
The University Of Sheffield.

# The tumour microenvironment as a potential therapeutic target in breast cancer

A thesis submitted in partial fulfilment of the requirements for the degree of
Doctor of Philosophy by

**Marie-Therese Haider**

Supervised by
Prof. Ingunn Holen and Prof. Nicola Brown

The University of Sheffield
Faculty of Medicine, Dentistry and Health
Department of Oncology and Metabolism

Submitted by August 2016

## Acknowledgements

Firstly, I would like to thank my supervisors Prof. Ingunn Holen and Prof. Nicola Brown for their truly extensive support, help, guidance and encouragement throughout my PhD. Thank you so much!

A special thank you goes to Dr. Penelope Ottewell and Dr. Hannah Brown who both taught me so many techniques. Thank you for answering my never-ending list of questions, I could not have completed this work without you!

A big thank you goes to Alyson Evans and Mark Kinch for cutting all my histological sections, and not giving up when I continuously asked for "deeper levels". A big thank you goes to Diane Lefley, Beka Armstrong and Rachel Rodham for their help, support and guidance with all my *in vivo* experiments.

I also want to thank all people in the Bone Analysis Laboratory and the Flow Cytometry Core Facility for their assistance. Russell Hughes, for answering all my questions about flow cytometry, Holly Evans, for help with the μCT analysis, Darren Robinson for help with confocal/fluorescence microscopy – thank you very much.

Thank you so much Victoria Cookson for all your moral support, calming me down, helping me out and listening to whatever I was complaining and worrying about.

Also, thank you to the McAllister laboratory for having me in Boston, and especially to Jessalyn Ubellacker for making my stay amazing.

Last but not least the most important "THANK YOU" goes to my amazing family for their continuous and never-ending support and encouragement over the last years. Thanks for giving me the strength to follow my goals and for always believing in me – I hope I made you proud.

**Funding bodies**

My PhD studies were funded by Breast Cancer Now, UK.


Further funding was kindly provided by:







## Declaration

I hereby declare that this thesis is a presentation of my original research work under the guidance of my supervisors Prof. Ingunn Holen and Prof. Nicola Brown. All work was performed by myself; any contribution by others is clearly indicated in the corresponding methodologies section. Where samples have been obtained through collaborative work every effort has been made to indicate this clearly.

For work published prior to presentation in this thesis the consent from all authors to reproduce obtained data sets has been obtained. Permission of reproduction is granted for the following manuscripts:

Haider M-T, Holen I, Dear TN, Hunter K, Brown HK. **Modifying the osteoblastic niche with zoledronic acid *in vivo*—Potential implications for breast cancer bone metastasis.** Bone. 2014;66(100):240-250.

DOI: http://dx.doi.org/10.1016/j.bone.2014.06.023

Haider MT, Hunter KD, Robinson SP, Graham TJ, Corey E, Dear TN, Hughes R, Brown NJ, Holen I. **Rapid modification of the bone microenvironment following short-term treatment with Cabozantinib *in vivo*.** Bone 2015;81: 581-592.

DOI: http://dx.doi.org/10.1016/j.bone.2015.08.003

## Abstract

Increasing evidence suggests that breast cancer (BC) progression involves interaction between the tumour and the surrounding stroma, the tumour microenvironment (TME). Work presented in this thesis is based on the hypothesis that anti-cancer therapies influence the bone microenvironment (BME), contributing to enhanced treatment efficacy. Thus, the BME was established as a therapeutic target for BC using *in vivo* models, imaging and molecular analysis.

Novel evidence of early effects of the bisphosphonate Zoledronic acid (ZOL) on cells other than the osteoclast, its' main target, are presented. Indeed a single, clinically relevant dose rapidly affected osteoblasts, bone volume, bone marrow microvasculature and extra cellular matrix (ECM) composition as early as 3 days after treatment *in vivo*. Based on the finding that BC cells preferentially locate to osteoblast-, and ECM-rich trabecular bone and that BC cell location in bone could be challenged in a ZOL-modified microenvironment, osteoblasts were identified as a potential key component of the metastasis niche and a novel therapeutic target for BC bone metastasis.

Additionally this work provides evidence that the tyrosine kinase inhibitor Cabozantinib (CBZ) affects bone structure, growth plate chondrocytes and haematopoietic bone marrow cells including megakaryocytes in naïve mice. Effects on osteoblasts and osteoclasts varied between animal model and treatment schedule, however, these studies suggest that therapeutic response to CBZ in patients with bone metastasis may be partially mediated via the BME.

Although ZOL affects a variety of BM-derived cells, first evidence is given that modification of the BME with ZOL is not sufficient to affect peripheral BC re-growth following cessation of successful combination therapy.

Collectively work presented in this thesis contributes important knowledge to the inadequately characterised, initial events of bone metastasis; and provides strong evidence that the BME contributes to treatment success in metastatic BC, however its role in primary disease needs to be established.

## Publications

The publications arising from my doctoral studies include:

**A) Publications with peer review process – Manuscripts**

(1) **M.T. Haider**, K.D.Hunter, S.P.Robinson, T.J.Graham, E.Corey, T.N.Dear, R.Hughes, N.J.Brown, I.Holen (2015) *Rapid modification of the bone microenvironment following short-term treatment with Cabozantinib in vivo*. In: Bone 81 (2015) 581-592.

(2) **M.-T.Haider**, I.Holen, T.N.Dear, K.Hunter, H.K.Brown (2014) *Modifying the osteoblastic niche with zoledronic acid in vivo – Potential implications for breast cancer bone metastasis.* In: Bone 66(0) (2014) 240-250.

**B) Publications with peer review process – published abstracts from national and international conferences**

Oral presentations:

(1) **MT. Haider*,** PD. Ottewell, DV. Lefley, NJ. Brown, I.Holen *Peripheral tumour re-growth following combination therapy – role of the bone microenvironment* 13.-17.05.2016 – 43rd Annual European Calcified Tissue Society Congress 2016; Rome, Italy; In: *Bone Abstracts* (2016) 5 CABSOC2.4, DOI:10.1530/boneabs.5.CABS.OC2.4

(2) **MT.Haider*,** I.Holen, K.Hunter, HK.Brown *Tumour cells home to osteoblast-rich areas – effects of a single dose of Zoledronic acid on the bone metastatic niche in vivo* 25.-26.06.2014 - Bone Research Society Annual Meeting 2014; Sheffield, UK; In: Frontiers, Bone Research Society Abstracts, Annual Meeting 2014, OC4, DOI: 10.3389/978-2-88919-300-4

(3) **MT.Haider,** I.Holen, HK.Brown* *Zoledronic acid affects osteoblasts in vivo with potential implications for the bone metastasis niche* 05.-06.09.2013 - 4th Joint Meeting of the Bone Research Society and the British Orthopaedic Research Society; Oxford, UK; In: Frontiers, Bone Research Society Abstracts, 2013, OC38 , DOI: 10.3389/978-2-88919-174-1

Poster presentations:

(1) P.Ottewell, H.Brown, G.Allocca, **MT.Haider**, N.Brown, I.Holen*. *The bone microenvironment as a master regulator of tumour cell dormancy in breast cancer – evidence from novel in vivo models* 09-12.06.2016 24th Biennial Congress of the European Association for Cancer Research; Manchester, UK; In: European Journal of Cancer (2016), Volume 61, Supplement 1, S74-S75, DOI: 10.1016/S0959-8049(16)61259-5

(2) **JM.Ubellacker*,** MT.Haider, T.Laszewski, I.Holen, SS.McAllister *Elucidating the impact of zoledronic acid on the bone microenvironment: Implications for breast cancer* 30.11.-03.12.2015 – American Association for Cancer Research, Tumor Metastasis Meeting, Austin, Texas, USA, In: Cancer Research 76(7 Supplement) (2016) IA07-IA07, DOI: 10.1158/1538-7445.TUMMET15-A67

(3) **MT.Haider,** K.Hunter, I.Holen, NJ.Brown* *Short-term in vivo administration of Cabozantininb induces rapid modification of the bone marrow vascularity* 03.-06.06.2015 - 28th European Society for Microcirculation and 8th European Vascular Biology Organisation Meeting 2015; Pisa, Italy, In: Journal of Vascular Research (2015), Vol.52, Suppl. 1, 28, DOI:10.1159/000433497

(4) **MT. Haider*,** K.Hunter, NJ.Brown, I.Holen *Rapid modification of the bone microenvironment in vivo following short-term Cabozantinib administration* 25.-28.04.2015 - 4th Joint Meeting of European Calcified Tissue Society and International Bone and Mineral Society; Rotterdam, The Netherlands, In: IBMS BoneKEy 13, Article number: 685 (2015), P107, DOI:10.1038/bonekey.2015.53

(5) **MT.Haider*,** HK.Brown, K.Hunter, NJ.Brown, I.Holen *Rapid modification of the in vivo bone marrow vascularity following short-term administration of Cabozantinib* 16.-17.04.2015 – 65th meeting of the British Microcirculation Society; Manchester, UK, In: Microcirculation (2015), Volume 22, Issue 8, pages 753-781, PP10, DOI: 10.1111/micc.12212

**C) Further publications with peer review process – National and Local Meetings**

(1) **MT.Haider*,** J.M.Ubellacker, H.K.Brown, P.D.Ottewell, G. Allocca, N.J.Brown, S.S.McAllister, I.Holen Modification of the bone microenvironment – potential consequences on breast cancer bone metastasis 03.-04.04.2016 SEARCHBreast "*In vivo* models of breast cancer" workshop in Glasgow, UK

(2) **MT. Haider*,** HK.Brown, K.Hunter, NJ.Brown, I.Holen *The bone microenvironment as a therapeutic target in advanced breast cancer - evidence from in vivo models of bone metastasis* 07.-09.10.2015 – British Association of Cancer Research special meeting Breast Cancer - Bridging gaps in our knowledge to improve patient outcome; Newcastle, UK

(3) **MT. Haider*,** HK. Brown, K. Hunter, NJ. Brown, I. Holen *The tumour microenvironment – still underestimated as a mediator of anti-cancer therapy?* 15. – 16.06.2015 – The Medical School Research Meeting; University of Sheffield, Sheffield, UK

(4) **MT. Haider*,** K.Hunter, N.J.Brown, I.Holen *Short-term administration of Cabozantinb (CBZ) causes significant modification of the bone microenvironment* 05.12.2014 - 5th Mellanby Centre Research Day; Sheffield, UK

(5) **M.T.Haider*,** I.Holen, K.Hunter, H.K. Brown *Effects of a single dose of zoledronic acid on the bone metastasis niche in vivo* - 16.07.2014 - 17.06.2014 The Medical School Research Meeting, University of Sheffield, Sheffield UK

* indicates presenting author

## Table of Contents

**List of Figures**

**List of Tables**

**List of common abbreviations**

| Abbreviation | Meaning |
|---|---|
| Ab | Antibody |
| ABC | Avidin Biotin Complex |
| AL | Alendronate |
| AOI | Area of interest |
| ATCC | American Type Culture Collection |
| AVCs | Angiogenic vascular cells |
| BCA | Bicinchoninic acid assay |
| BM | Bone marrow |
| Bm | Bone marrow |
| BMDCs | Bone marrow derived cells |
| BME | Bone microenvironment |
| BP | Bisphosphonate |
| $Ca^{2+}$ | Calcium |
| CAFs | Cancer-associated fibroblastic cells |
| CBZ | Cabozantinib |
| cDNA | ComplementaryDNA |
| CLO | Clodronate |
| CTCs | Circulating tumour cells |
| CXCR4 | C-X-C chemokine receptor type 4 |
| DAB | 3, 3'-diaminobenzidine |
| DAPI | 4',6-diamidino-2-phenylindole |
| $dH_2O$ | Deionised water |
| dia | Diaphysis |
| DMSO | Dimethyl sulfoxide |
| DNA | Deoxyribonucleic acid |
| DOX | Doxorubicin |
| DTC | Disseminated tumour cells |
| ECM | Extra cellular matrix |
| EDTA | Ethylenediaminetetraacetic acid |
| ELISA | Enzyme-linked immunosorbant assays |
| EOP | End of procedure |
| ep | Epiphysis |
| ETI | Etidronate |
| GFP | Green fluorescent protein |
| GP | Growth plate |
| $H_2O$ | Water |
| $H_2O_2$ | Hydrogen peroxide |
| HCl | Hydrochloric acid |
| HGF | Hepatocyte growth factor |
| hr | Hour |
| HSCs | Haematopoietic stem cells |
| IBAN | Ibandronate |
| IGF-1 | Insulin-like growth factor 1 |

| | |
|---|---|
| IICs | Infiltrating immune cells |
| Ils | Interleukins |
| $lN_2$ | Liquid nitrogen |
| LOX | Lysyl oxidase |
| M-CSF | Macrophage colony stimulating factor |
| MDSCs | Myeloid derived suppressor cells |
| MET | Hepatocyte growth factor receptor |
| met | Metaphysis |
| min | Minutes |
| min | Minute |
| MIP-1α | Macrophage inflammatory protein |
| MMPs | Matrix metalloproteinases |
| MSC | Mesenchymal stem cells |
| MSCs | Mesenchymal stem cells |
| NBP | Nitrogen containing bisphosphonate |
| NNBP | Non-nitrogen containing bisphosphonate |
| Ob | Osteoblast |
| Oc | Osteoclast |
| OPG | Osteoprotegerin |
| OPN | Osteopontin |
| PAM | Pamidronate |
| PBS | Phosphate-buffered saline |
| PDGF | Platelet-derived growth factor |
| PFA | Paraformaldehyde |
| PINP | Procollagen type I N propeptide |
| PTH | Parathyroid hormone |
| PTHrP | Parathyroid hormone-related protein |
| PVP | Polyvinylpyrrolidone |
| qRT-PCR | Quantitative Real Time Polymerase Chain Reaction |
| RANK | Receptor activator of nuclear factor-kB |
| RANK | Receptor activator of nuclear factor kappa-B |
| RANKL | Receptor activator of nuclear factor kappa-B ligand |
| RIS | Risedronate |
| RNA | Ribonucleic acid |
| RT | Room temperature |
| RTKs | Receptor Tyrosine Kinases |
| SDF-1 | Stromal cell-derived factor 1 |
| sec | Second |
| SREs | Skeletal related events |
| TAMs | Tumour associated macrophages |
| Tb | Trabeuclar bone |
| TGF-β | Transforming growth factor-β |
| TME | Tumour microenvironment |
| TNF-α | Tumour necrosis factor alpha |

| | |
|---|---|
| TRAP | Tartrate-resistant acid phosphatase |
| VEGF | Vascular endothelial growth factor |
| VOI | Volume of interest |
| ZOL | Zoledronic acid |
| μCT | Micro-computed tomography |

# Chapter 1 – Introduction

### 1.1. Breast cancer and breast cancer metastasis to bone – Statistics

Breast cancer is one of the most common cancers in Europe (464,000 cases; 13.5% of all cancer cases diagnosed in 2012) [1]. Steady improvements in screening methods and therapy, awareness and early detection have led to excellent prognosis for patients. Nevertheless, it remains the leading cause of death from cancer in women. Progress in the treatment of primary breast cancer has resulted in doubling of the 10-year net survival rates, which is currently at nearly 78% [2]. The skeleton is the most favoured site of metastasis in breast cancer and around 70% of patients with advanced disease will develop bone metastases [3]. These patients experience high morbidity caused by skeletal-related events (SREs) due to the osteolytic nature of the disease [3]. Survival rates at this stage are poor, only 15% of patients diagnosed with stage IV breast cancer (metastatic spread to other organs of the body) will survive their disease for up to five years [4]. Given that advanced disease is incurable, and the lack of routine markers for early detection of bone metastases, emphasises the need for new treatment strategies and novel therapeutic approaches to improve the long-term survival of patients with advanced breast cancer.

### 1.2. The tumour microenvironment (TME)

Over the last decade, research has moved away from the hypothesis that cancer cells alone result in development and progression of the disease. The tumour microenvironment (TME), the cellular environment in which the cancer exists, in addition to the surrounding matrix and signalling molecules is widely acknowledged to contribute to disease progression; and offers a broad field for research investigation and treatment intervention. A number of aspects of the contribution of the TME are established (*e.g.* the role of endothelial cells in tumour angiogenesis [5-7]), whereas others including the impact of the TME in mediating response to anti-cancer therapy, activation of invasion and metastasis [8, 9], remain under-researched and poorly defined. Understanding the complexity of how components of the TME co-operate with cancer cells is instrumental to ultimately establish more successful anti-cancer treatment.

#### 1.2.1 Composition of the TME and contribution to disease progression

The complexity of tumour–stroma interactions and the role of the TME has been actively researched and reviewed over the last decades [10-12]. Therefore only a short summary will be provided here, with a more detailed discussion concerning the role of the bone microenvironment (BME) in breast cancer growth in the next sections. On a cellular level, the TME comprises a broad spectrum of subpopulations. For simplification Hanahan and Coussens have grouped these into three compartments including **(1) Angiogenic Vascular**

**Cells** (AVCs) **(2) Infiltrating Immune Cells** (IICs, including tumour associated macrophages, TAMs) and **(3) Cancer-Associated Fibroblastic cells** (CAFs) [10].

Briefly, CAFS are suggested to be the most prominent compartment of the TME in breast cancer [13]. Given the physiological role of fibroblasts in wound healing, inflammation and ECM remodelling, their activated presence in the TME is predominant as tumours are considered "chronic, non-healing wounds". The origin of CAFs remains unclear but they may be derived from resident fibroblasts [14], bone marrow derived cells that are actively recruited and/or cancer cells that under-go active epithelial-mesenchymal transition (EMT) [15]. There is currently no specific set of markers to identify CAFs as they are a heterogeneous population, similar to the tumour itself. The role of CAFs in cancer progression, invasion and metastasis has been extensively reviewed [13]. Briefly these cells produce a variety of soluble factors that all contribute to drive the disease (*e.g.* hepatocyte growth factor (HGF), transforming growth factor-β (TGF-β), stromal derived factor-1 (SDF-1), vascular endothelial growth factor (VEGF), interleukins (IL-6) *etc.*), in addition to matrix metalloproteinases (MMPs), thereby affecting several hallmarks of cancer [8, 9, 16].

Macrophages derived from haematopoietic origins physiologically contribute to tissue repair and defence against foreign pathogens; and are often thought to be the first cells arriving at sites of infection and/or wounds. Macrophages are one of the most abundant cell populations at the tumour site (termed tumour associated macrophages, TAMs). They are generally not tumouricidal unless tumour-derived factors including interleukins (Ils) and TGF-β activate/promote M2 macrophage polarisation (the tumour-growth-promoting subtype) [17]. TAMs are generally associated with poor prognosis due to their ability to promote tumour angiogenesis (*e.g.* via epidermal growth factor (EGF), VEGF, platelet-derived growth factor (PDGF), tumour necrosis factor alpha (TNFα), CCL2, CXCL8, *etc.*) [18, 19], migration (*e.g.* EGF, MMPs, *etc.*), metastatic spread (preparing the metastatic site through VEGFR1, CCR2, and CX3CR1) [20], and immunosuppression – all recently reviewed in detail [21].

In addition to macrophages also other infiltrating immune cells such as neutrophils and subsets of T-cells, can have both tumour promoting and inhibiting functions – processes mediated via microenvironmental factors including for example interferons (IFNs) and TGF-β. As a key component in inflammation they contribute to tumour growth partially via the secretion of pro-tumorigenic factors including EGF, TGF-β, PDGF, HGF and VEGF [22].

The contribution of AVCs including pericytes, endothelial cells and smooth muscle cells has been extensively characterised in tumour development. Briefly they contribute to tumour growth via providing nutrients and oxygen, facilitate trafficking of growth promoting factors as well as cells to and from the tumour and allow cancer cell dissemination and metastasis. In turn, cancer cells induce the so-called ‘’angiogenic switch“. This involves the induction of tumour angiogenesis through detachment of perivascular cells and vessel dilation, followed by angiogenic sprouting, formation and maturation of new vessels to provide essential nutrients and oxygen [23, 24]. This results in increased rate of tumour growth [6, 7, 25]. In their extensive review Hanahan and Coussens have elegantly summarised and illustrated key contributions of cells of the TME to cancer growth – see Figure1.

Of relevance to breast cancer, the mammary stroma is comprised of following components: adipocytes, pre-adipocytes, fibroblasts, blood vessels, inflammatory cells, as well as extracellular matrix [26]. Stromal cells in the developing mammary gland, as well as growth factors and cytokines are associated with breast cancer growth and progression – reviewed in [26].

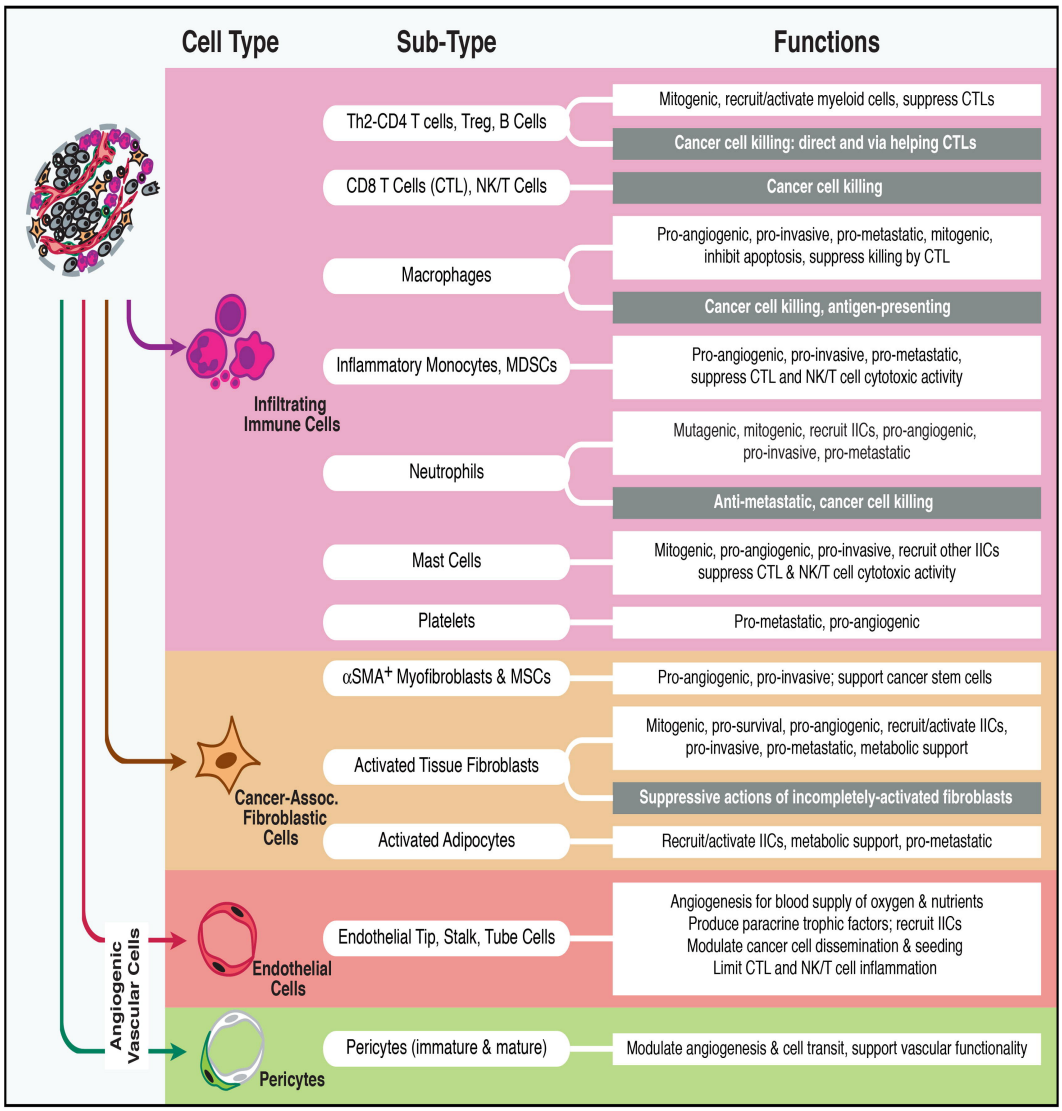


**Figure 1 Contribution of the tumour microenvrionment to cancer growth.**
A myriad of cell populations contribute to the „Hallmarks of Cancer“ [9]. „Reprinted from **Accessories to the Crime: Functions of Cells Recruited to the Tumor Microenvironment**
D. Hanahan, L.M. Coussens, Accessories to the crime: functions of cells recruited to the tumor microenvironment, Cancer Cell 21(3) (2012) 309-22. Copyright © 2012 Elsevier Inc. Terms and Conditions; with permission from Elsevier. doi:10.1016/j.ccr.2012.02.022

#### 1.2.1.1. Recruitment of bone marrow-derived cells to promote tumour growth

Growing attention is paid to bone marrow-derived cells (BMDCs) and their contribution to breast cancer growth. Many of the stromal cells present within the TME are mobilised host cells from distant tissues including the bone marrow and spleen, illustrated in Figure 2. Recruitment of BMDCs involves the release of tumour-derived factors including granulocyte-colony stimulating factor (G-CSF), VEGF, TGF-β, osteopontin (OPN), lysyl oxidase (LOX) and stromal cell-derived factor 1 (SDF-1) [27-29]. SDF-1 is a key regulator of bone marrow retention and homing of haematopoietic stem and progenitor cell populations (HSCs, HSPCs)[30, 31]. G-CSF in contrast causes mobilisation of HSCs or prevents their homing to bone marrow niches [32]. Additionally the bone matrix protein OPN is required for the pro-tumorigenic function of BMDCs in tumour xenograft models [27]. Studies have shown that BMDCs contribute to vascularisation and growth of primary tumours. Formation of a complex vascular network is a pre-requisite of tumour growth and in addition to the sprouting from pre-existing vessels, BMDCs including haematopoietic-, endothelial progenitor cells and mesenchymal stem cells are recruited to promote tumour angiogenesis and growth [33-35]. It is also suggested that recruitment of BMDCs is detrimental for the early stages of tumour angiogenesis, whereas residual BMDCs may contribute to later tumour growth [33]. In addition tumour-derived chemoattractants including VEGF, colony stimulating factor 1 (CSF-1) and CCL2 (Chemokine (C-C Motif) Ligand 2) drive the accumulation of TAMs derived from mononuclear bone marrow progenitor cells in the tumour stroma [36]. TAMs produce angiogenic factors including VEGF and angiopoietin [37-40], which stimulates the recruitment of further BMDCs including mast cells, neutrophils, myeloid-derived suppressor cells and leukocytes [36, 40, 41]. The role of BMDCs in mediating primary breast cancer (re)-growth is further discussed in Chapter 3; and illustrated in Figure 2 below. However, the contribution of BMDCs is not limited to primary tumour growth, which became evident by studies reporting that VEGFR1+ve bone marrow-derived haematopoietic progenitor cells home to pre-metastatic sites where they form clusters prior to the arrival of tumour cells [28, 42]. Here the role of BMDCs in metastasis is stressed by the observation that metastasis did not occur in the absence of BMDC recruitment [28].

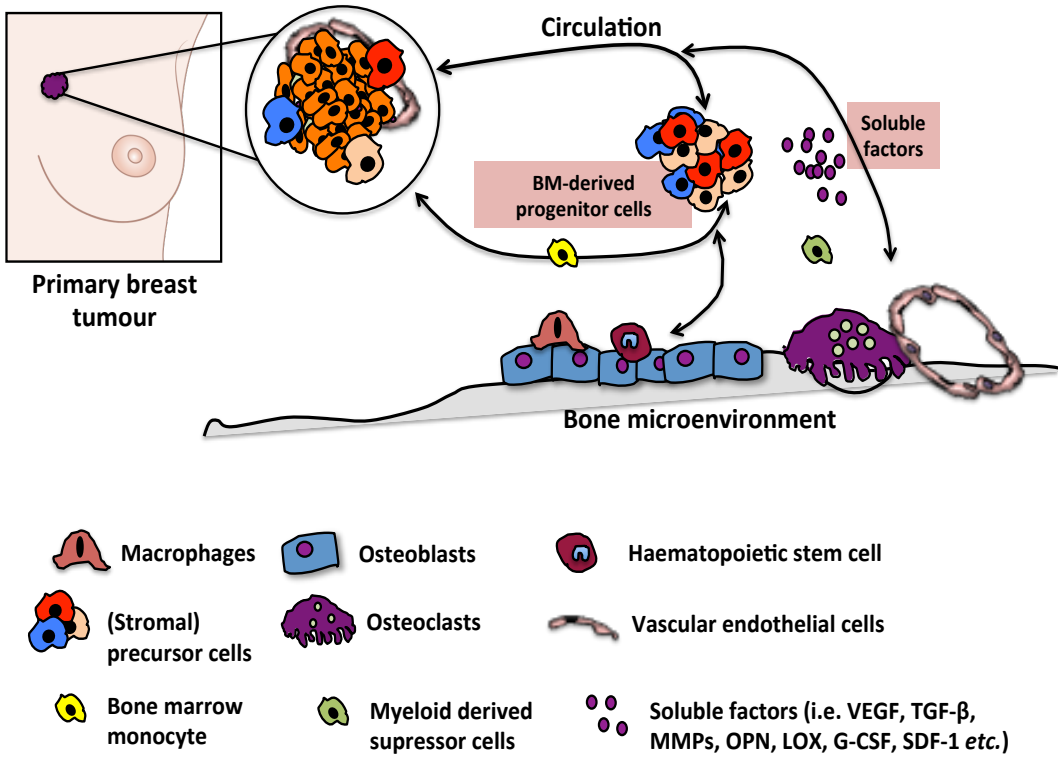


**Figure 2 Bone marrow-derived precursor cells (BMDCs) - contribution to primary breast cancer growth.**
Cancer cells secrete various growth factors, cytokines and chemokines, which results in the recruitment of bone marrow-resident precursor cells. These cells actively promote disease progression. However, whether these cells get activated whilst still in the bone marrow or at the site of tumour growth is still unclear. The complex tumour-stroma crosstalk gives room for therapeutic targeting.

### 1.2.2 The TME - Summary

In summary, the composition of the TME is complex and our increased understanding of the tumour-stroma crosstalk resulted in the development of therapeutic agents that target not only the tumour cells but also the microenvironment. This includes for example agents that affect the tumour vasculature such as bevacizumab, sunitinib, sorafenib, erlotinib and gefitinib. Other approaches are to enhance tumour immunity by targeting myeloid derived suppressor cells, T-, and B-cells. Various chemokines that recruit BMDCs including TAMs, as well as inflammatory signalling pathways are explored as therapeutic targets. Agents that disrupting the interaction between tumour cells and the ECM as well as the bone microenvironment are investigated and/or used in clinical practice including for example

integrin inhibitors and anti-resorptives such as bisphosphonates and Denosumab (discussed in section 1.5.1. and 1.5.2.).

### 1.3. The bone microenvironment (BME)

Besides lung, liver and brain, bone is the preferred site for breast cancer metastasis. Around 70% of patients with advanced disease will develop bone metastases [3], hence indicating the potential for therapeutic modification of the bone microenvironment (BME). In addition, physiological interaction between breast and bone is apparent, especially during the process of childbearing and breastfeeding. Lactation as well as suckling requires the release of large amounts of calcium ($Ca^{2+}$) from the skeleton. Both processes involve alterations in parathyroid hormone (PTH), parathyroid hormone-related protein (PTHrP), calcium ($Ca^{2+}$), RANK/RANKL signalling (Receptor activator of nuclear factor kappa-B/ligand; key regulatory pathway of osteoclastogenesis and drivers of bone remodelling), calcitonin, vitamin D3, gonadotropin-releasing hormone, prolactin and estradiol [43-45]. During pregnancy and breastfeeding this commonly results in increased bone resorption and bone loss, which is rapidly reversible after weaning [46]. A key regulator of serum $Ca^{2+}$ levels is PTH through its' effects on bone (release of $Ca^{2+}$/bone remodelling) and kidney (increase $Ca^{2+}$ resorption, phosphate excretion and 1,25 dihydroxyvitamin D formation). Decreased $Ca^{2+}$ levels result in rapid, increased secretion of PTH, followed by osteoclastic bone resorption to release $Ca2^{+}$ stored in the skeleton, a tightly regulated feedback mechanism. However, PTH can have both anabolic (bone building) and catabolic (bone destroying) functions, depending on exposure and concentration (intermittent = anabolic, continuous = catabolic [47]).

#### 1.3.1. Bone composition and function

Bone is a dynamic organ composed of a mineral phase (hydroxyapatite), an organic phase including lipids, and water. The organic phase can be divided into **(1) structural proteins** including type I collagen, fibronectin, and **(2) non-collagenous proteins** such as proteoglycans, osteopontin, osteonectin, matrix metalloproteinases and phosphatases [48]. These building blocks are produced by cells of mesenchymal origin, including both osteoblasts and fibroblasts. Two structural subtypes of bone are observed: **(1) trabecular** (around 20% of the skeleton, high metabolic activity) and **(2) cortical** bone (about 80% of the skeleton, less active, provides mechanical strength) [49].

#### 1.3.1.1. Key bone cells and function

Briefly, the bone marrow hosts two distinct stem cell populations, haematopoietic and mesenchymal stem cells (HSCs and MSCs), with each having different progenies. HSCs give rise to all lymphoid and myeloid linage cells finally differentiating into immune cells, megakaryocytes, myeloid cells (monocytes/ macrophages/ granulocytes) and erythrocytes [50]. MSCs in contrast differentiate to give rise to adipocytes, bone and connective tissue-forming cells including chondrocytes, osteoblasts and myoblasts (Figure 3). In addition the bone marrow is comprised of a dense, interconnected vascular system (endothelial cells arising from hemangioblasts similar to HSCs [30]), which maintains haematopoiesis and osteogenesis [51, 52].

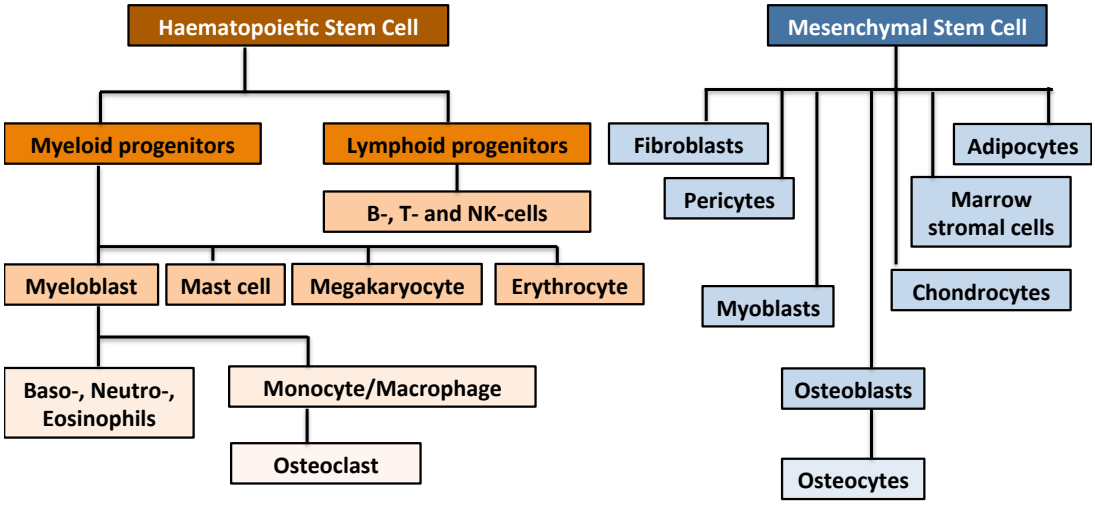


**Figure 3 Origin of cells of the bone microenvironment.**
The bone marrow hosts two distinct stem cell populations, haematopoietic and mesenchymal stem cells (HSCs and MSCs), with each having different progenies.

The three key cells responsible for maintaining bone structure and function include **(1) the bone resorbing osteoclast, (2) the bone forming osteoblast** and **(3) the mechanosensory osteocyte**, the most abundant cell type in bone.

**Cells of the osteoblast family:** MSCs differentiate into osteoblast precursors (so-called osteoprogenitors characterised by expression of osterix and Runx2 [53, 54]) followed by maturation into active, bone forming osteoblasts (characterised by expression of Osteocalcin). Osteoblasts are generally round in shape, characterised by a large golgi complex, abundant endoplasmatic reticulum and found in clusters lining bone surfaces [55]. After a short phase of active bone formation the terminal fate of osteoblasts is to become buried in bone, upon which they are classified as osteocytes, or exist quiescent

on bone surfaces as bone lining cells characterised by a flattened morphology with few organelles [56]. Being embedded within the bone matrix and their tight connection with neighbouring cells through various cell processes allows osteocytes to sense mechanically-induced matrix-strain and to consequently relay signals to surrounding cells to respond to mechanical stimuli [55, 57] .

**Osteoclasts:** Derived from haematopoietic cells of the myeloid lineage, osteoclast precursors differentiate into large, multinucleated osteoclasts (tartrate-resistant acid phosphatase TRAP+ve, cathepsin K+ve); a process controlled by receptor activator of nuclear factor-kB (RANK, or TNFSF11) and macrophage colony stimulating factor (M-CSF). Osteoclasts are responsible for breaking down and resorbing mineralised matrix. Only when in contact with mineralised bone surfaces, osteoclasts generate distinct membrane domains including the ruffled membrane, bind to resorption sites via αvβ3 integrin molecules and create a unique, isolated microenvironment known as the sealing zone. Hydrogen ions are pumped into this sealing zone creating a low pH (4.5), which in combination with collagenolytic enzymes (Cathepsin K, MMPs) degrades the bone matrix [58].

**Connective tissue cells – Fibroblasts:** Another mesenchymal-derived cell type abundant in the BME includes fibroblasts. Fibroblasts synthesize and secrete extracellular matrix (ECM) molecules including collagens, fibronectin and proteoglycans in addition to ECM-degrading proteases, thereby contributing to connective tissue maintenance. Physiologically quiescent or resting spindle-shaped fibroblasts are found embedded within the ECM. Next to their contribution of ECM synthesis and deposition, quiescent fibroblasts become activated by tissue injury or associated stimuli (*e.g.* transforming growth factor-β (TGFβ), platelet-derived growth factor (PDGF) and interleukin-6 (IL-6)), thus contributing to wound healing, tissue repair and regeneration [59, 60]. During bone repair, fibroblasts start to lay down ECM to aid vascular ingrowth. Once vascular ingrowth is progressing a collagen matrix is laid down, osteoid secreted and finally mineralised by osteoblasts. In addition they contribute to haematopoiesis by secreting cytokines including GM-CSF, IL-6 and M-CSF, macrophage inflammatory protein (MIP-1α), monocyte chemotactic protein-1 (MCP-1), interferon-γ [61-63]. Fibroblasts also contribute to angiogenesis, in example through production of HGF, basic fibroblast growth factor (bFGF) and thrombospondin [64].

#### 1.3.1.2. Physiological bone remodelling

Cross-talk between osteoblasts and osteoclasts is regulated in time and space during the process of bone remodelling. Remodelling takes place in distinct sites termed basic multicellular units (BMUs). This ensures maintenance of tissue turnover and is a tightly "coupled" process involving resorption of bone by osteoclasts followed by osteoblast-mediated bone formation [65]. The hypothesis of communication between osteoblasts and osteoclasts by Rodan and Martin [66] resulted in the discovery of the RANK/RANKL, osteoprotegerin (OPG) signalling cascade, and its importance during bone remodelling [67-72].

Briefly, the remodelling cycle consists of distinct phases including activation, resorption, reversal formation and finally termination of the cycle [65], schematically illustrated in Figure 4.

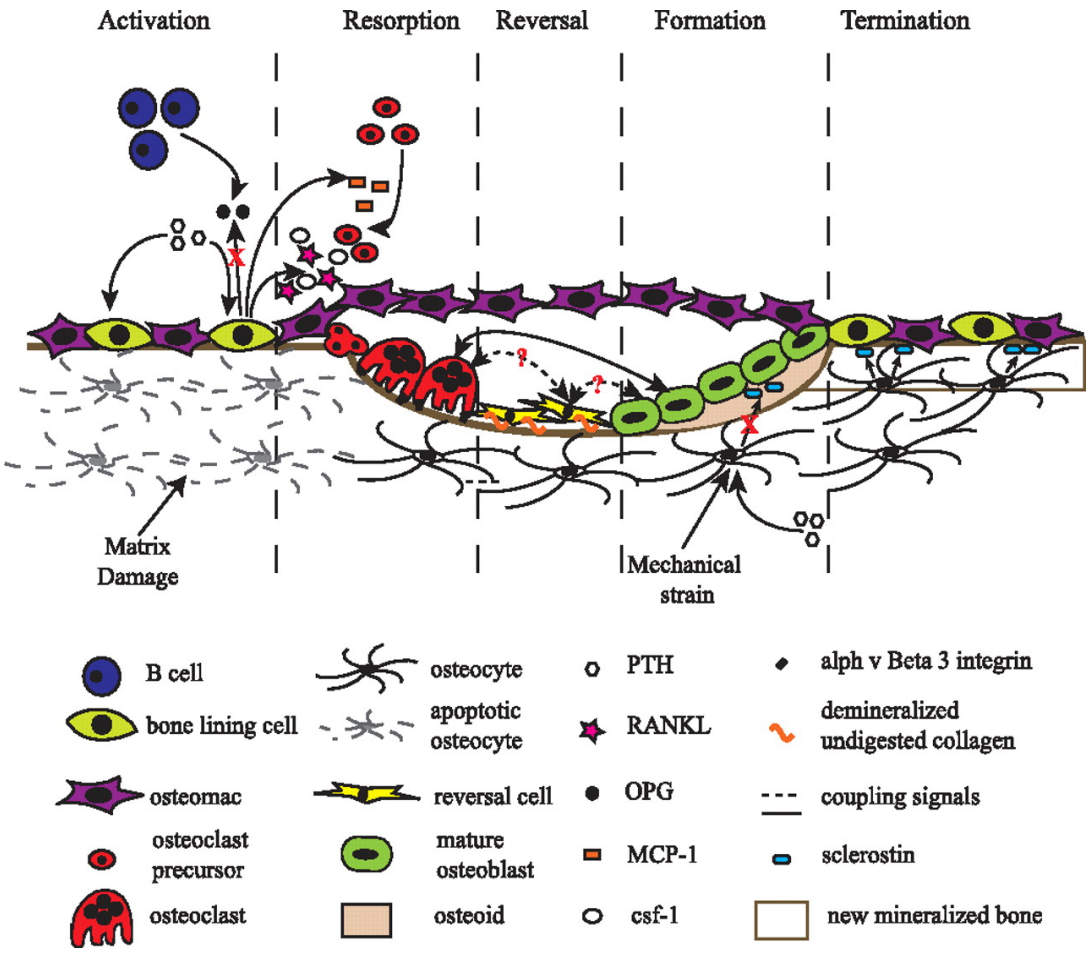


**Figure 4 Schematic representation of a Bone Mineral Unit (BMU) and the associated bone-remodeling process.**
The remodelling cycle consists of distinct phases including activation, resorption, reversal formation and finally termination of the cycle. Each phase is tightly regulated by the interaction of various bone cells. „This research was originally published in The Journal of Biological Chemistry. L.J.Raggatt, N.C. Partridge.Cellular and molecular mechanisms of bone remodelling.*J Biol Chem* 285(33) (2010) 25103-8. ©2010 by the American Society for Biochemistry and Molecular Biology, Inc; with permission from American Society for Biochemistry and Molecular Biology". doi: 10.1074/jbc.R109.041087

The remodelling cycle is activated through an initial stimulus including **(1)** mechanical stress sensed by osteocytes affecting IGF-I, a factor known to be required for MSC differentiation [73]; **(2)** PTH as an endocrine bone remodelling signal or **(3)** reduced TGF-β concentrations resulting from osteocyte apoptosis during tissue damage [74]. Next osteoclast precursors are recruited to the resorption site followed by their differentiation into mature, multinucleated osteoclasts. Completion of osteoclast precursor differentiation requires expression of macrophage colony stimulating factor (M-CSF) and RANKL by osteoblastic stromal cells and binding to the corresponding receptors RANK and c-fms on osteoclast precursors [67, 71, 75]. RANK/RANKL mediated osteoclast maturation

is inhibited by OPG, a decoy receptor for osteoblastic RANKL and negative regulator of bone resorption, which is also produced by osteoblasts (Figure 4) [69]. Signalling downstream the RANK/RANKL, M-CSF/c-fms signalling axes result in activation of NF-kB, NFATc1 and c-fos [68, 76] leading to expression of osteoclast specific genes including TRAP, cathepsin K and b3 integrins. Osteoclastic bone resorption is systemically regulated by 4 main hormones, PTH and 1,25-dihydroxy vitamin $D_3$ stimulating and oestrogen and calcitonin reducing bone resorption directly or indirectly. PTH and 1,25-dihydroxy vitamin $D_3$ are key regulators of calcium homeostasis; by stimulating osteoclastic bone resorption, both are required to maintain serum $Ca^{2+}$ concentrations to avoid clinical manifestations including hypo- and hypercalcemia. The resorption site is isolated by a membrane ring known as the sealing zone and low pH in combination with collagenolytic enzymes ultimately lead to degradation of the bone matrix [58]. During the reversal and formation phase an equal amount of previously resorbed bone needs to be removed and replaced by new matrix; known as coupling [77]. Reversal of bone resorption is proposed to be initiated by mononuclear cells of still unknown origin, called “reversal cells” [74]. During this phase, any remaining collagen is removed and the bone surface is prepared for the subsequent formation of new matrix by osteoblasts [56]. The signals that couple formation and resorption of bone remain a subject of debate, but are suggested to include bone matrix-derived factors including ILs, TGF-β, osteoclast-osteoblast-derived signals including EphB4-ephrin-B2 [78] and Sphingosine 1-phosphate [79], or mechanical stimulation via osteocytes [73, 74]. Mesenchymal-derived osteoblast precursors differentiate into mature osteoblasts mediated via PTH, ILs, bone sialoprotein (BSP), osteocalcin and osteopontin [56]. Osteoblastogenesis is further driven by bone morphogenic proteins (BMPs), wnt signalling, Notch signalling and the transcription factors Runx2 and osterix. Once equal amounts of resorbed bone has been formed, mature osteoblasts undergo apoptosis, revert to bone lining cells or become embedded in the mineralised matrix as osteocytes.

In addition other cells present in the bone marrow are suggested to contribute to bone remodelling, for example megakaryocytes. Platelet-producing megakaryocytes reside in the bone marrow and mice deficient in the transcription factors GATA-1 and NF-E2 have increased megakaryocyte number accompanied by elevated osteoblast numbers and increased bone volume [80]. *In vitro,* osteoblast proliferation is increased by the presence of megakaryocytes [80] and direct cell-to cell contact between both cell types is suggested to occur via gap junctions [81] and/or integrins [82]. However, further studies are required

to determine the role of megakaryocytes in bone remodelling *in vivo* (discussed in more detail in Chapter 4).

### 1.4. The TME in breast cancer bone metastasis

The multi-step process of metastasis development involves **(1) colonisation** of the bone marrow by circulating tumour cells (CTCs), **(2) survival and/or dormancy** in specialised microenvironments or "niches", followed by **(3) reactivation** and development into actively proliferating micrometastases [83]. The metastatic cascade has been described as less efficient than growth at primary sites, mainly due to the obstacles faced upon arrival at the distant organs; and only a small subset of cells will eventually initiate metastatic outgrowth [84, 85]. For example, studies using B16F1 murine melanoma cells in a C57Bl/6 mouse model of liver metastasis showed that a total of about 80% of injected cells survived the extravasation into the secondary organ (data from 90 minutes and 3 days post injection). In contrast, 13 days post injection only 36.2% of injected cells were still present of which 0.07% were present as micrometastases (4-16 cells), 0.02% as macrometastases, with the remaining cells being ''solitary"/dormant cells (Ki67 –ve, TUNEL –ve) [84]. Similar effects were observed in prostate cancer models, DiD-labelled tumour cells (dye retaining cells are here defined as quiescent) could be detected in tibiae of mice 24hrs after intra-cardiac injection, which accumulated over the first week and then rapidly declined over time. However, DiD-labelled, quiescent cells were still detected in bone 6 weeks post injection showing that mitotic quiescence cells persist in bone until a still unknown signal triggers proliferation [85].

Beside lung, liver and brain, breast cancer cells (''seeds") preferentially metastasise to bone (''soil"), a concept based on Steven Paget's seed and soil theory that *„when a plant goes to seed, its seeds are carried in all directions; but they can only live and grow if they fall on congenial soil"* [86]. Bone provides such a ''congenial soil" as it undergoes constant remodelling thereby providing an ideal microenvironment for disseminated breast cancer cells through a constant supply of soluble factors (*e.g.* RANKL, ILs, TGF-β and high $Ca^{2+}$ levels [87-89]).

#### 1.4.1. The concept of niches

Based on Paget's seed and soil theory [86] the concept that distinct supporting microenvironments ("niches") promote survival, and/or proliferation of metastatic tumour cells was established [86]. Circulating breast tumour cells have a high affinity for bone, in particular areas of active bone remodelling [90]. Not only the complex interplay between

osteoblasts and osteoclasts, but also the presence of various other bone marrow-derived (precursor) cell populations (BMDCs) and soluble factors (*e.g.* OPN, MMPs, *etc.*), make bone an attractive site (a "metastatsis niche") for disseminated tumour cells (DTCs).

Within bone, the proposed metastasis niche is comprised of various individual entities of BMDCs comprising a **(1) haematopoietic, (2) endosteal and (3) (peri-) vascular niche** [31]**.** Emerging data also implicate a role for the **immune-** and **bone marrow adipocyte niche** in bone metastasis [91, 92]. The interaction and overlap between the niches remain to be established. This has resulted in the generalised term of the "metastasis niche" that is thought to regulate homing, survival and dormancy of tumour cells [31, 92-96]. The following sections will discuss the role of the BME in the early and late(r) stages of bone metastasis.

### 1.4.2. Formation of pre-metastatic niches

Development of metastatic disease was previously considered the last step in disease progression however, in about 30% of patients with early-stage breast cancer, presence of micro-metastases in the bone marrow at the time of diagnosis has been reported [97]; which is associated with poor prognosis.

Although exact mechanisms that guide tumour cells towards the metastatic site remain to be established, current thinking is that tumour cells themselves modify the distant microenvironment, for example through systemic factors, that make it more attractive for the disseminated tumour cells (DTCs) [28, 98, 99] - Figure 5. Consequently the formation of these supportive microenvironments (pre-metastatic niches) involves primary tumour-derived factors (*e.g.* VEGF, placental growth factor (PIGF), TNF-α, TGF-β, LOX, G-CSF, miRNAs) as well as recruitment of BMDCs including macrophages [18, 28, 42].

Lysyl oxidase (LOX), an enzyme that plays a key role in extracellular matrix and collagencrosslinking, for example has been associated with breast cancer metastasis and increased risk for bone relapse in ER -ve breast cancer patients [29]. Recent studies using the syngeneic 4T1-BALB/c immunocompetent mouse model of spontaneous metastasis ($LOX^{high}$) showed that the formation of osteolytic lesions preceded the arrival of tumour cells in bone. Similar results were observed when injecting recombinant LOX into both immunocompetent and immunocompromised mice, which resulted in formation of local osteolytic lesions and increased bone resorption markers. These data suggest that high levels of LOX could drive the development of osteolytic lesions independent of the presence of tumour. In contrast, formation of osteolytic lesions was decreased when LOX

activity was silenced using either 4T1shLOX tumours ($LOX^{low}$) or a specific antibody against LOX. *In vitro* addition of recombinant LOX stimulated osteoclastogenesis independent of the presence of RANKL, decreased proliferation and increased terminal differentiation of primary calvarial mouse osteoblasts. Similar effects on differentiation of the human osteoblast SaOS-2 cell line was observed when cultured with cancer-conditioned medium from $LOX^{high}$ 4T1 cells when compared to control. In summary, LOX shifted the balance of bone remodelling towards osteoclastic bone resorption, confirmed by quantification of osteoblasts (reduced) and osteoclasts (increased) in bones of 4T1scr bearing mice when compared to 4T1shLOX tumour bearing mice. These studies also suggested the formation of specialised niches within the BME upon LOX-mediated pre-metastatic focal osteolytic lesion generation that supported colonisation of circulating tumour cells. Following intracardiac 4T1 injection mice were injected with hypoxic 4T1 conditioned medium +/- simultaneous treatment with the bisphosphonate Zoledronic acid. Addition of Zoledronic acid significantly reduced tumour cell colonisation and development of bone metastases, suggesting beneficial effects of bisphosphonate treatment for patients with $LOX^{high}$ tumours (*e.g.* ER -ve). These intriguing findings highlight the potential for novel therapeutic intervention in the treatment of bone metastases by targeting tumour-derived systemic factors [29].

In addition, by injecting different cell lines into the contralateral flanks of mice, McAllister and colleagues showed that ''instigator'' cell lines were capable of inducing the growth of ''responder'' cells in the opposite flank, which was not observed after injection of matrigel or ''non-instigators". Growth of ''responders" was mediated by mobilised bone marrow cells and analysis of blood plasma suggested that tumour-instigation was mediated by osteopontin (OPN). In addition ''instigators" also increased the frequency of lung metastases, which was reduced by inhibition of OPN by shRNA [27]. In addition, Kaplan and colleagues demonstrated that haematopoietic VEGFR1+ve bone marrow cells appear to home to bone marrow sites where they form clusters prior to the arrival of tumour cells [28, 42]. Recently it has also been shown that pancreatic ductal adenocarcinoma-derived exosomes are selectively uptaken by liver Kupfer cells, resulting in the establishment of a pro-inflammatory, metastasis-supporting environment [98].

However, besides these few studies there is minimal data demonstrating that systemic factors influence bone metastases, whether systemic factors released from DTCs are also released from distant (primary tumours) to influence the BME or which systemic

factors are necessary to create a favourable microenvironment for DTCs; critical questions raised in a recent review by Ubellacker and McAllister [100] .

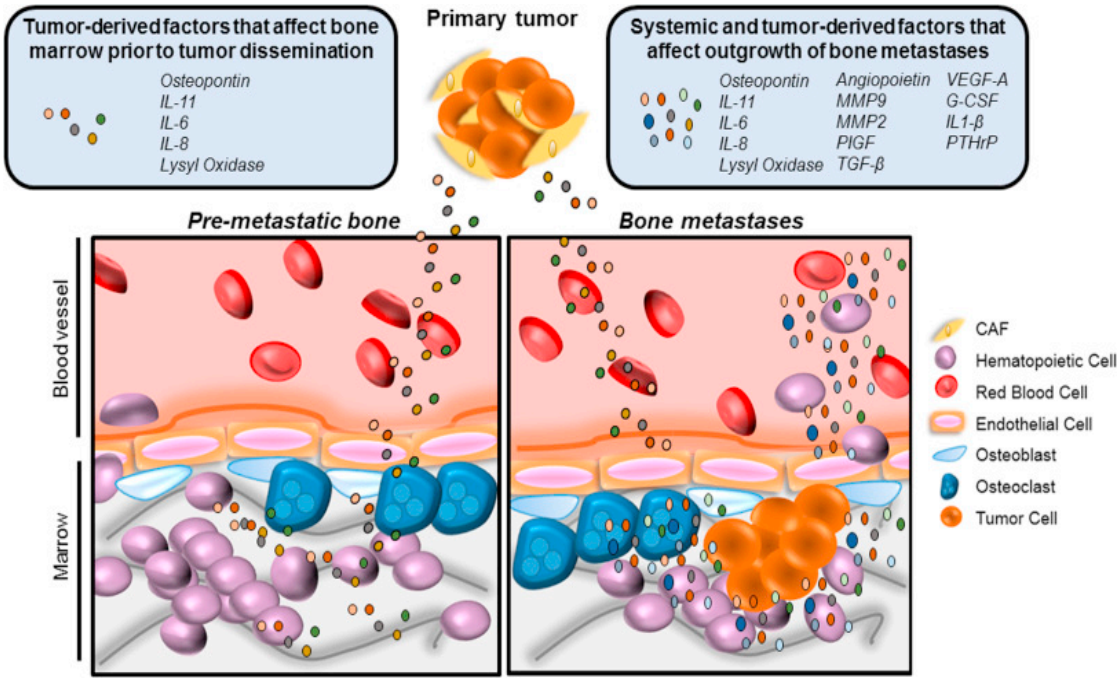


**Figure 5 The pre-metastatic niche and the role of systemic factors in bone metastases.**
Studies suggest that disease progression might be mediated through systemic factors, derived from both the BME and the TME. However these remain relatively unexplored. Reprinted from J.M. Ubellacker, S.S. McAllister, The unresolved role of systemic factors in bone metastasis, Journal of Bone Oncology © 2016 The Authors, Published by Elsevier GmbH, under Creative Commons Attribution-NonCommercial-No Derivatives License (CC BY NC ND), https://creativecommons.org/licenses/by-nc-nd/4.0/, doi:10.1016/j.jbo.2016.03.009.

### 1.4.3. The role of the BME in the early stages of breast cancer bone metastasis

Given that bone metastases are incurable once established in bone, increasing our knowledge about the mechanisms that direct tumour cells towards bone and subsequent bone marrow colonisation will facilitate the design of drugs that could specifically target these early steps of metastatic disease.

Colonising tumour cells will be exposed to a heterogeneous BME upon arrival, which could determine whether they will actively proliferate, stay quiescent/dormant or die. A recent review suggested that long-term dormancy might be supported when tumour cells face quiescent/static microenvironments (*e.g.* endosteal surfaces covered by bone lining cells, stable vasculature [101]), whereas active, dynamic microenvironments

including areas of osteoclastic bone resorption and sprouting vasculature [101] support active proliferation and/or reactivation of dormant tumour cells [83].

Bone is a major site of haematopoiesis thereby providing a reservoir of HSCs (HSC niche). BMDCs suggested to comprise the endosteal (osteoblasts, osteoclasts, adipocytes) and (peri-) vascular niche (vascular endothelial cells, pericytes) regulate self-renewal, differentiation and proliferation of HSCs [102-104] through production of cytokines and intracellular signals in addition to cell-to-cell contact (integrins, cadherins *etc.*) [102, 103, 105-107]. Tumour cells are capable of responding to these niche signals and various chemokines and their receptors have shown to be involved in directing cancer cells towards the metastasis niche, with the best studied being the CXCL12/CXCR4 axis. CXCL12 or stromal cell-derived factor-1 (SDF-1) is produced and secreted by bone marrow stromal cells, primarily the osteoblast, endothelial and epithelial cells [108]. Signalling takes place through its cognate receptor CXCR4, expressed on haematopoietic, stromal and endothelial cells; and in high levels on various cancer cell lines (prostate: PC3, C42B [95], breast: MDA-MB-231 [109]). Homing of HSCs to the marrow niche is partially regulated by CXCR4/CXCL12 chemotactic signalling [110], and there is evidence that tumour cell homing to bone is mediated similarly [95]. For example, Shiozawa and colleagues demonstrated that human prostate cancer cells compete with HSCs for niche localisation [95]. In support of this, CXCR4 overexpression in MDA-MB-231 cells increases bone metastasis [111]. Very recently, it has been demonstrated that the CXCR4-antagonist AMD3100 resulted in mobilisation of breast cancer cells from the bone marrow into the circulation in female SCID mice, and both newly and established metastases were anchored in the bone marrow by CXCR4/SDF-1 interactions [112]. Further niche signals are suggested to include OPN [27], vascular adhesion molecule-1 (VCAM-1), very late antigen-4 (VLA-4, α4β1 integrin), intercellular adhesion molecule-1 (ICAM-1) and N-cadherin [94, 96]. Whether homing/colonising tumour cells prefer HSCs and/or other progenitor niches has yet to be determined, as all are closely associated with each other being located adjacent to endosteal surfaces. The endosteal niche has recently risen in prominence and osteoblasts and osteoclasts are considered key cells in the early events of metastasis development [85, 90, 94]. Whether osteoblasts are indeed part of the metastasis niche is subject to debate [113], and is discussed in Chapter 3.

Based on the observation that adipokines, including leptin, mediate migration of MDA-MB-231-fLuc-EGFP breast cancer cells to human bone tissue fragments *in vitro* also highlighted the importance of adipocytes, one of the most abundant stromal components

in the BME, in breast cancer cell osteotropism and early colonisation [92]. Direct cell contact between adipocytes and cancer cells of the bone marrow compartment was observed when co-cultured with human bone fragments [92]. Another level of complexity is added given that the (peri)-vascular niches may also support DTCs to establishment in bone not only by providing oxygen and nutrients but also through endothelial-derived angiocrine stimulation [114]. It is also hypothesised that regulation of tumour cell dormancy in bone could partially be mediated through the (peri)-vascular niche [101]; which will be discussed in the following section.

#### 1.4.3.1. Tumour cell dormancy - microenvironmental control

The relapse of cancer patients with no clinical evidence of disease after their initial treatment is caused by DTCs that remain in a reversible, quiescent/dormant state upon dissemination to the secondary organ. Elimination of DTCs is currently not possible given the resistance of dormant tumour cells to conventional therapy [115], and the lack of insight into the mechanisms of this stage. Briefly three molecular mechanisms involved in tumour dormancy have been suggested. This includes cellular dormancy where cells arrest in G0-G1 phase of the cell cycle or angiogenic dormancy where tumour cells are unable to recruit new blood vessels required for the supply of oxygen and growth-supporting nutrients. By recognising foreign pathogens and transformed cells the body's immune system eliminates most cancer cells however a subset persists in immunological dormancy (immunosurveillance) [116]. Various microenvironmental-derived factors are suggested to be involved in tumour cell dormancy including thrombospondin [101], growth arrest specific protein 6 (GAS6) and its cognate receptor annexin II and AXL [96], as well as BMPs, wnt proteins and IL-6 [83, 91]. A recent review by Quayle and colleagues discusses molecular drivers in breast and prostate cancer cell dormancy in greater detail [117]. With the lack of suitable experimental *in vivo* models our understanding of tumour cell dormancy remains limited, especially with regards to mechanistic regulation.

Given the multi-step process of metastasis and that DTCs travel via haematogenous routes to the secondary organ, this raised the hypothesis that vascular endothelial cells and their surrounding basement membrane could be key regulators of tumour cell dormancy. Specific factors released by endothelial cells, so-called angiocrine factors, are thought to regulate tumour growth through the establishment of vascular niches. Angiocrine signals may include adhesion molecules including ICAM1, VCAM1, E- and P-selectin, chemokines such as ILs, monocyte chemotactic protein (MCP1), SDF1 and various growth factors including BMPs, TGF-β and VEGFA [94, 114]. Furthermore

angiocrine signals are suggested to be involved in recruitment of inflammatory cells, thus contributing to immune dormancy [114]. VCAM-1 for example is hypothesised to regulate activation of indolent/dormant micrometastases through the recruitment of integrin α4β1+ve osteoclast progenitors and promotion of osteclast activity, key for initiation of the vicious cycle [118]. Further studies in a mouse model showed that dormant (defined as Ki-67–ve) MDA-MB-231 and T4-2 breast cancer cells were observed residing directly on microvascular endothelium of lung and bone marrow, confirmed *in vitro* using organotypic microvasculature cultures. Here thrombospondin (TSP-1) was defined as an endothelial-derived tumour suppressor based on the finding that TSP-1 was reduced in the location of sprouting neovasculature, an area where tumour growth was accelerated. This was also due to the high presence of tumour-growth promoting factors such as TGF-β at sprouting vasculature. In contrast quiescent/dormant tumour clusters were often associated with stable vasculature (data from *in vitro* cultures and zebra fish models) [101]. In summary, in vascular niches dormancy is suggested to be induced/maintained through the balance of pro- (VEGF, PDGF, FGF and angiopoietin) and anti-angiogenic factors (TSP-1, angiostatin) [101, 119]. Given the dormancy-regulating role of TSP-1, other components of the BME, such as megakaryocytes and platelets may be key regulators of dormancy. Absence of TSP-1 from circulating platelets, the terminal differentiation state of megakaryocytes, has been shown to reduce the ability of platelets to inhibit tumour angiogenesis during the initial stages of tumour growth in a mouse model of lewis lung carcinoma [120].

With regards to immunological dormancy, dormant tumour cells (breast and lung) showing stem-like characteristics (*e.g.* $CD44^{high}/CD24^{low}$) were able to enter a slow-cycling state by autocrine overexpression of DKK1, thus silencing the wnt signalling pathway. In addition this slow-cycling state allowed the cells to significantly down-regulate cell surface natural killer-cell-activators, rendering them resistant to NK-cell-mediated elimination [91]. This suggests a potential mechanism by which quiescent/dormant cells are protected from immune surveillance. Depletion of NK-cells resulted in metastatic outgrowth, showing that these quiescent cells have the capacity to enter immune surveillance whilst maintaining the ability to re-initiate metastasis. The authors suggest that a decrease in NK cell cytotoxicity could be used as a marker for disease relapse in cancer patients [91].

Recent studies also showed that in model systems of multiple myeloma, tumour cells colonise endosteal, osteoblast-rich niches as early as 1-3 days post injection; a niche suggested to support tumour cell survival and dormancy [115]. Using the lipophilic membrane dye DiD, that is lost during active cell proliferation but retained in “dormant”

cells, allowed detection of dormant cells in *vivo*, with differential gene expression (*e.g.* VCAM-1, AXL) compared to proliferating ($DiD^{low/neg}$) populations. In agreement conditioned medium from osteoclastic cells stimulated myeloma cell proliferation *in vitro*. *In vivo* increased osteoclast activity reduced the presence of dormant myeloma cells in bone, suggesting re-activation of these cell populations based on osteoclast activity [115]. However, whether dormancy mechanisms observed in multiple myeloma, a haematological malignancy of the bone marrow, are relatable to solid breast or prostate bone metastasis, remains to be established.

### 1.4.4. Role of the BME during late(r) stages of bone metastasis

Once established in bone, tumour cells gradually take over control of the microenvironment, a process known as the vicious cycle [121]. Herein the finely tuned balance of bone remodelling is disturbed resulting in osteolytic, osteoblastic or mixed lesions; predominantly osteolytic in breast cancer.

By inducing increased RANKL expression on osteoblasts and stromal cells [122], breast cancer cells stimulate osteoclastogenesis and bone resorption. This is especially prominent in patients with severe osteolysis showing increased serum RANKL/OPG ratio when compared to healthy individuals [87]. In a murine model, PTHrP overexpressing MCF-7 breast cancer cells developed bone metastases earlier and to a greater extent when compared to parental cells, based on imbalanced RANKL/OPG ratio upon breast-cancer-cell-mediated PTHrP secretion [122]. Briefly, a variety of other osteolytic tumour derived factors including ILs, TNF-α, GM-CSF, MIP-1α, MCP-1 and VEGF [23, 123, 124] are present during metastatic tumour growth in bone; (reviewed in [125]), and alterations in bone remodelling induced for example by ovariectomy are known to accelerate tumour growth in pre-clinical models [126]. Additionally, breast cancer cells have been shown to secrete factors that affect osteoblast differentiation including for example DKK1 [127, 128]. Besides the cancer cell directly affecting osteoblasts and osteoclasts, the increased bone resorption in turn results in the release of growth factors from the bone matrix such as TGF-β, $Ca^{2+}$ and BMPs, that drive tumour growth. Thereby a “vicious cycle” between bone destruction and tumour growth is established [129, 130].

## 1.5. Targeting the BME in breast cancer bone metastasis – current standard of care

As discussed previously, homing of breast tumour cells to bone and establishment of osteolytic disease involves interaction with the BME, stimulating tumour growth

progression through the vicious cycle. Given the clinical features of bone metastases (in particular pain) treatment often involves anti-neoplastic therapy in addition to palliative regimens, with the latter including analgesics, radiotherapy and surgery to improve quality of life. Therefore agents that target the osteoclast-osteoblast crosstalk have been developed, leading to the clinical use of osteoclast-targeted agents including bisphosphonates and the RANKL inhibitor Denosumab, the current standard of care. In addition multiple novel anti-resorptive agents are under investigation including inhibitors for Cathepsin K (Odanacatib), Src (Dasatinib, Saracatinib), Activin A (Sotatercept) or mTOR (Everolimus). However, targeting osteoclasts is not sufficient to eliminate cancer growth in bone and anti-resorptive agents are thus commonly combined with other anti-cancer drugs including chemotherapy regimes [3, 131-135].

### 1.5.1. Bisphosphonates

The anti-resorptive bisphosphonates (BPs) are the standard of care for skeletal disorders that are characterised by excessive bone resorption including osteoporosis, Pagets disease as well as cancer-induced bone disease. BPs inhibit bone resorption by having high affinity for bone mineral where they are internalised by osteoclasts during active bone resorption and interfere with various biochemical processes that will be discussed below. The use of BPs, in particular Zoledronic acid (ZOL) will be addressed in greater detail here, as this agent was used in two of the Chapters presented in this thesis (see Chapter 3 + 5).

#### 1.5.1.1. Structure and mechanism of action

Their high affinity to bone is mediated via the P-C-P motif, usually enhanced by the presence of a hydroxyl group in the R1 side chain. The structure of the R2 side chain determines the anti-resorptive potency, marking the two classes of BPs: nitrogen (NBPs) and non-nitrogen containing BPs (NNBPs) – see Table 1.

**Table 1 Classification of bisphosphonates and their potency.**

| Classification | Structural feature of R2 side chain | Example | Increased potency → |
|---|---|---|---|
| Non-nitrogen containing | Absence of amino group | Clodronate (CLO)<br>Etidronate (ETI) | |
| Nitrogen containing | Presence of primary amino group | Pamidronate (PAM)<br>Alendronate (AL) | |
| Nitrogen containing | Presence of secondary or tertiary amino group | Ibandronate (IBAN)<br>Risedronate (RIS)<br>Zoledronate (ZOL) | |

Both classes of BPs induce apoptosis however, via different mechanisms. Briefly, NNBPs are metabolised into AppCp-type metabolites, cytotoxic analogues of ATP that accumulate in the cytoplasm and induce apoptosis by inhibiting the mitochondrial adenine nucleotide translocase (ANT)[136]**.** NBPs in contrast induce apoptosis via inhibiting farnesyl pyrophosphate synthase (FPP) a key enzyme of the mevalonate pathway. Inhibition of FPP results in reduced prenylation of small GTPases such as Ras, Rab, Rho and Rac resulting in loss of osteoclast function and consequently osteoclast apoptosis [137]. NBPs can also induce apoptosis via the production of ApppI (triphos- phoric acid 1-adenosin-50-yl ester 3-(3-methylbut-3-enyl) ester), an endogenous ATP analogue. Accumulation of isopentenyl pyrophosphate isomerase (IPP) results from the inhibition of FPP and is then converted into ApppI inducing osteoclast apoptosis via inhibiting ANT - Adenine nucleotide translocator, also known as the ADP/ATP translocator [138]. Given the importance of the mevalonate pathway and GTPases in cell physiology BPs can theoretically affect every cell type however, given their high affinity to bone, osteoclasts were identified as the main target of BPs.

#### 1.5.1.2. Anti-tumour effects of BPs

Extensive pre-clinical studies have reported anti-tumour effects of BPs, in addition to their bone-preserving activity, *in vitro* [139-142] and *in vivo* [143-146]. Initial studies investigated the use of BPs as single treatment in models of cancer-induced bone disease from prostate, breast and myeloma cells. In agreement reduced osteolysis was observed as a consequence of BP treatment (ZOL, IBAN, PAM, RIS, ETI). Data on BP effects on intra-osseous tumour burden were conflicting, with some reporting no effects or increased tumour burden. However, the majority of studies observed a reduction of tumour burden in bone, especially in breast cancer models (reviewed in detail in [147]).

The majority of studies concluded that anti-tumour effects of BPs are bone-mediated, predominantly via the inhibition of osteoclast-mediated bone resorption and disruption of the vicious cycle of bone metastasis; and no effects at peripheral sites being achieved unless high and/or repeated dosing is used. Studies comparing RIS with analgoues exhibiting a lower bone mineral affinity and a lower anti-resorptive activity [145, 148] revealed that anti-tumour effects were irrespective of the bone sparing activities, however the RIS-analogue with 300-fold lower anti-resorptive activity than the original compound did not reduce growth of B02 bone metastases. This suggests that anti-tumour effects of BPs are mainly mediated via their anti-resorptive activities. In contrast, data from

mice lacking functional osteoclasts showing reduced melanoma burden in bone upon ZOL (pre)-treatment support osteoclast independent anti-tumour effects of ZOL [143]. However, these studies did not determine effects of BPs on soft tissues, suggesting a microenvironmental-dependent anti-tumour effect. With regards to soft tissue tumour burden there are reports of both increased [149] and reduced tumour burden [150] upon BP treatment. It still remains unclear whether effects of BPs on cancer cells are direct or via indirect anti-tumour effects, yet it is likely that a combination of both mechanisms are involved in inhibition of bone metastases. This is supported by data from Gao *et al.*, showing reduced osseous tumour burden and decreased soft tissue burden [150], which suggests that BPs exert direct effects on cancer cells, but not necessarily independent of the BME.

Indeed, BPs including ZOL have been shown to inhibit proliferation, migration, adhesion and invasion *in vitro* [141, 142, 148]. However, most *in vitro* studies used high doses and/or prolonged exposure consequently resulting in drug levels that are not achievable *in vivo*. Evaluation of pharmacokinetics and dynamics of ZOL in patients with cancer and bone metastases showed anti-resorptive effects 24hrs after infusion that were maintained over 28 days, supporting the clinical schedule of 4mg infusions every 3-4 weeks [151]. Peak plasma concentrations of ZOL (1-2μM) decline rapidly to 1% after 24hrs, with a short serum half-life of about 1hr [151]. However the drug remains bound to bone for years, exerting prolonged effects after a single administration [152], suggesting that release of stored BPs from bone mineral during osteoclast mediated bone resorption (reaching peaks up to 1000μM in the resorption pits [153]) could expose DTCs to cytotoxic BP concentrations in bone. However exact molecular mechanisms remain to be established, with the major difficulty remaining to separate between direct effects on cancer cells and those that are mediated via alterations of the BME. In clinical practice the BP ZOL is given as a single, intravenous infusion every 3-4-weeks and given the high doses and frequent administrations in experimental studies, effects on cells other than the bone is highly unlikely in the clinical setting. For example, only weekly and daily administration, not a single dose, of ZOL did result in convincing anti-tumour effects in pre-clinical models [146, 154].

The effects of NPBs on FPP synthase suggests that these agents have potential to affect any cell type as long as sufficient amounts can be internalised. Various *in vitro* and *in vivo* studies have identified osteoclasts and macrophages as the key targets of NBPs, due to their high endocytic capacity [38, 148, 155-157]. However, emerging data are indicating

further cell types in bone as potential targets of BPs, including the osteoblast [158] or vascular endothelial cells [159] with potential consequences on both, primary and metastatic breast cancer growth. Bone is a highly vascularised organ [51, 160]; however, surprisingly few studies have established the effects of ZOL on (vascular) endothelial cells within the bone although anti-tumour effects of ZOL are suggested to be partially mediated via its anti-angiogenic properties. The data are mainly from *in vitro* experiments [161-163], with a notable lack of studies investigating the effects of BPs on vasculature *in vivo*. Reduced vessel thickness and increased vessel numbers after long-term ZOL-treatment (4 weeks) in mice [159], decreased levels of circulating endothelial progenitor cells ($CD34^+/133^-/VEGFR2^+$) in ZOL-treated patients suffering from osteonecrosis of the jaw [164], and reduced differentiation of MSCs into endothelial cells after BP treatment (*in vitro,* ZOL, AL [165]) suggest the ability of ZOL to affect the *in vivo* bone marrow vasculature. In agreement with this, cancer patients receiving BP treatment have decreased serum/plasma levels of VEGF, a potent angiogenic factor, as well as altered levels of γ-IFN, IL-6 and PDGF [166, 167]. Similar effects of ZOL on cytokine and chemokine levels have been observed in mice [37, 168]. Macrophages, especially TAMs, are considered potent targets of BP treatment [38, 155] and ZOL increases levels of apoptosis as well as accumulation of unprenylated Rap1A *in vitro* and *in vivo* [38, 155]. Recently it has also been demonstrated that ZOL impaired prostate cancer induced M2 macrophage polarisation and prevented M2-mediated fibroblast activation, resulting in reduced subcutaneous tumour growth and lung metastasis in a murine prostate cancer model [169]. A further potential target of BP treatment could include myeloid-derived suppressor cells (MDSCs), a cell type increased in the bone marrow, blood and spleen of patients with solid tumours [170]. Intra-tumoural depletion of $CD11b^+/Gr\text{-}1^+$ MDSCs, reduced infiltration of $CD\text{-}11b^+/Gr\text{-}1^+/F4/80^+$ cells into the tumour stroma and decreased presence of these cells in peripheral blood has been observed after ZOL treatment [37, 170, 171]. Whether this was due to direct effects of ZOL on MDSCs, or mediated via ZOLs' effects on bone remains unclear. Melani and colleagues for example suggest that reduced intra-tumoural presence of MDSCs could be mediated through impaired bone marrow mobilisation by ZOL-induced reduction of MMP-9, a factor required for MDSC function and mobilisation [37]. In addition, ZOL resulted in a reduction of the number of clonogenic colony-forming progenitor cells present in bone marrow [37]. Injection of fluorescently labelled BPs *in vivo* allowed identification of further cellular targets of these drugs. They found that CD14+ve bone marrow monocytes internalised fluorescently labelled RIS-analogues *in vivo* and caused an accumulation of unprenlyated Rap1a (24hrs-7days post single dose), suggesting

potential effects of BPs on bone marrow monocytes [172]. However, Wolf and colleagues did not observe increased rates of apoptosis or necrosis, nor effects on differentiation of CD14+ve monocytes from healthy individuals, when cultured under increasing concentrations of ZOL (24hr treatment with 0.1-10 μM)[173]. Additionally, effects of BPs including ZOL have been observed on γδ T cells, fibroblasts as well as HSCs [159, 162, 174]. For example, IBAN, PAM and ZOL reduced viability of fibroblasts *in vitro* [162], and repeated treatment with ZOL has shown to expand HSCs *in vivo* [159]. With regards to γδ T cells, BPs are known to promote Vg9Vd2Tcell chemotaxis and cytotoxicity *in vivo* [175].

To summarise, BPs have the potential to affect a wide variety of BMDCs, in addition to modifying levels of growth factors and cytokines involved in tumour growth, both within and outside bone [38, 155, 156, 163, 166, 174, 176]. Potential anti-cancer effects of BPs are illustrated in Figure 6; however as discussed previously novel cellular as well as systemic mediators of treatment response are emerging. The role of the BME in mediating peripheral, primary tumour (re)-growth in the presence and absence of BPs will be discussed in Chapter 5.

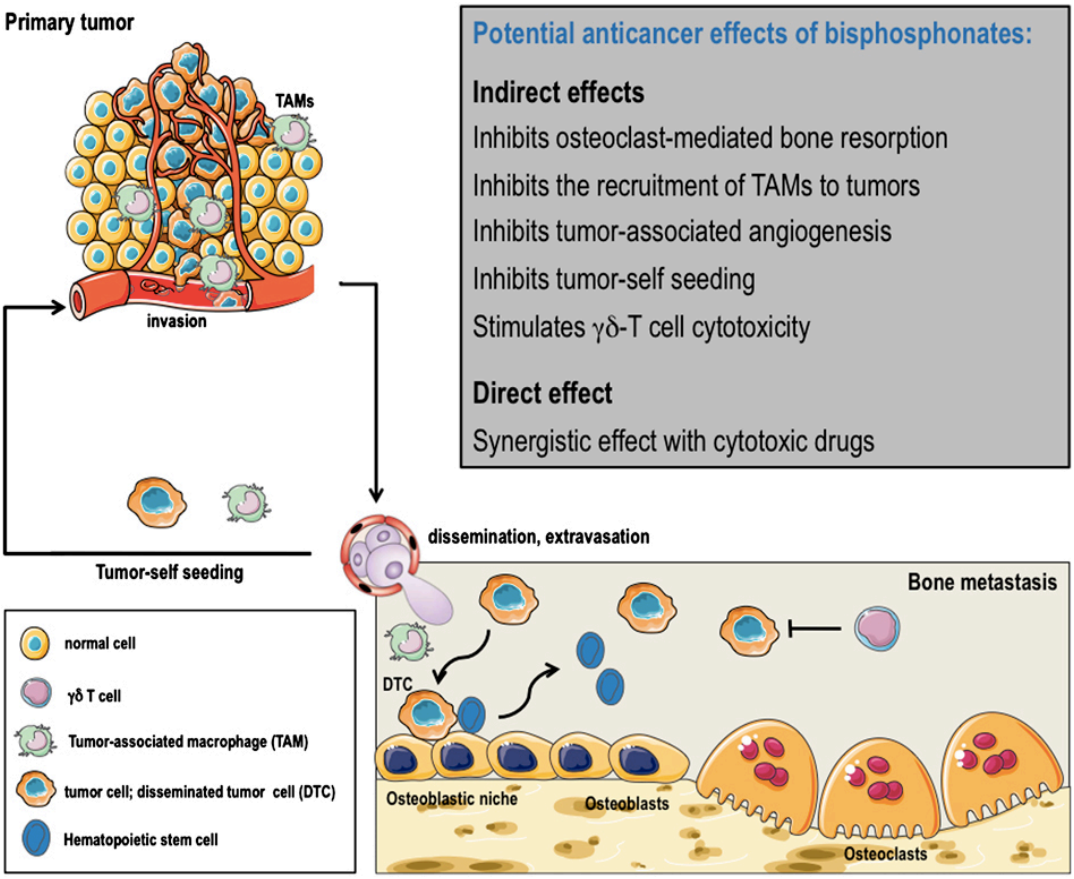


**Figure 6 Potential anticancer effects of bisphosphonates *in vivo*.**
Various *in vitro* and *in vivo* studies have identified osteoclasts and macrophages as the key targets of NBPs, due to their high endocytic capacity [38, 148, 155-157]. However, emerging data are indicating further cell types in bone as potential targets of BPs. Reprinted by permission from Macmillan Publishers Ltd: Bone Key Reports P. Clezardin, Mechanisms of action of bisphosphonates in oncology: a scientific concept evolving from antiresorptive to anticancer activities, BoneKEy Rep 2, Article number 267 (2013), Bone Key Reports, Copyright © 2013, Rights Managed by Nature Publishing Group". doi:10.1038/bonekey.2013.1

### 1.5.1.3. BPs in the clinical setting

The clinical benefits of BPs are well established in metastatic prostate and breast cancer as well as advanced multiple myeloma, with reduced skeletal morbidity and reduced risk of developing skeletal related events (SREs) including fractures, spinal cord compression and pain being reported [134, 177].

Initial clinical studies tested the efficacy of BPs in preventing breast cancer bone metastasis, reporting survival benefits including improved disease-free survival (DFS) and prolonged overall survival following clodronate treatment in patients with primary stage I-III breast cancer [178, 179]. This led to several subsequent clinical trials investigating the potential of combining adjuvant ZOL with endocrine therapy, aromatase inhibitors and chemotherapy in breast cancer patients [132, 133, 135, 180, 181]; including the ZO-FAST, AZURE, ANZAC and ABSCSG-12 trials. Detailed trial informations are listed in Table 2.

Briefly, the ZO-FAST study in postmenopausal women with hormone receptor-positive early breast cancer receiving adjuvant letrozole +/- ZOL, reported benefits in disease free survival in the ZOL cohort [135, 181], with similar results being observed in the Austrian Breast and Colorectal Cancer Study Group trial-12 (ABCSG-12) [180]. In contrast, the adjuvant use of ZOL in addition to standard therapy in the AZURE trial did not show a difference in DFS in the overall study population. However, sub-group analysis showed substantial benefits for postmenopausal women [133]. Following the completion of several clinical trials with differential inclusion/exclusion criteria, study populations, trial designs and conflicting results, **menopausal status has emerged as the benefit-limiting factor of adjuvant ZOL** [133, 180]. This became evident with the meta-analysis from the Early Breast Cancer Trials Collaborative Group (EBCTCG), summarising that for the entire population (18766 women involved in 26 randomised trials) BPs had little effect on clinical outcomes for the overall population (post- and premenopausal) [182]. Benefits were often only borderline significant, whereas prolonged time till first distant recurrence in bone, overall breast cancer recurrence, distant recurrence at any site and breast cancer mortality were improved in postmenopausal women receiving ZOL. It is therefore concluded that adjuvant ZOL is beneficial for postmenopausal women only [182]. In agreement with this subgroup analysis the importance of ZOLs impact on the BME depending on menopausal status has also been demonstrated in experimental studies *in vivo* [183].

**Table 2 Clinical trials of adding ZOL in the adjuvant setting.**
DFS = disease-free survival, IDFS = invasive DFS, ZOL = Zoledronic acid

| Study | Patients | Outcome | Ref. |
|---|---|---|---|
| ZOL in the adjuvant setting | | | |
| **Adjuvant Zoledronic Acid to Reduce Recurrence (AZURE trial)** Open-label, international, multicentre, randomised, controlled, parallel-group phase 3 trial 59/84 months follow up | • 3360 patients, female >18 years<br>• Stage II or III breast cancer<br>• Standard adjuvant systemic treatment alone (control group) or with 4 mg ZOL | **Overall population**<br>• No difference DFS, IDFS overall survival and distant recurrence<br>• ZOL reduced the development of bone metastases<br>• ZOL protected against fractures<br>**Patients >5 years post menopause**<br>• Improved IDFS<br>• Reduction in risk of extraskeletal recurrence | [132, 133] |
| **Austrian Breast and Colorectal Cancer Study Group trial-12 (ABCSG-12)** Randomised, controlled, open-label, two-by-two factorial, multicentre trial 62/94.4 months follow-up | • 1803 patients, female<br>• Premenopausal<br>• Endocrine-receptor-positive early-stage (stage I-II) breast cancer receiving goserelin (to induce menopause), anastrozole or tamoxifen with or without ZOL (4mg) | • ZOL improved DFS<br>• ZOL reduced the relative risk of DFS events (disease recurrence or death)<br>• No effect on risk of death | [180, 184] |
| **Zoledronic acid (zoledronate) for postmenopausal women with early breast cancer receiving adjuvant letrozole (ZO-FAST study)** Open-label, multicentre, randomised study | • 1065 patients, female<br>• Postmenopausal<br>• Oestrogen- and/or progesterone-receptor-positive [ER+/PR+] stage I, II, or IIIA early breast cancer<br>• Adjuvant letrozole with immediate ZOL or delayed (fractures, low T-score) | **Immediate ZOL vs. delayed ZOL**<br>• Immediate ZOL improved lumbar spine and hip bone mineral density<br>• Reduced DFS events (disease recurrence or death) vs. delayed ZOL<br>• Reduced local and distant disease recurrences vs. delayed ZOL<br>• Bone metastases were more common in the delayed ZOL group<br>• Improved DFS vs no ZOL treatment | [135] |

Several studies using BPs in the adjuvant setting have also been performed in prostate cancer and multiple myeloma, summarised in [177]. Briefly, in men with locally advanced prostate cancer addition of ZOL to radiotherapy and androgen suppression (RADAR trial) decreased prostate-specific antigen (PSA) progression and reduced the need

for secondary therapeutic intervention, but this was limited to patients with a Gleason score of 8–10 (histopathological grading system, 8-10=cells are poorly differentiated) [185]. In the ZEUS study, standard prostate cancer therapy +/- ZOL in high risk localised prostate cancer patients, addition of ZOL was not effective in preventing bone metastases [186]. A recent meta-analysis compared several randomised controlled trials assessing the use of standard of care +/- docetaxel or BPs for men with high-risk localised or metastatic hormone-sensitive prostate cancer. Here no evidence of improved survival was reported when BPs were added to standard care in patients with locally advanced disease [187]. In multiple myeloma, clodronate increased overall survival in patients without vertebral fracture at study entry when compared to placebo [188]. In a separate trial ZOL improved progression-free and overall survival and reduced SREs when compared with clodronate [189, 190]. In summary, besides reducing SREs, myeloma and prostate cancer patients did not benefit from prolonged survival when BPs were administered in the adjuvant setting.

Whereas BPs have been extensively explored in the adjuvant setting, little is known about their role in neoadjuvant therapy, given before surgical removal of the primary tumour. Recently, addition of ZOL to neoadjuvant chemotherapy in breast cancer has also been explored, showing conflicting results, but again with some benefits mainly for postmenopausal women (see Table 3, further discussed in Chapter 5) [191-193].

In summary, in breast cancer survival benefits from ZOL depend on menopausal status. If this is adopted into clinical practice as adjuvant therapy, this could save several lives per year in the UK alone, given that between 2011 and 2013 each year almost half (48%) of patients diagnosed with *in situ* breast cancer in the UK were over the age of 60 [194].

**Table 3 Clinical trials of adding ZOL in the neoadjuvant setting.**
DFS = disease-free survival, IDFS = invasive DFS, ZOL = Zoledronic acid, pCRb = pathological complete response in the breast, pCR = pathological complete response in the breast and lymph nodes, RITS = Residual Invasive Tumour Size

| Study | Patients | Outcome | Ref. |
|---|---|---|---|
| **ZOL in the neoadjuvant setting** | | | |
| **Addition of zoledronic acid to neoadjuvant chemotherapy does not enhance tumor response in patients with HER2-negative stage II/III breast cancer (NEOZOTAC trial)** National, multicenter, randomized study | • 250 patients, female >18 years<br>• Stage II/III, HER2-negative breast cancer<br>TAC (docetaxel, adriamycin and cyclophosphamide) chemotherapy +/- ZOL (4 mg within 24hrs after chemotherapy) followed by granulocyte colony-stimulating factor on day 2 | **Overall population**<br>• No difference in pCR in breast<br>• No improved objective response rates - no significant difference in decrease of the sum of diameters of tumor lesions (MRI)<br>**Postmenopausal**<br>• Numerical benefit in favor of treatment with ZOL, but did not reach statistical significance<br>• No improved objective response rates (MRI) | [195] |
| **Evaluation of Chemotherapy Prior to Surgery With or Without Zometa for Women with Locally Advancer Breast Cancer** Open label, Phase 2 randomized trial | • 120 patients, female<br>• Post and premenopausal<br>• Clinical stage II–III newly diagnosed breast cancer<br>4mg ZOL or no ZOL concomitant with neoadjuvant epirubicin plus docetaxel | • ZOL reduced presence of disseminated tumour cells in bone marrow at 3 months follow up<br>• ZOL increased bone mineral density<br>• No difference in DFS at 12 and 24 months | [191] |
| **Neoadjuvant arm of the AZURE trial** | • 205 patients, female<br>• Neoadjuvant chemotherapy (anthracyclin or taxane) +/- ZOL (4mg) | • ZOL reduced RITS<br>• No difference in axillary nodal involvement<br>• ZOL nearly doubled pCR (6.9% vs. 11.7%) | [192] |
| **A meta-analysis - Effects of neoadjuvant chemotherapy with or without zoledronic acid on pathological response** | Individual patient data from four prospective randomised clinical trials neoadjuvant chemotherapy +/- ZOL; data from 750 patients pooled | **Total study population**<br>• ZOL did not affect pCRb and pCR<br>• No benefits in pre/perimenopausal women<br>**Postmenopausal women**<br>• ZOL increased pCRb (significant) and pCR (7.8% vs.14.6%, p=0.076) | [193] |
| **AdditioN of Zoledronic Acid to Chemotherapy (ANZAC)** | • 40 patients female<br>• invasive breast cancer<br>• >18 years<br>• no evidence of metastatic disease<br>neoadjuvant chemotherapy (fluorouracil, epirubicin, cyclophosphamide every 3 weeks +/- 4mg ZOL, followed by 3 cycles of docetaxel | • no evidence of a direct antitumor effect<br>• addition of ZOL to chemotherapy in postmenopausal women decreases serum levels of the activin inhibitor, follistatin | [196] |

### 1.5.2. Denosumab

RANKL plays a key role in bone remodelling and a further osteoclast-targeted agent currently used for the treatment of cancer-induced bone disease is Denosumab (XGEVA®), a fully human monoclonal IgG2 antibody against RANKL, paralleling the role of OPG. By inhibiting RANK/RANKL signalling, Denosumab can inhibit survival, formation and activation of osteoclasts resulting in decreased bone resorption [197].

Initial studies in a mouse model of breast cancer, MDA-MB-231 breast cancer cells injected intracardially into athymic BALB/c-nu/nu mice, showed that recombinant OPG (25mg/kg, 3x weekly for 4 weeks) prevented osteolytic lesions, decreased number and size of skeletal tumour nests per mouse, consequently resulting in an 80% decrease in total skeletal tumour burden when compared to vehicle control [198]. In a separate study the potency of RANKL–inhibition with OPG to that of BPs in murine models of osteoclast-mediated hypercalcemia using C-26 colon adenocarcinoma cells was compared. OPG (0.2-5mg/kg) suppressed hypercalcemia at longer and faster rates than the BP ZOL in the C-26 tumour model (OPG: 25-96hrs vs. ZOL: 48-96hrs) [199]. In agreement with this a dose-dependent, inhibitory effect on osteoclasts in femurs of rB6CSFe-da-CsfnP$^{(op/op)}$ mice, accompanied by remarked reduction in tumour size of 2472 murine sarcoma cells in bone was observed after OPG treatment (0.1, 0.5, or 5.0 mg/kg, daily) when compared to the vehicle treated cohort [200].

The anti-resorptive properties of Denosumab have been reported in clinical trials of bone metastasis and Denosumab is approved at a dose of 120mg subcutaneously every 3-4 weeks for the prevention of SREs in patients with bone metastases from solid tumours. Denosumab appeared to be superior when compared to ZOL in preventing SREs [201, 202], representing a novel alternative treatment option. However, overal survival, disease progression, and rates of adverse events (AEs) and serious AEs were similar between the ZOL and Denosumab group [201].

With regards to using Denosumab in the adjuvant setting, the Austrian Breast and Colorectal Cancer Study Group Trial-18 compared Denosumab vs. placebo in postmenopausal women receiving adjuvant aromatase inhibitors. Compared with the placebo group, patients receiving Denosumab had a significantly delayed time to first clinical fracture, indicating that adjuvant denosumab significantly reduces aromatase inhibitor-induced fractures in postmenopausal patients with breast cancer [203]. Another

exciting study in patients with high-risk early breast cancer is currently on-going aiming to establish if denosumab prevents disease recurrence and prevents survival benefits (ClinicalTrials.gov Identifier: NCT01077154). The pharmacokinetic and dynamic properties of Denosumab are quite different when compared to BPs, and inhibition of osteoclast resorption by Denosumab is reversible when treatment is terminated, whereas BPs remain stored in bone and might still be active for suppression of bone remodelling.

### 1.6. Further approaches to target the TME/BME in breast cancer bone metastasis

Vascularisation is a key requirement for tumour growth and is regulated by pro- and anti-angiogenic factors produced by both tumour cells as well as stromal cells. Key regulating factors include vascular-endothelial growth factor (VEGF), platelet-derived growth factor (PDGF), epidermal growth factor (EGF) and fibroblast growth factor (FGF), with their corresponding receptors. The VEGFR tyrosine kinase receptor family – VEGFR-1, -2, and -3 – mediate angiogenesis and lymphangiogenesis by activating signalling cascades in endothelial cells. VEGFR-2 is considered to be the most prominent signalling receptor in tumour angiogenesis and formation of new blood vessels is required for tumours to progress and metastasise as they supply oxygen, nutrients and the "route" to secondary organs [25].

The concept of targeting angiogenesis in cancer therapy was initially proposed by Folkman [6, 7, 25]. One of the first agents showing proof-of principle that targeting the microenvironment in addition to cancer cells is effective was bevacizumab, a recombinant humanised VEGF-neutralising monoclonal antibody (mAb). Pre-clinical models using the murine bevacizumab-equivalent A4.6.1 showed reduced tumour growth of multiple human cancer cell lines in mice in addition to inhibition of metastasis development; with additive and synergistic effects when combined with chemotherapy or radiotherapy (reviewed in [204]). In clinical practice combining bevacizumab with capecitabine was generally well tolerated and increased response rates in patients with metastatic breast cancer previously treated with an anthracycline and a taxane. However, this did not translate into survival benefits [205]. Combination of bevacizumab with sorafenib (a tyrosine kinase inhibitor of PDGFR and VEGFR) in patients with confirmed adenocarcinoma of the breast with evidence of metastatic disease did not increase survival, with minimal effects on the previously treated metastatic disease and resulted in substantial toxicity [206]. Effects of bevacizumab in the metastatic setting are modest. Studies have revealed life-threatening side effects when using angiogenesis inhibitors in general leading to complications in physiological processes including wound healing, kidney and heart function as well as

reproduction, and/or other fatal adverse events including gastrointestinal tract perforation, neutropenia or haemorrhage. Further FDA approved anti-angiogenic compounds include sorafenib (targets RAF/MEK/ERK pathway and tyrosine kinases VEGFR/PDGFR) and sunitinib (VEGFR-1, VEGFR-2, fetal liver tyrosine kinase receptor 3 (FLT3), KIT (stem-cell factor receptor), PDGFRα and β). Although early clinical benefits have been documented in the treatment of many cancer types, the effects of VEGF-targeted therapies are not long lasting. This shows that cancers have the ability to develop resistance against VEGF therapy, but the detailed mechanisms behind this remain unclear [207]. In addition, very little is known about the effects of anti-angiogenic agents on the BME as these drugs were mainly designed to target the tumour vasculature.

Given the concerning safety profile of anti-angiogenic agents and minimal effects on prolonged survival, these agents are not routinely used in the treatment of metastatic breast cancer.

### 1.6.1. Targeting the VEGF/HGF axis in breast cancer (bone metastasis) with Cabozantinib

Over recent years tyrosine kinase inhibitors (TKIs) have emerged as novel cancer-microenvironment targeting agents, as they showed to have effects on cells of the osteoclast and/or osteoblast lineage [208]. This is likely to arise from the target receptors being expressed on both cancer as well as bone cells [208-215].

Receptor Tyrosine Kinases (RTKs) consist of an extra-cellular N-terminal domain, a transmembrane part and a C-terminal intra-cellular domain with tyrosine kinase activity; and are the second largest class of cell-surface receptors. There is an ATP binding cleft between the N- and C-termial lobes [216, 217]. Ligand binding causes dimerization of the receptor followed by stimulation of the intrinsic protein tyrosine kinase activity, subsequently resulting in signal-transduction cascades leading to alterations in cell physiology and/or gene expression. Tyrosine kinases are enzymes that transfer donor molecules to substrates, resulting in protein phosphorylation (*e.g.* ADP-ATP).

Tyrosine kinases can be inhibited either by direct binding to the receptor ligand and competing with ligand binding, both of which occur extracellularly. Further approaches include inhibiting the kinase activity thus inhibiting phosphorylation of the receptor and subsequent downstream signalling, such as the RAS-MAPK and PI3K-AKT pathways, NF-κB and Wnt/GSK-3β/ β-Catenin. Cabozantinib (XL184, Exelixis, San Francisco, herein referred to as CBZ), is a potent inhibitor of VEGFR2 and MET (the receptor for HGF) and has also

shown activity against various other kinases associated with tumour pathobiology including KIT, RET, AXL, TIE2, and Fms-like tyrosine kinase 3 [218]. The mechanism of action of CBZ is illustrated in Figure 7 below.

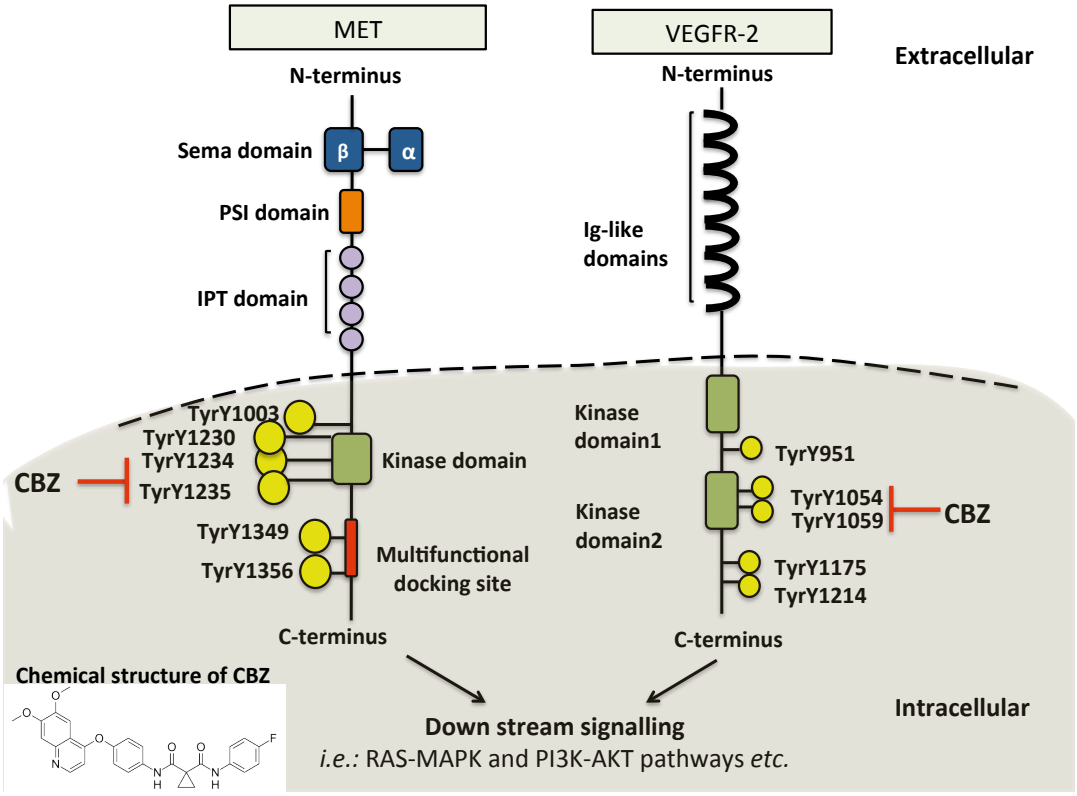


**Figure 7 MET and VEGFR2, tyrosine kinase receptors targeted by Cabozantinib.**
Extracellular MET is composed of three domains including a semaphorin (Sema) domain, a PSI domain (present in plexins, semaphorins and integrins) and 4 IPT (immunoglobulin-plexin-transcription) domains. Tyrosine kinase activity is intracellular. Tyrosine kinase (Tyr) Y1234/5 positively regulate enzyme activity, in contrast to TyrY1003. Signal transducers and adaptors are recruited to the docking site upon receptor activation [219]. The extracellular domain of VEGFR-2 includes 7 Ig-like domains, intracellular 2 tyrosine kinase domains with autophosphorylation sites are present (TyrY1054/59 are required for maximum kinase activity)[220]. Cabozantinib (CBZ), the small molecule multiple tyrosine kinase inhibitor targets MET and VEGFR-2.

Although our understanding of the mechanisms of tumour cell resistance to anti-VEGF therapy remains limited, one potential mechanism might include the induction of hypoxia due to inhibition of the VEGF pathway, consequently resulting in up-regulation of MET expression [221]. HGF is the only known ligand for the receptor tyrosine kinase MET. MET/HGF signalling is instrumental in embryogenesis, cell proliferation, motility and survival in addition to angiogenesis and wound healing [222-225]. High levels of MET in

cancer are associated with poor prognosis and are known to promote tumour invasion, metastasis, growth and survival [226]. Simultaneously targeting the VEGFR/MET axis with the small molecule tyrosine kinase inhibitor CBZ therefore appears a promising therapeutic approach. As a competitive ATP inhibitor [218, 227] CBZ crosses the cell membrane, mimics ATP binding and thereby inhibits phosphorylation and subsequent downstream signalling of the target receptors [218]. Studies by Yakes and colleagues demonstrated high affinity, but reversible binding for MET and VEGFR-2 [218] and metabolism occurs in the liver via CYP3A4 and CYP2C9. Peak plasma concentrations of CBZ have been found 2-5 hours post administration and the predicted effective half-life is 55 hours. CBZ is therefore administered daily [228].

CBZ has been approved for the treatment of metastatic medullary thyroid cancer (MTC) by the US Food and Drug Administration in November 2012. In a double-blind, phase III trial comparing CBZ with placebo in patients with metastatic MTC, CBZ prolonged progression free survival (11.2 vs. 4 months) when compared to placebo [229]. Various studies have investigated the effects of CBZ on tumour cells *in vitro,* reporting reduced viability, proliferation, migration and invasion of breast, lung, prostate and gastric cancer cells [218, 230]. The majority of pre-clinical studies have been performed in prostate cancer models of bone metastasis showing reduced tumour growth, not only in bone but also of subcutaneously transplanted tumours [230-233]. Besides these promising results there are limited numbers of studies using models of breast cancer to my knowledge [218], which are discussed in Chapter 4. However, there is a rational for studies in breast-cancer bone metastasis models given that in addition to RANK/RANKL signalling [69] the MET and VEGF signalling pathways regulate the tightly balanced coupling between osteoblasts and osteoclasts as both cell types express target receptors [209-212]; and that breast cancer cells express MET receptor, which is correlated with poor prognosis and increased aggressiveness [226].

CBZ has demonstrated promising results in a phase II randomised discontinuation trial with castration-resistant prostate cancer (CRPC) patients including improvements in bone scans in 68% of patients, with 12% showing complete response. This correlated with partial response of tumour lesions and pain relief. Soft tissue lesions decreased in 72% of evaluable patients and progression-free survival after in the CBZ cohort was 23.9 vs. 5.9 weeks in the placebo group. This study also reports a reduction in serum total alkaline phosphatase and plasma cross-linked C-terminal telopeptide I collagen [234]. Another trial in patients with CRPC who received chemotherapy prior to CBZ reported similar results

[235]. Given the rapid and complete resolution of disease in bone scans, a phenomenon hardly ever observed among therapies with proven survival benefits, raises the possibility that CBZ might interfere with imaging of radionuclides during bone remodelling. A study tested this hypothesis by surgically inducing bone remodelling in naïve mice and performed $^{18}$F–sodium fluoride ($^{18}$F-NaF) positron emission tomographic (PET) and technetium 99m–methylene diphosphonate ($^{99m}$Tc-MDP) single-photon emission computed tomographic (SPECT) scans before and after CBZ or related inhibitor administration (axitinib for VEGFR, crizotinib for MET, single or combined treatment). A remarked reduction in radiotracer uptake in the CBZ treated group was observed when compared to the control group, whereas this was not observed by inhibiting the VEGFR/MET signalling axis with axitinib or crizotinib. These studies therefore provide the first evidence that bone scan resolution after CBZ treatment could be a tumour-independent effect, raising the need to carefully interpret the peviously described results [236]. Nevertheless in all these studies CBZ was associated with reduced pain [237]. However, due to the results of the COMET-1 trial - a Phase III, randomized trial comparing treatment with CBZ to treatment with prednisone among men who had already progressed after earlier treatment on standard of care therapy – failed to meet the primary end point of extending overall survival in men with metastatic castration resistant prostate cancer (CBZ arm: 11.0 vs. Prednisone arm: 9.8months), **ClinicalTrials.gov Identifier:** NCT01605227.

This trial failure explains the limited clinical studies of CBZ in breast cancer bone metastasis however, Cabozantinib (60mg daily) mono-therapy has recently also shown evidence of antitumor activity in a phase II study of CBZ in metastatic triple-negative breast cancer patients [238] (**Clinical trial information:** NCT02260531). Further studies for the use of CBZ in advanced breast cancer are recruiting. This includes "A Phase II Trial of Cabozantinib in Women With Metastatic Hormone-Receptor-Positive Breast Cancer With Involvement of Bone" (ClinicalTrials.gov Identifier: NCT01441947) and "A Phase II Study of Cabozantinib Alone or in Combination With Trastuzumab in Breast Cancer Patients With Brain Metastases" (**ClinicalTrials.gov Identifier:** NCT02260531).

Recent news from the METEOR trial [239] shows significant benefits in overall survival and progression-free survival in patients with advanced renal cell carcinoma (http://www.exelixis.com/investors-media/press-releases). Patients with bone metastasis at baseline showed median overall survival of 20.1 months (CBZ) versus 12.1 months (everolimus); **ClinicalTrials.gov Identifier:** NCT01865747. In addition CBZ has now been

FDA-approved for the treatment of patients with advanced renal cell carcinoma (RCC) who have received prior anti-angiogenic therapy [240].

In summary, CBZ is showing promise against various types of advanced cancer in clinical trials, with potential to explore this agent further in patients with breast cancer bone metastasis.

### 1.7. Summary, conclusion and outstanding questions

In summary, the TME is increasingly recognised as a key component of tumourigenesis and response to therapy. Breast cancer preferentially metastasizes to bone, hence indicating the potential for therapeutic modification of the BME.

To date very little is known on how the BME responds to anti-cancer therapy, which is detrimental to treatment success or failure. A better understanding of how novel and existing anti-cancer agents mediate their effects is therefore crucial to improve treatment regimens and to elucidate how this affects the interactions between tumours and their microenvironment. Detailed characterisation of the response of the naïve BME is needed to elucidate if therapeutic agents exert their anti-cancer activity via direct, indirect, or dual mechanisms.

Dissemination of tumour cells appears to occur early on in the disease and in about 30% of patients with early-stage breast cancer, presence of micro-metastases in the bone marrow at the time of diagnosis has been reported [97]. Once progressing in bone the disease is considered incurable, though patients, with metastasis found in bone only, may live for several years as long as the cancer-induced bone disease is controlled. To effectively treat and/or prevent the breast cancer bone metastasis, a deeper understanding of how breast cancer cells establish themselves in bone is needed and it is of great clinical relevance to characterise the early steps of the disease, including the homing of tumour cells to bone. The bone metastasis niche is suggested to regulate tumour cell homing, survival and progression in bone [31, 42, 92, 94, 101, 105, 112]. However, outstanding questions remain concerning the precise cellular composition of the niche, the role of the osteoblasts during the early stages of bone metastasis [94, 113], how niche components interact [51] as well as how it is modified during treatment.

Recent clinical data have shown the efficacy of BPs in the adjuvant setting [131, 132, 135, 182]. This will result in increasing use in patients without evidence of bone metastasis. Given that the microenvironment of primary breast tumours is partially composed of BMDCs, a key role of the BME in mediating peripheral breast cancer (re)-

growth is expected. BMDCs, as well as their precursors, may be affected by anti-cancer treatment and thereby directly or indirectly contribute to therapeutic response on peripheral tumour growth. To date it remains unclear how therapeutic modulation of the BME affects peripheral tumour (re)-growth.

### 1.8. Hypothesis, aims and objectives

Work presented in this thesis aims to establish the role of the tumour microenvironment (TME) in breast cancer using a variety of *in vivo* models. To address these aims, the following hypothesis will be tested:

***The bone microenvironment (BME) mediates response to anti-cancer therapy in breast cancer.***

#### 1.8.1. Aims and objectives

To test the above hypothesis this thesis aims to address the following:

- **Aim 1: Establish the response of the BME to anti-cancer therapy *in vivo.***
    - Determine the early effects of a single, clinically relevant, dose of the anti-resorptive agent Zoledronic acid (ZOL) on key bone cells.
    - Characterise the effects of short-term administration of Cabozantinib, a tyrosine kinase inhibitor of MET and VEGFR-2, on the naïve BME.
    - Determine if the bone metastasis niche is affected by ZOL treatment and potential consequences on tumour cell homing to bone.

- **Aim 2: Determine the role of the BME in peripheral breast cancer (re)-growth.**
    - Establish a tumour re-implantation model to study the role of the BME in primary breast cancer re-growth.
    - Assess whether reduced tumour growth after combination therapy is altered when tumours are transplanted into animals with a modified BME.

# Chapter 2 – Materials and Methods

## 2.1. List of Materials and Equipment

### 2.1.1. Laboratory reagents and Kits

| Reagent or Kit | Supplier |
|---|---|
| 10X Casein | Vector Laboratories, SP-5020 |
| 1mg/mL Geneticin 10131 | Gibco, Life technology |
| 30% Hydrogen Peroxide | VWR Chemicals Prod23622.296 |
| 30% Hydrogenperoxide | VWR Chemicals, 23622.298 |
| ABC | Vectastain, PK-6100 |
| Acetic acid | AnalaR VWR, 100001 CU |
| Alizarin Red S | SIGMA, A5533 |
| Cabozantinib, XL184 | Exelixis, South San Francisco, CA |
| Calcein | SIGMA, C0875 |
| Chloroform | Sigma-Aldrich, C2432 |
| Citric Acid | AnalarR, Prod.100813M |
| Citric acid | AnalaR, 100813M |
| Copper(II)sulfate, 0.1mol/l | Fulka Analytical, 35185 |
| DAB | Vector Laboratories, SK-4100 |
| Dako Target Retrieval Solution | Dako, S1699 |
| Dimethylformamide | Fisher Chemicals |
| DMEM culture medium | Gibco 61965-026 |
| Doxorubicin hydrochloride | 2mg/mL, PL20075/0109, PA1390/022/001 |
| DPX mountant | VWR, 360294H |
| EDTA | SIGMA, 03620 |
| Eosin | Atom Scientific LTD, RRSP35-A |
| Ethanol | Fisher Scientific, E/0665DF/17 |
| Ethanol | Sigma-Aldrich, 24103-1L-R |
| Fast green FCF | Sigma-Aldrich, 44715 |
| Gelatine | SIGMA, G1890 |
| Gill's haematoxylin solution modified according to Gill II | Merck, HX249494 |
| High Capacity RNA-to-cDNA™ Kit | Applied Biosystems® Cat.No.: 4387406 |
| Hydrochloric acid (HCl) | AnalaR VWR, 10125 |
| Luciferin | Perkin Elmer |
| Methanol | AnalaR NORMAPUR, Prod.20847.307 |
| MouseTRAP™ Assay | Immunodiagnostic systems, SB-TR103 |
| Naphthol AS-BI phosphate (sodium salt) | SIGMA, N-2125 |
| Normal Goat Serum | Vector Laboratories, S-1000 |
| O.C.T. compound, mounting media for cryotomy | VWR, 361603E |
| Pararosaline | SIGMA, P-3750 |
| PBS for *in vivo* studies | Gibco by Life Technologies, pH7.4, 100-10-015 |
| Paraformaldehyde PFA | SIGMA, P6148 |
| Phosphate Buffered Saline Tablets | Oxoid, BR0014G |
| Pierce BCA Protein Assay Reagent A | Thermo Scientific, 23223 |

| | |
|---|---|
| Proto Gel Acrylamide | Geneflow, A2-0072 |
| Proto Gel Resolving Buffer | Geneflow, B9-0012 |
| Proto Gel Stacking buffer | Geneflow, B9-0014 |
| PVP | Sigma-Aldrich, PVP40 |
| Rat/Mouse PINP EIA | Immunodiagnostic systems, AC-33F1 |
| RBC lysis buffer | eBioscience |
| RNA Clean & Concentrator Kit | Zymo Research (ZEC174900) |
| RNAlater Tissue Collection Solution | Ambion, Life Science Technologies, AM7021 |
| RPMI culture medium | Gibco 61870-10 |
| Safranin O Solution | SIGMA, HT90432 |
| Safranin O Solution | Sigma-Aldrich, S2255 |
| Sodium acetate trihydrate | SIGMA, S-9513 |
| Sodium Bicarbonate (NaHCO3) | SIGMA, S5761 |
| Sodium Hydroxide pellets (NaOH) | Fisher Scientific, 5/4920/53 |
| Sodium tartrate (dihydrate) | SIGMA, S-4797 |
| Taab Medium Grade LR White Resin | Taab Laboratory Equipment Ltd, L012 |
| Toluidine Blue O | SIGMA, T0394 |
| TRI Reagent | SIGMA, T9424 |
| Triton-X 100 | Sigma-Aldrich, X100-500ML |
| Tween 20 | Fisher, T14206160 |
| Tween 20R | Fisher Chemical, T/4206/60 |
| VECTASHIELD® Mounting Media with DAPI | Vector Laboratories, H1200 |
| Vibrant® CM-DiI Cell-Labeling Solution | Life Technologies, V-22888 |
| Vibrant® DID Cell-Labeling Solution | Life Technologies, V22887 |
| Zoledronic acid | Novartis |

### 2.1.2. Softwares used for data analysis

| Software | Supplier |
|---|---|
| CTAnalyser software | SkyScan, Bruker microCT, CT-Analyser version 1.14.4.1 |
| Fiji (ImageJ) | ImageJ, Version 2.0.0-rc-24/1.49m |
| GraphPad Prism software | Prism, Version 6.0c |
| LAS AF | Leica Microsystems CMS GmbH, Version 2.6.3 build 8173 |
| Living Image 4.0 software | Caliper Life Sciences |
| NIS-Elements-software | Nikon Instruments, Version 4.30 |
| Nrecon | SkyScan, Bruker microCT, Version 1.6.9.9 |
| OsteoMeasure | OsteoMetrics |
| SDS 2.1 software | Applied Biosystems 7900HT Fast Real-Time PCR System |
| Tree Star FlowJo | FlowJo, vX.07 |
| Volocity software | Improvision, Version 4.3.2 |

### 2.1.3. Antibodies used

| Antibody | Supplier |
|---|---|
| Alexa Fluor® 555, goat anti-rat IgG | LifeTechnologies, A21434 |
| Alexa Fluor® 647, goat anti-rat IgG | LifeTechnologies, A21247 |
| Anti-CD31 (Ms) from Rat | DIA-310, Dianova |
| Anti-Mouse CD11b Alexa Fluor® 488 | eBioscience, Clone M1-70, Cat.No.:53-0112-80 |
| Anti-Mouse CD41 PE | eBioscience, Clone: eBioMWReg30, Cat. No: 12-0411-81 |
| Anti-Mouse TER-119 APC | Anti-Mouse TER-119 APC (eBioscience, Clone: TER-119, Cat. No: 17-5921-81) |
| Biotinylated anti Mouse IgG (H+L), made in horse | Vector BA-2000 |
| Biotinylated Goat-anti-Rat IgG | Vector BA-9401 |
| Brilliant Violet 421™ anti-mouse CD45 Antibody | BioLegend, Clone 30-F11, Cat.No: 103133 |
| c-Met [pY1230/34/35] Rb recombinant monoclonal | Invitrogen, Clone 5H27L59 |
| Endomucin V.7C7, rat monoclonal | Santa Cruz, sc-65495 |
| goat-anti-rat IgG FITC conjugated | ZyMax 81-951 |
| Monoclonal Mouse Anti-Human Ki67 | DAKO, Clone MIB-1 |
| Met Antibody (C-28) | sc-161, Santa Cruz |
| Pe-Cy7 anti-mouse Ly-6G/Ly-6C (Gr-1) | Clone RB6-8C5, Cat.No.:108415 |
| Polyclonal Goat Anti-Mouse Iggs HRP, | Dako, P0447 |
| Rat anti-mouse CD34 | MCA1825GA, AbD Serotec |

### 2.1.4. TaqMan Real-Time PCR-Assays

| Gene | Taq Man ID |
|---|---|
| B2M | Mm00437762_m1, Thermo Fisher Scientific |
| HPRT | Mm00446968_m1, Thermo Fisher Scientific |
| Abl1 | Mm00802029_m1, Thermo Fisher Scientific |
| RANKL | Mm00441906_m1, Thermo Fisher Scientific |
| RANK | Mm00437135_m1; Mm00437132_m1, Thermo Fisher Scientific |
| OPG | Mm00435451_m1, Thermo Fisher Scientific |
| Vegfa | Mm01281449_m1, Thermo Fisher Scientific |
| Sox9 | Mm00448840_m1, Thermo Fisher Scientific |

### 2.1.5. Machines used

| Machine | Supplier |
|---|---|
| 2200 TapeStation Instrument | Agilent Technologies |
| ABI PRISM 7900HT Sequence Detection System | Applied Biosystems |
| Agilent RNA ScreenTape assay | Agilent Technologies |

| | |
|---|---|
| Benchtop Centrifuges | MSE Mistral 2000; Heraeus FRESCO21; 5810R, Eppendorf; Eppendorf Centrifuge 5810; Beckman Microfuge Lite; Beckman GPR |
| Confocal Microscope | Nikon A1 inverted |
| Cryostat | 5030 Microtome, Bright |
| Cryostat | MICROM HM560 |
| Desktop X-ray microtomograph | SkyScan 1172, Bruker microCT |
| Dry Heating bath | Labnet International |
| FACSCalibur | Becton Dickinson |
| Glass bottomed Dish 12mm | Thermo Scientific, 150680 |
| Gradient Thermo Cycler | MJ Research, PT-200 |
| Inverted widefield fluorescence microscope | Leica DMI 4000B, Leica AF6000LX |
| IVIS® Lumina II | Perkin Elmer |
| Leica AF6000LX inverted | Leica |
| Leica DM1000 | Leica |
| Leica DMRB upright microscope | Leica |
| LSRII | BD BioSciences |
| Multiphoton Confocal Microscope | Zeiss LSM510 NLO Inverted |
| Nanodrop 2000 | Thermo Scientific |
| Nanodrop ND-1000 Spectrophotometer | Nanodrop Wilmington, DE |
| Olympus BX53 microscope | Olympus BX53 |
| Superfrost ® Plus Slides | Thermo Scientific, J1800AMNZ |
| Thermomoxer Comfort | Eppendorf |
| Vortexer | Rotamixer, Hook&Tucker Instruments |
| Water bath | Grant JB Series |

## 2.2. Methods

***In vitro* work**

### 2.2.1. Cell lines

For experiments establishing the role of the BME in peripheral breast cancer growth, Dr. Penelope Ottewell (University of Sheffield, UK) kindly provided the GFP expressing MDA-G8 cell line. This cell line has been originally derived from MDA-MB-436 (triple negative) breast cancer cells [241]. Tumour cell homing to bone was established using the MDA-MB-231-NW1-luc2 cell line, transfected with luciferase and kindly provided by Dr. Ning Wang (University of Sheffield, UK). This cell line was derived from the MDA-MB-231 ATCC breast cancer cell line.

### 2.2.2. Thawing and freezing of cells

For long-term storage cell lines were kept in liquid nitrogen ($lN_2$). For culture, cells were removed from $lN_2$ and rapidly thawed in a 37°C water bath. 9mL corresponding medium containing 10% foetal bovine serum (FBS) was added followed by centrifugation at 800rpm for 5min. The cell pellet was re-suspended in 10mL fresh medium and cells plated into a T75 flask. For freezing, cells were washed in PBS (2x), dislodged using trypsin/EDTA, re-suspended in medium and centrifuged for 5min at 800rpm (Beckman GPR fitted with rotor GH3.7; ≈160xg). Cell number was determined and $1x10^6$ cells/mL aliquoted in their corresponding growth medium supplemented with 10% DMSO. Cells were frozen in Mr. Frosty™ Freezing Container (Thermo Scientific; achieves a cooling rate of -1°C/minute which is optimal for cells) at -80°C prior to long-term storage in $lN_2$.

### 2.2.3. Cell culture

Cultures were maintained and grown in T75 or T125 flasks containing the appropriate medium for each cell type at 37°C, 5% $CO_2$. Sub-culturing was performed in sterile tissue culture hoods and took place depending on confluence (about 70-80% prior to sub-culture). To sub-culture cells were washed twice with 5mL sterile PBS, 1mL trypsin/EDTA added followed by incubation at 37°C for 2-5min to detach adherent cells. To neutralise the trypsin/EDTA cells were re-suspended in fresh medium (if required cell number determined) followed by centrifugation at 800rpm (Beckman GPR fitted with rotor GH3.7; ≈160xg) for 5min. The cell pellet was re-suspended in 10mL fresh medium and a ratio of cells (commonly 1:10) plated into a T75 flask containing fresh growth medium. DMEM supplemented with 10% FBS was used for MDA-231-NW1-luc2 and RPMI supplemented with 10% FBS for MDA-G8 cells.

### 2.2.4. Determination of cell number

Cell number was determined using a haemocytometer and where applicable a viable cell count was performed using trypan blue exclusion principle. Briefly, a single cell suspension was prepared and an aliquot (10µL) transferred into the haemocytometer followed by counting the total cell number of all 4 sets of 16 corner squares (according to standard operating procedures). To determine the total number of cells the average of all 4 sets was calculated and multiplied by $1x10^4$ and the volume from which the original cell sample was obtained. For trypan blue staining cells were mixed 1:2 with trypan blue prior to transferal into the haemocytometer and the dilution factor incorporated when estimating total cell number.

### 2.2.5. Labelling cells with lipophilic dyes – DiD and CM-DiI

Dialkylcarbocyanines such as DiD and CM-DiI are lipophilic tracers that are incorporated into cell membranes, thereby staining the entire cells and allowing their detection by fluorescence. Here the lipophilic membrane dyes DiD and CM-DiI were used to map the location of cancer cells in bone by immunofluorescence and two-photon microscopy.

Labelling of cells with the dyes was performed to manufacturers instructions. Briefly, cells were trypsinised and dislodged as described before and suspensions of $1x10^6$ cells/mL prepared in serum free medium (for DiD) or HBSS/D-PBS (for CM-DiI). 5µL dye per $1x10^6$ cells/mL were added to the suspension. For DiD staining cells were incubated for 20min at 37°C in the dark. For CM-DiI labelling suspensions were incubated for 5min at 37°C followed by 15min on ice. Following incubation with the dye cells were centrifuged (800rpm, 5min), re-suspended and washed 2 times in sterile PBS prior to injection.

## *In vivo* work

### 2.2.6. Ethics

For all experiments animals were housed in the University of Sheffield Biological Service Unit to the required guidelines. All experiments were performed in compliance with the UK Animals (Scientific Procedures) Act 1986 and were reviewed and approved by the local Research Ethics Committee of the University of Sheffield (Sheffield, UK). Studies were performed under Home Office Project Licence 40/3531 (PPL, Prof. NJ Brown) or 40/2972 (Prof. C Eaton). Until my UK Home Office personal license (PIL40/10913, December 2013) was granted, *in vivo* work was kindly performed by Dr. Hannah Brown, University of Sheffield as indicated in Chapter 3.

### 2.2.7. Animals

Male and female immunocompromised BALB/c nude mice were ordered form Charles River (UK) or Harlan (UK) as indicated for each study respectively. Genetically engineered mice expressing GFP +ve cells of the osteoblastic lineage (pOBCol2.3GFPemd crossed to BALB/c nude) were kindly provided from Leeds Institute for Molecular Medicine (UK). By expressing GFPemd in cells of the osteoblast lineage this immunocompromised mouse model (BALB/c nude background as described in detail in [158]) allowed a detailed investigation of the effects of anti-cancer therapies on osteoblastic cells and the link between disseminated cancer cells and resident osteoblasts. With aging the composition of the BME changes, including the presence of myeloid and lymphoid lineages in the bone marrow in addition to alterations in intrinsic HSC properties such as proliferation and differentiation. In addition, mesenchymal stem cells change their proliferation and differentiation capacity during aging, which is potentially associated with the increased bone loss in adulthood [242]. Young mice (6-8-weeks old) with high bone turnover/immature skeleton and older mice (9-17-weeks old) with a mature skeleton enabled to assess effects of anti-cancer therapeutics in different BMEs were therefore used in my experiments. In addition I also incorporated male mice in a subset of studies. For collaborative studies with the McAllister Laboratory, Boston, USA 6-week old female immonocompromised NCr-Nu (nude), CrTac:NCr-Foxn1$^{nu}$ mice (herein referred to as NCr-Nu (nude); Taconic Laboratories (Hudson, NY)) were used. These mice are derived from an original cross between the BALB/c inbred nude and NIH(S) outbred nude mice.

### 2.2.8. Preparation of injectables and drug administration

#### 2.2.8.1. Luciferin

Luciferin (D- Luciferin potassium salt) was prepared and kindly provided by Anne Fowles (University of Sheffield, UK), and administered intraperitoneally at a concentration of 30mg/kg.

#### 2.2.8.2. Intracardiac injection of breast cancer cells

Briefly, MDA-MB-231 breast cancer cells were harvested and DiD or DiI labelled as described previously. To prevent clump formation, cells were passed through a 100µm nylon mesh prior to injection. Mice were anaesthetised using isoflurane and complete anaesthesia was confirmed by the pinch reflex. Correct position of the needle was assessed by the bright red colour of oxygenated blood drawn into the syringe prior to slow injection of the cell suspension (containing $1x10^5$ cells) into the left ventricle. Injection was

performed using 1mL insulin syringes with 27-gauge needles. Following intracardiac injection mice were put into an incubator to recover and closely monitored. For experiments presented in Chapter 3, intracardiac injections were performed by Dr. Hannah Brown, University of Sheffield, UK or Jessalyn Ubellacker, Boston, USA.

#### 2.2.8.3. Subcutaneous injection of MDA-436 cells

Cell number was determined as described previously and 100µL ($5x10^5$ cells) injected subcutaneously into the right flank using 1mL syringes, 25-gauge needle.

#### 2.2.8.4. Intravenous injection of Doxorubicin

Clinical grade Doxorubicin was kindly provided from Weston Park Cancer Hospital (2mg/mL). A drug suspension with 2mg/kg Doxorubicin was prepared in PBS and sterile filtered prior to intravenous injection. The drug was prepared fresh for each day. To dilate tail veins animals were placed in an incubator at 35°C for at least 15min. For injection mice were placed in a bench top restrainer fitted onto a heating pad and 100µL drug suspension were slowly injected into the tail vein using insulin syringes (27-gauge needle).

#### 2.2.8.5. Zoledronic acid

Zoledronic acid was provided as the hydrated disodium salt ([1-hydroxy-2-1H-imidazol-1-yl)ethylene]bisphosphonic acid (Novartis). A 10mg/mL stock solution was prepared by Ms. A Evans in PBS and stored in aliquots at -20°C. A 100µg/kg suspension in PBS was prepared fresh prior to injection, sterile filtered and 100µL injected intraperitoneally using 1mL syringes (25-gauge needle).

#### 2.2.8.6. Cabozantinib

Cabozantinib (XL184), kindly provided by Exelixis Inc. (South San Francisco, California, USA) was prepared in sterile filtered $dH_2O$. To aid dissolution of the drug 5µL 1N HCl per 3mg/mL CBZ were added according to company recommendations. The drug suspension was prepared fresh on the day of administration and given within 1hr of preparation in a dose volume of 200µL by oral gavage.

#### 2.2.8.7. Phosphate buffered saline - PBS

PBS served as a vehicle control for all *in vivo* experiments as not otherwise specified. Sterile filtration was performed prior to injection and 100µL injected using the same route as for the respective experimental drug.

### 2.2.9. *In vivo* imaging

The Illumatool Lightning System was used to image the presence of GFP+ve cells *in vivo* using a Retiga EX-B camera with QCapture software (Version 2.70.0). Prior to *in vivo* live

imaging using IVIS Lumina II system mice were anaesthetised using isoflurane. Briefly, anaesthetised mice were placed into a dark box imaging chamber with a 12.5cm field of view and focus on subject height. Grey scale images were taken and animals imaged for luciferase signal. Relative fluorescence was visualised and overlaid with the grey scale images using pseudo colours and Living Image software. Auto Settings were used for image acquisition.

***Ex vivo* analysis**

### 2.2.10. Sample collection and processing

#### 2.2.10.1. Blood samples

Blood was collected at experimental endpoints. Animals were intraperitoneally injected with 50µL pentobarbiturate, deep anaesthesia confirmed using the pinch reflex. Blood was retrieved from the heart using a 1mL syringe, 25-gauge needle and placed in 1.5mL Eppendorf tubes after removal of the needle. To obtain serum, blood was allowed to clot at ambient temperature followed by 10min centrifugation at 10,000rpm (Beckman Microfuge Lite with rotor F1802B; ≈7150xg), 4°C. The clear supernatant (serum) was removed and pipetted into fresh Eppendorf tubes. Serum samples were stored at -80°C for later analysis. For flow cytometric analysis of whole blood samples, blood was collected as described before but the collection syringe and needle were pre-wetted with Heparin (50µL).

#### 2.2.10.2. Fixation of soft tissue samples for histological analysis

Soft tissues were fixed in 4% paraformaldehyde (PFA, prepared in PBS, pH 7.4) for 48hrs and subsequently transferred into 70% ethanol, processed by the University of Sheffield Bone Biology Lab and embedded in paraffin. For staining sections with a thickness of 3µm were cut by Alyson Evans, University of Sheffield.

#### 2.2.10.3. Fixation of bone samples for histological analysis

For **paraffin embedding** long bones were fixed in ice cold 4% PFA (prepared in PBS, pH 7.4) for 48-72hrs and decalcified in 0.5M EDTA/0.5% PFA (prepared in PBS, pH8) for 2 weeks at 4°C, constant shaking. Tissues were then embedded in paraffin and sections of 2 non-serial levels with a thickness of 3µm were cut by Mark Kinch and Alyson Evans, both University of Sheffield.

For **frozen sections embedded in gelatine** a protocol kindly provided by Dr. Anjaly Kusumbe, Max Plank Institute, Munich was followed. On day of cull, tibiae were fixed in ice cold 4% PFA (pH 7.4, in PBS) for 4hrs at 4°C. Next samples were washed 3x5min in PBS,

decalcified in 0.5M EDTA (pH 8, in PBS) for at least 24hrs. Once decalcified, samples were washed 3x5min in PBS and subsequently transferred into a 20% sucrose/2% Polyvinylpyrrolidone (PVP) solution (prepared in PBS) and incubated overnight at 4°C. On the following day bones were incubated in a water bath at 60°C in a solution containing 8% gelatine/ 20% sucrose/ 2% PVP for 45min prior to transferal into cryomolds. The gelatine solution was allowed to solidify for at least 30min followed by transferal of the samples into the -80°C freezer for long-term storage. Sections of 30µm thickness were cut using a cryostat (MICROM HM560).

For **calcein analysis** a protocol provided and optimized by Orla Gallagher, Bone Analysis Laboratory Sheffield was followed. Dissected spines were fixed in 70% ethanol for at least 48hrs, lumbar vertebra 4 isolated and stored in the dark until further processing. Vertebrae were infiltrated with alcohol (2x 80% IMS, 2x 90% IMS, 2x 100% pure ethanol for 48hrs each at ambient temperature) prior to transferal into Taab Medium Grade LR White Resin (Taab Laboratory Equipment Ltd; 3 changes for 48hrs each) at 4°C. Next samples were placed in plastic moulds and the LR White Resin allowed to polymerise at 55°C overnight for up to 24hrs. Sections for histomorphometric analysis were then cut by Orla Gallagher, Bone Analysis Laboratory Sheffield.

#### 2.2.10.4. Micro computed tomography (µCT) analysis

For µCT analysis bones were either scanned within the 48-72hr time frame of 4% PFA fixation or whilst in 10% Formalin solution. To determine effects of anti-cancer therapeutics on bone, trabecular bone volume (depicted as bone volume per tissue volume, BV/TV in %), trabecular number (Tb.N. in $mm^{-1}$), trabecular thickness (Tb.Th. in mm) and cortical bone volume (BV in $mm^{-3}$) were analysed using a SkyScan 1172 or 1272 (SkyScan). Tibiae were scanned using a currency of 200mA, 51kV, a 0.5mm aluminium filter and a medium camera resolution of 2000x1024 or 2016x1344 respectively. Pixel size for all scans was set to 4.3µm. For each sample images were reconstructed using NRecon software. A bone volume of interest (VOI) was determined by interactively drawing on the obtained two-dimensional images. Analysis was started from a fixed offset (0.5mm for trabecular bone and 1.2mm for cortical bone analysis) after a reference line was set at the lower part of the growth plate (Figure 8). Analysis was performed covering a length of 1.0mm for each bone. Obtained grey scale images of the VOI were converted into binary images (thresholds were consistent within one study) and bone parameters calculated using CTAn software.

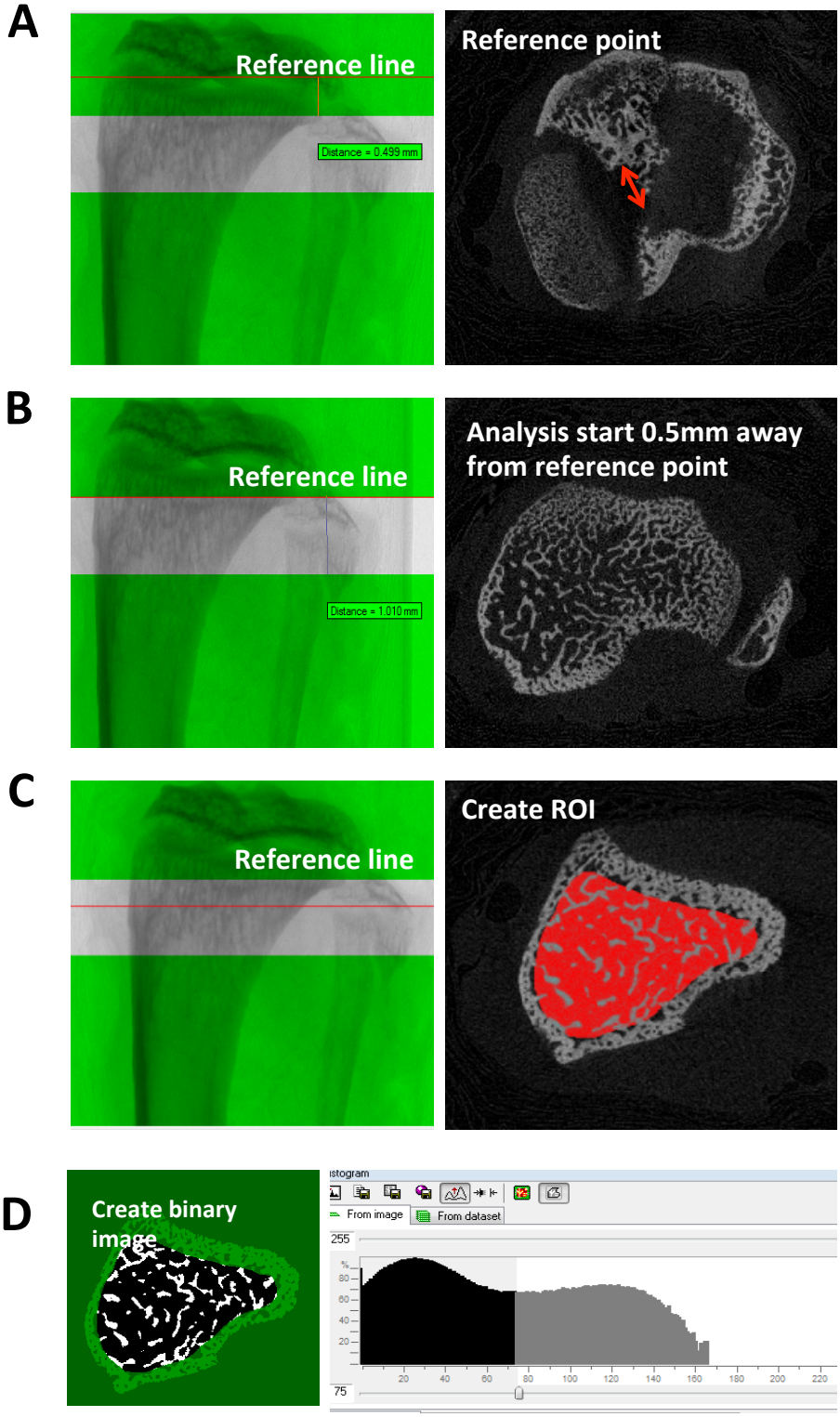


**Figure 8 Schematic workflow of µCT analysis.**
(A) A point of reference was set at the growth plate ("growth plate bridge", indicated by red arrow heads in A). Analysis was started from a fixed offset (B) after this reference point covering an area of 1.0mm for each bone (C). It was interactively drawn around the volume of interest (VOI) (C) and binary images created (D).

#### 2.2.10.5. Immunohistochemistry

A range of staining procedures were applied to identify cells on histological bone and/or soft tissue sections.

##### 2.2.10.5.1. Haematoxylin and Eosin (H&E) staining

H&E staining can be used to visualise numerous different tissue structures as nuclei are stained in blue by haematoxylin, whereas cytoplasm and connective tissue appears in various intensities of pink. H&E staining of paraffin embedded tissue sections was performed according to standard operating procedures developed by the Bone Analysis Laboratory, University of Sheffield. Briefly, 3µm sections of paraffin embedded tissue sections were dewaxed in xylene (2x5min), rehydrated through decreasing concentrations of alcohol (99%, 99%, 95% and 70%, 1min each) to distilled water. Samples were then incubated in Gill's Haematoxylin solution for 2 minutes followed by "bluing" in running tap water for 5 min, 5min incubation in 1% eosin solution and another washing step in running tap water until completely clear. Slides were dehydrated through alcohols (70%, 95%, 99%, 99%), cleared in xylene and mounted and cover slipped using DPX [(distyrene), plasticizer (tricresyl phosphate) and xylene] mounting medium.

##### 2.2.10.5.2. Tartrate-resistant acid phosphatase (TRAP) staining

Bone resorbing osteoclasts express TRAP. To analyse number, size and presence of osteoclasts in bone, histological samples were stained for TRAP according to standard operating procedures developed by the Bone Analysis Laboratory, University of Sheffield. Sections were dewaxed and rehydrated to $dH_2O$ as described previously followed by 5min incubation in pre-warmed acetate-tartrate buffer at 37°C. Sections were then immersed in naphtol AS-BI phosphate/dimethylformamide solution in acetate tartrate buffer for 30min at 37°C – the optimal temperature for this enzyme. Consequently sections were incubated in sodium nitrite/ pararosaniline/ acetate-tartrate buffer containing solution for 15min at 37°C. Counterstaining was performed using Gill's Haematoxilin prior to dehydration through alcohol and xylene, mounting and cover slipping. Table 4 shows the composition of buffer solutions for TRAP staining and gives quantities of reagents to stain 10 histological samples.

**Table 4 Composition of buffers for TRAP staining**

| BUFFER SOLUTION | | | | | | PRE WARM | SOLUTION A | | | SOLUTION B | | | | | |
|---|---|---|---|---|---|---|---|---|---|---|---|---|---|---|---|
| No. of Slides | Sodium Acetate (g) | $H_2O$ (ml) | Acetic Acid (ml) | Total Acetate-TartrateBuffer Volume (mls) | Sodium Tartrate (g) | Prewarm Slides Acetate-Tartrate Buffer (ml) | Naphthol AS-BI phosphate (g) | Dimethyl formamide (ml) | Solution A Acetate-Tartrate Buffer (ml) | Sodium Nitrite (g) | $H_2O$ (ml) | Para Rosaniline (ml) | Total Volume of Para Rosaniline-Nitrite (ml) | Solution B Para Rosaniline-Nitrite Volume Required (ml) | Solution B Acetate-Tartrate Buffer (ml) |
| 10 | 5.44 | 200 | 50 | 250 | 4.6 | 50 | 0.02 | 1 | 50 | 0.08 | 2 | 2 | 4 | 2.5 | 50 |

#### 2.2.10.5.3. Visualisation of proteoglycan using Safranin-O and Toluidine Blue staining

The cationic dyes Safranin-O and Toluidine blue were used to visualise acidic proteoglycan in growth plate cartilage on histological sections of tibiae.

Safranin-O staining was used to stain cartilage/proteoglycan. Cartilage and mucin are stained in red, nuclei in black and background (bone) in green. Briefly, rehydrated and dewaxed sections were incubated in Weigert's iron hematoxylin working solution (solution A: Hematoxilin/95% alcohol, Solution B: 29% Ferric chloride in $dH_2O$/concentrated HCl; 1:1) for 5 min, washed in $dH_2O$ followed by de-staining in acid ethanol prior to staining with Fast Green solution (Sigma-Aldrich) for 5 min at ambient temperature. Slides were then rinsed with 1% acetic acid and immersed in 0.1% Safranin – O solution for 5min followed by mounting with DPX.

Toluidine blue, a metachromasia dye, stains acidic proteoglycan and was next to Safranin O staining used to visualise alterations in growth plate cartilage. Bone sections were dewaxed and hydrated as described and immersed in Toluidine blue working solution (Toluidine Blue O, Sigma Aldrich; 1% NaCL pH = 2.3) at ambient temperature for 3min, followed by clearing in running $dH_2O$, dehydration through alcohols and cover slipping.

#### 2.2.10.6. Immunofluorescence

##### 2.2.10.6.1. Visualisation of GFP+ve osteoblastic cells

To visualise the presence of GFP+ve osteoblastic cells in bone, paraffin embedded bone sections were dewaxed as described previously, followed by mounting with VECTASHIELD® Mounting Media with DAPI**.** Images were acquired using a Leica DMI4000B microscope and LAS AF Lite software.

##### 2.2.10.6.2. Visualisation of the bone marrow vasculature

To visualise effects of anti-cancer drugs on the bone marrow vasculature, immunofluorescence staining against the vascular endothelial cell marker Endomucin and CD31 was performed on either paraffin embedded bone sections or gelatine embedded sections (1:100, Endomucin V.7C7, rat monoclonal, Santa Cruz, sc-65495) and CD31 (1:100, DIA-310: Anti-CD31 (Ms) from Rat (Clone: SZ31)). Endomucin is expressed in venous endothelium and as well as capillaries, whereas it is not present on arterial endothelium. CD31 (or platelet endothelial cell adhesion molecule-1, PECAM-1) is expressed on cell surfaces of platelets, neutrophils, embryonic and mature endothelial cells; and involved in cell-to-cell adhesion.

With a recommended working concentration of 1:50-1:500 for immunohistochemistry the 1:100 working solution of the Endomucin Antibody has previously been optimised in our laboratory group and was based on previously published experiments by Kusumbe and colleagues [51]. Dianova recommended a starting concentration of 1:20 for immunohistochemistry, the CD31 antibody was initially tested at a concentration of 1:50 and 1:100. Vascular staining was observed at both concentrations with 1:100 being ultimately used for all further experiments. Appropriate negative controls where incorporated by emitting the primary antibody. No fluorescence signal was observed on these samples.

###### 2.2.10.6.2.1. Visualisation of the bone marrow vasculature on paraffin embedded sections

The protocol for paraffin embedded bone sections was optimised with kind advice from Dr. Russell Hughes, University of Sheffield (UK). Histological sections of tibiae were dewaxed and rehydrated prior to antigen retrieval in Tris-buffer (pH9) for 15min at 95°C in a waterbath. Heated slides were allowed to stand at ambient temperature for 10min prior to washing in Tris buffered saline (TBS), blocking in 5% normal goat serum/3% bovine serum albumine (BSA) followed by overnight incubation in primary antibody (1:100, Endomucin V.7C7, rat monoclonal, Santa Cruz, sc-65495) at 4°C. After washing in TBS, sections were

incubated in secondary antibody (1:200, Alexa fluor 555, goat anti-rat Igg, LifeTechnologies, A21434) at ambient temperature for 1hr followed by washing in TBS and mounted with VECTASHIELD® Mounting Media with DAPI. Images were acquired using a Leica DMI4000B microscope and LAS AF Lite software (20x objective) or a Nikon A1 confocal microscope with NIS Elements software (40x objective). Visualisation of the bone marrow vasculature on gelatine embedded sections

To visualise effects of anti-cancer agents on the bone marrow vasculature I was kindly provided with a protocol from Dr. A Kusumbe, Max Plank Institute, Munich (Germany). Briefly, immunofluorescence staining against the vascular endothelial cell marker Endomucin (1:100, Endomucin V.7C7, rat monoclonal, Santa Cruz, sc-65495) and CD31 (1:100, DIA-310: Anti-CD31 (Ms) from Rat (Clone: SZ31)) was performed. 30µm thick frozen sections of tibiae were left to defrost at ambient temperature for 20min followed by re-hydrating the tissue with PBS and 20min incubation in 0.3% Triton X-100. Slides were then rinsed 3 times in PBS followed by incubation in 5% goat serum (in PBS, blocking solution) for 30min at ambient temperature. Primary antibody (prepared in blocking solution) was applied to incubate for 2hrs at ambient temperature or 4°C over night. This was followed by 3 rinses in PBS to remove unbound antibody and samples were incubated in secondary antibody (1:200, Alexa fluor 555, goat anti-rat Igg, LifeTechnologies, A21434, prepared in PBS) for 1hr at room temperature followed by 3 rinses in PBS and mounting with VECTASHIELD® Mounting Media with DAPI. DAPI was left to settle for 5min followed by sealing the coverslips with nail polish. Slides were stored at 4°C until image acquisition.

Images were acquired using the Nikon A1 Confocal microscope (NIS-Elements-software Version 4.30, CFI Plan Fluor 20x MI (NA 0.75), 403nm and 562nm laser) or the Nikon inverted Ti eclipse microscope (NIS-Elements software Version 4.30, Plan Apo 20x (NA 0.75)). For a subset of samples Z-stacks of 20µm depth (0.9µm intervals, 23 steps) were acquired and 3D projections reconstructed using Fiji (ImageJ, Version 2.0.0-rc-24/1.49m, Image>Stacks>3D projections). For others tile scans (6x6 or 8x8) were aquired. Appropriate negative controls were included (omitting the primary antibody).

#### 2.2.10.7. Assessing histological slides

As not indicated separately all histological analysis of bone samples was performed on 3µm thick sections of two non-serial sections (20µm apart).

#### 2.2.10.7.1. Osteoblasts and osteoclasts

Osteoblast quantification was performed on H&E or TRAP stained sections, osteoclasts were quantified on TRAP-stained bone sections according to standard operating procedures developed by the Bone Analysis Laboratory, University of Sheffield. Histopathological support was kindly provided by Dr. K Hunter (University of Sheffield, UK).

Briefly, osteoblasts were identified by their characteristic cuboidal shape, a distinct single nucleus, large golgi complex and violet appearance after H&E staining. Osteoblasts function as an entity of bone forming cells and were therefore found in groups of at least 3 cells lining the bone surfaces. (Fig.9). Osteoclasts were identified by their multiple nuclei and bright pink appearance after TRAP staining as illustrated in Figure 9. Bone cell number (here represented as osteoblast and osteoclast number/mm trabecular bone surface) and size was determined. Using OsteoMeasure software (OsteoMetrics), it was interactively drawn around areas of interest including: osteoblast surface (the surface covered by bone forming osteoblasts), osteoclast surface (the surface resorbed by osteoclasts), osteoclast volume (depicted as osteoclast size in $mm^2$) and trabecular bone surfaces. A schematic illustration and an example screenshot using OsteoMeasure can be seen in Figure 10.

A list of parameters used for analysis can be seen in Figure 10). Osteoblast and osteoclast number/mm trabecular bone surface was started 125µm from the last hypertrophic chondrocyte stack away covering all trabecular bone surfaces, using a 10x objective. Cortical bone was excluded for analysis. For a subset of studies presented in Chapter 3 an offset of 200µm was used and a 20x objective due to an upgrade of the OsteoMeasure system and provision of a new camera and microscope (Olympus BX53 microscope). This is indicated separately under the corresponding data sets (Chapter 3).

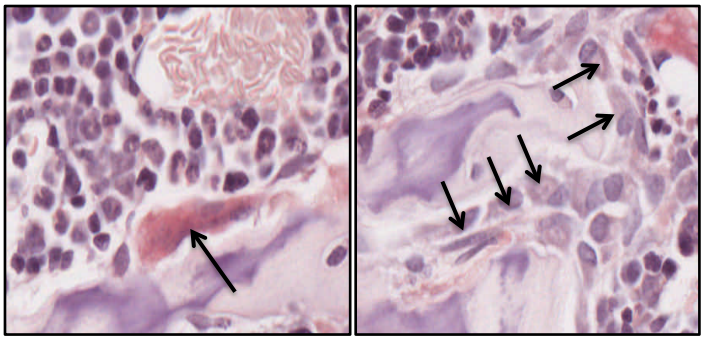

| Osteoclast | Osteoblast |
|---|---|
| Multiple nuclei | Single, distinct nucleus |
| Ruffled border | Large golgi complex |
| In contact with bone surface | Appear in groups |
| Pink, TRAP positive | Cuboidal shape |
| Resorption lacunae | In contact with bone surface |

**Figure 9 Identification parameters for osteoblasts and osteoclasts on histological sections.**

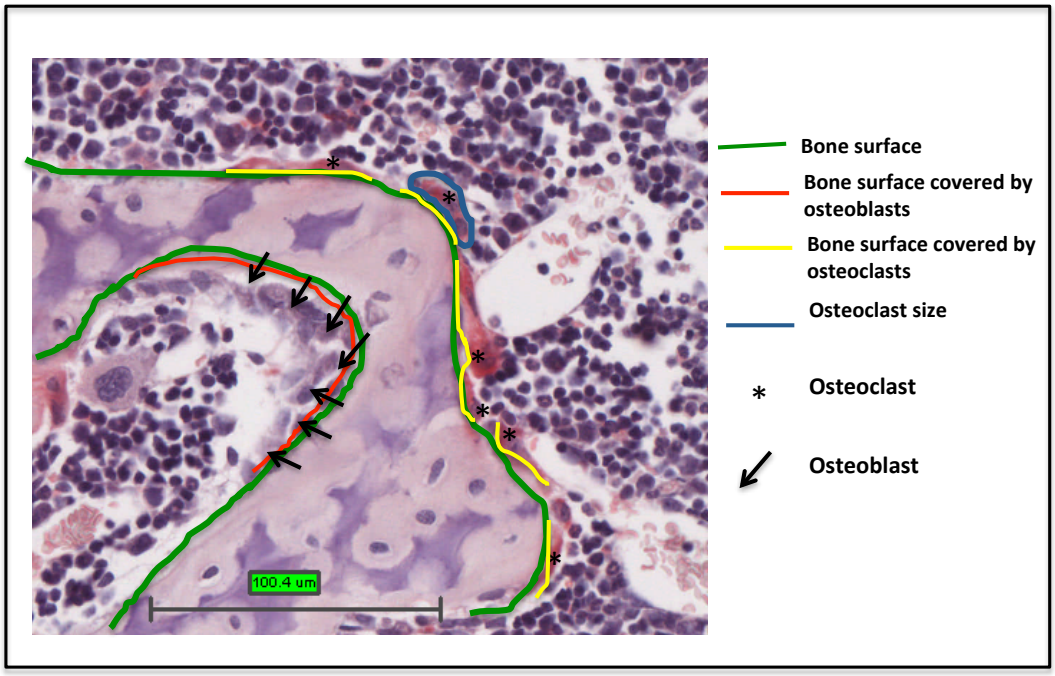


**Figure 10 Illustration of bone cell quantification using OsteoMeasure software.**
Osteoblasts (black arrow head) and osteoclasts (asterisk) lining all trabecular bone surfaces (green) were identified and quantified by interactively drawing around the parameters of interest.

#### 2.2.10.8. Serum measurments by ELISA

##### 2.2.10.8.1. TRAP

Tartrate-resistant acid phosphatase (TRAP) is expressed by osteoclasts when actively resorbing bone and this enzymatic assay was therefore used to measure osteoclast activity in serum samples. MouseTRAP$^{TM}$ Assay from Immuno Diagnostic Systems (SB-TR103) was used to determine osteoclast-derived tartrate-resistant acid phosphatase form 5b (TRACP 5b). The assay was performed according to manufacturer's guidelines. Anti-mouseTRAP Antibody (100µL) was added to the 96-well plate, incubated for 60min at room temperature (RT) on a micro plate shaker, prior to washing wells with Washing solution. Calibrator and Control solutions (100µL/well) were added to assigned wells in duplicates. 0.9% NaCl (75µL/well) followed by serum samples (25µL/well) were pipetted into the remaining wells in duplicate. Releasing Reagent (25µL/well) was added using a multichannel pipette and the plate was incubated at RT for 60min with shaking. The previously mentioned washing step was repeated followed by a 2hr incubation with Substrate Solution (100µL/well) at 37°C. Finally Stop Solution (NaOH, 25µL/well) was added and absorbance was read within 30 min of adding the Stop Solution at 405nm using a MRXII Dynex Technologies plate reader. Standard curves were generated, experimental sample concentrations calculated and expressed in U/L.

##### 2.2.10.8.2. Rat/Mouse PINP Enzyme immunoassay

The bone matrix consists partly of Type I collagen. Bone forming osteoclasts release precursor type I procollagen which can be used as a marker to determine bone formation. Rat/Mouse PINP Enzyme immunoassay for the quantitative determination of N-terminal propeptide of type I procollagen (PINP) (Immunodiagnosticsystems (AC-33F1) was therefore used to monitor osteoblast activity in serum samples. Briefly, Control and Calibrator (50µL/well) were added to the assigned wells of the antibody coated 96-well plate in duplicates. Samples (5µL/well) and Sample diluent (45µL/well) were pipetted in duplicate to the appropriate wells before PINP Biotin (50µL/well) was added to all wells and the plate was incubated for 1hr at RT on a microplate shaker. After washing with Washing buffer, Enzyme Conjugate (150µL/well) was added and the plate was incubated for 30min at RT. Washing of wells was repeated and the plate was incubated with TMB substrate (150µL/well) for 30 min at RT. Last Stop Solution (HCl, 50µL/well) was added and absorbance at 450nm was measured using a Spectra Max plate reader (Molecular Devices). Standard curves were generated, experimental sample concentrations calculated and expressed in ng/mL.

### 2.2.10.9. Gene expression analysis using long bones

A representative workflow can be seen in Figure 11 below and is described in the following section.

On day of sacrifice, tibia and femur were isolated and all muscle tissue removed using scissors and scalpel. Bones were immediately preserved in RNAlater Tissue Collection Solution (Ambion, Life Science Technologies), followed by splitting into halves and manually scraping out the bone marrow using scalpels and razor blades. Bones were then snap frozen in $lN_2$ prior to storage at -80°C for further analysis.

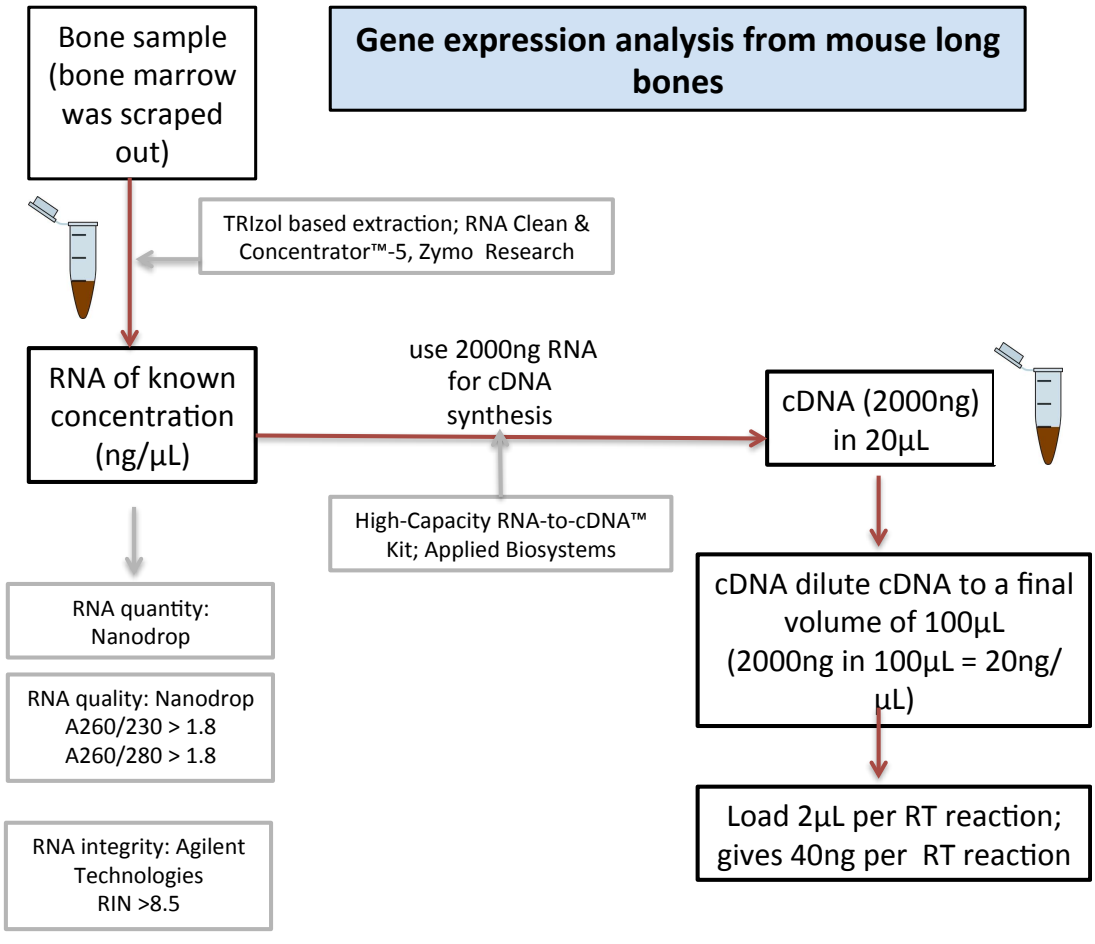


**Figure 11 Schematic workflow of gene expression studies.**
RNA from long bones was extracted using TRIZol and RNA Clean& Concentrator Kit, quantitiy and quality assessed followed by cDNA synthesis, and loading the samples into a 384-well plate for qRT-PCR analysis.

#### 2.2.10.9.1. RNA extraction

For RNA extraction snap frozen bones were pulverised using mortar and pestle under constant addition of $lN_2$. Tibia and femur from one leg of each mouse were pooled for RNA extraction to ensure sufficient concentration of extracted RNA. RNA was extracted using standard phenol-chloroform TRIzol RNA extraction in combination with the RNA Clean & Concentrator Kit from Zymo Research (ZEC174900). Briefly, 1mL TRIzol® (Sigma) was added per 100mg pulverised bone tissue. Samples were incubated at ambient temperature for 10min followed by centrifugation at 12,000rpm (Beckman Microfuge Lite with rotor F1802B; ≈10300xg) for 10min at 4°C to pellet insoluble high fat content. The supernatant was transferred to a fresh Eppendorf tube and 100µL chloroform/millilitre TRIzol® were added. Samples were incubated for 15min at ambient temperature followed by centrifugation at 12,000rpm (Beckman Microfuge Lite with rotor F1802B; ≈10300xg) for 15min at 4°C. The aqueous RNA phase was transferred into a fresh Eppendorf tube and an equal volume of 100% ethanol was added prior to transferral into a Zymo-Spin IC column. RNA Clean & Concentrator Kit from Zymo Research (ZEC174900) was used according to manufacturers guidelines. Briefly, the sample was centrifuged for 30sec, followed by addition of 400µL RNA Prep Buffer. After centrifugation RNA was washed twice using RNA Wash Buffer and eluted in a final volume of 20µL of DNAse/RNAse free $H_2O$.

#### 2.2.10.9.2. Assessment of RNA quality and quantity

RNA was quantified using a Nanodrop ND-1000 Spectrophotometer (Nanodrop Wilmington, DE). An A260/280 ratio of 1.8-2.2 and an A260/230 of 2.0-2.2 was accepted for pure RNA [243], and only these samples were used for cDNA synthesis.

RNA integrity was analysed using Agilent RNA ScreenTape assay (Agilent Technologies) and 2200 Tape Station Instrument (Agilent Technologies). The RNA integrity number (RIN) algorithm was used to analyse the entire electrophoretic trace of an RNA sample for the presence of degradation products. The resulting RIN number ranges from 1 to 10, with 1 being the most degraded and 10 being the most intact RNA. RIN number takes into account the ratio between the ribosomal peaks at 28S and 18S in mammalian samples. In my experiments RIN numbers ranged from 8.3 to 10.

#### 2.2.10.9.3. cDNA synthesis

2µg of RNA was reverse transcribed in a total volume of 20µL using High Capacity RNA-to-cDNA™ Kit (Applied Biosystems®) according to manufacturers instructions (See Table 5 below). For each sample a "Reverse transcription (Enzyme Mix) negative control" was

loaded, therefore each sample was prepared in two replicate tubes. In addition a tube containing "DNAse/RNAse free water" only was also prepared to ensure no contamination in the reagents (see Table 5).The reaction was performed using a thermal cycler at 37°C for 60min, 95°C for 5min and held at 4°C, followed by long-term storage at -20°C. The resulting first-strand complementary DNA (cDNA) worked as a template for real-time quantitative polymerase chain reaction (qRT-PCR) – composition of the reaction mix is seen in Table 6 below. Species-specific TaqMan® assays (Life Technologies) were used to analyse the expression of selected genes of interest (GOI).

**Table 5 Reagents used for cDNA synthesis**

| Volume (µL) | | | |
|---|---|---|---|
| **Reagent** | **Sample** | **Negative sample control (no reverse transcriptase)** | **Negative (no RNA) control** |
| **2X RT Buffer** | 10 | 10 | 10 |
| **20 X Enzyme Mix** | 1 | - | 1 |
| **RNA** | Up to 9µL (concentration of 1µg) | Up to 9µL (concentration of 1µg) | - |
| **DNAse/RNAse free $H_2O$** | Filled up to a final volume of 20µL | Filled up to a final volume of 20µL | 9 |
| **Total reaction volume** | 20 | 20 | 20 |

**Table 6 Composition of the PCR reaction mix**

| **Reagent** | **Volume (µL)** |
|---|---|
| **2X TaqMan® Universal PCR Master Mix (Applied Biosystems)** | 5 |
| **RNAse/DNAse free $H_2O$** | 2.5 |
| **20X TaqMan® Gene Expression Assay (Applied Biosystems)** | 0.5 |
| **cDNA** | 2 |

### 2.2.10.9.4. Selection of house keeping gene

During relative quantitation of a qRT-PCR experiment the expression of a gene of interest (GOI) in one sample (*e.g.* control group) is compared to the expression of the same GOI in another sample (*e.g.* treatment group). To correct for sample-to-sample variation data are normalised to an invariant, stable endogenous control, a so-called housekeeping gene

(HKG). The quality of normalised expression data can therefore only be as good as the quality of the HKG itself. Any variation of the HKG will result in artifactual changes [244], and therefore HKG have to be selected carefully for each experiment. Here, expression levels of B2M, HPRT1 and Abl1 were assessed but only B2M was stable expressed and therefore used as a HKG for all experiments described in Chapter 4 (HKG validation was performed according to guidelines obtained from [245]). In addition efficiency of both HKG and GOI were assessed using a standard curve of serially diluted cDNA (1, 1:10, 1:100, 1:1000) was performed for each housekeeper and GOI. Results were plotted with input nucleic acid quantity (log of dilution) on the X-axis and Ct-value on the Y-axis (see Fig.12). The efficiency was calculated using following formula: Efficiency=$10^{(-1/\text{-slope})}$-1 where the slope of the standard curve indicates the PCR efficiency. PCR efficiency ranged between 90-110%, the accepted range for TaqMan assays [246].

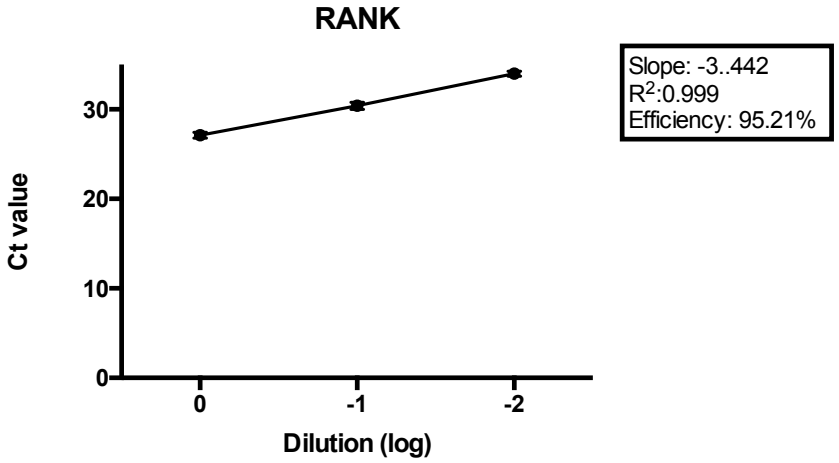


**Figure 12 Representative graph showing House Keeping Gene efficiency.**

#### 2.2.10.9.5. Quantitative Real Time Polymerase Chain Reaction (qRT-PCR)

qRT-PCR was performed using the ABI PRISM 7900HT Sequence Detection System (Applied Biosystems) and SDS 2.1 software. The PCR program consisted of an initial hold 50°C for 2min, an activation step at 95°C for 10min and 40 cycles at 95°C for 15sec followed by annealing for 1min at 60°C. A FAM non-fluorescence detector and a passive ROX reference signal were used. A baseline (the initial steps of the PCR where there is little change in fluorescence signal) of cycles 3-15 and a threshold (the level of signal that represents a significant increase over the calculated baseline signal) of 0.2 were used. This allowed the determination of the threshold cycle (Ct), the cycle number at which the fluorescent signal

of the reaction crosses the threshold. Ct values are inversely proportional to the expression of the target meaning that decreased amount of template = higher cycle number. Ct values ≥34 were excluded from analysis.

#### 2.2.10.9.6. Analysis – Relative quantification

Relative quantification shows the expression of the GOI relative to a HKG. Obtained Ct-values are expressed as a fold change in expression of the „treated samples" relative to the „control samples". Briefly, the ΔCt value was calculated from obtained Ct-values of the GOI by normalising to the Ct-value oft he HKG using the formula ΔCt=Ct(GOI)-Ct(HKG). Next, the ΔΔCt was calculated as follows: ΔΔCt=ΔCt(GOI)-ΔC(HKG). This is followed by determination of $2^{-\Delta\Delta Ct}$, the fold change.

### 2.2.11. Statistical Analysis

Statistical analysis was performed using GraphPad Prism Version 6.0. To determine whether the effects of anti-cancer therapeutics on bone and key bone cells were statistically significant unpaired Student's t-test or 2-way ANOVA with Bonferroni's post-test was used. T-test is usually applied when the test samples follow a normal, Gaussian distribution. In my studies I used small n-numbers (n=3-5), and most statistical normality tests require higher n-numbers to test for normal distribution of the samples (*e.g.* Shapiro-Wilk test requires n≥7 or D'Agostino & Pearson omnibus test n≥8). I decided to use t-test when analysing bone parameters including bone volume, bone cell number and serum levels of bone resorption/formation markers given the following:

- Tight error bars and small sample-to-sample variation were obtained when analysing bone parameters in previous experiments in our laboratory and by myself [154, 158, 247].
- In Chapter 4 I obtained samples from collaborative experiments to assess treatment effects of the tyrosine kinase inhibitor CBZ on growth plate chondrocytes (n=9-10). These n-numbers allowed me to assess normal distribution of values obtained for the hypertrophic and resting/proliferating chondrocyte zone. Using the D'Agostino & Pearson omnibus test, which tests the null-hypothesis that "all the values are sampled from a Gaussian distribution", showed that both parameters were normally distributed.
- In addition one can assume that when a distribution is normal, the mean and median will be equal. Mean and median of analysed parameters were in most analyses nearly identical. For example effects of a single dose of ZOL on trabecular

bone volume 3 days after PBS or ZOL treatment (n=3-4): PBS: Mean: 2.25 % vs. Median: 2.14%; ZOL: Mean: 3.66% vs. Median: 3.62%.

- When analysing data sets using Mann-Whitney test (assuming that samples are not from a normally distributed population), statistics were similar to that obtained from t-test.

Given the high variance in tumour growth, tumour size, microvascular density, necrotic core area and proliferation data were assessed using Mann-Whitney test.

# Chapter 3 - Modification of the bone metastasis niche with Zoledronic acid *in vivo* – consequences on tumour cell homing to bone

Part of this work has been published in "Haider M-T, Holen I, Dear TN, Hunter K, Brown HK. **Modifying the osteoblastic niche with zoledronic acid *in vivo*—Potential implications for breast cancer bone metastasis.** Bone. 2014;66(100):240-250. Reproduced with permission from Elsevier, Copyright © 2014 The Authors Published by Elsevier Inc. under the terms of the Creative Commons Attribution-NonCommercial-ShareAlike License (CC BY NC SA). (http://creativecommons.org/licenses/by-nc-sa/3.0/), DOI: 10.1016/j.bone.2014.06.023

### 3.1. Summary

Bone metastasis is the most common complication of advanced breast cancer. The majority of cancer patients die because of metastatic disease, not from their primary tumour. Once the cancer has spread to bone treatment remains restricted to palliative care. The cancer-induced bone disease is often treated with bone-sparing agents including the bisphosphonate Zoledronic acid (ZOL). Importantly, the lack of effective anti-metastatic therapy reflects the gap in our understanding of the underlying biology of tumour cell spread to bone. In clinical trials ZOL has shown to reduce recurrence of breast cancer in bone, which is suggested to be partially mediated by modification of the BME surrounding the disseminated tumour cells. However, the exact mechanisms behind this effect remain unknown.

The hypothesis to be tested in this chapter is that **ZOL modifies key components of the bone metastasis niche including osteoblasts and osteoclasts *in vivo*, with potential consequences on tumour cell homing to bone and metastatic outgrowth.**

Briefly, this chapter presents a detailed characterisation of the early effects of ZOL on key cells of the bone metastasis niche *in vivo* and will discuss how therapeutic modification of the niche affects breast cancer cell homing to bone. A single injection of ZOL rapidly altered the cellular (osteoblast and osteoclast number as well as activity) and extra-cellular (bone structure, extracellular matrix) composition of the bone metastasis niche in 6-week old, naïve mice as early as 3 days post treatment. In addition alterations in the structural organisation of the bone marrow vasculature were observed 3 days after ZOL injection when compared to control. Injection of MDA-MB-231 breast cancer cells at day 5, when ZOL induced effects reached their peak, demonstrated that breast cancer cells appear to preferentially home to osteoblast-rich trabecular bone areas, which could be altered when they arrive in a ZOL-modified microenvironment

In conclusion, a single dose of ZOL caused significant changes in the bone area suggested to contain the metastasis niche. Osteoblasts may be key components of the bone metastasis niche and therefore a potential therapeutic target in breast cancer.

## 3.2. Introduction

The skeleton is the most favoured site of metastasis in patients with advanced breast and prostate cancer. Both are likely to account for nearly 80% of all cases of metastatic disease and show the highest morbidity caused by skeletal related events (SREs) due to osteolytic and/or osteoblastic bone lesions [3]. Currently there is a lack of biological markers that could be used for routine diagnosis and bone metastases are usually detected radiologically once bone lesions are established. At this stage treatment remains palliative and often includes agents that prevent bone resorption by inhibiting osteoclast differentiation and/or apoptosis. The cancer-associated bone disease is therefore often targeted by Denosumab, the monoclonal antibody to RANKL, or bisphosphonates (BPs), with ZOL being the most potent one [248]. Both compounds primarily target osteoclasts but have also shown to affect other cell types in bone including osteoblasts [249], HSCs and vascular endothelial cells [159].

Briefly, the nitrogen-containing BP ZOL inhibits key enzymes of the intracellular mevalonate pathway by targeting the enzyme farnesyl pyrophosphate synthase (FPP synthase). Inhibition of FPP results in a lack of prenylation of downstream signalling proteins resulting in loss of osteoclast function and consequently osteoclast apoptosis [138, 250].

The progression from primary to secondary or metastatic tumour is a highly controlled process including detachment of tumour cells from the ECM, intravasation into surrounding tissue, lymph and/or blood vessels, circulation, attachment to the vessel wall and extravasation into the secondary organ [251]. The extent and aggressiveness of primary tumours has long been thought to be the main risk factor for the development of secondary disease. However, it became clear that also small primary tumours could cause metastatic relapse, often at much later time points. This suggests that dissemination of malignant cells (DTCs) to bone is an early event and tumour cells may reside in a dormant state within the bone for many years [252, 253]. With treatment remaining palliative once the tumour cells proliferate in bone, a potent therapeutic approach is to prevent and/or target the early steps of bone metastasis including the homing of tumour cells to secondary sites. Increasing our understanding about the metastatic spread is therefore detrimental for developing effective therapies.

As discussed previously Steven Paget almost 100 years ago already proposed that therapies to modify the microenvironment that supports tumour growth might be of equal

importance as therapies targeted against cancer cells themselves [86]. General consensus is that bone marrow-derived cells (BMDCs) make up a "metastasis niche", a tumour growth-promoting milieu within the bone, which regulates tumour cell homing, survival and dormancy. The niche is suggested to be comprised of various entities of BMDCs including (1) a hematopoietic stem cell niche, (2) an endosteal niche (osteoblasts, osteoclasts, mesenchymal stem cells, adipocytes) and (3) a (peri)-vascular niche [101], discussed in greater detail in Chapter 1, Section 1.4.

Recent work has highlighted that the microenvironment comprising microscopic bone lesions is primarily comprised of osteoblastic cells [94] and suggests that OCs are not critical in the earliest stages of bone metastases but rather at later stages of disease progression [93]. DTCs are suggested to take advantage of similar molecular mechanisms that regulate HSC homing and retention including the CXCL12/CXCR4 signalling axis which might involve the osteoblast as a key mediator [103]. *In vitro* CXCL12 (or SDF-1) is expressed on a variety of cells of the BME including osteoblasts and endothelial cells [254, 255]. In addition CXCR4, the receptor for CXCL12, is expressed on a variety of cancer cells including breast and prostate [255, 256]. Using prostate cancer models Shiozawa and colleagues have shown that tumour cells compete with HSCs for the occupancy of the haematopoietic niche [95]. This suggests that cancer cells might use the CXCL12/CXCR4 pathway whilst homing to the osteoblastic niche in bone. This is supported by data from Price and colleagues who have recently demonstrated that both, newly and established metastases are anchored in the bone marrow by CXCR4/SDF-1 interactions [112]; a factor highly expressed by osteoblastic cells. Whether osteoblasts are indeed part of the metastasis niche is subject to debate [113] and was experimentally addressed within this chapter.

Several clinical trials support beneficial effects of ZOL for breast cancer patients in the adjuvant setting [132, 179, 180, 182]. The AZURE (BIG 01/04) clinical trial reported that increased risk of bone metastasis seemed to be associated with high serum PINP (osteoblast activity) levels at baseline (study entry) when compared to patients with low PINP. Although this was not relevant for overall distant disease recurrence, it suggests a potential role of osteoblasts in breast cancer recurrence in bone, and a novel therapeutic target. Importantly, there was also a reduced incidence of bone metastases in women (post-menopausal) receiving ZOL in addition to standard adjuvant therapy [132].

In agreement several *in vivo* studies have reported a reduction in cancer-induced bone disease when osteoclastic bone resorption was inhibited by early administration of BPs (BP pre-treatment prior to tumour cell injection) in the development of bone metastasis. In addition, preventative schedules appear to slow down disease progression. Initiating ibandronate treatment (10μg/kg/day) upon appearance of osteolytic lesions in femurs of rats reduced progression of these lesions however, tumour growth was not eliminated [144]. In contrast, when ibandronate treatment was started 3 days prior to tumour cell injection, the development of osteolytic lesions was inhibited and expansion of osteolytic areas slowed down [144]. In agreement with this, a study by van der Pluijm *et al.* showed that pre-treatment (2 days prior to injection of MDA-231-B/luc+) with olpadronate (1.6μmol/kg/day), delayed the progression and decreased the development of bone metastases in addition to reducing the establishment of osteolytic lesions [257]. The authors suggest that preventative schedules reduce tumour growth by inhibiting the release of tumour growth factors by osteoclastic bone resorption, a mechanism well known for driving progression of cancer-induced bone disease [257]. Additionally BPs have shown to inhibit invasion, a pre-requisite for the establishment of metastatic disease, of PC-3 and MDA-MB-231 prostate and breast cancer cells in in a dose dependent fashion with ZOL being the most potent agent [142].

Taken together these data suggest that the bone metastasis niche generates a beneficial microenvironment for disseminated tumour cells in bone and that osteoblasts might be one of the key components of this niche.

### 3.3. Hypotheses

- A single dose of ZOL rapidly alters the cellular and extracellular composition of the bone metastasis niche.
- ZOL-induced modification of the bone metastasis niche alters tumour cell homing to bone and metastatic outgrowth *in vivo*.

### 3.4. Aims and Objectives

- Establish the early effects (Day 3-10) of a single, clinically relevant dose of ZOL (100μg/kg) on the bone metastasis niche *in vivo* by assessing alterations in
    - Osteoblast number and activity
    - Osteoclast number and activity
    - Extracellular matrix composition
    - Bone marrow vasculature
- Determine if the presence of tumour cells in bone is altered when they encounter a ZOL-modified microenvironment.
    - Do tumour cells home to specific areas in bone?

### 3.5. Material and methods

Methods not described below can be found in the general methods section, Chapter 2. A summary of methods applied is listed in Table 7 below.

**Table 7 Summary of methods applied in Chapter 3**

| Method | Parameters analysed | Equipment |
|---|---|---|
| Microcomputed tomography | -Trabecular bone volume (BV/TV in %)<br>-Trabecular number (TB.N. in $mm^{-1}$)<br>-Trabecular thickness (Tb.Th. in mm) | -SkyScan 1172/1272 scanner (SkyScan)<br>-NRecon software<br>-CTAn software |
| **Histological assessment** | | |
| Tartrate-resistant acid phosphatase staining (TRAP) | -Osteoclast number per mm of trabecular bone surface<br>-Osteoclast size (in $mm^2$) | -OsteoMeasure software (OsteoMetrics)<br>-Leica DMRB upright microscope |
| Haematoxylin and Eosin staining (H&E) | -Osteoblast number per mm trabecular bone surface | -OsteoMeasure software (OsteoMetrics)<br>-Leica DMRB upright microscope<br>-Olympus BX53 microscope |
| Toluidine blue staining | -Alterations in growth plate area<br>-Visualise proteoglycan<br>-Quantification of growth late area per tissue area | -OsteoMeasure software (OsteoMetrics)<br>-Leica DMRB upright microscope |
| Immunofluorescence/confocal microscopy | -Visualisation of Endomucin positive vascular endothelial cells | -Leica DMI4000B microscope (20x objective)<br>-Leica AF6000LX inverted microscope (20x objective)<br>- LAS AF Lite software<br>-Nikon A1 confocal microscope with NIS Elements software (40x objective)<br>-Nikon inverted Ti eclipse, NIS-Elements software Version 4.30, Plan Apo 20x (NA 0.75)<br>-Cryostat (MICROM HM560) |
| **Tumour cell homing to bone** | | |
| Two-photon microscopy | -Presence of tumour cells in bone | -Bright OTF Cryostat with a 3020 microtome (Bright Instrument Co. Ltd, Huntingdon, UK)<br>-Zeiss LSM510 NLO upright multiphoton/confocal microscope (Carl Zeiss Inl, Cambridge, UK). A 20x/0.8 lens<br>-LMS software version 4.2 (Zeiss)<br>-Volocity 3D Image Analysis software 6.01 (PerkinElmer, Cambridge, UK) |
| Flow cytometry | - Presence of tumour cells in bone marrow and blood | -FACS Calibur |
| **Enzymatic analysis** | | |
| MouseTRAP™ Assay | -Osteoclast activity | -MouseTRAP™ Assay from immunodiagnostic systems (SB-TR103) |
| Rat/Mouse PINP Enzyme immunoassay | -Osteoblast activity | -Rat/Mouse PINP Enzyme immunoassay for the quantitative determination of N-terminal propeptide of type I procollagen from immunodiagnostic systems |
| **Statistical analysis** | | |
| Statistical analysis | -Experimental datasets | -Prism GraphPad |

### 3.5.1. Cell lines

The triple negative MDA-MB-231-NW1-luc2 cell line was kindly provided by Dr. Wang, University of Sheffield, UK. For collaborative experiments with Dr. McAllister, Boston USA the MDA-MB-231-GFP-IV cells, stably transfected with e-GFP by Dr. Ottewell, University of Sheffield, was used. The here used MDA-MB231-GFP-IV cell line is derived from MDA-MB-231 cells that underwent repeated passaging *in vivo,* however does not have the full bone-homing phenotype described in [258]. The MDA-MB231-B02-FII was kindly provided by J. Ubellacker, Harvard School of Medicine, USA. Cell cultures were maintained as described in Chapter 2, Section 2.2.3.

### 3.5.2. Substance preparation

#### 3.5.2.1. Zoledronic acid

Zoledronic acid (ZOL) was supplied as the hydrated disodium salt ([1-hydroxy-2-1H-imidazol-1-yl)ethylene]bisphosphonic acid from Novartis. The drug suspension at a concentration of 100µg/kg was prepared fresh on the day of injection in PBS and sterile filtered (45µm filter) prior to intraperitoneal injection (100µL) using 1mL syringes, 25-gauge needle.

### 3.5.3. Experimental design

Intracardiac tumour cell injections in this chapter have been performed by Dr. Hannah Brown, University of Sheffield. Until the receipt of my Home Office Personal License she kindly performed the ZOL or PBS treatments. For collaborative experiments, *in vivo* work was performed by Jessalyn Ubellacker, Boston, USA.

#### 3.5.3.1. Establishing short-term effects of ZOL on the bone microenvironment *in vivo*

The early effects of a single dose of ZOL on osteoblasts and osteoclasts were elaborated in 6-week old immunocompromised BALB/c nude mice (n=3-4/group; BALB/c-Nude[Foxn1-Crl], Charles River, UK). Collaborative experiments with Dr. Sandra McAllisters group were performed using 6-week old female NCr-Nu (nude), CrTac:NCr-Foxn1$^{nu}$ mice (herein referred to as NCr-Nu (nude). In these experiments 1X Hank's Balanced Buffer Solution (HBSS) was used as a vehicle control.

Experimentally animals were randomised into two groups and received a single dose of (1) Zoledronic acid (100µg/kg, 100µL, i.p., equivalent to the 4mg infusion used in the treatment of cancer-induced bone disease [241]) or (2) sterile vehicle control (100µL, i.p.) on day 0. Previous studies in immunocompromised and/or immunocompetent mice have shown no effect of ZOL on bone and bone cells 24hrs after a single dose, but reduced

osteoblast and osteoclast numbers on day 15 post treatment when compared to control [154, 158]. To determine how quickly ZOL affects the BME, mice were culled 3, 5, 8 and 10 days after treatment – See Fig.13.

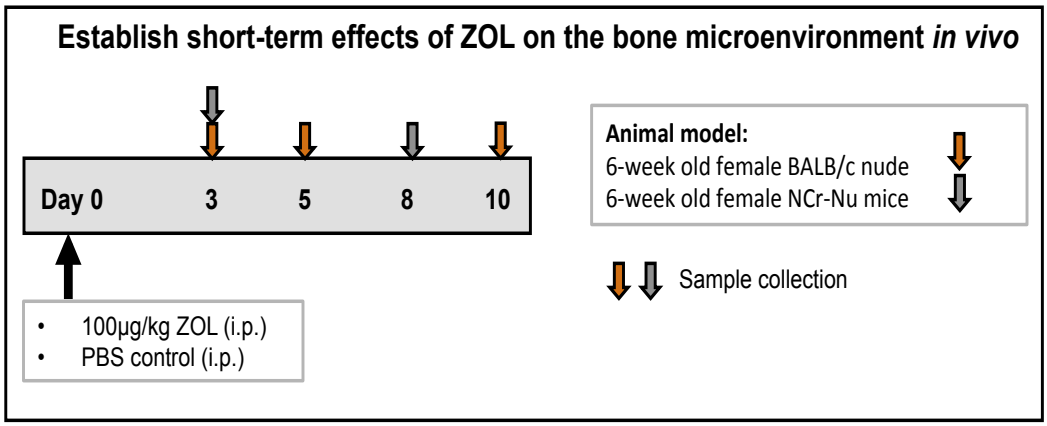


**Figure 13 Experimental outline – Establish early effects of Zoledronic acid on the *in vivo* bone microenvironment.**
To determine the early effects of Zoledronic acid (ZOL) on the *in vivo* BME 6-week old female BALB/c nude (n=3-4/group) or NCr-Nu (nude), CrTac:NCr-Foxn1$^{nu}$ mice (n=5/group) were treated with a single, clinically relevant dose of ZOL (100µg/kg, 100µL, i.p.) or vehicle control (100µL, i.p.). Samples (indicated by green and red arrow head) were collected 3, 5, 8 and 10 days post injection.

#### 3.5.3.2. Establishing if therapeutic modification of the bone microenvironment with ZOL alters tumour cell homing to bone

To establish if therapeutic modification of the BME with ZOL affects tumour cell homing to bone and whether osteoblasts are key components of the bone metastasis niche 8–13-week old female immunocompromised mice expressing GFP+ve cells of the osteoblastic lineage were used (homozygote and heterozygote nude, BALB/cAnNCrl.Cg-Tg(Col1a1-GFP)Row Foxn1$^{nu/nu}$, described in greater detail in [158], referred to as GFP-Ob$^{+}$, n=4/group for 2 independent experiments). Mice were randomised and received either (1) a single dose of ZOL (100µg/kg, 100µL, i.p.) or (2) sterile PBS control (100µL, i.p.) on day 0. To assess if tumour cell homing to bone is altered when the cells arrive in a ZOL-modified BME, animals were injected intracardiac with 1x10$^{5}$ DiD labelled MDA-MB-231-NW1 (luc2 positive) breast cancer cells on day 5, the time point where ZOL-induced modification of the BME reached its' peak. Samples were collected on day 10 – see Fig.14.

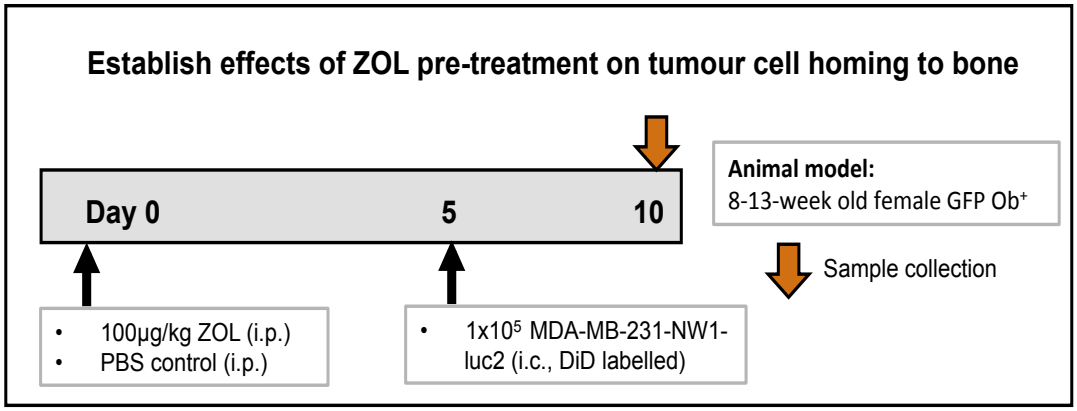


**Figure 14 Experimental outline to establish the effects of Zoledronic acid pre-treatment on tumour cell homing to bone.**
Effects of ZOL pre-treatment were established in 8-13-week old female mice expressing GFP+ cells of the osteoblastic lineage (n=4/group for two individual experiments, GFP-Ob$^{+}$). Mice were treated with a single dose of Zoledronic acid (100µg/kg, 100µL, i.p., ZOL) or PBS control (100µL, i.p.). 5 days post injection 1x10$^{5}$ DiD labelled MDA-MB-231-NW1-luc2 breast cancer cells were injected intracardiac.

To further characterise the effects of ZOL on tumour cell homing to bone I collected bone samples from collaborative experiments performed in Dr. Sandra McAllisters laboratory, Brigham and Women's hospital, Boston, USA. In these experiments 6-week old female NCr-Nu (nude), CrTac:NCr-Foxn1$^{nu}$ mice were injected with a single dose of ZOL (100µg/kg, 100µL, i.p.) or HBSS (100µL, i.p.) on day 0. Three days post treatment both control and treated mice were randomly assigned into two groups receiving (1) 1x10$^{5}$ cM-DiI labelled MDA-MB-231-B02-FII or (2) 1x10$^{5}$ CM-DiI labelled MDA-MB-231-GFP-IV cells (i.c.). Samples were collected 5 days post cancer cell inoculation (day 8) – See Fig.15. McAllister and colleagues were most interested in assessing the effects of a single dose of ZOL on HSCs *in vivo,* with potential to further establish consequences on tumour cell homing and metastatic outgrowth in bone. These studies have shown rapid effects on HSCs 72hrs post ZOL treatment in the NCr-Nu (nude) mice, hence the intracardiac inoculation of tumour cells 72hrs post pre-treatment.

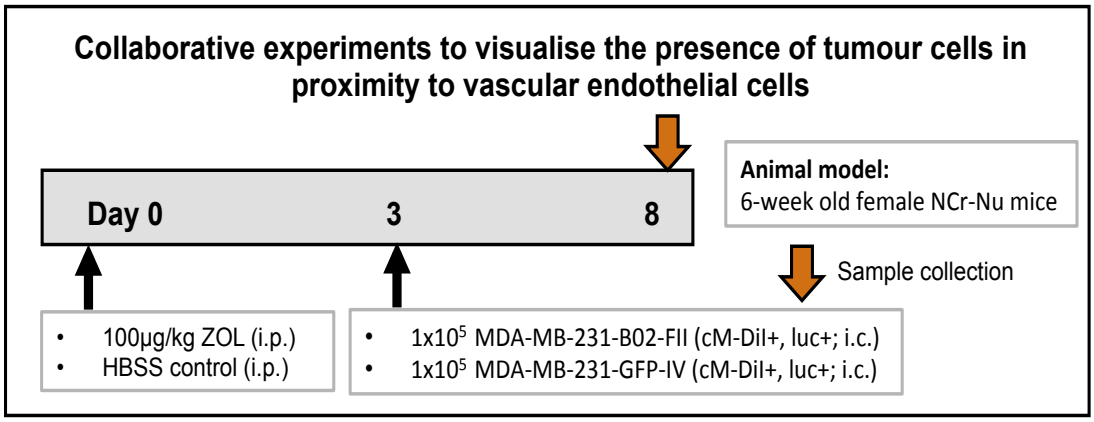


**Figure 15 Experimental outline – Collaborative experiments**
In collaborative experiments the effects of ZOL pre-treatment on tumour cell homing to bone were established in 6-week old female NCr-Nu (nude), CrTac:NCr-Foxn1$^{nu}$ mice (n=5/group). Animals were treated with a single dose of ZOL (100µg/kg, 100µL, i.p.) or HBSS control (100µL, i.p.). Three days post injection 1x10$^5$ cM-DiI- labelled MDA-MB-231-GFP-IV or MDA-MB-231-B02-FII breast cancer cells were injected intracardiac and effects on tumour cell homing to bone assessed on day 8 (5 days post i.c. injection). Here I collected bone samples to visualise tumour cells in proximity to vascular endothelial cells.

#### 3.5.3.3. Pilot experiment to establish if pre-treatment with a single dose of ZOL affects the development of bone metastasis

To establish the consequences of ZOL pre-treatment on the development of bone metastasis, immunocompromised 6-week old female GFP Ob$^+$ mice received a single dose of ZOL (100µg/kg, 100µL, i.p.) or PBS (100µL) on day 0 followed by intracardiac injection of 1x10$^5$ MDA-MB-231-NW1-luc2 cells (performed by Dr. HK Brown, University of Sheffield) on day 5 as described in Chapter 2, section 2.2.8.2 (n=6/group). Development of bone metastases was monitored 2x weekly using bioluminescence signalling and visualised using the IVIS system as described in Chapter 2, section 2.2.9. This experiment was performed in 2 "batches" (6 days apart between experiment start) due to a subset of mice having lower body weight thus potentially complicating recovery from intracardiac injections. Data are represented as mean tumour number per mouse and corresponding time points for each "batch" pooled (*e.g.* tumour growth on day 11 post i.c. injection from experiment 1 pooled with day 12 post i.c. injection from experiment 2). The experiment was terminated upon observation of first signs of morbidity (Day 32 and 36 respectively).

### 3.5.4. Sample collection and analysis

#### 3.5.4.1. Bone cell quantification on histological sections

Osteoblasts and osteoclasts/mm trabecular bone surfaces were scored on 2 non-serial histological sections (3µm, H&E or TRAP-stained) using OsteoMeasure as described in Chapter 2, Section 2.2.10.7.1.

#### 3.5.4.2. Quantification of the proteoglycan-rich area

Toluidine blue staining to visualise ZOL-induced alterations to extracellular matrix composition was performed as described in Chapter 2, Section 2.2.10.5.3. The proteoglycan-rich area in the bone (in particular in the epiphysis) was quantified using OsteoMeasure software (OsteoMetrics), Leica DMRB upright microscope and a 2.5x objective. It was interactively drawn around the area of interest (AOI), which comprised the proteoglycan-rich growth plate and all trabecular bone surfaces (with dark purple staining) directly connected to the epiphysis (see Fig.16 for schematic illustration). All cortical bone surfaces were excluded from analysis as well as trabecular bone surfaces not directly connected to the dense network of trabeculi at the epiphysis – see Figure 16.

#### 3.5.4.3. Bone cell activity

Serum was collected as described in Section 2.2.10.1, Chapter 2 and PINP levels (osteoblast activity) or TRAP levels (osteoclasts) measured using ELISA according to manufacturers instructions (Section 2.2.10.8.1/2, Chapter 2). For collaborative experiments the PINP ELISA was performed in conjunction with J. Ubellacker, using plasma samples of mice treated with ZOL or PBS. In these experiments the Mouse procollagen I N-terminal peptide, PINP ELISA Kit (MyBioSource MBS703389) was used.

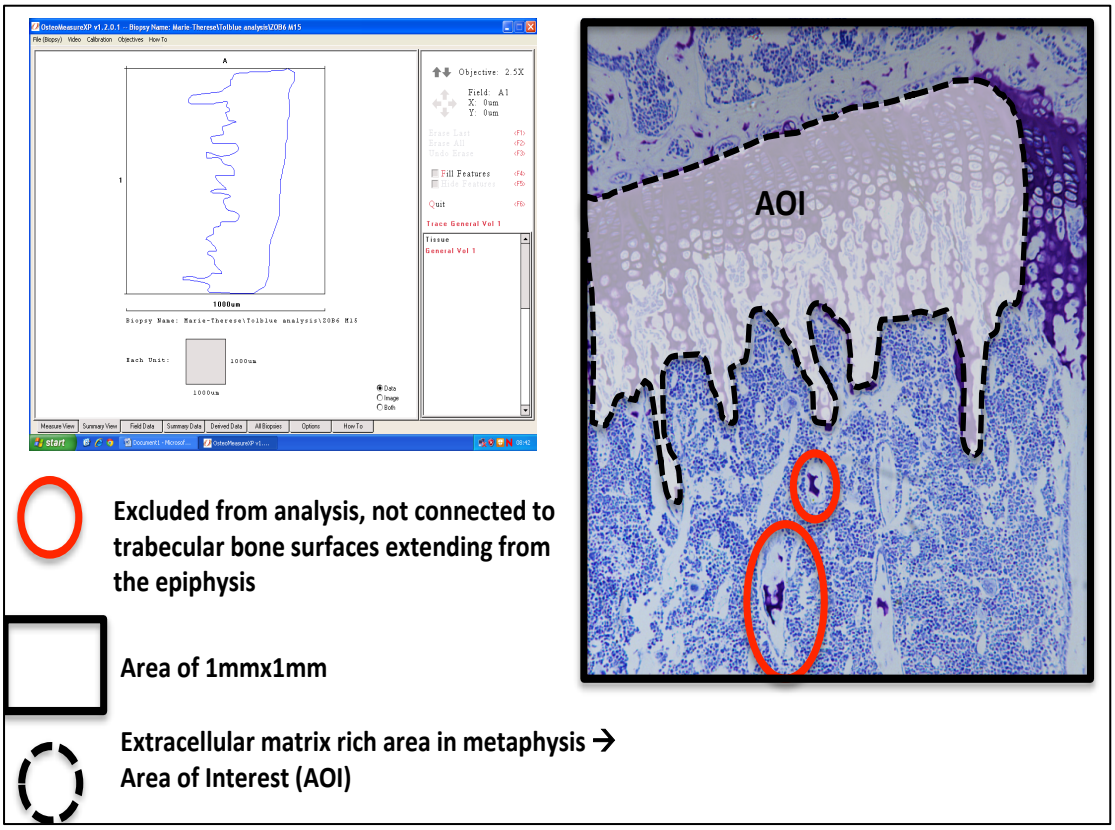


**Figure 16 Quantification of extracellular matrix (ECM)/ proteoglycan rich area in bone.**
Using OsteoMeasure software it was interactively drawn around the area of interest (AOI) which covered the proteoglycan-rich epiphysis and all trabecular bone surfaces directly connected to it. Bone disconnected from the trabeculi extending the epiphysis were excluded from analysis (red circle). OsteoMeasure software was used, using an Leica DMRB upright microscope, 2.5x objective. Proteoglycan-rich matrix area (in $mm^2$) was quantified for a total region of interest of $1mm^2$ for each sample. All cortical bone surfaces were excluded from analysis. Toluidine blue stained histological sections of tibiae were used for quantification (3µm thick, paraffin embedded)

### 3.5.4.4. Bone samples for µCT analysis

µCT analysis for 6-week old female BALB/c nude mice was performed as described in Section 2.2.10.4, Chapter 2. For NCr-Nu (nude) mice a SkyScan 1272 (SkyScan) was used. Femurs were scanned using 200mA, 51kV, a 0.5mm aluminium filter, medium camera resolution of 2016x1344 and pixel size set to 4.3µm. Images were reconstructed using NRecon software and a bone volume of interest (VOI) was determined by interactively drawing on the two-dimensional images. Analysis was started from a fixed offset 0.7mm away from the lower part of the growth plate covering a length of 1.5mm. Obtained grey scale images of the VOI were converted into binary images (threshold 95-225) and bone parameters calculated using CTAn software.

#### 3.5.4.5. Bone samples for two-photon microscopy

To visualise presence of single tumour cells in bone using two-photon microscopy dissected bones were wrapped in foil on day of sacrifice, snap frozen in $lN_2$ and stored at -80°C. One day before analysis bones were embedded in Optimal Cutting Temperature (OCT) medium (VWR, 361603E) in plastic moulds and left to settle at -80°C. On day of analysis the growth plate was exposed using a Bright OTF Cryostat with a 3020 microtome (Bright Instrument Co. Ltd, Huntingdon, UK). For imaging the tibia was placed on a glass bottom dish with the exposed growth plate facing downwards, covered by aluminium foil and immediately taken to the Zeiss LSM510 NLO upright multiphoton/confocal microscope (Carl Zeiss Inl, Cambridge, UK). A 20x/0.8 lens and visual light were used to focus on the edge of the growth plate prior to visualisation of bone and tumour cells using corresponding lasers. LMS software version 4.2 (Zeiss) was used, MTS files and temporary databases were generated for each individual sample and a stack area of 2104µm x 2525µm with 70µm depth captured. Presence of CM-DiI and DiD labelled tumour cells was visualised using a 543nm and 633nm laser respectively. Bone was visualised using the 900nm laser (Coherent, Santa Clara, CA.). Quantification of DiD+ve events within selected regions of interest was analysed using the Volocity 3D Image Analysis software 6.01 (PerkinElmer, Cambridge, UK). Two-photon microscopy and analysis to quantify the presence of DiD+ve tumour cells was kindly performed by Dr. HK Brown, University of Sheffield UK (Fig.32). Once trained on the two-photon microscope I indeed performed the two-photon scans for a subset of samples from collaborative experiments described in Fig.17, to visualise the presence of CM-DiI+ve MDA-MB-231-B02-FII cells in bone (see Figure 33/34).

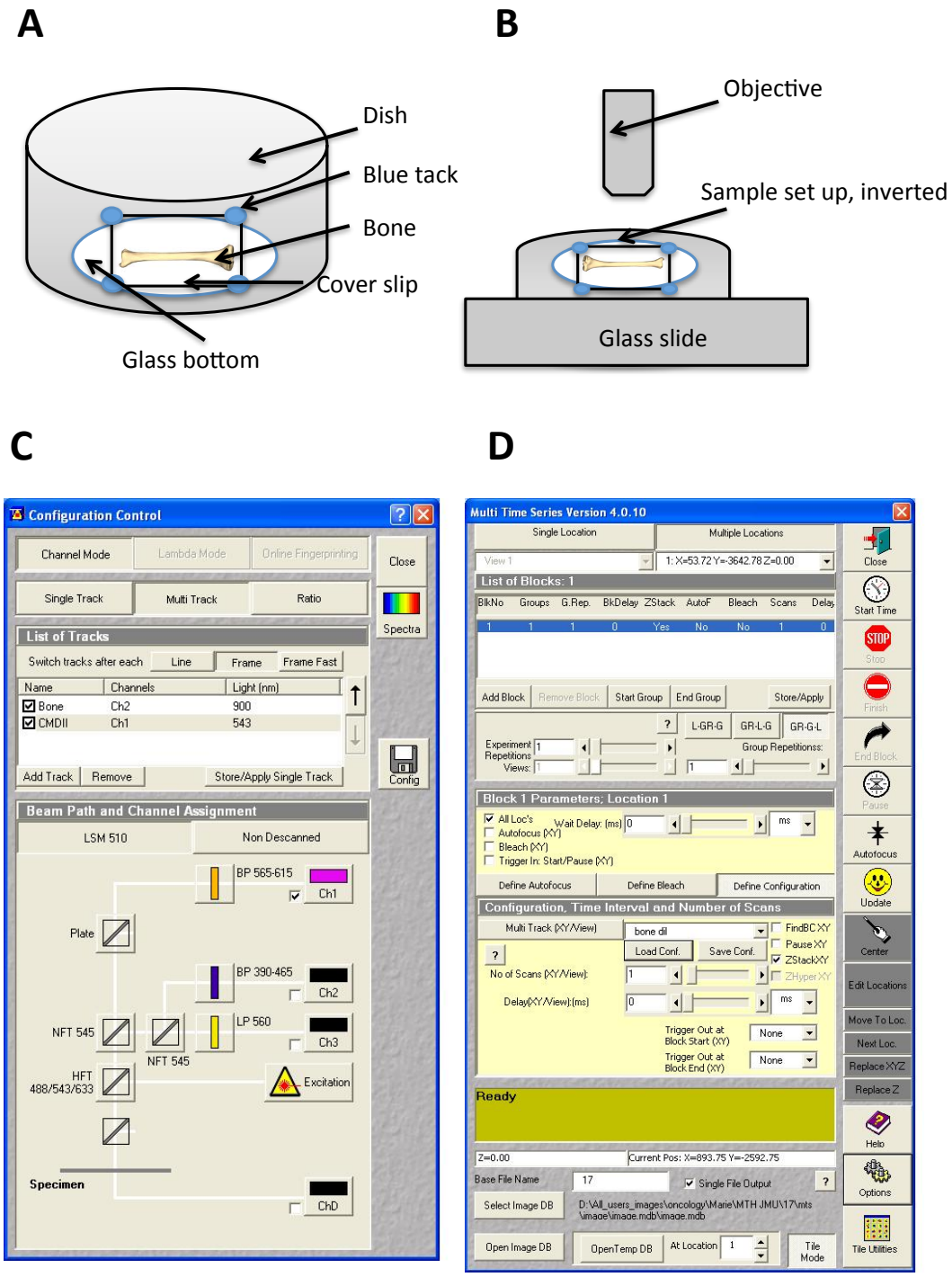


**Figure 17 Experimental setup for two-photon analysis.**
(A&B) shows the set up of the bone sample for two-photon analysis, (C) representative laser settings (top) and tile scan settings (bottom) for the detection of CM-DiI positive tumour cells in bone for collaborative experiments. Multi Time Series (MTS) settings are illustrated in (D).

#### 3.5.4.6. Flow cytometry

Presence of DiD+ve tumour cells in the bone marrow and circulation was assessed using flow cytometry. Briefly, whole blood was collected in syringes pre-wetted with heparin and total blood volume retrieved from each mouse recorded. Red blood cells were lysed using the Whole blood erythrocyte lysing kit (R&D) according to manufacturers instructions. To collect bone marrow, hind legs were dissected and the end bit of the bones cut off and bone marrow flushed by inserting a 25G needle attached to a 10mL syringe filled with PBS. Flushing was repeated until the bones appeared translucent and samples pooled for each treatment group. Bone marrow flushes were centrifuged at 1500rpm (MSE mistral 2000; ≈403xg) for 3min at ambient temperature, the supernatant discarded and cell pellets resuspended in 1X Whole blood erythrocyte lysing kit (R&D). Red blood cell lysis was performed according to manufacturers guidelines. Samples were passed through a 70µm nylon cell strainer prior to analysis in PBS containing 10% FBS. The number of circulating DiD+ve events was assessed by flow cytometry using the Red 633nm laser on the LSRII flow cytometer (BD Biosciences). Flow cytometry samples were run by the Flow Cytometry Core Facility, University of Sheffield. Bone marrow and blood samples were pooled for each treatment group respectively, and experiments repeated twice.

#### 3.5.4.7. Visualise presence of tumours cells at experimental endpoint

To visualise presence of established tumours in organs and bones at experimental endpoint, organs and bones were excised and bioluminescence signal was visualised using the IVIS system.

#### 3.5.4.8. *Ex vivo* organ cultures

To establish whether ZOL treatment causes tumour cells to home to other (non bone) sites *ex vivo* organ cultures of lung, liver, brain, spleen, remaining bone marrow and blood suspensions were prepared. Briefly, organs were mechanically disrupted using scissors and scalpels, passed through a 100µm cell strainer and plated into 6-well plates containing DMEM + GlutaMAX + Pyruvate supplemented with 10%FCS, 5% Pen Strep, 5% fungizone. After 48hrs growth media was additionally supplemented with 1 mg/mL G418 to select for MDA-MB-231-NW1-luc2 breast cancer cells using antibiotic pressure. Medium was changed every other day and cells left to grow for 2 weeks at 37°C, 5% $CO_2$. Tumour cell growth was then visualised by bioluminescence using IVIS.

#### 3.5.4.9. Visualisation of ZOL-induced alterations to the bone marrow vasculature

Immunofluorescence staining against the vascular endothelial cell marker Endomucin (1:100, Endomucin V.7C7, rat monoclonal, Santa Cruz, sc-65495) and CD31 (1:100, DIA-310: Anti-CD31 (Ms) from Rat (Clone: SZ31)) was performed to visualise ZOL-induced effects on bone marrow vasculature as described previously in Chapter 2, Section 2.2.10.6.2.2.

#### 3.5.4.10. Statistical Analysis

Statistical analysis was performed using GraphPad Prism Version 6.0. Analysis was done using unpaired Student's t-test or 2-way ANOVA with Bonferroni's post-test. Statistical tests applied are specified underneath the corresponding figures or if no graphs are presented next to the raw data.

### 3.6. Results

I first established the effects of a single, clinically relevant, dose of ZOL (100µg/kg, i.p.) on bone and key bone cells in 6-week old female BALB/c nude mice, the xenograft model later used in all tumour studies. Establishing the duration of the effects of a single dose of ZOL in this animal model was of great importance as the majority of studies published to date have used repeated and/or clinically irrelevant dosing schedules [38, 159, 183, 241, 247, 259, 260]. This enabled the design of later experiments so that the arrival of tumour cells in bone coincided with the time point when ZOL-induced alterations to the BME had reached their peak.

#### 3.6.1. A single dose of ZOL rapidly affects bone volume and structure

The early effects of ZOL (100µg/kg) on trabecular and cortical bone volume of tibiae were established 3, 5 and 10 days post treatment using µCT analysis.

As early as 3 days after a single dose of ZOL trabecular bone volume (bone volume/tissue volume in %) of tibiae was nearly doubled when compared to control ($p \leq 0.01$, Fig.18A, Table 8). The increase in trabecular bone volume was maintained 10 days after injection ($p \leq 0.01$, Fig.18A, Table 8). Similarly, ZOL increased trabecular number on day 3 ($p \leq 0.05$; ≈63% increase) and 10 ($p \leq 0.01$; ≈71% increase) when compared to control (Fig.18B, Table 8). Trabecular thickness was significantly elevated 3 days ($p \leq 0.05$, Fig.18C, ≈16% increase, Table 8) post ZOL treatment whereas a reduction was determined on day 10 ($p \leq 0.05$, Fig.18C, Table 8, ≈12.5% decrease). Representative µCT cross sections are shown in Fig.18E&F.

**Table 8 Effects of a single dose of Zoledronic acid (ZOL, 100µg/kg) on bone.**
Trabecular bone volume (BV/TV in %), trabecular thickness (Tb.Th. in mm) and number (Tb.N. in $mm^{-1}$) was assessed 3, 5 and 10 days post treatment. ns is non-significant, * is $p \leq 0.05$, ** is $p \leq 0.01$; 2-way ANOVA with Bonferroni post-test, data show Mean±SEM, n=3 PBS, n=4 ZOL.

| | BV/TV (%) | | | Tb.Th. (mm) | | | Tb.N. ($mm^{-1}$) | | |
|---|---|---|---|---|---|---|---|---|---|
| **Day** | PBS | ZOL | p | PBS | ZOL | p | PBS | ZOL | p |
| **3** | 7.21 ± 1.39 | 13.40 ± 1.18 | ** | 0.032 ± 0.001 | 0.037 ± 0.001 | * | 2.25 ± 0.36 | 3.66 ± 0.28 | * |
| **5** | 12.60 ± 1.20 | 15.28 ± 1.20 | ns | 0.036 ± 0.001 | 0.036 ± 0.001 | ns | 3.52 ± 0.37 | 4.27 ± 0.42 | ns |
| **10** | 11.25 ± 1.30 | 17.01 ± 0.95 | * | 0.040 ± 0.001 | 0.035 ± 0.001 | * | 2.80 ± 0.23 | 4.81 ± 0.22 | ** |

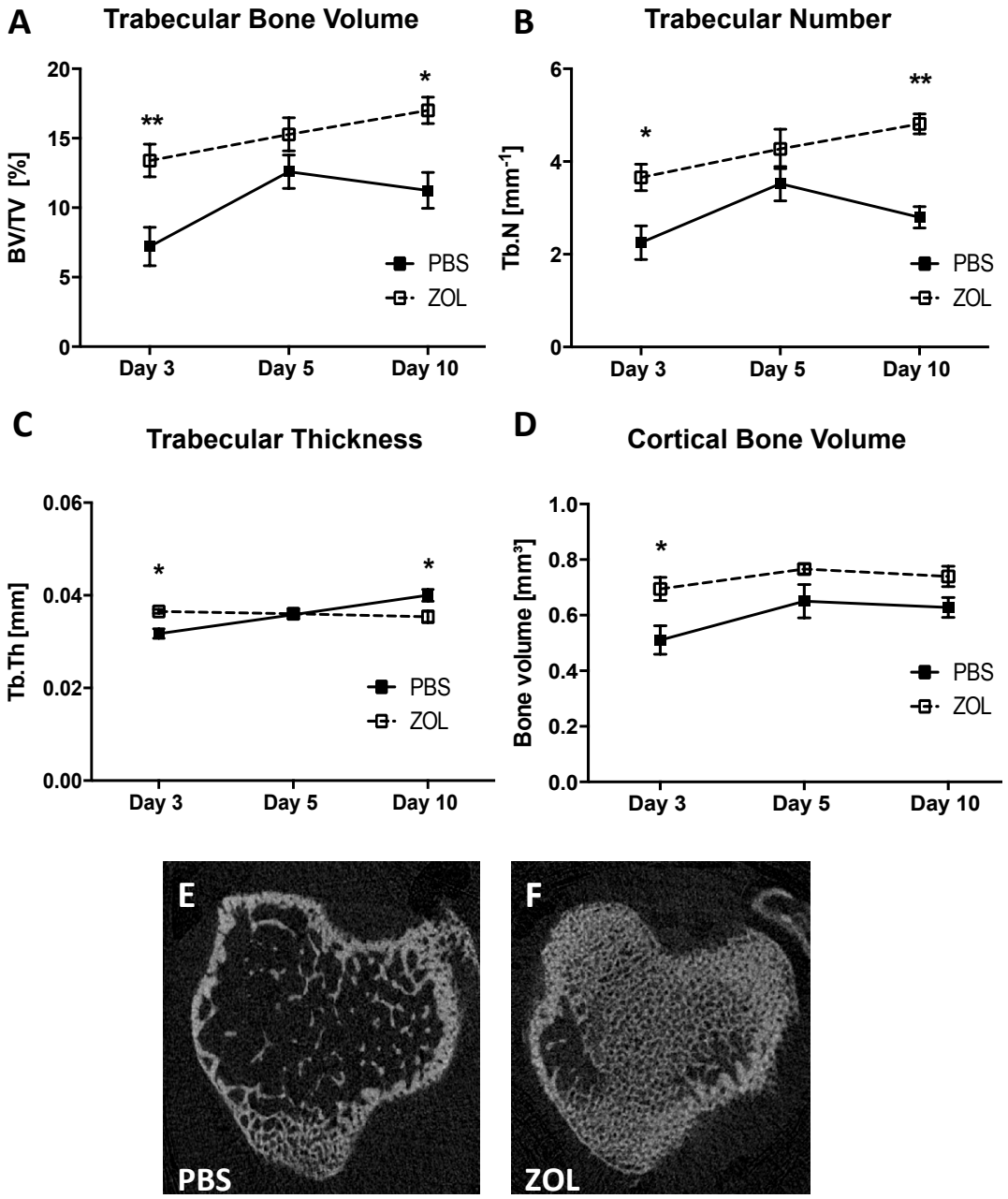


**Figure 18 Effects of a single dose of Zoledronic acid on bone volume and structure of tibiae.**
6-week old female BALB/c nude mice received a single dose of Zoledronic acid (ZOL, 100µg/kg, i.p.) or sterile PBS control on day 0. (A) Effects on trabecular bone volume (in % ), (B) number (in $mm^{-1}$) and (C) thickness (in mm) were determined using µCT analysis. Effects on cortical bone volume (in $mm^3$) are shown in (D). n=3 for PBS, n=4 for ZOL, * is p≤0.05, ** is p≤0.01, ns is non-significant, Two-way ANOVA with Bonferroni post-test, data show Mean±SEM. (E) shows representative cross sections from tibiae 10 days after (PBS) and (F) 100µg/kg ZOL injection, 0.5mm away from the epiphyseal growth plate.

I could not detect a significant increase in trabecular bone volume (HBSS: 8.13 ± 1.09% vs. ZOL: 10.56 ± 1.06%) and number (HBSS: 2.37 ± 0.24$mm^{-1}$ vs. ZOL: 3.23 ± 0.29$mm^{-1}$) 3 days post ZOL treatment relative to the control cohort when analysing femurs of 6-week old NCr-Nu (nude), CrTac:NCr-*Foxn1*$^{nu}$ mice, probably due to the small sample number and/or the early time point post ZOL treatment.

In 6-week old female BALB/c nude mice cortical bone volume of tibiae was significantly increased 3 days after a single dose of ZOL (PBS: 0.51 ± 0.05$mm^3$ vs. ZOL: 0.69 ± 0.04$mm^3$, p≤0.05, Fig.18D). The difference in cortical bone volume 5 and 10 days post injection did however not reach statistical significance (Day 5: PBS: 0.65 ± 0.06$mm^3$ vs. ZOL: 0.76 ± 0.02$mm^3$, Day 10: PBS: 0.63 ± 0.04 vs. ZOL: 0.74 ± 0.04, Fig.18D).

To summarise, both trabecular and cortical bone volume are rapidly increased following a single dose of ZOL, indicating substantial and quick response of bone to anti-cancer therapy in this model system (young mice with rapid bone turnover).

### 3.6.2. A single dose of ZOL rapidly modifies the cellular composition of the BME

I aimed to provide a detailed characterisation of the effects of ZOL on key bone cells, including osteoblasts and osteoclasts. In addition I wanted to determine the time point when ZOL-induced effects on the BME had reached their maximum as well as the duration of the effect(s). Therefore the number of osteoblasts and osteoclasts per mm trabecular bone surface was determined 3, 5, 8 and 10 days after one dose of ZOL (100µg/kg) or control on H&E and TRAP stained histological sections of tibiae (3µm thick, 2 non-serial levels).

#### 3.6.2.1. A single dose of ZOL rapidly alters osteoclasts

Bisphosphonates are potent inhibitors of osteoclastic bone resorption inducing apoptosis via interfering with the mevalonate pathway [261]. This experiment aimed to establish the acute (Day 3-10) effects of a single dose of ZOL on osteoclast number, activity and size.

There was a rapid and significant drop in osteoclast number 3 days post injection onwards (Day 3: p≤0.0001, ≈94% reduction; Day 5: p≤0.0001, ≈89% decrease, Table 9, Fig.19A). The osteoclast number in ZOL treated mice remained significantly decreased 10 days post injection (Day 10: p≤0.001, Table 9, ≈70% decrease, Fig.19A) when compared to control, however a slight increase compared to the earlier time points was observed. Histological TRAP-stained sections illustrating the effects of ZOL on osteoclasts are shown in Fig.23 below.

**Table 9 Effects of a single dose of Zoledronic acid on osteoclast number.**
Effects of a single dose of Zoledronic acid (100µg/kg) on osteoclasts in 6-week old BALB/c nude mice was assessed on two non-serial histological sections of TRAP stained tibiae 3,5 and 10 days post treatment. *** is p≤0.001, **** is p≤0.0001; 2-way ANOVA with Bonferroni post-test, data show Mean±SEM, n=3 PBS, n=4 ZOL.

| Osteoclast number/mm trabecular bone surface | | | |
|---|---|---|---|
| Day | **PBS** | **ZOL** | **p** |
| **3** | 7.30 ± 0.50 | 0.46 ± 0.050 | **** |
| **5** | 8.33 ± 1.25 | 0.91 ± 0.16 | **** |
| **10** | 7.88 ± 0.74 | 2.40 ± 0.60 | *** |

Collaborative experiments with Dr. McAllisters laboratory group in Boston, USA allowed me to analyse the effects of a single dose of ZOL (100µg/kg) on osteoclasts in a different mouse model. I was kindly provided with bone samples of tibiae of 6-week old female NCr-Nu (nude) mice. In agreement with my previous experiments, a significant reduction in osteoclast number/mm trabecular bone surface compared to control was detected 3 days after ZOL treatment (HBSS: 3.51±0.19 vs. ZOL: 0.30±0.06, p≤0.0001, Fig.20A), slowly starting to return to control levels by day 8 (HBSS: 3.51±0.56 vs. ZOL: 1.83±0.22, p≤0.05, Fig.20A).

Morphology of the remaining osteoclasts after ZOL treatment appeared altered in both 6 week old female BALB/c nude and NCr-Nu (nude) however this did not reach statistical significance (**BALB/c nude:** Day 3: PBS: $1.05x10^{-4} \pm 4.10x10^{-6}mm^2$ vs. ZOL: $1.59x10^{-4} \pm 3.35x10^{-5}mm^2$; Day 5: PBS: $9.70x10^{-5} \pm 4.16x10^{-6}mm^2$ vs. ZOL: $1.67x10^{-4} \pm 1.44x10^{-5}mm^2$; Day 10: PBS: $9.83x10^{-5} \pm 6.69x10^{-6}mm^2$ vs. ZOL: $1.42x10^{-4} \pm 1.69x10^{-5}mm^2$, Fig.19C, **NCr-Nu (nude):** (Day 3: HBSS: $1.99x10^{-4} \pm 3.14x10^{-5}$ $mm^2$ vs. ZOL: $1.21x10^{-4} \pm 1.71x10^{-5}$ $mm^2$; Day 8: HBSS: $1.06x10^{-4} \pm 2.14x10^{-5}$ $mm^2$ vs. ZOL: $1.25x10^{-4} \pm 1.24x10^{-5}$ $mm^2$, Fig.20B).

The reduction in osteoclast number lining trabecular bone surfaces was mirrored by a rapid and significant reduction in serum TRAP levels (used as a measure of osteoclast activity) three (PBS: 7.18 ± 1.94 U/L vs. ZOL: 2.46 ± 0.28 U/L, p≤0.001, Fig.19B) and five (PBS: 5.69 ± 0.52 U/L vs. ZOL: 1.97 ± 0.08 U/L, p≤0.01) days after administration of ZOL. Serum TRAP levels reached that of control mice on day 10 (PBS: 3.88 ± 0.33 U/L vs. ZOL: 2.61 ± 0.37 U/L, Fig.19B) reflecting the osteoclast quantification data.

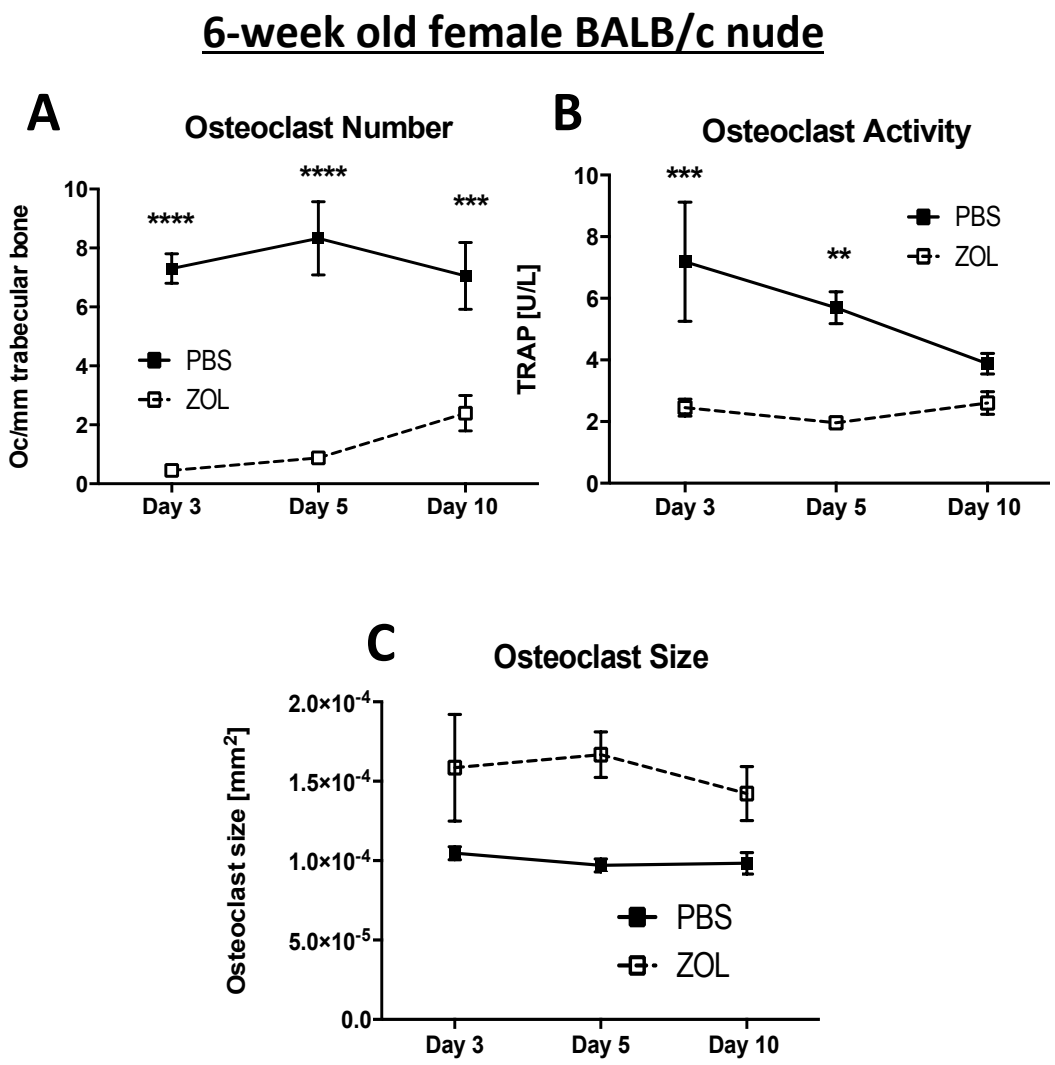


**Figure 19 Effects of a single dose of zoledronic acid on osteoclasts in 6-week old female BALB/c nude mice.**

6-week old female BALB/c nude mice received a single dose of Zoledronic acid (ZOL, 100µg/kg, i.p.) or sterile PBS control on day 0. Effects on (A) osteoclast number/mm trabecular bone surface, (B) osteoclast activity (serum TRAP levels) and (C) osteoclast size was assessed 3, 5 and 10 days post injection. n=3 for PBS, n=4 for ZOL, Day 5: n=4/group for TRAP, ** is p≤0.01,*** is p≤0.001,**** is p≤0.0001, Two-way ANOVA with Bonferroni post-test, data show Mean±SEM.

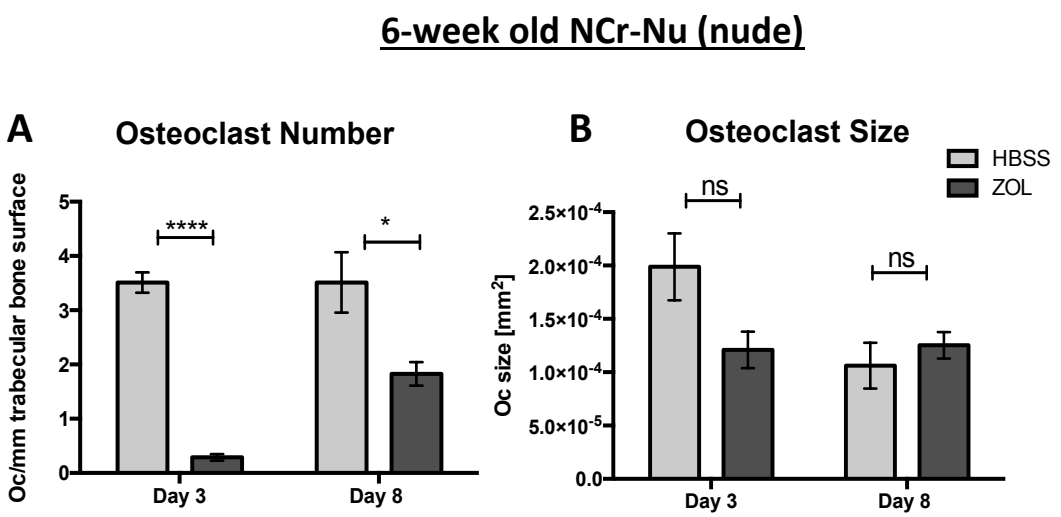


**Figure 20 Effects of a single dose of zoledronic acid on osteoclasts in 6-week old female NCr-Nu (nude) mice.**
6-week old female NCr-Nu (nude) mice received a single dose of Zoledronic acid (ZOL, 100µg/kg, i.p.) or HBSS control. Effects on (A) osteoclast number/mm trabecular bone surface and (B) osteoclast size was assessed 3 and 8 days post injection Day 3: n=4/group, Day 8: n=5 for PBS, n=4 for ZOL, **** is p≤0.0001, * is p≤0.05, ns is non-significant. Student's t-test, data show Mean±SEM.

In summary, a single and clinically relevant dose of ZOL rapidly affects the number and activity of osteoclasts *in vivo.* ZOL-induced effects on osteoclasts reached their peak 3 days after the single injection and started to return to control levels from day 10 onwards.

#### 3.6.2.2. Effects on osteoblasts

To establish if the increased bone volume following ZOL administration is a result of increased osteoblast-mediated bone formation the number of osteoblasts lining trabecular bone surface and their activity (measured by serum PINP levels) was determined.

Interestingly, osteoblast number/mm trabecular bone surface in ZOL treated mice decreased significantly from day 5 onwards when compared to control (PBS: 14.73 ± 1.79 vs. ZOL: 6.62 ± 0.88, p≤0.05, Fig.22A). The drop in the number of osteoblasts lining trabecular bone surfaces was even more prominent by day 10 (PBS: 15.65 ± 3.06, vs. ZOL: 5.66 ± 0.85, p≤0.01, Fig.22A). Histological TRAP-stained sections illustrating the effects of ZOL on osteoclasts are illustrated in Fig.23 below. The reduction in osteoblast number was reflected by a drop in serum PINP levels (used as a measure for osteoblast activity). Osteoblast activity was reduced from day 3 onwards (Day 3: PBS: 281.0 ± 76.70 vs. ZOL: 65.62 ± 4.69ng/mL, p≤0.01; Day 5: PBS: 157.1 ± 55.43ng/mL vs. ZOL: 63.00 ± 6.03ng/mL; Day 10: PBS: 91.05 ± 12.56ng/mL vs. ZOL: 78.22 ± 12.98ng/mL, Fig.22B).

In addition a significantly higher osteoblast per osteoclast ratio compared to control mice (PBS: 2.13 ± 0.39% vs. ZOL: 21.39 ± 3.67%, p≤0.0001, Fig.22C) was observed 3

days after the single dose of ZOL normalised to control levels on day 10 (PBS: 2.48 ± 0.69% vs. ZOL: 2.93 ± 0.79% Fig.22C).

Similar effects were observed when analysing bone and plasma samples from 6-week old female NCr-Nu (nude) mice that had received a single dose of ZOL (100µg/kg, i.p.). In agreement with the effects of ZOL observed in 6-week old female BALB/c nude mice, osteoblast number/mm trabecular bone surface (Day 3: HBSS: 9.92±1.64 vs. ZOL: 2.88±0.68, p≤0.01; Day 8: HBSS: 10.87±1.35 vs. ZOL: 1.05±0.51, p≤0.001, Fig.21A) and PINP plasma levels (Day 3: PBS: 198.2 ± 38.91 pg/mL, vs. ZOL: 79.02 ± 3.803 pg/mL, p≤0.05; Day 8: PBS: 268.9 ± 11.11 pg/mL vs. ZOL: 132.9 ± 32.29 pg/mL, p≤0.01, Fig.21B) were significantly reduced 3 and 8 days after the single dose of ZOL.

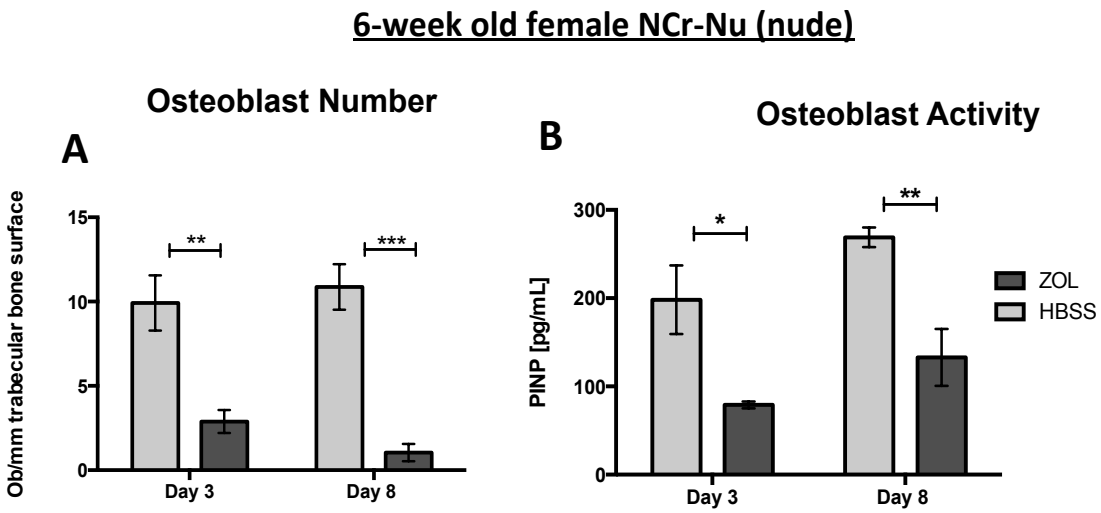


**Figure 21 Effects of a single dose of Zoledronic acid on osteoblasts in 6-week old female NCr-Nu (nude) mice.**

6-week old female NCr-Nu (nude) mice received a single dose of Zoledronic acid (ZOL, 100µg/kg, i.p.) or sterile HBSS control on day 0. Effects on (A) osteoblast number/mm trabecular bone surface and (B) osteoblast activity (serum PINP levels) was assessed 3 and 8 days post injection Day 3: n=4/group, Day 8: n=5 for PBS, n=4 for ZOL, *** is p≤0.001, ** is p≤0.01,* is p≤0.05, ns is non-significant. Student's t-test, data show Mean±SEM.

# 6-week old female BALB/c nude

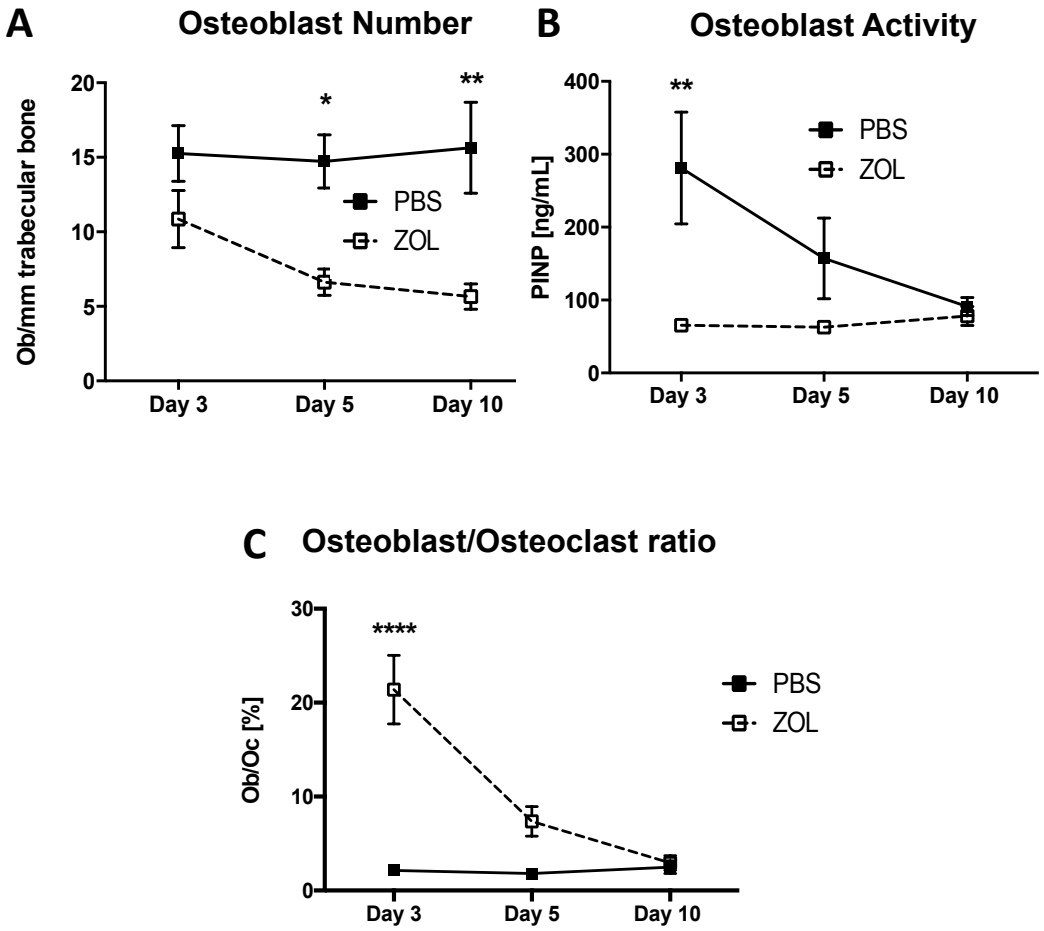


**Figure 22 Effects of a single dose of Zoledronic acid on osteoblasts in 6-week old female BALB/c nude mice.**

6-week old female BALB/c nude mice received a single dose of Zoledronic acid (ZOL, 100µg/kg, i.p.) or sterile PBS control on day 0. Effects on (A) osteoblast number/mm trabecular bone surface, (B) osteoblast activity (serum PINP levels) and (C) osteoblast/osteoclast ratio was assessed 3, 5 and 10 days post injection. n=3 for PBS, n=4 for ZOL, Day 5: n=4/group for PINP, * is p≤0.05,** is p≤0.01,**** is p≤0.0001, Two-way ANOVA with Bonferroni post-test, data show Mean±SEM.

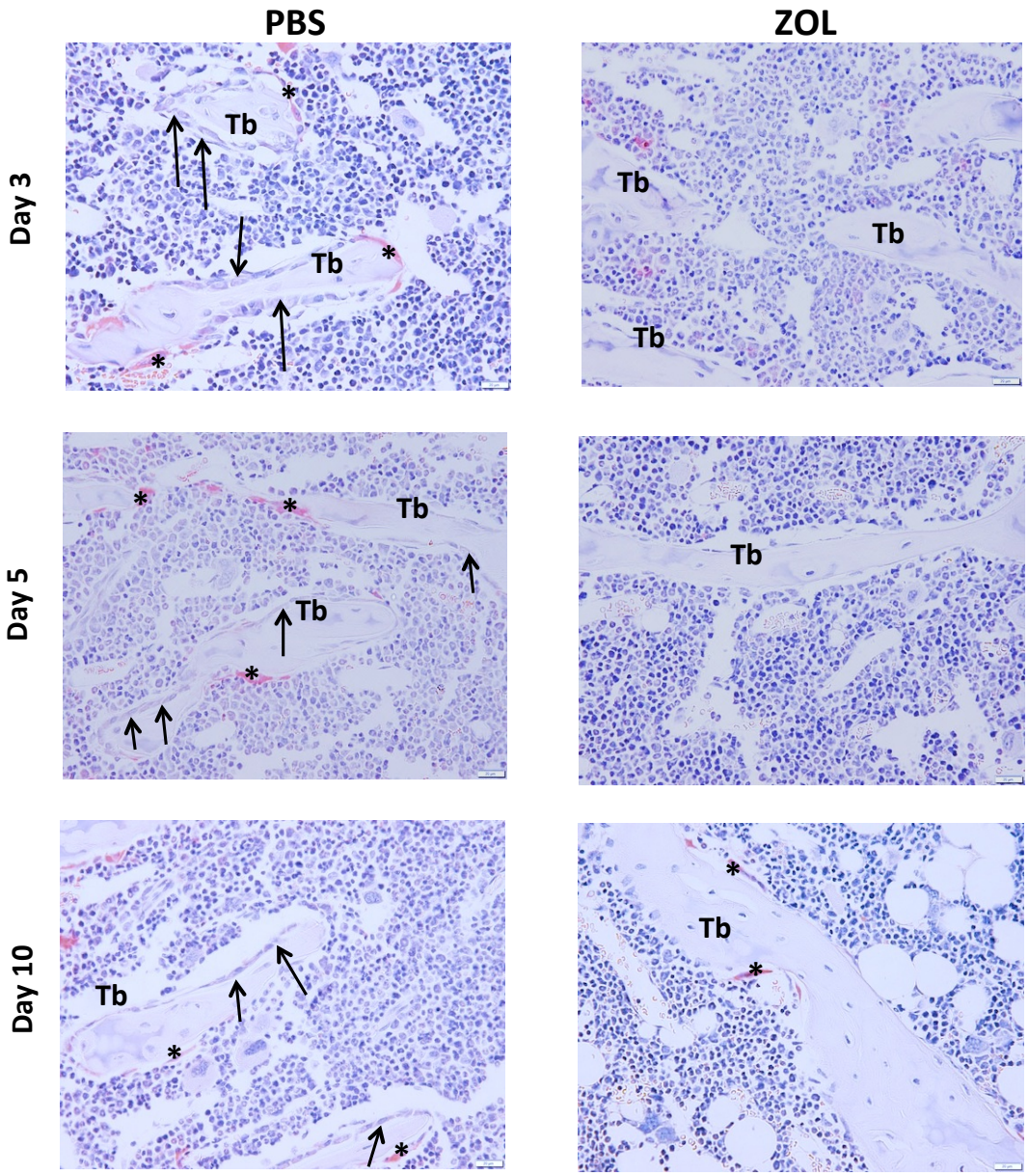


**Figure 23 Histological TRAP stained sections illustrating the effects of a single dose of Zoledronic acid on osteoblasts and osteoclasts *in vivo*.**

6-week old female BALB/c nude mice received a single dose of Zoledronic acid (ZOL, 100µg/kg, i.p.) or sterile PBS control on day 0. Effects on osteoblasts and osteoclasts were assessed 3,5 and 10 days post injection. Representative TRAP stained sections of tibiae from (left panel) PBS and (right panel) ZOL treated mice are illustrated. Black arrowheads point out osteoblasts, osteoclasts are indicated with black asterisk. Tb= trabecular bone. Scale bar is 20µm, 40x objective, Olympus BX53.

Taken together, these data support that ZOL does not only affect bone resorbing osteoclasts but also rapidly decreased activity and number/mm trabecular bone surface of bone forming osteoblasts in these experiments.

#### 3.6.2.3. Effects of Zoledronic on extracellular matrix composition

Osteoclasts are responsible for initiating the remodelling of calcified cartilage into cancellous bone. At the edge of the growth plate newly formed cartilage (either from chondrocytes or osteoblasts) gets resorbed by osteoclasts. To determine if the rapid reduction in osteoclast number and activity after the single dose of ZOL affects the presence of proteoglycan-rich extra cellular matrix (ECM) ZOL-induced modification of the proteoglycan rich ECM was visualised using toluidine blue staining and quantified using OsteoMeasure.

The single injection of ZOL significantly increased the proteoglycan-rich matrix area in the metaphysis which stretched deeper into the extending front of the growth plate in ZOL treated mice when compared to control from day 5 onwards (Day 5: PBS: 0.321 ± 0.015mm$^2$ vs. ZOL: 0.449 ± 0.023mm$^2$, p≤0.05, Fig.24A&C). The proteoglycan rich area extended even further down the metaphysis 10 days after ZOL treatment (Day 10: PBS: 0.313 ± 0.021mm$^2$ vs. ZOL: 0.480 ± 0.028mm$^2$, p≤0.01, Fig.24A&C). The ZOL-induced increase in bone volume may therefore be a result of elevated endochondral ossification, as this excess matrix is normally resorbed by osteoclasts. Similar results were observed in female NCr-Nu (nude) mice (Day 3: HBSS: 0.371 ± 0.021mm$^2$ vs. ZOL: 0.473 ± 0.022mm$^2$, p≤0.05; Day 8: 0.347 ± 0.012mm$^2$ vs. ZOL: 0.539 ± 0.0190 mm$^2$, p≤0.01, Fig.24B).

To summarise, a single dose of ZOL does not only affect the cellular but also the extra-cellular composition of the bone metastasis niche.

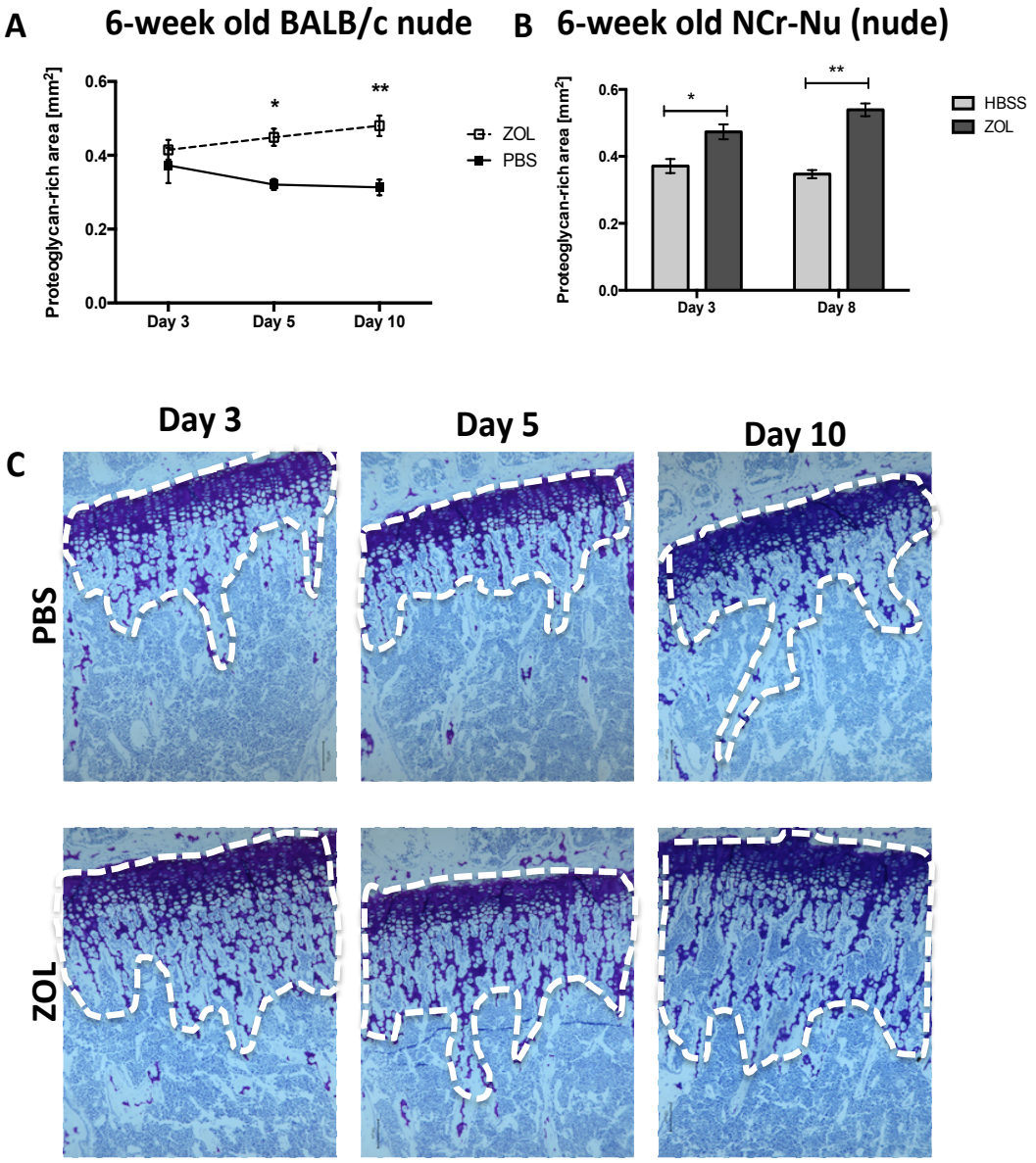


**Figure 24 Visualisation of ZOL-induced effects on extracellular matrix composition.**
Alterations in proteoglycan/extracellular matrix composition of the epiphysis and metaphysis of tibiae were visualised by Toluidine blue staining on 3µm sections of tibiae from 6-week old female BALB/c nude mice. OsteoMeasure software was used to quantify the proteoglycan-rich area (white dashed line, shown in C) 3, 5 and 10 days after a single dose of ZOL (100µg/kg, bottom panel) or PBS control (top panel). n=3/group and time point, only one histological level was quantified. 2-way ANOVA with Bonferroni's post-test. ** is p≤0.01, * is p≤0.05.). Scale bar is 100µm. (B) quantification data for 6-week old NCr-Nu (nude) mice Day 3: n=4 for PBS, n=3 for ZOL, Day 8: n=3/group. Student's t-test. Data show Mean±SEM.

### 3.6.3. Effects of Zoledronic acid on the bone marrow vasculature

By using fluorescent markers against endothelial cells work published by Kusumbe *et al.* provided detailed information about the organisation, functional specialisation and precise function of the skeletal vasculature in mice [51]. Vasculature in the methaphysis is described as straight columns being interconnected by vessel loops or arches. Vasculature in the diaphysis in contrast was highly branched. Additionally both metaphyseal and diaphyseal vasculature were interconnected forming one vascular bed [51]. As ZOL induced rapid modification in the cellular es well as extracellular BME I aimed to visualise if the single dose of ZOL also alters the bone marrow vasculature. Therefore I performed immunofluorescence staining against the vascular endothelial cell marker Endomucin on 30µm sections of tibiae from mice treated with 100µg/kg ZOL or PBS control (samples were collected 3 days post injection from collaborative experiments, NCr-Nu nude mice).

In the control cohort (2 out of 3) I observed distinct connection and organisation of Endomucin +ve vasculature in the metaphysis and diaphysis as described in [51], with long, branched tubular vessels occupying the metaphysis and a more sinusoidal patterning in the diaphysis (representative images shown in Fig.25A-D, 26A-L).

The organisation and interconnection between the metaphyseal and diaphyseal vasculature appeared to be affected by ZOL treatment (3 out of 3). There appeared to be increased numbers of small, dilated and rounded vessels in the diaphysis 72 hours after the single injection of ZOL (2 out of 3, qualitative data). The third biological replicate showed small vessels, but these were not rounded or dilated, Fig.25&26. The presence of endothelial vascular cells is detrimental for endochondral ossification at the epiphysis. Given the observed alteration to the structural organisation of the epiphysis and increased trabecular bone volume, I assessed potential alterations in CD31+ve vascular endothelial cells adjacent to the epiphysis. However, no apparent difference in organisation and structure of the CD31+ve bone marrow vasculature was observed 3 days after treatment in the ZOL-treated cohort when compared to the control cohort (Fig.27).

To summarise, a single dose of ZOL appears to alter structural organisation of the bone marrow vasculature 3 days after injection.

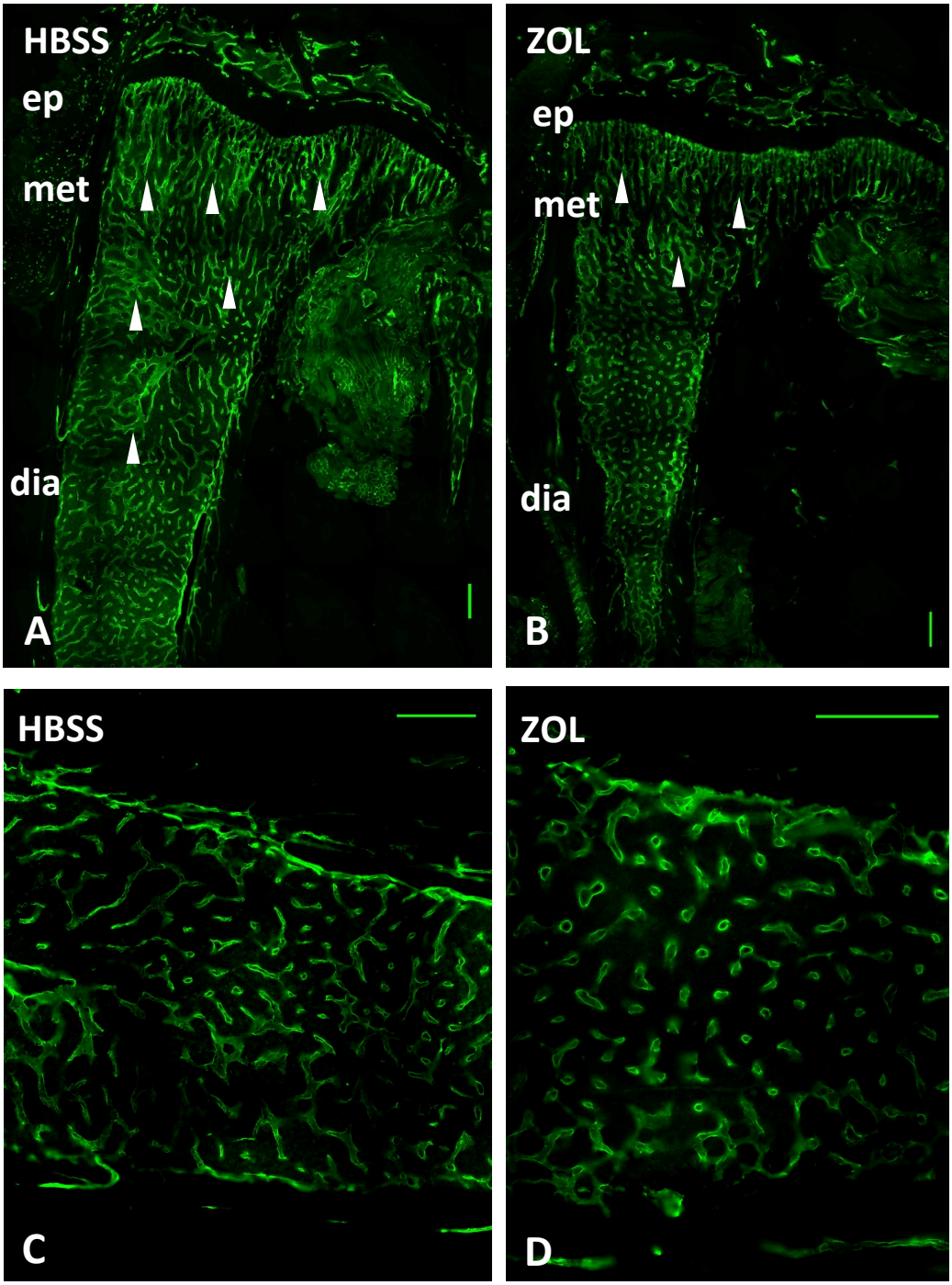


**Figure 25 Effects of a single dose of Zoledronic acid (ZOL) on bone marrow vasculature.**
3 days after a single dose of (A&C) HBSS (100µL, i.p.) or (B&D) 100µg/kg ZOL (100µL, i.p.) right tibiae of 6-week old NCr-Nu (nude), CrTac:NCr-Foxn1$^{nu}$ mice were collected. Treatment effects on on bone marrow vasculature was visualised using immunofluorescence staining against the vascular endothelial cell marker Endomucin on 30µm thick sections of gelatine embedded tibiae. (A-D) 8x8 tile scans captured with 20x objective using the Nikon Eclipse Ti, NIS-Elements-software Version 4.30, CFI Plan Fluor 20x MI (NA 0.75), Endomucin+ve vascular endothelial cells = green (Alexa555) Ep is epiphysis, met is metaphysis, dia is diaphysis. Scale bar is 250µm.

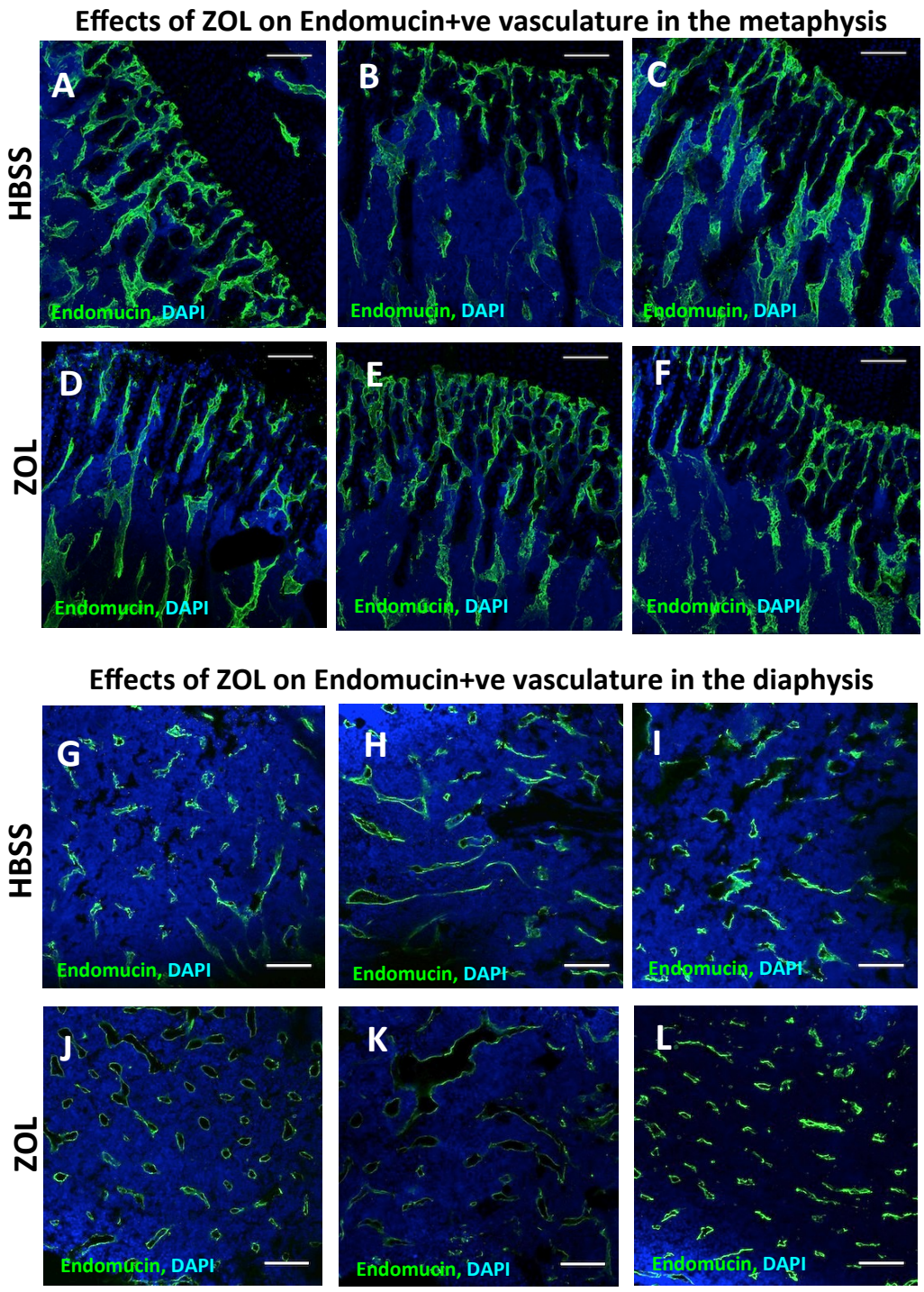


**Figure 26 Visualisation of the effects of a single dose of Zoledronic acid (ZOL) on bone marrow vasculature.**

3 days after a single dose of (A-C,G-I) HBSS (100µL, i.p.) or (D-F,J-L) 100µg/kg ZOL (100µL, i.p.) right tibiae of 6-week old NCr-Nu (nude), CrTac:NCr-Foxn1$^{nu}$ mice were collected. Treatment effects on bone marrow vasculature in the metaphysis (A-F) and (G-L) diaphysis were visualised using immunofluorescence staining against the vascular endothelial cell marker Endomucin on 30µm thick sections of gelatine embedded tibiae. (A-F) Z-stacks with a depth of 20µm and (G-L) confocal images, both aquired with Nikon A1 Confocal microscope, NIS-Elements-software Version 4.30, CFI Plan Fluor 20x MI (NA 0.75), Endomucin+ve vascular endothelial cells = green (Alexa555), nuclei = blue (DAPI). Scale bar is 100µm. n=3/group.

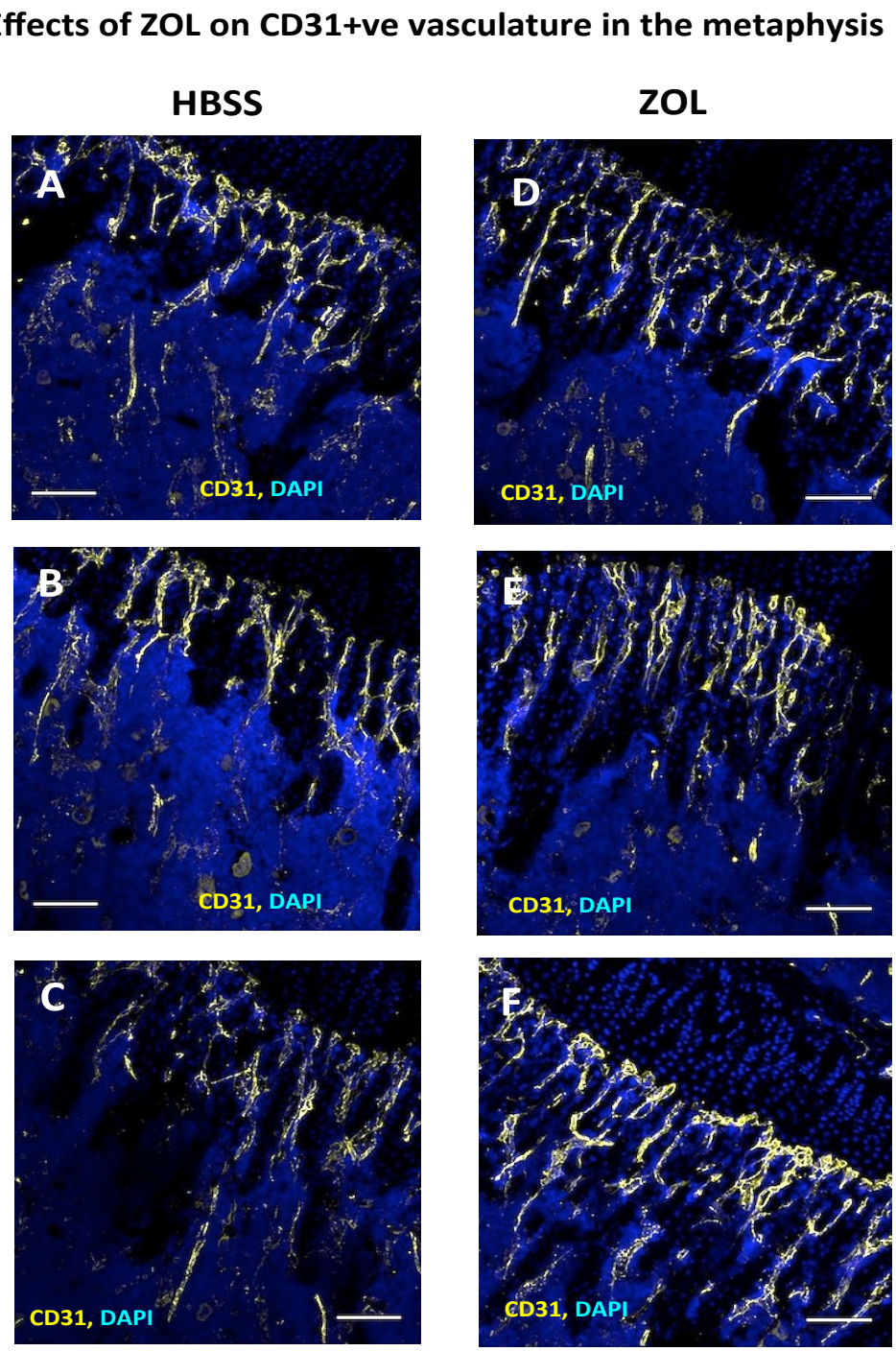


**Figure 27 Effects of a single dose of Zoledronic acid (ZOL) on CD31+ve bone marrow vasculature.** 3 days after a single dose of (A-C) HBSS (100µL, i.p.) or (D-F) 100µg/kg ZOL (100µL, i.p.) right tibiae of 6-week old NCr-Nu (nude), CrTac:NCr-Foxn1$^{nu}$ mice were collected. Effects of ZOL on CD31+ve bone marrow vasculature in the metaphysis was visualised using immunofluorescence staining against the vascular endothelial cell marker CD31 on 30µm thick sections of gelatine embedded tibiae. Z-stacks with a depth of 20µm were aquired using the Nikon A1 Confocal microscope, NIS-Elements-software Version 4.30, CFI Plan Fluor 20x MI (NA 0.75), CD31+ve vascular endothelial cells = yellow (Alexa555), nuclei = blue (DAPI). n=3/group.

### 3.6.4. Effects of ZOL pre-treatment on tumour cell homing

Two independent experiments using mature (8-13-week old) female BALB/c mice (heterozygote or homozygote nude, n=4/group in each experiment) with GFP expressing cells of the osteoblastic lineage were performed to assess if the ZOL-induced alterations to the BME affect tumour cell homing to bone *in vivo*. Briefly, mice were injected with a single dose of ZOL (100µg/kg, i.p.) or PBS on day 0 followed by intracardiac injection of DiD labelled MDA-MB-231-NW1 (luciferase+ve) tumour cells on day 5, when the previous experiments had shown that ZOL effects on the BME were most prominent. Samples were collected 5 days after tumour cell injection and the presence and location of tumour cells in circulation, soft tissue and bone assessed.

To confirm the therapeutic effects of ZOL in these experiments one mouse/group was sacrificed 5 days after the single dose of ZOL and trabecular bone volume determined using µCT. As expected, trabecular bone volume was higher after administration of ZOL when compared to control (PBS: 14.81% vs. ZOL: 16.72%, Fig.28A) and histological slides of tibiae additionally demonstrated the expected reduction in osteoblast number at this time point (Fig.28B).

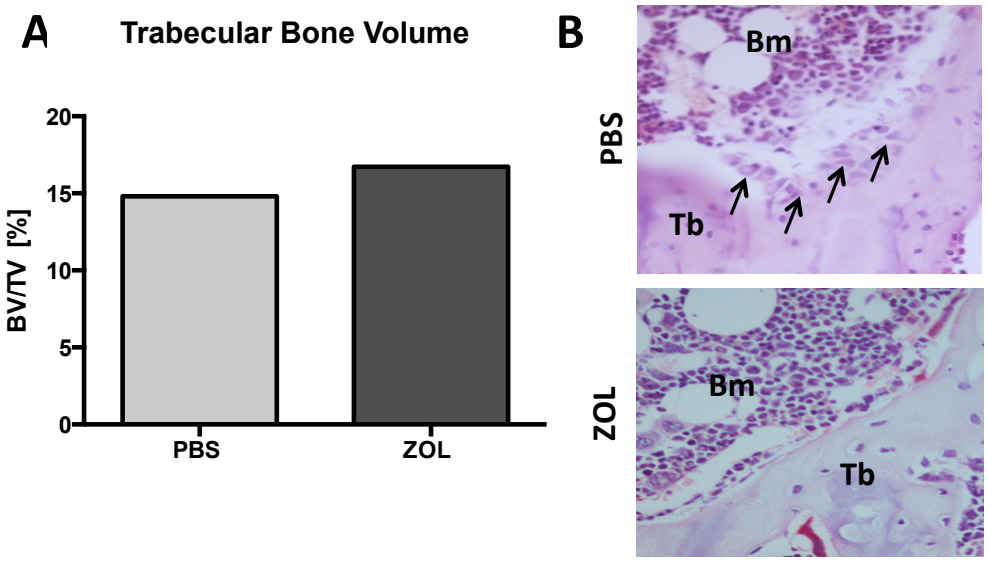


**Figure 28 Confirmation of ZOL-induced effect on the BME in the bone metastasis studies.**
(A) Trabecular bone volume of tibiae of 8-13-week old female GFP-Ob$^{+}$ mice 5 days after a single dose of ZOL, the time point of tumour cell injection was determined using µCT analysis (n=1/group). The reduction in the number of osteoblasts (indicated by black arrow heads) is illustrated in (B) on TRAP-stained histological sections of tibiae. Tb = Trabecular bone, Bm = bone marrow.

### 3.6.4.1. Circulating tumour cells

Circulating tumour cells are often associated with poor prognosis and suggested to be early predictors of metastases in breast cancer patients. Flow cytometry was used to quantify the number of circulating DiD+ve tumour cells in blood 10 days after ZOL treatment (5 days post i.c. injection of breast cancer cells) to assessed if pre-treatment with the bisphosphonate affects the number of circulating breast cancer cells.

Both of the independent experiments suggested a reduction in the number of circulating tumour cells per millilitre of blood (Experiment 1: PBS: 183.27 events/mL vs. ZOL: 2.55 events/mL, Fig. 30A; Experiment 2: PBS: 295.33 events/mL vs. ZOL: 31.43 events/mmL, Fig.30C). To confirm the reduction of tumour cells in the circulation, blood was collected on day of sacrifice, pooled for all animals per treatment group and an aliquot of 50µL plated in 6-well plates and cultures maintained for 2 weeks. Using selective pressure *in vitro* (DMEM + GlutaMAX + Pyruvate supplemented with 10%FCS, 5% Pen Strep, 5% fungizone, and 1 mg/mL G418) the decrease of tumour cells in blood following ZOL treatment was confirmed by bioluminescence signal of luc2 positive MDA-MB-231-NW1 cells (Fig.29). These findings suggest that ZOL reduces the number of circulating tumour cells in blood.

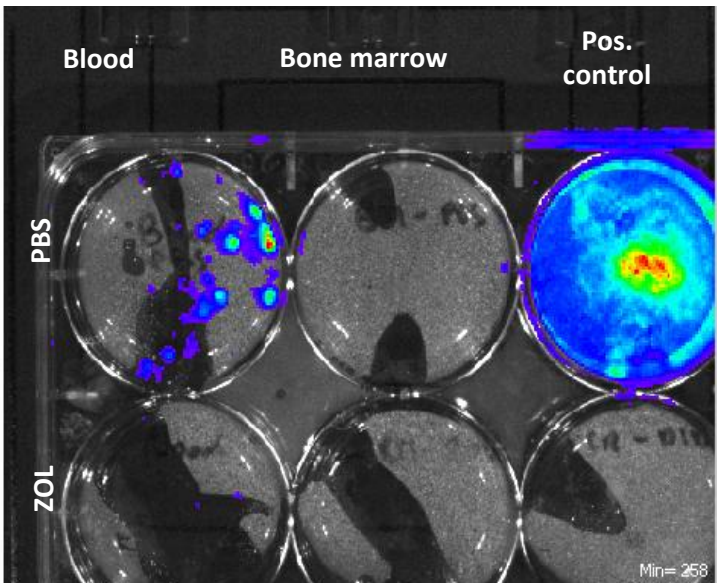


**Figure 29 Presence of tumour cells in *ex vivo* blood and bone marrow cultures.**
Blood and bone marrow was collected on day of sacrifice, pooled for all animals per treatment group and an aliquot of 50µL plated in 6-well plates and cultures maintained for 2 weeks. The decrease of tumour cells in blood following ZOL treatment was confirmed by bioluminescence signal of luc2 positive MDA-MB-231-NW1 cells. These findings suggest that ZOL reduces the number of circulating tumour cells in blood.

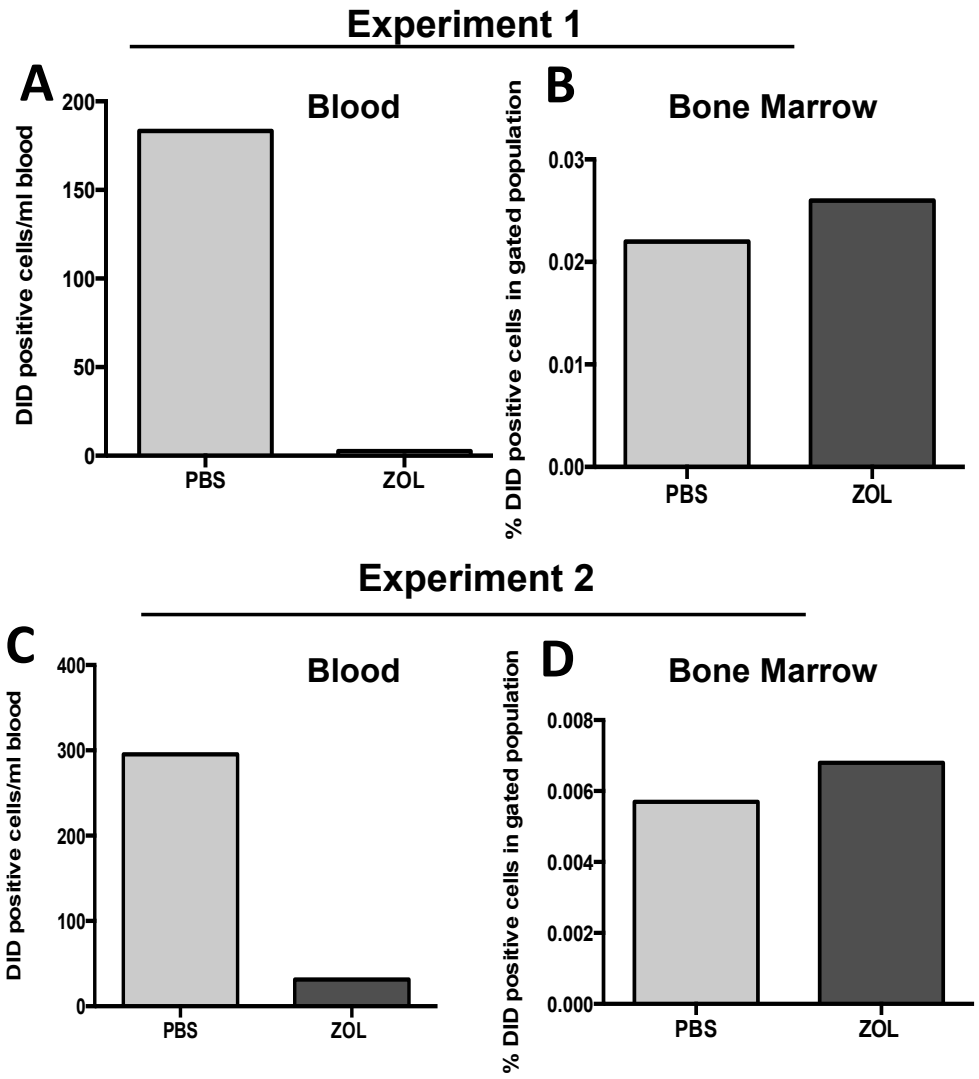


**Figure 30 Presence of tumour cells in circulation and bone marrow after Zoledronic acid pre-treatment.**

5 days post intra-cardiac injection of $1x10^5$ DiD labelled MDA-MB-231-NW1 (luc+) breast cancer cells the presence of circulating tumour cells in blood (A&C) was assessed using flow cytometry. Bone marrow (B&D) was flushed and analysed for the presence of DID+ events in the gated population. 2 independent experiments (n=4/group in each experiment) were performed and each time bone marrow and blood samples of all mice/group were pooled for analysis.

#### 3.6.4.2. Presence of tumour cells in soft tissues

To determine if tumour cells home to sites other than bone *ex vivo* cultures of organs collected at experimental endpoint were performed and selected for MDA-MB-231-NW1 cells using antibiotic pressure. No tumour cells were detected in these cultures except in the lung culture of one out of 4 mice of the ZOL group.

#### 3.6.4.3. Presence of tumour cells in bone

To assess if ZOL pre-treatment affects the number of tumour cells homing to bone the presence of DiD+ve tumour cells in bone marrow flushes of mice was analysed using flow cytometry. The percentage of tumour cells in bone was not greatly affected by pre-treatment with ZOL (Experiment 1: PBS: 0.018% vs. ZOL: 0.028%; Experiment 2: PBS: 0.005% vs. ZOL: 0.007%, Fig. 30B&D) suggesting that ZOL pre-treatment does not affect the actual number of tumour cells homing to bone. However, tumour cells could not be detected when culturing a suspension of bone marrow cells collected at the experimental endpoint under antibiotic pressure *in vitro*.

In previous experiments performed during a research internship [158] I determined that ZOL treatment primarily affects osteoblasts on trabecular bone surfaces, but osteoblasts were still visible in the dense growth plate area. To assess if the presence or absence of osteoblasts and the ZOL induced alteration in ECM in this area of bone affects tumour cell location within bone, their presence was mapped using two-photon microscopy and immunofluorescence.

By using two-photon microscopy three different regions of interest (ROI) were analysed including the growth plate (ROI-2, osteoblast-rich in both treatment groups), trabecular bone (ROI-3, osteoblast rich in PBS vs. osteoblast-depleted in ZOL treated group) and the total analysed area (ROI-1 = ROI-2 + ROI-3, Fig.31A-C). Cortical bone was excluded for analysis and data from the two separate experiments were combined (n = 6/treatment group).

In agreement with data obtained from the flow cytometry experiments, analysing the presence of DiD+ve events between the treatment groups revealed that a single dose of ZOL did not affect the overall number of tumour cells homing to bone (data represented as DiD+ve events, **ROI 1:** PBS: 504.7 ± 135.2 vs. ZOL: 501.1 ± 28.49, Fig.32 A&B). No difference in tumour cell number between the groups was observed when analysing the different areas (**ROI 2:** PBS: 113.7 ± 46.38 vs. ZOL: 208.7 ± 30.49; **ROI 3:** PBS: 391.0 ± 117.2 vs. ZOL: 292.4 ± 45.32, Fig.32A&B).

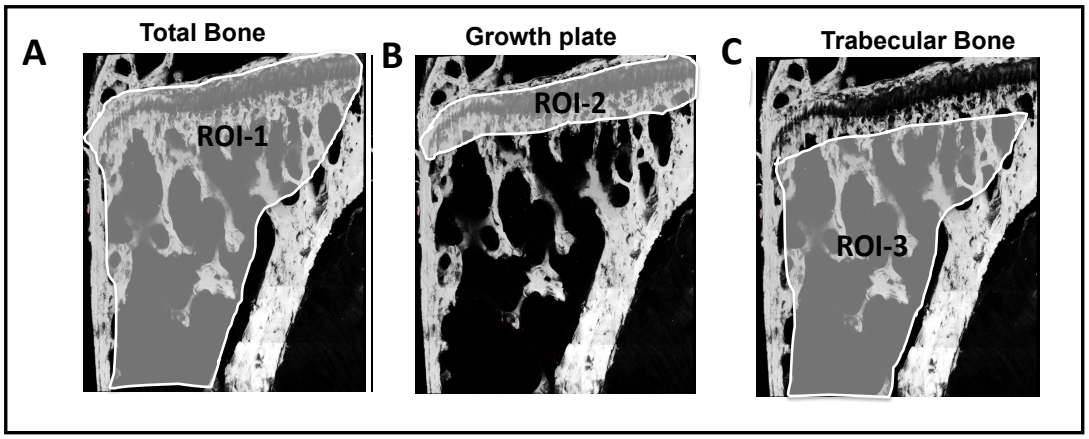


**Figure 31 Effects of Zoledronic acid pre-treatment on tumour cell homing between treatment groups for three different areas in bone.**
8-13-week old female BALB/c nude mice were pre-treated with a single dose of Zoledronic acid (ZOL, 100µg/kg, i.p., 100µL) or PBS control (i.p., 100µL) on day 0. Five days later $1x10^5$ DiD labelled MDA-MB-231-luc2-NW1 cells were injected intracardiac and the number of tumour cells (DiD positive events/$mm^3$ bone marrow) was determined for three different areas in bone including (A) total bone (ROI-1), (B) the growth plate area (ROI-2) and (C) trabecular bone areas (ROI-3) on day 10. ROI = region of interest.

However, in the PBS treated mice more DiD+ve events were detected in the osteoblast-rich trabecular bone area **(ROI-3)** compared to the growth plate **(ROI-2)** (ROI-2: 113.65 vs. ROI-3: 391.03, p=0.0625, Fig.32A) although this did not reach statistical significance. In contrast, pre-treatment with ZOL appeared to blunt this preferential distribution (ROI-2: 208.67 vs. ROI-3: 292.44, p =0.2959, Fig.32B) towards the osteoblast- and ECM-rich growth plate area.

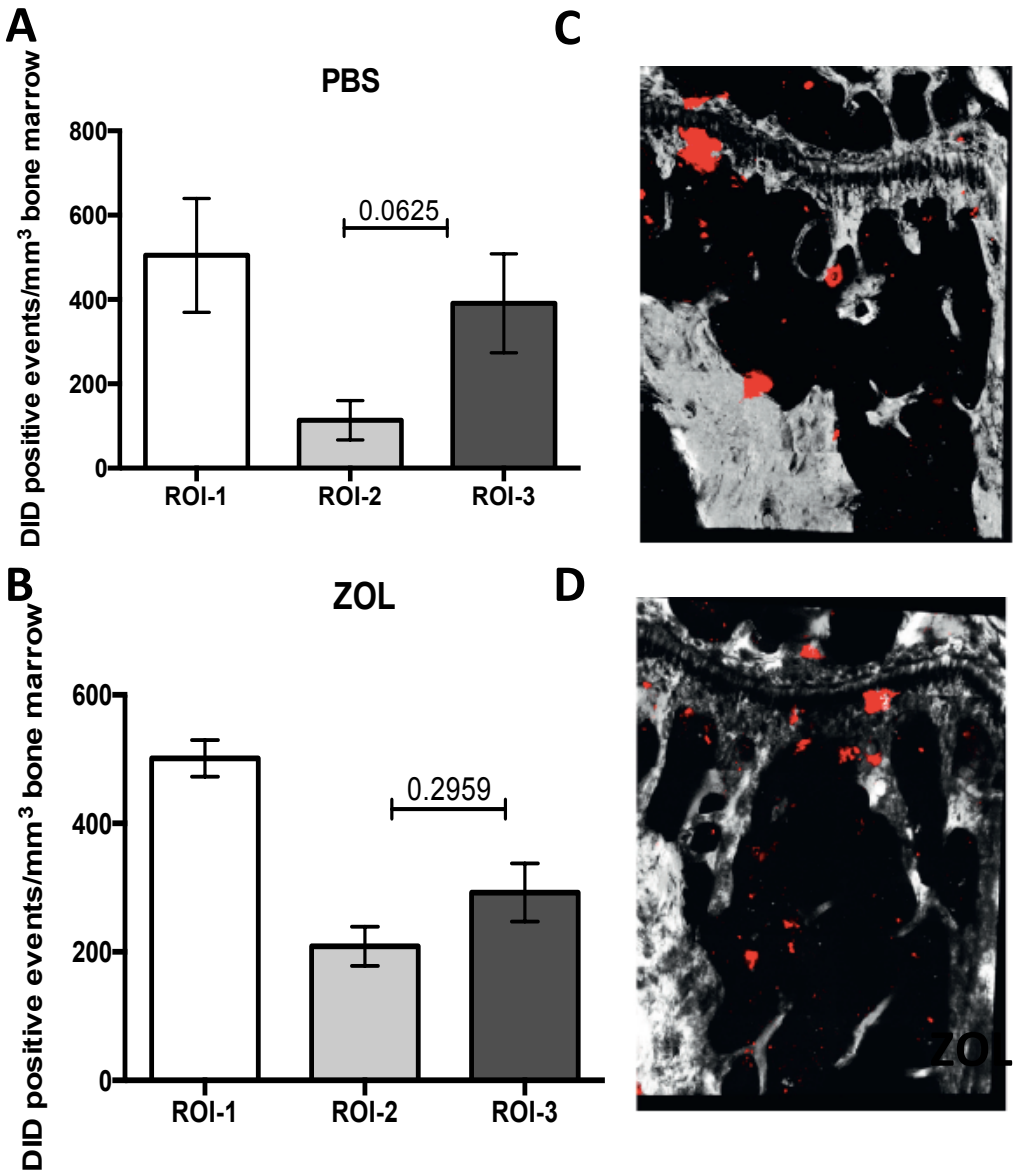


**Figure 32 Analysis of location of tumour cells in three different areas of bone by two-photon microscopy.**

8-13-week old female BALB/c nude mice were pre-treated with a single dose of Zoledronic acid (ZOL, 100µg/kg, i.p., 100µL) or PBS control (i.p., 100µL) on day 0. Five days later $1x10^5$ DiD labelled MDA-MB-231-luc2-NW1 cells were injected intracardiac. Data from two independent experiments (n=4/group in each experiment) were pooled for analysis (n=6/group). To determine if tumour cells preferentially home to specific areas in bone presence of DiD positive tumour cells (in red) was analysed for total bone (ROI-1), the growth plate area (ROI-2) and trabecular bone areas (ROI-3) on day 10. (A) shows data for PBS and (B) for ZOL pre-treated mice. Representative two-photon scans are shown in (C) for PBS and (D) for ZOL. Data show Mean±SEM, Student's t-test

These data suggest that breast cancer cells appear to preferentially home to bone areas that are rich in osteoblasts as well as extracellular matrix and that the location of tumour cells in bone can be altered when they arrive in a modified microenvironment.

Using bones from collaborative studies I aimed to assess whether ZOL pre-treatment affects the homing of two sub-clones of MDA-MB-231 (CM-DiI+ve) breast cancer cells using two-photon microscopy. Due to limited amounts of samples I could not perform quantitative analysis, however, CM-DiI+ve events were observed irrespective of HBSS or ZOL pre-treatment in both cell lines – see Figure 33.

To visualise whether tumour cells home close to endothelial cells and/or whether they get trapped in the bone marrow microvasculature, I performed immunofluorescence staining against vascular endothelial cells using the endothelial cell marker Endomucin. I was kindly provided with gelatine embedded bone samples from collaborative experiments performed at Dr. McAllister's laboratory. In these experiments mice were pre-treated with a single dose of ZOL (100µg/kg) or control and $1x10^5$ cM-DiI labelled breast cancer cells (MDA-MB-231-GFP-IV or MDA-MB-231-B02-FII) injected 3 days post treatment. Samples were collected 5 days post tumour cell injection (Fig.34). I was able to detect single tumour cells by using fluorescence microscopy (2 animals/group assessed). The majority of tumour cells appeared to be in close proximity to trabecular bone surfaces or vascular endothelial cells or even both. This suggests that tumour cells localise to areas that are rich in vascular cells and adjacent to bone surfaces, but this needs confirmation and quantification in separate studies.

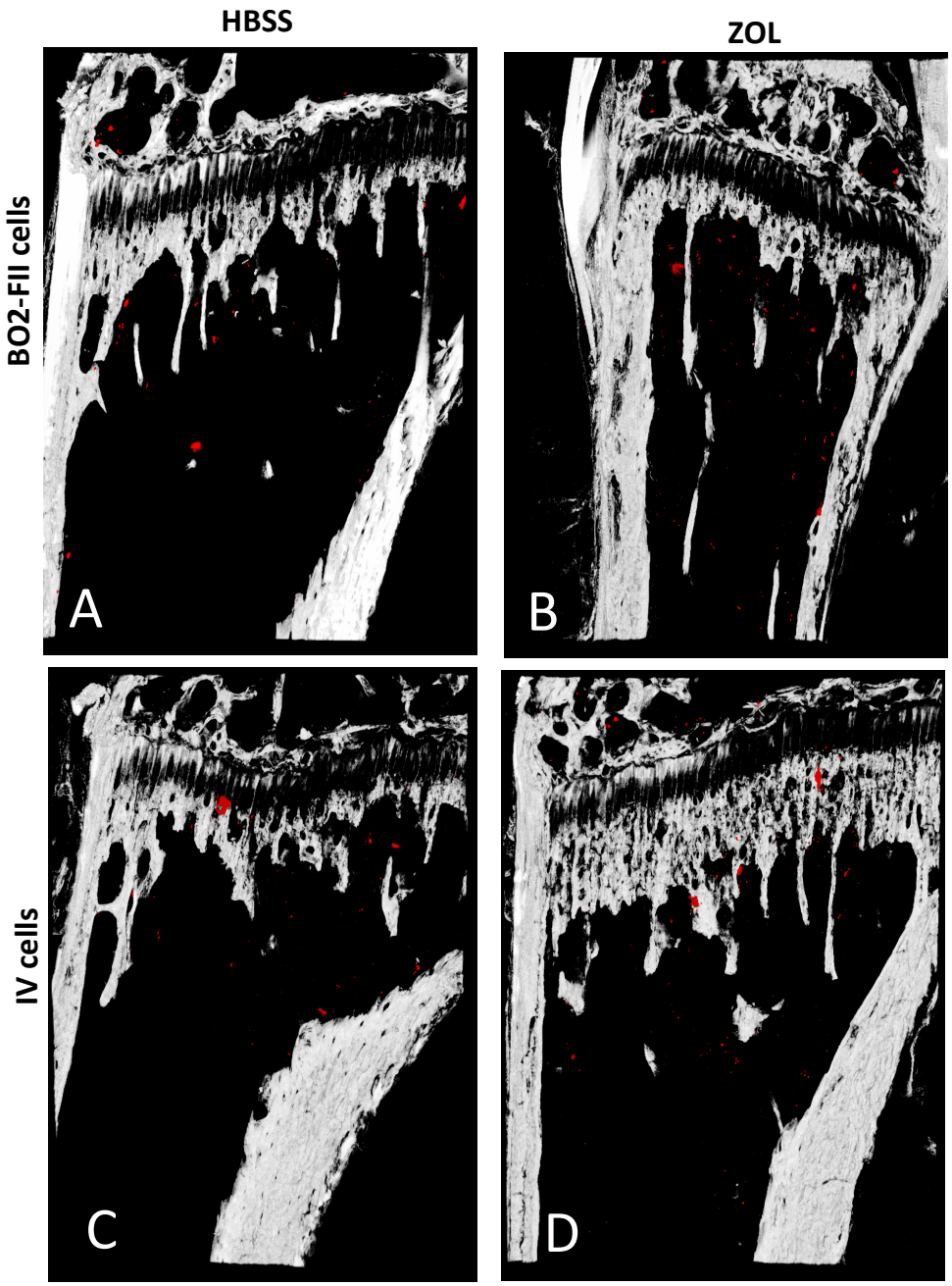


**Figure 33 Effects of Zoledronic acid pre-treatment on homing of two MDA-MB-231 breast cancer sub-clones to bone.**

6-week old female NCr-Nu (nude) mice were injected with a single dose of (A,C) HBSS control or (B&D) 100µg/kg Zoledronic acid (ZOL) on day 0 followed 72hrs later by intracardiac injection of $1x10^5$ cM-DiI labelled (A&B) MDA-MB-231 B02-FII cells or (C&D) MDA-MB-231- IV cells. Presence of tumour cells (red, cM-DiI positive events) in bone (white) was mapped using two-photon microscopy.

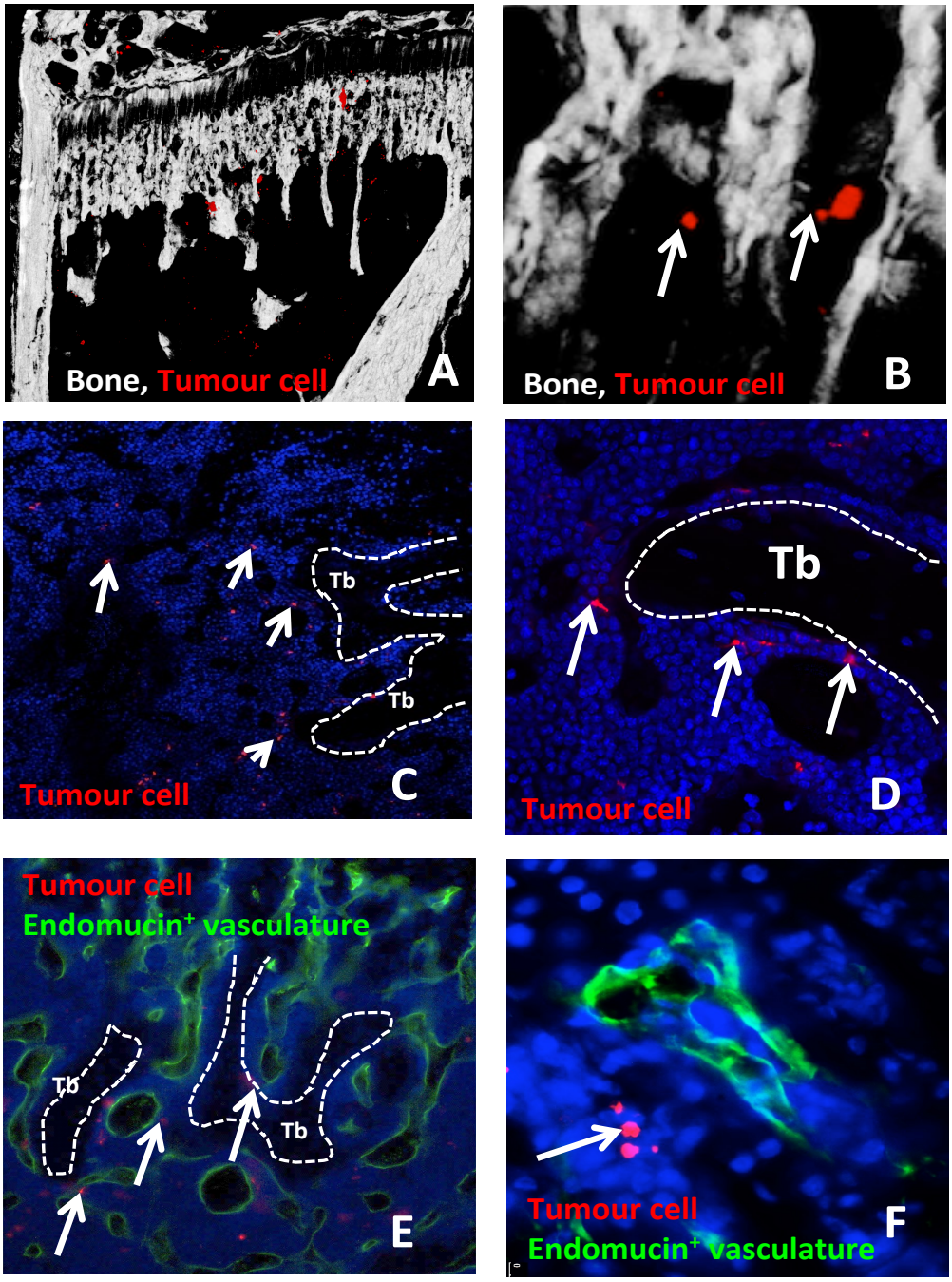


**Figure 34 Detection of tumour cells in bone by two-photon and fluorescence/confocal microscopy.**

CM-DiI+ve MDA-MB-231-B02 or MDA-MB-231-IV tumour cells (in red) were detected in bone (white) by two-photon microscopy (A&B) and fluorescence/confocal microscopy (C-F). (C&D) shows single tumour cells (red) in great proximity to trabecular bone (Tb) and within the bone marrow, nuclei stained in blue with DAPI. (E&F) shows presence of tumour cells in great proximity to trabecular bone surfaces (Tb) and vascular endothelial cells (green) within mouse tibiae. Samples are representative images from 6-week old female NCr-Nu (nude) mice 8 days after intracardiac injection of $1x10^5$ MDA-MB-231-BO2FII cells.

### 3.6.5. Effects of ZOL pre-treatment on breast cancer progression in bone

To establish if pre-treatment with ZOL affects breast cancer growth in bone 6-week old female nude GFP-Ob$^{+}$ mice received a single injection of ZOL (100µg/kg, 100µL, i.p.) or PBS (100µL, i.p.) on day 0 followed by intra-cardiac injection of 1x10$^{5}$ DID labelled MDA-MB-231-NW1-luc2 breast cancer cells on day 5. Tumour growth was monitored 2x weekly using IVIS imaging.

At the experimental endpoint (day 33-35) there was no difference in the mean number of tumours established per mouse between the two groups (PBS: 1 vs. ZOL: 0.8) suggesting that a single pre-treatment with ZOL is not sufficient to affect metastatic breast cancer growth (Fig.35). When imaging excised limbs and organs on day of sacrifice, tumour cells (bioluminescence signal) were detected in the lung (PBS: 2 vs. ZOL: 1), long bones (PBS: 2 vs. ZOL: 0) and the ribs (PBS: 1 vs. ZOL: 0) (n=5/group).

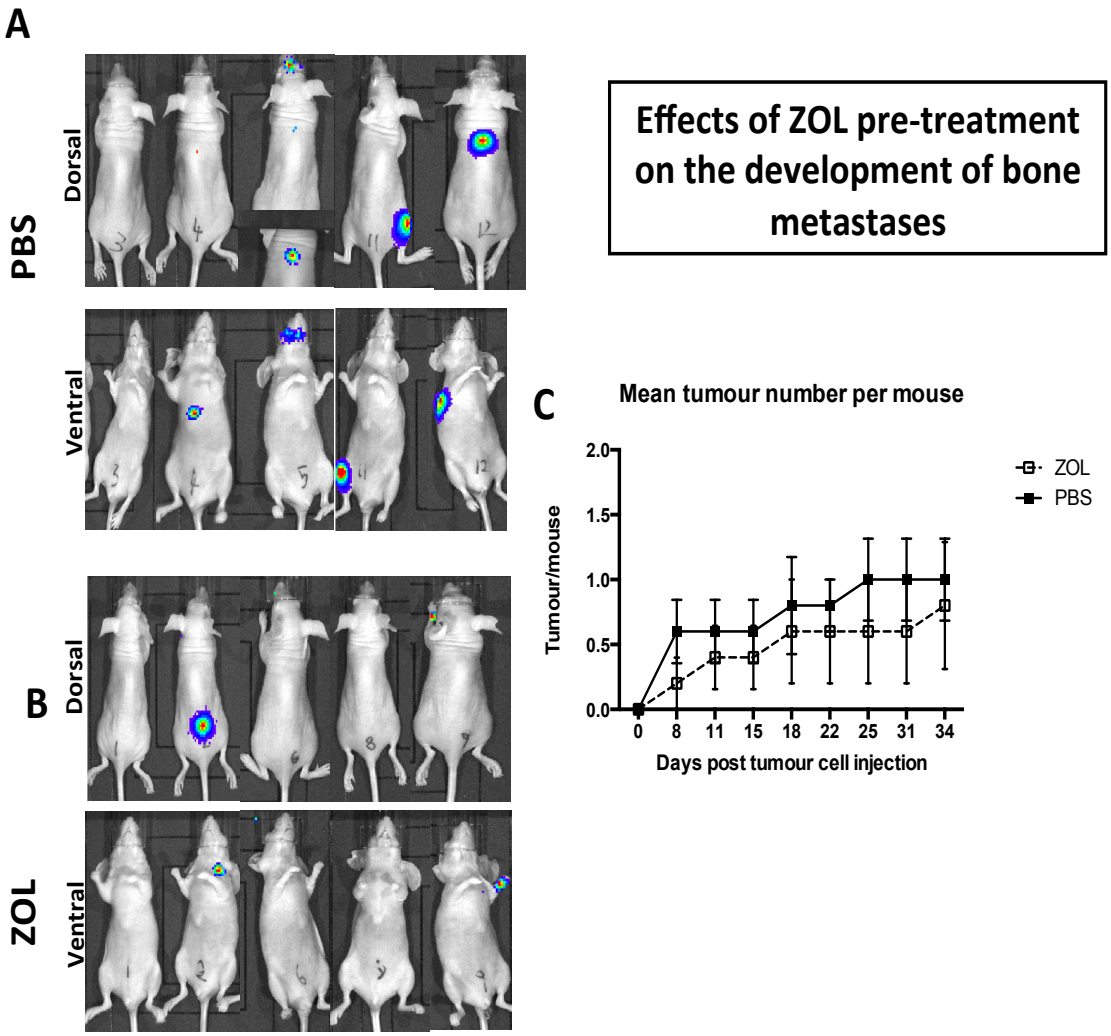


**Figure 35 Effects of Zoledronic acid (ZOL) pre-treatment on the development of bone metastases.** Potential differences in the development of bone metastases after a single injection of 100µg/kg ZOL or PBS control was assessed in 6-8-week old female BALB/c nude mice. $1x10^5$ MDA-MB-231-luc2-NW1 cells were injected 5 days post ZOL pre-treatment and development of tumours monitored by bioluminescence signal using IVIS. Dorsal and ventral representative IVIS images are shown in (A) for PBS and (B) for ZOL pre-treatment group (n=5/group), day 29/30 post injection. (C) shows mean tumour number/mouse over time (Mean ± SEM).

### 3.7. Discussion

This study investigated how a single, clinically relevant dose of the anti-resorptive agent ZOL affects bone cells, suggested to be key components of the bone metastasis niche. Osteoclasts and osteoblasts are in part driving the vicious cycle in late stage bone metastasis however, their role in the early events of metastasis development including tumour cell homing to bone and/or triggering subsequent metastatic outgrowth remains to be elucidated. This chapter presents the first detailed characterisation of the short-term effects of ZOL on both, osteoblasts and osteoclasts *in vivo* and discusses if modification of the BME with ZOL affects tumour cell homing to bone.

#### 3.7.1. Effects on bone volume and structure

Bisphosphonates are standard of care for pathological conditions characterised by excess osteoclast-mediated bone resorption including osteoporosis and Paget's disease. In addition patients with advanced breast cancer often receive BPs in combination with chemotherapy to prevent the cancer-induced bone loss. It is well established that repeated treatment with the bisphosphonate ZOL increases bone volume. Pozzi *et al.* for example report increased trabecular bone volume and number in 5-week old female C57BL6 mice after weekly treatment with ZOL (0.05-1mg ZOL) for 3 weeks [262]. In agreement with this, Ottewell and colleagues determined increased trabecular and cortical bone volume in 6-week-old-female MF1 nu/nu mice bearing subcutaneous MDA-436 tumours after weekly administration of 100µg/kg ZOL for 6 weeks [241].

Importantly, these studies used administration schedules or doses that are not comparative to that in clinical use. Patients with cancer-induced bone disease receive a single, intravenous infusion of 4mg ZOL every 3-4 weeks. In my experiments I have investigated the early effects of a clinically relevant dose of ZOL (100µg/kg in mice = 4mg in humans [241]) on the naïve, *in vivo* BME. Interestingly trabecular bone volume in 6-week old female BALB/c nude mice was rapidly increased as early as 3 days after the single injection indicating rapid effects of ZOL on bone. This is in agreement with findings by Brown et. *al* reporting increased trabecular bone volume 15 and 23 days after a single injection of ZOL in 6-week old female BALB/c nu/nu mice [154], suggesting that repeated treatment with ZOL is not required to initiate ZOL-induced bone effects in these model systems.

#### 3.7.2. Effects on bone cells

Effects of BPs on osteocytes which comprise more than 90% of all cells within the bone matrix are reported. Plotkin and colleagues for example report that the BPs etidronate,

pamidronate, olpadronate and alendronate at doses of ($10^{-9}$M – $10^{-8}$M) inhibited dexamethasone induced apoptosis of murine MLO-Y4 osteocytic cells. These effects were lost at higher doses [263]. In my experiments I did not assess the acute effects of ZOL on osteocytes.

#### 3.7.2.1. Effects on osteoclasts

However, there is general consensus that osteoclasts are the main targets of BPs. The compounds high affinity for bone brings them into close contact with bone resorbing osteoclasts where they are embedded into the bone matrix until released during active bone resorption. BPs affect osteoclasts in various ways including their recruitment, differentiation, activity and viability [261]. Long-term and repeated treatment with BPs is known to reduce osteoclast activity and number *in vivo* [241, 262]. Pozzi *et al.* report that ZOL (0.05-1mg/kg ZOL weekly for 3 weeks) reduces osteoclast activity (assessed by TRACP5b serum levels) in 5-week old female C57BL6 mice [262]. In these experiments osteoclast number per bone perimeter was slightly reduced however this did not reach statistical significance. Furthermore, weekly doses of ZOL (100µg/kg) for 6 weeks caused a significant reduction in the percentage of cortical bone surface in contact with osteoclasts [241].

Cortical bone has a lower bone turnover rate when compared to trabecular bone and recent studies demonstrated that the tibial metaphysis is preferentially colonised by breast cancer cells in bone metastasis models [90, 264]. In my experiments I therefore only investigated effects of ZOL on osteoclasts lining trabecular bone surfaces. To my knowledge acute effects (3-5 days post injection) of a clinically relevant dose of ZOL on osteoclasts *in vivo* have not been established in great detail and effectiveness of various dosing schedules (high dose with reduced treatment intervals vs. lower doses with increased treatment intervals) are subject to debate [265]. I determined that a single dose of ZOL rapidly reduced the number of osteoclasts on trabecular bone surfaces of tibiae of 6-week old female BALB/c nude mice as early as 3 days post treatment when compared to control. A drop in osteoclast activity (measured by serum TRAP levels) by day 3 mirrored this finding. Analysing osteoclast numbers in tibiae of 6-week old female NCr-Nu (nude) mice support the rapid effect of ZOL on osteoclasts and similar effects were previously observed in immunocompetent BALB/c mice [158]. These findings suggest that a single dose of ZOL is sufficient to initiate rapid therapeutic effects on osteoclasts irrespective of the immune status of the animal model used. Importantly, effects on osteoclasts were transient and returned to control levels by day 8 and 10 respectively. This highlights the

importance of determining the acute effects of therapeutic agents on bone cells over various time points. In contrast, Fisher *et al.* reported increased osteoclast numbers 48hrs after a single dose of alendronate (5µg/kg) and ibandronate (150µg/kg and 1.25µg/kg), whereas no alteration of total osteoclast number in tibiae of rats 48hrs after administration of ZOL (333µg/kg) was observed [265]. However, in agreement with my findings Brown *et al.* reported that a single administration of ZOL does not only decrease osteoclast numbers/mm trabecular bone surface but also results in significant alterations in osteoclast morphology and increased osteoclast size 15 and 23 days after the single dose [154]. Repeated treatment with BPs causes the presence of "giant" osteoclasts [157, 266] and Fisher and colleagues proposed that higher doses of BPs are associated with changed osteoclast morphology (rounded), whereas flat osteoclasts were observed after low dose [265]. Importantly, they describe osteoclasts of ZOL treated rats as taller, rounded-up and plump with a 34% increased average height 48hrs after administration of a single (333µg/kg) dose of ZOL to male Sprague-Daley rats [265]. In addition, increased osteoclast apoptosis 48hrs after administration was observed [265]. Electronmicrographs of bones from adult rats injected twice with 0.4mg/kg of the BP alendronate followed by infusion with PTHrP to stimulate bone resorption resulted in a lack of ruffled borders and fewer vacuoles of osteoclasts attached to bone surfaces when compared to control suggesting that BPs partially inhibit osteoclastic bone resorption by interfering with ruffled boarder formation [153]. However, comparing *in vivo* experiments performed in rats with those performed in mice might not be appropriate. I have previously determined a significant increase in osteoclast size 3 days post ZOL administration in immunocompetent mice [158], however, I did not find any significant alterations in osteoclast morphology or osteoclast apoptosis in either 6-week old female BALB/c nude or NCr-Nu (nude) mice at analysed time points.

#### 3.7.2.2. Effects on osteoblasts

Although therapeutic effects of BPs might be dependent on their anti-resorptive properties there is increasing evidence that they also affect other cells of the BME [249, 262, 267].

Data on effects of BPs on osteoblasts are conflicting and vary depending on the experimental model, BP and dose used (reviewed in [268], however mainly focused on beneficial effects of BPs). Some report increased differentiation, proliferation and inhibition of apoptosis [249] whereas others report opposite effects. Briefly, low doses of BPs appear to have pro-osteoblastogenic effects whereas higher doses were found to exhibit inhibitory effects. For example Im *et al.* studied the effects of aledronate and

risedronate on primary human trabecular bone cells and MG-63 (osteoblast-like) cells *in vitro*. At high dose ($10^{-4}$M) both drugs inhibited proliferation of MG-63 cells whereas proliferation was stimulated at lower doses ($10^{-7}$M – $10^{-9}$M; peak effects reached after 72hr treatment). Aledronate and risedronate also increased alkaline phosphatase activity of MG-63 cells after 24hr treatment. Similarly aledronate ($10^{-8}$M) increased proliferation of human trabecular bone cells [249]. In addition, others report that both, ibandronate and ZOL stimulated proliferation of human osteoblasts after 72hrs ($10^{-8}$M to $10^{-5}$M) [269].

The significance of *in vitro* studies investigating the effects of BPs on osteoblasts however needs to be assessed. This is due to the rapid incorporation of BPs into bone causing only short exposure times of other cell types including osteoblasts to these compounds *in vivo*. There is only a limited number of published studies describing effects of BPs on osteoblasts *in vivo* [154]. Here I assessed the acute effects of a single, clinically relevant, dose of ZOL and showed that osteoblast number/mm trabecular bone surface and activity (measured by serum PINP levels) is rapidly decreased in 6-week old female BALB/c nude mice from day 5 post injection onwards. Similar results were obtained in immunocompetent mice, with significant effects on osteoblasts being observed from day 3 post treatment onwards and maximum reduction in osteoblast number reached on day 5 [158]. These observations were confirmed when analysing samples from independent experiments using NCr-Nu (nude) mice. In agreement others report reduced osteocalcin levels after 0.05-1mg/kg ZOL weekly for 3 weeks in female C57BL6 mice, suggesting reduced osteoblast activity [262]. A recent study by Brown *et. al* also found reduced osteoblast number and activity 15 days after a single administration of ZOL [154].

It is difficult to establish whether effects of ZOL on osteoblasts were due to a direct effect on these cells or indirectly via osteoclast coupling. Treatment of human osteoblasts for 72hrs with ZOL or pamidronate resulted in increased levels of OPG mRNA and OPG protein expression (measured by ELISA) with most potent effects at $10^{-8}$ to $10^{-6}$M, respectively [270]. This suggests that anti-resorptive effects of ZOL could be mediated through interference with the pro-differentiation and survival of osteoclasts by the RANK/RANKL/OPG axis mediated via osteoblasts. Considering the important role of osteoblasts in osteoclast differentiation, potential effects of BPs on osteoblasts might contribute to the observed reduction in osteoclast formation and activity following BP treatment.

To summarise I, have shown that a single dose of ZOL rapidly affects both osteoblast and osteoclasts *in vivo* demonstrating that repeated treatment cycles are not required for

initiation of bone effects. Effects on bone cells were transient for some parameters, highlighting the importance of measuring both cell number and activity over time.

### 3.7.3. Effects on growth plate cartilage

Next to the rapid alterations in bone volume and bone cell number ZOL treatment resulted in a significant accumulation of proteoglycan-rich extracellular matrix around the epiphyseal growth plate, thereby changing the physical environment in this area of bone. Skeletal growth of long bones is achieved during endochondral ossification, a process mediated by chondrocyte proliferation, secretion of ECM, hypertrophy, terminal differentiation and ultimately chondrocyte death. ECM secreted by chondrocytes is composed of aggrecan, hyaluronan, collagen, proteoglycans and other non-collageneous proteins. In addition these cells secrete various growth factors to regulate their proliferation and hypertrophy including BMPs, IGFs and VEGF (briefly reviewed in [271]). This in turn regulates the recruitment and invasion of cells to the ossification front to degrade and replace the cartilage matrix by ossified bone [53]. Both osteoclasts, osteoblasts and endothelial cells are required at the ossification front to maintain normal growth plate physiology. In the absence of osteoclastic activity (induced by the BP clodronate) trabecular bone of mice was elongated due to the inability of osteoclasts to invade the ossification centre [272]. However, vascular endothelial cells appear to be the first cells to invade the growth plate potentially independent of the presence of osteoclastic activity and BP treatment [272]. In addition osteoblasts are found at the ossification front where they deposit the bone matrix leading to the formation of trabecular bone surfaces. The increase in proteoglycan-rich ECM observed after ZOL treatment might therefore be a consequence of altered osteoblast and osteoclast number and activity.

### 3.7.4. Effects on the bone marrow vasculature

To visualise potential effects of ZOL on the BME I performed immunofluorescence staining for the endothelial cell marker Endomucin on gelatine embedded bone samples obtained during collaborative experiments in Boston, USA.

Any alteration in bone marrow vasculature prior to tumour cell dissemination could affect the accessibility and therefore colonisation of tumour cells in bone. A recent study by Ghajar *et al.* has elegantly demonstrated the role of the (peri)vascular niche in regulating tumour cell dormancy *in vivo* (mouse and zebra fish) and organotypic microvascular niches composed of human cells [101]. The authors conclude that stable

microvasculature contains a dormant niche, whereas metastatic outgrowth happens at sprouting neovasculature, a process mediated by thrombospondin-1. Furthermore in breast cancer patients actively proliferating macro-metastases were found in great proximity to endosteal surfaces whereas dormant breast cancer cells were predominantly located adjacent to perisinusoidal niches [112]. Whether the proposed endosteal niche overlaps with the vascular niche remains to be established however close interaction between those two is apparent: During bone formation osteoblasts are often detected adjacent to vascular endothelial cells, suggesting that entry of osteoblast precursors into developing bone is coupled to/directed by the invasion of blood vessels [53]; data supported by Kusumbe and colleagues demonstrating that osteogenesis and angiogenesis are closely coupled [51]. *In vitro* ZOL has shown to inhibit proliferation of HUVECs suggesting anti-angiogenic properties and potential of the drug to affect the *in vivo* bone marrow vasculature. Using MicrofilTM perfusion followed by µCT analysis, Soki *et al.* showed that 4-week old male mice treated with ZOL for 4 weeks (200µg/kg, 2x/week) had reduced vessel thickness and increased vessel numbers whereas the overall vessel volume fraction was not affected [159]. The physiological process of new blood vessel formation is a very rare event in the normal, healthy adult. In agreement with this no effects of ZOL on bone marrow vasculature was determined in 4-months old mice after 4 weeks of ZOL treatment [159]. In my experiments I observed alterations in the vascular architecture in 6-week old mice 3 days after a single dose of ZOL (100µg/kg). However this requires confirmation by quantitative analysis and multiple sections/samples. Also it remains to be elucidated whether the observed changes in structural organisation of the bone marrow vasculature after ZOL treatment is due to direct effects of the drug on endothelial cells or due to the altered bone structure.

### 3.7.5. Effects of ZOL pre-treatment on the bone metastasis niche

Targeting the BME with anti-resorptive agents including bisphosphonates has been standard of care for patients with cancer-induced bone disease and these agents are also proposed to exhibit direct and/or indirect anti-tumour effects *in vivo* [147, 273].

The AZURE (BIG 01/04) trial enrolled 3360 women with stage II and III breast cancer who received standard adjuvant therapy alone or in combination with 4mg ZOL. This study revealed reduced incidence of bone metastases in women receiving ZOL demonstrating beneficial effects of early ZOL-treatment [132]. Although the underlying mechanisms remain to be established, these may include a reduction in the survival and/or progression of disseminated tumour cells in bone. This is supported by data obtained in

model systems, showing that preventive regimens (*e.g.* administration of BPs prior to or at the time of tumour cell injection) appear more effective compared to therapeutic treatment of established tumours [147]. However, the focus of most preventive *in vivo* studies has been on reduction of tumour burden and the associated bone disease without assessing the effects that alterations to the BME may have on tumour cell homing to bone. In addition the AZURE trial suggested that patients with high PINP serum levels (a marker for osteoblast activity) at study entry had a higher risk of bone metastasis when compared to patients with low PINP [132]. However, potential consequences of BP treatment on osteoblasts and subsequent tumour cell homing to bone have not been investigated in this context.

Here I determined if ZOL pre-treatment and the therapeutic induced alterations to the BME affect tumour cell homing to bone *in vivo*. The significant alterations in osteoclasts and osteoblasts in addition to the accumulation of ECM in the growth plate 3-10 days post ZOL, raised the hypothesis that this could cause alterations to the location of the bone metastatic niche and subsequently affect tumour cell homing. Injecting MDA-MB-231 breast cancer cells 5 days post ZOL treatment – the time point when osteoblasts were depleted form trabecular bone surfaces - therefore allowed establishment of the role of osteoblasts in mediating tumour cell homing to bone. Additionally using two-photon microscopy and immunofluorescence enabled analysis of the presence of tumour cells in different areas of the metaphysis and whether this is modified by ZOL pre-treatment.

When tumour cells arrived in mice where the proposed bone metastasis niche area was modified by ZOL pre-treatment, their location and distribution appeared to be altered when compared to control. A trend towards enrichment of tumour cells in the same region of the metaphysis where ZOL had induced accumulation of ECM and where the remaining osteoblasts after treatment were located was observed. These findings need validation in independent experiments but suggest the presence of particular 'preferred' osteoblast-rich niche areas in bone. In support of this are findings reported by Sasaki and colleagues. In these experiments the authors pre-treated 3 week old nude mice daily for 7 days with risedronate (4µg/mouse, s.c.) prior to intracardiac injection of $1x10^5$ MDA-MB-231 breast cancer cells. Upon cancer cell injection risedronate treatment was discontinued in these experiments. At experimental endpoint (day 28) they report lower numbers of osteoclasts and that metastatic invasion of breast cancer cells was restricted to the area adjacent to the epiphyseal growth plate where new bone would have been formed after cessation of risedronate treatment (observations made by histology) [149]. Furthermore, a study by

Wang and colleagues reports abundant expression of alkaline phosphatase and collagen-I, both markers for osteoblastic lineage cells, in cells comprising "the microenvironment niche of microscopic bone lesions". Using breast cancer models (MCF-7, 4T1 or MDA-MB-361) they found that about 80% of cells in the niche were positive for ALP, 40-65% were positive for Col-I and only 20% were $CTSK^+$ (marker for osteoclastic cells) suggesting that the niche in early bone colonisation is primarily composed of osteoblastic cells [94]. Also niche cells expressed markers of osteognesis including RUNX2 and Osterix [94]. In addition tumour cells are thought to harvest resources such as growth factors including TGFb, BMPs, IGFs, FGFs, PDGFs that are stored in bone and released during osteoclast mediated bone remodelling [274] and osteoblast derived signals (in part required for HSC maintenance) including osteopontin, BMPs and RANKL, Notch signalling and PTH/PTHrP [102, 103]. Osteoblast derived adhesion molecules including osteopontin are suggested to be involved in tumour cell homing to bone. OPN for example interacts with the integrin receptor αvβ3 expressed on breast cancer cells and intravenous injection of αvβ3 over-expressing breast cancer cells has been associated with higher metastatic incidence *in vivo* [275]. These studies demonstrated that inhibition of αvβ3 with a nonpeptide antagonist (PSK1404) resulted in inhibition of osteoclast-mediated bone resorption in animal models of bone metastasis and blocked colonisation of αvβ3-expressing cancer cells [275]. Importantly, the mapping of individual tumour cells in bone still remains challenging and whether modification of other elements that influence tumour cell homing (*e.g.* the vascular niche, the HSC niche) are modified by ZOL remains to be established.

Additionally these data show that pre-treatment with a single dose of ZOL did not affect the overall number of tumour cells homing to bone assessed by both, flow cytometry and two-photon microscopy. Others investigated the effects of ZOL pre-treatment on B02 (a bone seeking derivative of the MDA-MB231 cell line) breast cancer cell homing to bone (assessed by luciferase activity) in 4-week old female BALB/c nude mice [146]. In agreement I did not observe any differences in development of bone metastases when comparing tumour burden in mice pre-treated with a single dose of ZOL or control. These findings suggest that repeated treatment with BPs is needed to induce a continuous inhibition of bone resorption thereby allowing reduction and/or inhibition of skeletal tumour burden. In agreement with this hypothesis Neudert *et al.* [144] and van der Pluijm [257] report beneficial effects of the BPs (ibandronate and olpadronate) on the development and progression of bone metastases when continuous treatment was initiated prior to injection of MDA-MB231 breast cancer cells *in vivo*. In support of my

findings a single dose of ZOL (100µg/kg) 1 day prior to intravenous injection of B02 breast cancer cells did not affect luciferase activity (a measure of skeletal tumour burden) 14 days post injection, or reduce the area of bone lesions by day 32 [146]. When weekly and daily treatment was initiated 1 day prior to tumour cell injection reduced luciferase activity was observed suggesting that the need of repeated dosing with ZOL to successfully reduce the establishment of metastatic disease in bone [146]. In agreement, repeated treatment with ZOL is shown to increase elimination of disseminated breast cancer cells in breast cancer patients [191]. Importantly reduced osteoclast activity is supposed to be the major mechanism behind the anti-tumour capacity of BP. However, also mice with defective osteoclasts receiving ZOL or control 10 and 3 days prior to intra-arterial injection of B16 melanoma cells showed an 88% decrease in tumour growth in bone when compared to control. This study suggests a potential osteoclast – independent effect of N-BPs in the treatment of bone metastasis [143].

### 3.8. Summary and Conclusion

In summary, this study presents novel evidence that a single, clinically relevant dose of ZOL rapidly induces significant alterations to both the cellular component and the extracellular matrix of the metaphysis, the area of bone comprising the metastatic niche. Although the total number of breast cancer cells in bone was not altered, there was a trend towards accumulation of tumour cells in osteoblast- and proteoglycan-rich areas after ZOL pre-treatment. In addition these data are the first to show that breast cancer cells appear to preferentially localise to specific regions in the metaphysis, but that they may home to other areas if challenged by an altered microenvironment. These findings also support that osteoblasts are a key component of the metastasis niche.

# Chapter 4 - Characterising the effects of Cabozantinib on the bone microenvironment *in vivo* – the potential role of Met and VEGFR-2

Part of this work has been published in "Haider MT, Hunter KD, Robinson SP, Graham TJ, Corey E, Dear TN, Hughes R, Brown NJ, Holen I. **Rapid modification of the bone microenvironment following short-term treatment with Cabozantinib *in vivo*.** " Bone 2015;81: 581-592. 

DOI: http://dx.doi.org/10.1016/j.bone.2015.08.003

## 4.1. Summary

Cabozantinib (CBZ) is targeted against multiple receptor tyrosine kinases involved in tumour pathobiology, including hepatocyte growth factor receptor (MET) and vascular endothelial growth factor receptor 2 (VEGFR-2). CBZ demonstrated promising results in patients with advanced prostate cancer with resolution of lesions visible on bone scans, implicating a potential role of the bone microenvironment (BME) as a mediator of CBZ effects.

I performed the first detailed characterisation of the effects of short-term administration of CBZ (30mg/kg, 5 and 8 doses) on the *in vivo* BME in the absence of tumour. Studies were performed in a variety of animal models of different age, sex and strain allowing me to establish the therapeutic response to CBZ in different microenvironments.

8 administrations of CBZ resulted in increased trabecular thickness and further significant effects on the BME were observed including a decrease in osteoclast and increase in osteoblast numbers/mm trabecular bone surface compared to control mice. Irrespective of administration schedule or animal model, administration of CBZ resulted in an elongation of the growth plate, in particular the hypertrophic chondrocyte zone. In addition male and female BALB/c nude mice had increased numbers of megakaryocytes and altered bone marrow vasculature following CBZ treatment. Importantly, effects of CBZ on the BME were transient and rapidly lost upon treatment termination.

These data reveal that short-term administration of CBZ induces rapid, reversible effects on the BME, highlighting a potential role in mediating therapeutic response to CBZ.

## 4.2. Introduction

Effective suppression of bone metastasis requires therapeutic targeting of both the tumour and the BME, hence use of agents with multiple targets may provide an opportunity to improve outcome for patients with skeletal metastases. Cabozantinib (CBZ) targets multiple receptor tyrosine kinases (RTK) including hepatocyte growth factor receptor (MET) and vascular endothelial growth factor receptor 2 (VEGFR-2) and has potential as an anti-tumour agent for use in patients with bone metastasis.

Bone metastasis involves complex crosstalk between tumour cells and cells of the BME including osteoclasts, osteoblasts, haematopoietic and vascular cells. Despite expression on tumour cells, CBZ target receptors are also expressed by a number of cell types in bone including osteoblasts and osteoclasts [209-212, 218]. In addition to RANK/RANKL signalling, the MET and VEGF signalling pathways regulate the tightly balanced coupling between osteoblasts and osteoclasts, as both cell types express target receptors [209-212] and are therefore potentially affected by CBZ. CBZ further inhibits phosphorylation of KIT, RET, AXL, TIE2, and FLT3 [218] all of which might be involved in bone remodelling as well as bone cell biology [208, 213-215]. In this study I have focused on exploring the potential role of MET and VEGFR in the bone effects of CBZ although other kinases might also contribute to the observed effects.

Clinical studies including a phase II randomised discontinuation trial of CBZ in patients with advanced prostate cancer demonstrated clinical activity, including increased resolution in bone scans, reduction in serum marker levels of bone remodelling, in addition to pain relief in more than 60% of evaluable patients [234, 235, 237]. Pre-clinical studies using *in vivo* models of prostate cancer bone metastasis showed a decrease in tumour volume, tumour necrosis, suppression of tumour growth in addition to altered bone remodelling following long-term CBZ treatment, suggesting tumour cells [218, 230] (see Table 10-12, Figure 36) as well as cells of the BME as potential cellular targets of CBZ [231, 233].

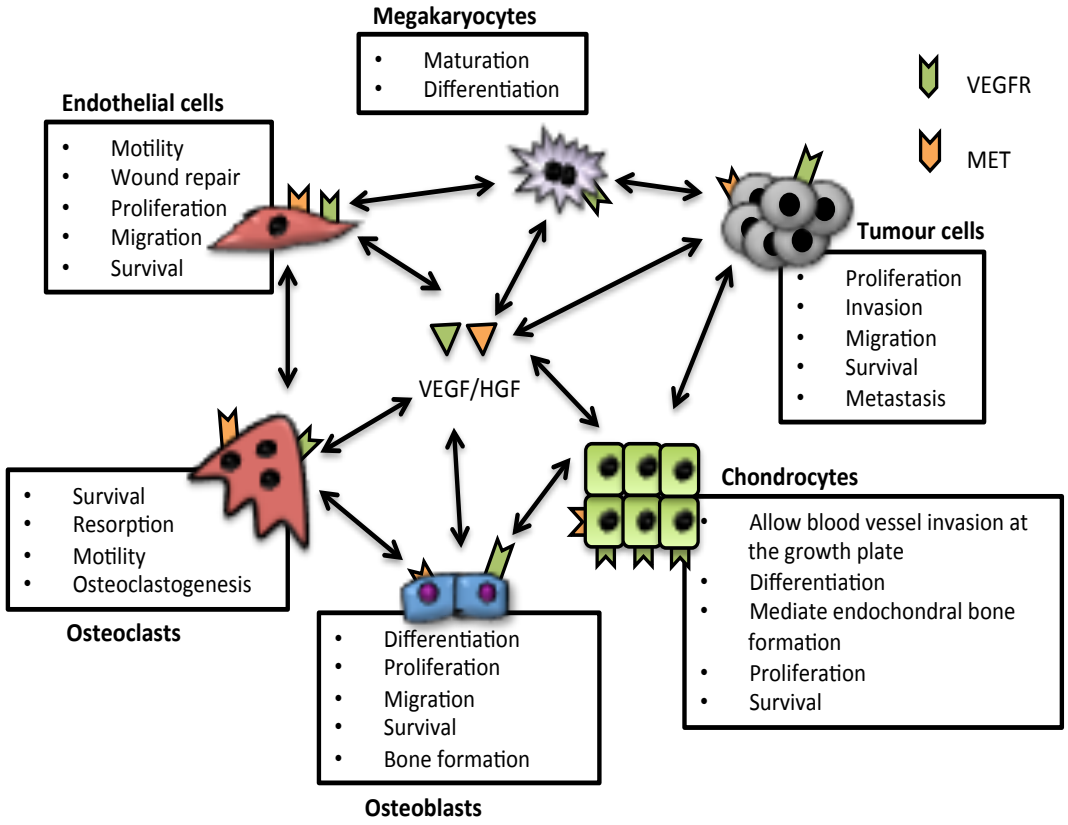


**Figure 36 Schematic representation of the involvement of VEGF and HGF signalling in bone remodelling and tumour development.**
Target receptors of Cabozantinib (CBZ) including VEGFR and MET, both are expressed on tumour cells as well as on cells of the BME and involved in regulating their proliferation, differentiation and survival. Cells of the BME are therefore representing potential therapeutic targets of CBZ.

Effects of CBZ on tumour cells *in vitro* and *in vivo* are well established [218, 230, 231, 235]. Briefly, CBZ resulted in decreased viability, proliferation, migration and invasion of breast, lung, prostate and gastric cancer cells *in vitro* [218, 230], in addition to decreased prostate cancer growth in bone [230-233]. In breast cancer xenograft models CBZ resulted in dose dependent inhibition of primary MDA-MB-231 breast tumour growth (in the mammary fat pad) and/or stable disease (3-60mg/kg, daily for 14 days). CBZ did not promote the formation of lung metastasis in these experiments (see Table 10) [218]. Importantly, despite the frequent diagnosis of bone metastasis in patients with advanced breast cancer, effects of CBZ in this setting have not been established yet.

**Table 10 Effects of CBZ on breast cancer growth *in vivo.***
Data summarised from results published by Yakes *et al.* [218]. Note that these experiments did not involve experiments assessing the role of CBZ in prevention and/or treatment of breast cancer-induced bone disease.

| Animal model | Dose of CBZ | Treatment duration | Effects on tumour |
|---|---|---|---|
| Female nu/nu mice, $1x10^6$ MDA-MB-231 breast cancer cells injected subcutaneously into the mammary fat pad | 1,3,10,30,60 mg/kg | Daily oral administration for 14 days once tumours reached 100,500 or 1000mg | Dose-dependent inhibition at 3 and 10-mg/kg doses<br>Stable disease at 30- and 60mg/kg |
| Female nu/nu mice, intra-venous injection of $1x10^6$ MDA-MB-231 breast cancer cells to assess lung metastasis formation | 60mg/kg | Daily oral administration for 28 days | No promotion of lung metastasis when compared to control mice |
| Female nu/nu mice, $1x10^6$ MDA-MB-231 breast cancer cells injected sub cutaneously into the mammary fat pad | 100mg/kg | Daily oral administration for 4 days once tumours reached 100mg | Tumors were resected at 4 and 8 hours after the first dose and 4 hours after consecutive doses<br><br>Early effects:<br>Increased tumor hypoxia at 8 and 4 hours after the first and second dose<br><br>Later effects:<br>Elevated levels of apoptotic (78-fold) and hypoxic (85-fold) cells after the third dose<br>Reduction in Ki67 (55%) and MECA-32 (75%) |

Importantly, these pre-clinical and clinical data strengthen the hypothesis that observed treatment response might be partially mediated by cells of the BME. However previously mentioned studies did not assess the direct effects of CBZ on the BME in great detail. *In vitro* assays determining the impact of CBZ treatment on bone cells showed effects of the therapeutic agent on both osteoblasts and osteoclasts – summarised in greater detail in Table 11. CBZ inhibited differentiation, proliferation and overall resorptive activity in RAW

264.7 pre-osteoclastic cells in two independent studies [230, 276]. However, *in vitro* data on osteoblastic cells are contradictory, with some reporting increased mineralisation and alkaline phosphatase (ALP) activity [231], whereas others found no effects of CBZ on mineralisation [230] and biphasic effects on ALP [230, 276].

The few studies investigating and reporting effects of CBZ on bone cells *in vivo* were all performed in models of prostate cancer-induced bone disease [230, 231, 233, 235]. Indeed, initial observations of these experiments on tumour-free bone in mice [230, 231] indicate that CBZ may have direct effects on the BME. The authors report inhibitory effects of CBZ on osteoclasts [230, 233] and stimulatory effects on osteoblasts [230, 232], summarised in greater detail in Table 12 below. However, the extensive loss of bone, combined with the profound effects of increasing tumour burden in this setting, could mask the effects of therapies on the BME.

**Table 11 Effects of CBZ on bone cells *in vitro***

| Study | Bone cell line | Dose | Effects on bone cells |
|---|---|---|---|
| Nguyen *et al.* [231] | MC3T3 | 0.01-3µM | • Increased mineralisation<br>• Increased alkaline phosphatase activity<br>• Decreased proliferation |
| Stern *et al.* [276] | RAW 264.7 preosteoclast cells<br><br>MC3T3-E1 osteoblastic | 1-10µM | **Osteoblasts**<br>• Decreased RANKL expression<br>• Alkaline phosphatase – biphasic effects<br>• Decreased proliferation<br>• Reduced viability<br>**Osteoclasts**<br>• No effect on expression of RANK, cathepsin K, integrin αV, integrin β3, TRAP or NFATc1 after 24hr culture<br>• after RANKL induced osteoclastogenesis - reduction in activity after 5 day culture<br>• Decreased proliferation<br>• Reduced viability |
| Dai *et al.* [230] | Murine MC3T3 E1<br><br>ST-2 mouse bone marrow stromal cells,<br><br>RAW 264.7 mouse macrophage /monocytes | 0.01-5µmol/L | **Osteoblasts**<br>• Decreased viability<br>• Alkaline phosphatase – biphasic effects<br>• Decreased osteocalcin expression<br>• No effect on mineralisation<br>• Inhibited phosphorylation of VEGFR2<br><br>**Osteoclasts**<br>• Inhibited differentiation<br>• Inhibition of overall resorptive activity |

**Table 12 Reported effects of CBZ on tumour and bone cells *in vivo*.**
Oc is Osteoclast, Ob is osteoclast, tb is tumoured bone, i.t. is intra tibial, s.c. is subcutaneously. Note the lack of studies investigating the effects of CBZ on the tumour free bone microenvironment. n.a. = not assessed

| Study | Tumour model | Tumour growth | Effects on bone volume (tumour bearing bone) | Oc | Ob |
|---|---|---|---|---|---|
| **Nguyen *et. al* [231] Prostate cancer** | LnCaP 23.1 (i.t.) (androgen-sensitive,elict osteoblastic reaction) | Decreased (i.b.) | Decreased | n.a. | n.a |
| | C4-2B cells (i.t.) (castration resistant, elict mixed osteoblastic/osteolytic response) | Decreased (i.b.) | Increased | | |
| | C4-2B cells (s.c.) (androgen independednt, castration resistant, elict mixed osteoblastic/osteolytic response) | Decreased | n.a. | | |
| | BV/TV, Tb.N. increased, Tb.Sp. decreased in tumour-free bone | | | | |
| **Dai *et. al* [230] Prostate cancer** | LnCaP 35 (s.c.) (androgen dependent | Decreased | n.a. | Decreased | Increased |
| | Ace1luc cells (i.t.) (osteoblastic) | Decreased (i.b.) | Decreased | | |
| | C4-2Bluc (i.t.) (mixed) | Decreased (i.b.) | Increased | | |
| | PC-3luc (i.t.)(osteolytic) | No impact | No impact | | |
| | PC-3luc (s.c.) | Decreased | n.a. | | |
| | No affect on bone mineral content in tumour-free bone | | | | |
| **Graham *et. al* [233] Prostate cancer** | VCaP BM1/cr-luc cells (castration resistant, androgen dependent, osteoblastic) (i.t.) | Decreased (i.b.) | Increase in tumor-bearing to non-tumor-bearing limb/bone volume ratio Decreased exterior bone growth | Decreased | n.a. |
| **Schimmoller *et al*. [232] Prostate cancer** | CRPC ARCaPM (osteoblastic/osteolytic) (i.t.) | Decreased | Preserves bone volume and mineral content (tumour bearing bone) | No effects$^{(tb)}$ | Increased$^{(tb)}$ |

In summary, both clinical and preclinical studies have highlighted the potential of CBZ to partially mediate its treatment response by modifying cells of the BME. Therefore I have chosen to elucidate the effects of CBZ on bone in the absence of tumour.

### 4.3. Hypotheses

The overall hypothesis in this chapter is to test whether CBZ partially mediates treatment effects by targeting the BME. The following was hypothesised:

- Cabozantinib mediates treatment response in patients with bone metastasis by altering bone remodelling; thus disrupting the vicious cycle.
    - Cabozantinib reduces osteoclast activity and number in the absence of tumour.
    - Cabozantinib increases bone volume by reducing bone resorption and/or increasing osteoblast activity.
- Cabozantinib affects the bone marrow vasculature, which contributes to reduced tumour growth in bone.
- Further cell types of the BME (e.g. megakaryocytes, chondrocytes) express target receptors of Cabozantinib, hence effects of CBZ on these cell types contribute to therapeutic response.

### 4.4. Aims and objectives

Within the aim of this chapter was to determine:

- What is the effect of Cabozantinib on osteoblasts (number, activity)?
- What are the effects of Cabozantinib on osteoclasts (number, activity)?
- What are the effects of Cabozantinib on bone structure and volume?
- Does Cabozantinib affect other cell types in bone (vascular cells, megakaryocytes, bone marrow cells etc.)?
- Does Cabozantinib modify the expression levels of genes associated with bone remodelling?

## 4.5. Material and methods

A summary of methods and analysis used can be seen in Table 13 below.

**Table 13 Summary of methods, parameters analysed and equipment used in Chapter 4.**

| Method | Parameters analysed | Equipment |
|---|---|---|
| Microcomputed tomography | Bone integrity of tibia:<br>-Trabecular bone volume (BV/TV in %)<br>-Trabecular number (TB.N. in $mm^{-1}$)<br>-Trabecular thickness (Tb.Th. in mm) | -SkyScan 1172 scanner (SkyScan)<br>-NRecon software<br>-CTAn software |
| **Histological assessment** | | |
| Tartrate-resistant acid phosphatase staining (TRAP) | -Osteoclast number per mm of trabecular bone surface<br>-Osteoclast size (in $mm^2$) | -OsteoMeasure software (OsteoMetrics)<br>-Leica DMRB upright microscope |
| Haematoxylin and Eosin staining (H&E) | -Osteoblast number per mm trabecular bone surface<br>-Quantification of growth late area per tissue area<br>-Quantification of Megakaryocytes per $mm^2$ tissue area | -OsteoMeasure software (OsteoMetrics)<br>-Leica DMRB upright microscope |
| Safranin-O staining | -Alterations in growth plate area<br>-Visualise proteoglycan | -OsteoMeasure software (OsteoMetrics)<br>-Leica DMRB upright microscope |
| Immunofluorescence - microscopy | -Visualisation of Endomucin positive vascular endothelial cells<br>-Alterations in bone formation<br>-Bone formation rate<br>-Mineral apposition rate<br>-Mineralising surface (%) | -Leica DMI4000B microscope and LAS AF Lite software (20x objective)<br>-Nikon A1 confocal microscope with NIS Elements software (40x objective)<br>-OsteoMeasure software (OsteoMetrics)<br>-Leica DMRB upright microscope |
| **Enzymatic analysis** | | |
| MouseTRAP™ Assay | -Osteoclast activity | -MouseTRAP™ Assay from immunodiagnostic systems (SB-TR103) |
| Rat/Mouse PINP Enzyme immunoassay | -Osteoblast activity | -Rat/Mouse PINP Enzyme immunoassay for the quantitative determination of N-terminal propeptide of type I procollagen from immunodiagnostic systems |
| **Gene expression level** | | |
| Real time PCR – gene expression | -Expression of genes associated with bone remodelling | -TRIzol RNA extraction in combination with the RNA Clean & Concentrator Kit (Zymo Research)<br>-High Capacity RNA-to-cDNA™ Kit (Applied Biosystems®)<br>-ABI PRISM 7900HT Sequence Detection System (Applied Biosystems)<br>-SDS 2.1 software<br>-TaqMan ® Gene expression assays (Life Technologies) |
| **Bone marrow cellularity** | | |
| Flow cytometry | -Percentage of haematopoietic cells in bone marrow | -LSRII (BD Bioscience) |

| Protein expression | | |
|---|---|---|
| Western blot | -Met receptor phosphorylation | -(c-Met [pY1230/34/35] Rb recombinant monoclonal Ab, Invitrogen, Clone 5H27L59, 1:1500; Met Antibody (C-28), sc-161, Santa Cruz) |
| **Statistical analysis** | | |
| Statistical analysis | -Experimental datasets | -Prism GraphPad |

Methods not described below can be found in the general methods section in Chapter 2.

### 4.5.1. Substance preparation

#### 4.5.1.1. Preparation and administration of Cabozantinib

Cabozantinib (XL184, CBZ), a kind gift from Exelixis Inc., South San Francisco, California, USA) was prepared in sterile filtered $dH_2O$ according to company recommendations. Briefly, CBZ at a concentration of 30mg/kg was dissolved in sterile filtered $dH_2O$. The drug suspension was placed in an ultrasonic water bath for 1min followed by brief vortexing (cycle repeated 4 times). To aid dissolution and ensure better tolerability 5µL 1N HCl per 3mg/mL CBZ were added to the drug suspension as advised by Exelixis. The drug was administered via oral gavage needles attached to a 1mL syringe, immediately after preparation and suspensions prepared fresh every day.

#### 4.5.1.2. Preparation and administration of Calcein

Calcein intercorporates into newly calcified bone and was therefore used to monitor the rate of new bone formation following CBZ treatment. Calcein was prepared in 0.2% sodium bicarbonate and injected intraperitoneal at a concentration of 30mg/kg, 6 and 2 days pre cull.

### 4.5.2. Experimental design

As breast and prostate cancer preferentially metastasise to bone I incorporated male and female animals in my experiments. Using animals of different sex, age and strain additionally allowed me to establish the effects of CBZ in a range of microenvironments and to determine the degree of variability between these. Animal models included in these experiments are as follows: **1)** 6-week old male BALB/c nude mice, **2)** 6-week old female BALB/c nude mice (BALB/c-Nude[Foxn1-Crl]; both Charles River, UK), **3)** 8**–**9-week old female genetically engineered mice expressing GFP+ve cells of the osteoblastic lineage on a BALB/c nude background ((BALB/cAnNCrl.Cg-Tg(Col1a1-GFP)Row Foxn1nu/nu, described in [158], heterozygous, referred to as GFP $Ob^+$ mice) and **4)** 17-week old female genetically engineered GFP $Ob^+$ mice (both Leeds Institute for Molecular Medicine, UK). As bone remodelling is reduced with increasing age using two cohorts of mice, 8-9-week old female

GFP $Ob^+$ (n=4/group) with a high bone turnover and 17-week old female GFP $Ob^+$ (n=4/group) mice with a more mature skeleton allowed me to elaborate the effects of CBZ in these different BMEs. Breast cancer preferentially metastasises to bone hence indicating the potential of CBZ as a potential treatment for late stage disease. Therefore the majority of experiments were performed in female animal models.

#### 4.5.2.1. Treatment schedules

Previous studies give evidence to hypothesise rapid effects of CBZ on bone and/or bone cells. In a model of prostate cancer bone metastasis Graham and colleagues observed reduced number of osteoclasts in tibiae of both tumour-bearing and tumour-free mice after 15 days of treatment with CBZ (30mg/kg, daily) [233]. Additional studies by Doran *et al.* observed reduced radiotracer accumulation at the site of bone remodelling in mice with surgically (fracture)-induced bone remodelling after 7 administrations of 30mg/kg CBZ [236]. I therefore aimed to establish the short-term effects of 5 and 8 doses of CBZ on the naïve *in vivo* BME.

Animals were randomised in two groups receiving (1) 30mg/kg CBZ (200µL) or (2) sterile $H_2O$ control (200µL). 8-9-, and 17-week old GFP-$Ob^+$ mice (n=4/group) received 30mg/kg CBZ or sterile $H_2O$ control 5x weekly for 5 days (cumulative dose of 150mg/kg) and were culled 24hrs after the last treatment (Fig. 37A). 6-week old male and female BALB/c nude (n=4-5/group) as well as female 9-week old GFP $Ob^+$ mice (n=4/group) were administered 30mg/kg CBZ or sterile $H_2O$ control 5x weekly for 10 days (8 administrations in total, cumulative dose of 240mg/kg CBZ). Animals were culled 6hrs after the last treatment. To monitor the rate of bone formation Calcein (30mg/kg, 100µL, i.p., Sigma-Aldrich) was injected 6 and 2 days pre cull (for the 10 day treatment schedule) and 4 and 2 days pre cull (for the 5 day treatment course, 8-9-week old mice) respectively. Additional animals were culled on day 15 and 22 to assess the reversibility of effects 5 and 12 days after the last administration of CBZ, respectively (Fig. 37B).

An additional pilot experiment using 10-week old male C57BL/6J mice (n=3/4 group) receiving the previously described treatment schedule was performed for future method establishment. 1 animal per group was culled 3.5hrs post treatment termination, the remaining animals 24hrs after the last dose.

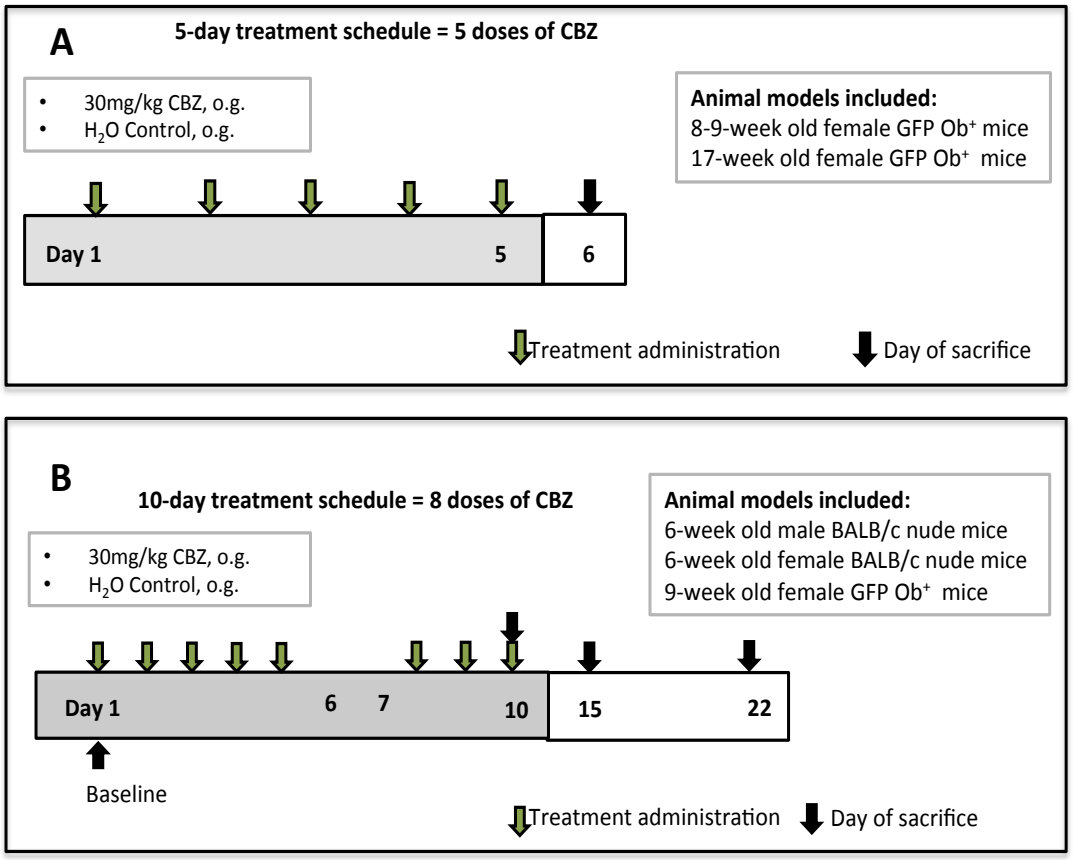


**Figure 37 Schematic outline of the *in vivo* studies investigating the effects of CBZ on the bone microenvironment.**
(A) 8-9- and 17-week old female GFP $Ob^+$ mice (n=4/group) received 30mg/kg Cabozantinib (CBZ) or sterile $H_2O$ control (CTRL) 5x weekly for 5 days via oral gavage. Animals were killed 24hrs after the last treatment administration. (B) Male and female 6-week old BALB/c nude as well as 9-week old female GFP $Ob^+$ mice (n=4-5/group) received 8 doses of 30mg/kg CBZ or sterile $H_2O$ control (CTRL). Animals were killed 6hrs after the last administration. To monitor if treatment effects of CBZ were maintained once treatment was terminated additional female BALB/c nude mice were culled 5 (Day 15) and 12 days (Day 22) after treatment termination.

To determine longer-term effects of CBZ on the BME I obtained paraffin embedded bone samples from collaborative experiments [231, 233]. These samples included contralateral, non-tumour bearing tibiae from castrated adult male NOD/SCID mice (injected intratibially with VCaP BM1/cr-luc prostate cancer cells, 30mg/kg CBZ daily for 15 days (n=6-7/group) [233], as well as tibiae from 6-week old castrated male beige SCID mice (injected intratibially with C4-2B prostate cancer cells, 60mg/kg CBZ 5x weekly for 6-weeks (n=9-10/group) [231].

### 4.5.3. Effects of CBZ on osteoblasts and osteoclasts

Number and activity of osteoblast and osteoclast was assessed as described in Chapter 2, Section 2.2.10.7.

### 4.5.4. CBZ-induced alterations in growth plate composition

To determine the effects of CBZ on growth plate chondrocytes, an area of interest (AOI) was interactively drawn around the total growth plate area, the resting/proliferating and hypertrophic chondrocyte zones using OsteoMeasure software (Fig.38A-C), 4x objective and a Leica DMRB upright microscope. Both growth plate areas of interest (AOIs, in $mm^2$) were then normalised to total epiphyseal growth plate area ($mm^2$) (Fig.38A-C) and data are presented as AOI ($mm^2$)/ total growth plate area (in $mm^2$). The total length of the growth plate was assessed usually covering 3-4 fields of view with each having a total area of 625µm x 625µm. Growth plate area/total tissue area for each sample was then calculated for 2 non-serial levels. Analysis was performed on H&E stained sections using a 4x objective.

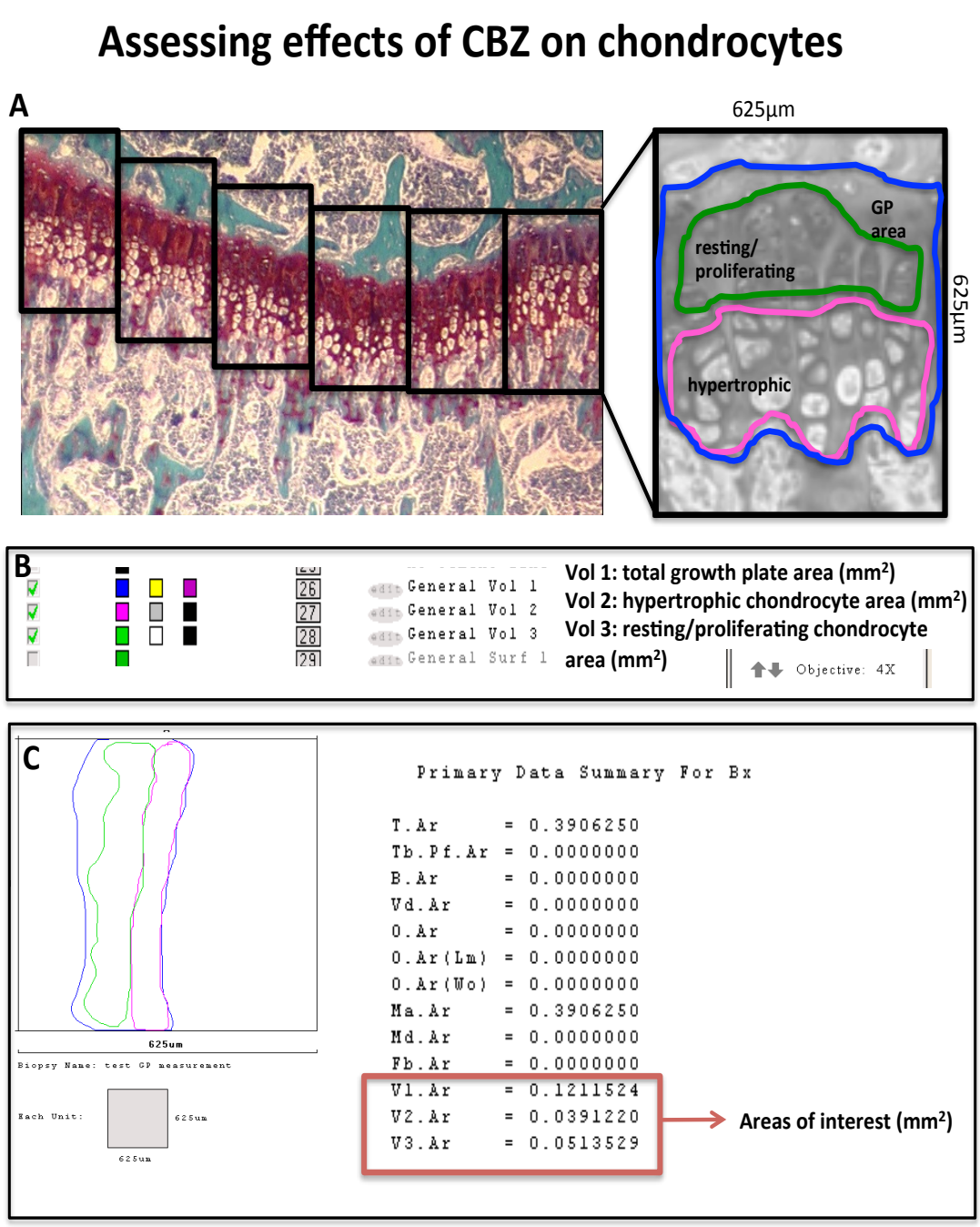


**Figure 38 Analysis of Cabozantinib effects on the growth plate chondrocytes.**
To determine effects of Cabozantinib treatment on growth plate chondrocytes it was interactively drawn around the total growth plate (GP) area (blue), the resting/proliferating (green) and hypertrophic (pink) chondrocyte area using OsteoMeasure, OsteoMetrics software, black squares represent fields of view with an area of 625x625µm. (A) Analysis was performed using a Leica DMRB microscope, 4x objective. (B) shows parameter specifications used for drawing around the separate zones. (C) shows representative data obtained from one field of view. For data representation individual growth plate zones (in $mm^2$) were normalised to total growth plate area (in $mm^2$), thereby representing the proportion of the individual zones per total growth plate area.

### 4.5.5. Quantification of bone marrow megakaryocytes

To assess alterations in bone marrow cellularity the number of megakaryocytes on 2 non-serial H&E stained histological sections was scored using OsteoMeasure software (OsteoMetrics) and a Leica DMRB upright microscope (10x objective). Megakaryocytes were identified by their characteristic shape and large lobulated nucleus (see Fig.39). All megakaryocytes per $mm^2$ tissue area were scored commencing 125µm away from the growth plate. An area with the length of 1250µm (5 fields of view with 250µm in length, measured on the medial side of the tibia) was assessed. Scored megakaryocyte number was then normalised to the total tissue area scored (see Fig. 39) and data are represented as megakaryocyte numbers/$mm^2$ tissue area.

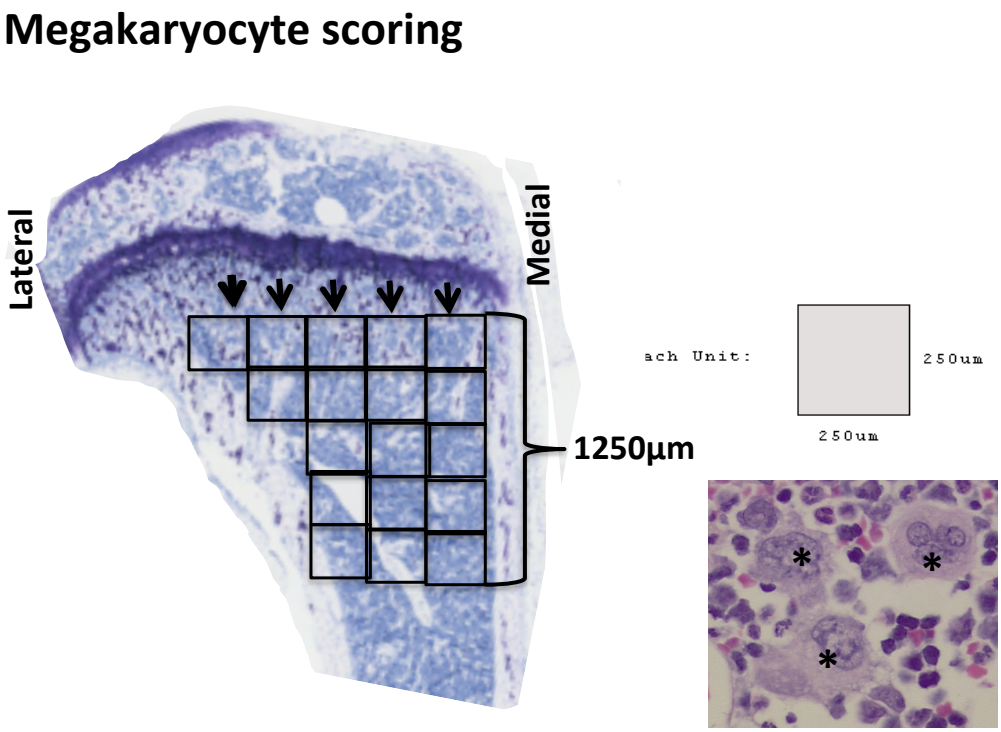


**Figure 39 Assessing efects of CBZ on megakaryocytes.**
Number of megakaryocytes was scored for a total tissue area with the length of 1250µm (measured on the medial side of the tibia). Number of megakaryocytes was then normalised to the total tissue area assessed. Each square represents a field of view with 250µm x 250µm. OsteoMeasure software, OsteoMetrics, Leica DMRB microscope and a 10x objective were used.

### 4.5.6. Visualisation of bone marrow endothelial vascular cells

To visualise effects of CBZ on the bone marrow vasculature immunofluorescence staining against the endothelial cell marker Endomucin was performed on 3µm histological sections of paraffin embedded tibiae as described in Chapter 2, Section 2.2.10.6.2. Images were acquired using a Leica DMI4000B microscope and LAS AF Lite software (20x objective) and a Nikon A1 confocal microscope with NIS Elements software (40x objective).

### 4.5.7. Assessment of bone formation rates using calcein double-labelling

Calcein intercorporates into newly formed bone and was therefore used to establish effects of CBZ on bone formation rate. Calcein analysis was performed on histological sections of lumbar vertebra 4 from 6-week old female BALB/c nude mice (n=4/group) that received 10-day treatment of 30mg/kg Cabozantinib (8 administrations) or $H_2O$ control, respectively.

Darren Lath, University of Sheffield, UK, kindly provided a protocol for Calcein analysis of long bones, which I adapted for the analysis of vertebrae for my experiments (see Figure 40). Analysis was performed using OsteoMeasure software (OsteoMetrics), a Leica DMRB upright microscope with a 10x objective. The following parameters were determined by manually drawing around the bone surfaces/calcein labels. The following table explains analysed parameters and data analysis:

**Table 14 Parameters analysed during assessment of calcein labelling**

| Parameter | Abbreviations | Definition |
|---|---|---|
| Mineralisation Surface (MS,%) = ((dL+0.5sL)/BPm.)x100 | dL: double label perimeter<br>sL: single label perimeter<br>BPm.: bone perimeter | Extent of actively mineralising bone surface |
| Mineral apposition rate (MAR, µm/day) = IL.W/number of days between injections | IL.W: inter-label width, distance between double labels | Distance between the labels divided by the time between labelling; rate at which osteoblasts are producing new matrix → measures Ob activity |
| Bone formation rate (BFR, $mm^2$ $x10^{-3}$/mm/day) = (MARx(dL+0.5sL))/BPm | See above | Multiplies the MAR by the fraction of bone surface that is labelled → takes into account how much of the bone surface is actively mineralising |

Information obtained from [277].

For vertebrae, analysis was started 250µm away from the growth plate and 250µm away from the cortical bone surface. All cortical bone surfaces were excluded from analysis. A total area comprising 9 squares of interest (each accounting for 250µmx250µm) was analysed. It was manually drawn around trabecular bone surfaces, single and double calcein labels using a 10x objective and OsteoMeasure software (Fig.40). Only one histological level per sample was assessed.

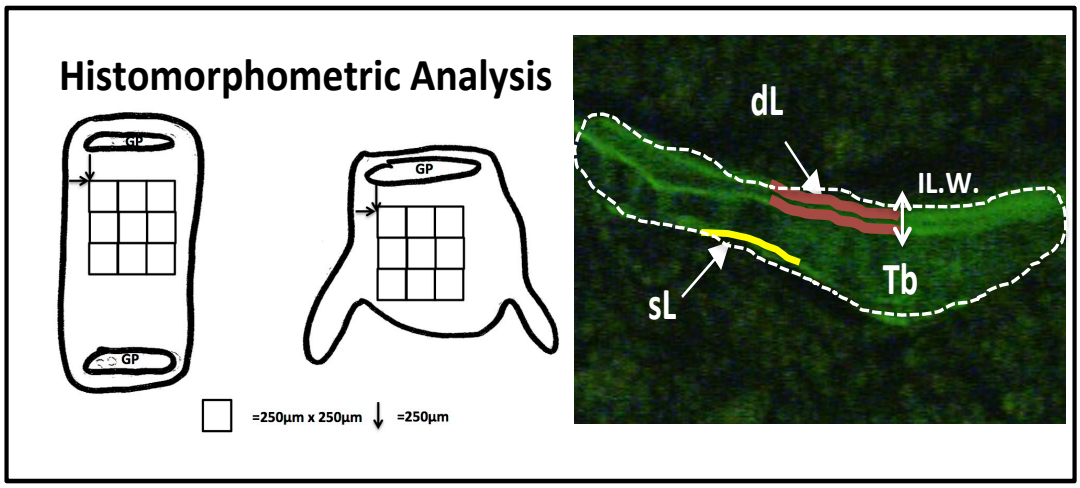


**Figure 40 Assessing effects of CBZ on bone formation using Calcein double-labelling.**
Analysis was started 250µm away from the growth plate and 250µm away from the cortical bone surface. All cortical bone surfaces were excluded from analysis. A total area comprising 9 squares of interest (each accounting for 250µmx250µm) was analysed. It was manually drawn around trabecular bone surfaces, single and double calcein labels using a 10x objective and OsteoMeasure software. Only one histological level per sample was assessed.

### 4.5.8. Gene expression analysis

On day of cull, bones were immediately preserved in RNAlater Tissue Collection Solution (Ambion, Life Science Technologies), followed by dividing into halves and manually scraping out bone marrow using scalpels and razor blades. Samples where then processed, RNA extracted and cDNA synthesised as described in Chapter 2, Section 2.2.10.9. Tibia and femur from each mouse were pooled to ensure sufficient concentration of extracted RNA.

Alterations in genes associated with bone remodelling was assessed using qRT-PCR. Genes of interest included OPG (Mm00435451_m1), RANKL (Mm00441906_m1), RANK (Mm00437135_m1; Mm00437132_m1), Vegf (Mm01281449_m1) and Sox9 (Mm00448840_m1). Data were normalised to B2M (Mm00437762_m1) expression levels (see Table 15 below).

**Table 15 Summary of genes analysed following Cabozantinib administration**

| Gene | Function |
|---|---|
| OPG (Osteoprotegerin) | Decoy receptor for RANKL; inhibits osteoclast differentiation, fusion, and activation; negative regulator of bone remodeling |
| RANK (Receptor Activator of NF-κB) | Essential for osteoclastogenesis |
| RANKL (Receptor Activator of Nuclear Factor NF-κB Ligand) | Required for osteoclastogenesis and osteoclastic bone resorption |
| Vegf (Vascular Endothelial Growth Factor) | Angiogenesis |
| Sox 9 | Transcription factor for chondrogenesis |

### 4.5.9. Flow cytometric evaluation of effects of CBZ on bone marrow cellularity – a pilot study

The effects of CBZ on bone marrow composition were confirmed by histopathologist Dr. Keith Hunter. I aimed to detect alterations in bone marrow cellularity after CBZ (30mg/kg, o.g.) or sterile $H_2O$ control in 10-week old male C57BL/6J mice receiving the previously described 10-day administration regimen using flow cytometry. Animals were sacrificed 3.5hrs post administration (n=1/group) and 24hrs post administration (n=3 for CTRL and n=2 for CBZ).

Right hind legs were dissected and soft tissue removed. Tibia and femur were separated, proximal end removed using a scalpel and the bone marrow was flushed out with 1mL FACS buffer (1%FBS in PBS (w/o $Mg^{2+}$, $Ca^{2+}$)) by inserting a 25G needle. Flushing was repeated 3 times or until the bone appeared translucent. Bone marrow aspirates from the right tibia and femur were pooled for each mouse and filtered through a 100-µm cell strainer (BD Falcon).

The 2mL cell aspirate was centrifuged at 2500rpm (MSE Mistral 2000; ≈1121xg) and resuspended in 1mL FACS buffer prior to aliquoting into individual tubes for analysis as outlined below. For each animal fluorescence minus one (FMO) controls were included as outlined in Table 16. Cell suspensions were centrifuged at 2500rpm (Heraeus FRESCO21; ≈600xg) at 4°C for 5 minutes and redissolved in 200µL FACS buffer containing appropriate antibodies (1µL of Ab per 200µL FACS buffer). Samples were stained for 30min in the dark using Anti-Mouse CD41 PE (eBioscience, Clone: eBioMWReg30 (MWReg30), Cat. No: 12-0411-81), Anti-Mouse TER-119 APC (eBioscience, Clone: TER-119, Cat. No: 17-5921-81), Brilliant Violet 421™ anti-mouse CD45 Antibody (BioLegend, Clone 30-F11, Cat.No: 103133) and LIVE/DEAD® Fixable Near-IR Dead Cell Stain (Life technologies, Cat.No.: L10119).

**Table 16 Sample preparation for flow cytometric analysis including relevant controls (Fluorescence Minus One)**

| For each mouse | |
|---|---|
| **Bone marrow flush (µL)** | **Labelling** |
| 150 | All-Ter119 |
| 150 | All-Viability |
| 150 | All - (Ter119+Viability) |
| 200 | All Abs |

Next samples were washed 2 times in FACS buffer (400µL, at 2500rpm, Heraeus FRESCO21, ≈600xg at 4°C) prior to immediate analysis using flow cytometry (LSRII, BD Bioscience). 600000 events were recorded for each sample, medium flow rate was used. Samples were run and gates set by the Flow Cytometry Core Facility, University of Sheffield, UK.

**Table 17 Laser settings for flow cytometric analysis and corresponding dyes**

| Emission/Filter | VOLTAGE | DYE |
|---|---|---|
| Red 780 | 555 | Near infrared |
| Violet 450 | 570 | Brilliant violet 421 |
| Blue 575 | 712 | PE |
| Red 660 | 692 | APC |

### 4.5.10. Western blot analysis for phosphorylated MET

To determine phosphorylation of MET snap frozen liver samples of 10-week old male C57BL/6J mice receiving the previously described 10-day administration course of CBZ were analysed for protein expression of MET and phosphorylated MET (24hrs post administration n=2 for CBZ and n=3 for CTRL; n=1/group 3.5hrs post administration). Liver samples were lysed using the Mammalian Cell Lysis Kit (Sigma Aldrich, MCL1-1K) with added Halt$^{TM}$ Protease & Phosphatase Inhibitor Cocktail (Thermo Scientific, Prod#78440). Protein concentration of lysates was assessed using the BCA assay and 50ng for each sample run on 10% gels. Gels were run at 200V for 1hr, transferred/blotted for 70min at 70V. Membranes were blocked in 5% BSA, incubated in primary antibody (c-Met [pY1230/34/35] Rb recombinant monoclonal Ab, Invitrogen, Clone 5H27L59, 1:1500; Met Antibody (C-28), sc-161, Santa Cruz), 1:100 as recommended by manufacturers instructions) overnight. Within the recommended dilution range of 1:100-1:1000 the Met antibody was tested at a concentration of 1:100-1:200; no expression was determined at a

concentration of 1:200, with clear bands obtained at a concentration of 1:100; the concentration used for further experiments. The c-Met [pY1230/34/35] antibody was tested at a concentration of 1:1000 and 1:1500; slight background was observed at 1:1000, which was eliminated by reducing the antibody concentration to 1:1500. The Secondary antibody was Anti-Rabbit IgG (Dako P0488, 1:30000). After membrane stripping (Restore™ Western Blot Stripping Buffer, Thermo Scientific) GAPDH (Ms mAB to GAPDH [6C5], Abcam, ab8245, 1:40000 (working concentration previously optimised in our laboratory)) was used as a loading control (secondary antibody: Polyclonal Goat Anti-Mouse Iggs HRP, Dako, P0447). Western blot optimisation was kindly assisted by Diane Lefley, Resarch Technician, University of Sheffield.

#### 4.5.11. Statistical Analysis

Statistical analysis was performed using GraphPad Prism Version 6.0. Analysis was done using unpaired Student's t-test or 2-way ANOVA with Bonferroni's post-test. Statistical tests applied are specified underneath the corresponding figures or if no graphs are presented next to the raw data.

## 4.6. Results

### 4.6.1. The BME is modified following 5-days of Cabozantinib administration

This study aimed to establish whether short-term treatment with CBZ affects the BME. I therefore initially administered 30mg/kg/day CBZ for 5 days (cumulative dose = 150mg/kg) and assessed osteoblast and osteoclast number per mm trabecular bone surface, in addition to bone volume and structure, as compared to $H_2O$ control. Two cohorts of mice were used; 8-9-week old female animals with a high bone turnover and 17-week old female animals with a more mature skeleton, allowing comparison of the effects of CBZ in these different bone BMEs (Fig.37A).

#### 4.6.1.1. CBZ effects on osteoblasts

Osteoblasts were identified based on their characteristic morphology and quantified on H&E-stained tissue sections. In addition, I used genetically engineered mice expressing GFP in cells of the osteoblastic lineage to confirm the effects of CBZ on osteoblasts by immunofluorescence (hereafter called GFP $Ob^+$, Fig.41 A&B). After 5 daily administrations of 30mg/kg CBZ, there were significantly increased numbers of osteoblasts lining the trabecular bone surfaces in 17-week old GFP $Ob^+$ mice (CTRL: 17.92 ± 2.11 vs. CBZ: 44.02 ± 3.63, $p \leq 0.001$, Fig.41C). This effect, was also seen in 8-9-week old GFP $Ob^+$ mice, although less prominent (CTRL: 20.60 ± 2.46 vs. CBZ: 31.96 ± 2.21, $p \leq 0.05$, Fig.41A&B,E). Despite the increase in osteoblast number, there was no significant difference in osteoblast activity (serum PINP levels) between the treatment groups (17-week old GFP $Ob^+$: CTRL: 33.17 ± 2.74ng/mL vs. CBZ: 39.90 ± 3.64ng/mL, Fig.41D; 8-9-week old GFP $Ob^+$: CTRL: 81.35 ± 6.97ng/mL vs. CBZ: 86.87 ± 22.52 ng/mL; Fig.41F).

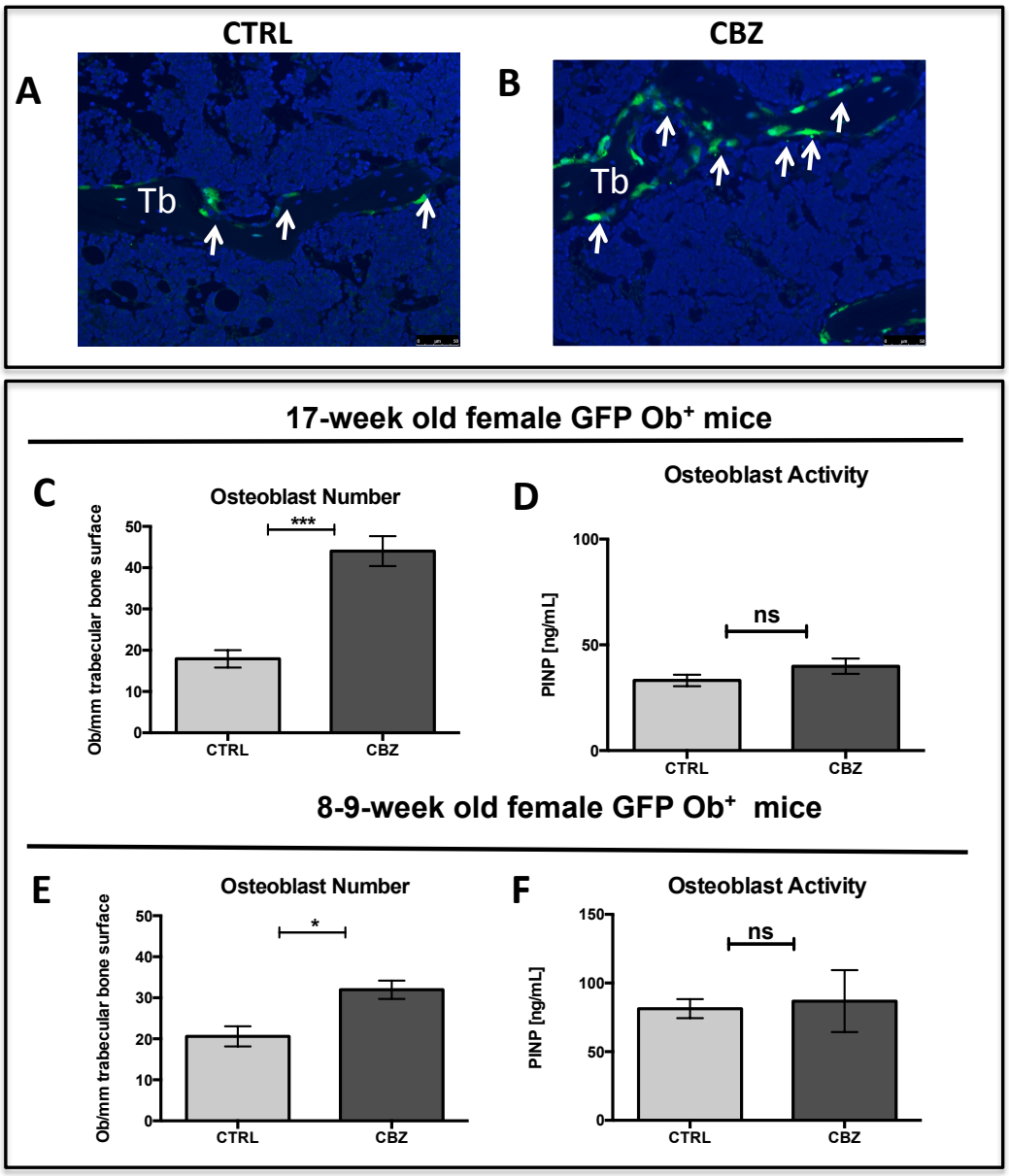


**Figure 41 Effects of 5-day treatment with Cabozantinib on osteoblasts.**
8-9 week old and 17-week old GFP $Ob^+$ mice received 5 doses of 30mg/kg Cabozantinib (CBZ) or sterile $H_2O$ control (CTRL). (A) Representative histological sections of tibiae showing GFP+ve osteoblastic cells lining trabecular bone surfaces by immunofluorescence, 20x objective. GFP+ve osteoblasts are shown in green. (C&E) Osteoblast number/mm trabecular bone surface and (D&F) osteoblast activity (measured by serum PINP levels), respectively after 5-day administration of Cabozantinib (CBZ, 30mg/kg) or $H_2O$ control (CTRL). (C&D) represents results for 17-week old (n=4/group) and (E&F) for 8-9-week old GFP $Ob^+$ mice (n=4/group). Osteoblast number/mm trabecular bone surface was scored on 2 non-serial histological H&E stained sections per sample. Student's t-test, ns is non significant,* is $p \leq 0.05$, *** is $p \leq 0.001$. All data show Mean±SEM. Tb = trabecular bone, osteoblast are indicated with white arrowheads.

#### 4.6.1.2. Effects on osteoclasts

The number of osteoclasts/mm trabecular bone surface was determined on TRAP-stained histological sections. Five daily administrations of CBZ induced a substantial reduction in osteoclast number/mm trabecular bone surfaces in 8-9-week old GFP $Ob^+$ mice compared to CTRL (CTRL: 6.91 ± 0.39 vs. CBZ: 3.95 ± 0.24, p≤0.001, Fig.42A&B, Fig.43A). In contrast, osteoclast number was not altered in older (17-week old) GFP $Ob^+$ mice (CTRL: 3.65 ± 0.37 vs. CBZ: 2.93 ± 0.43, Fig.43B), probably reflecting the age-related reduction in bone remodelling. Osteoclast activity (TRAP) was not affected by CBZ administration in either model (8-9-week old GFP $Ob^+$: CTRL: 7.82 ± 0.75 U/L vs. CBZ: 9.16 ± 1.50 U/L; 17-week old GFP $Ob^+$: CTRL: 11.14 ± 1.75 U/L vs. CBZ: 15.20 ± 1.50 U/L, Fig.43B,D). Osteoclast size was not altered in both mouse models following CBZ treatment when compared to control (8-9-week old GFP $Ob^+$: CTRL: $7.47x10^{-5}$ ± $4.94x10^{-6}mm^2$ vs. CBZ: $7.15x10^{-5}$ ± $2.04x10^{-6}mm^2$, Fig.43E; 17-week old female GFP $Ob^+$ mice: CTRL: $6.69x10^{-5}$ ± $7.11x10^{-6}mm^2$ vs. CBZ: 8.14± $3.49x10^{-6}mm^2$, Fig.43F).

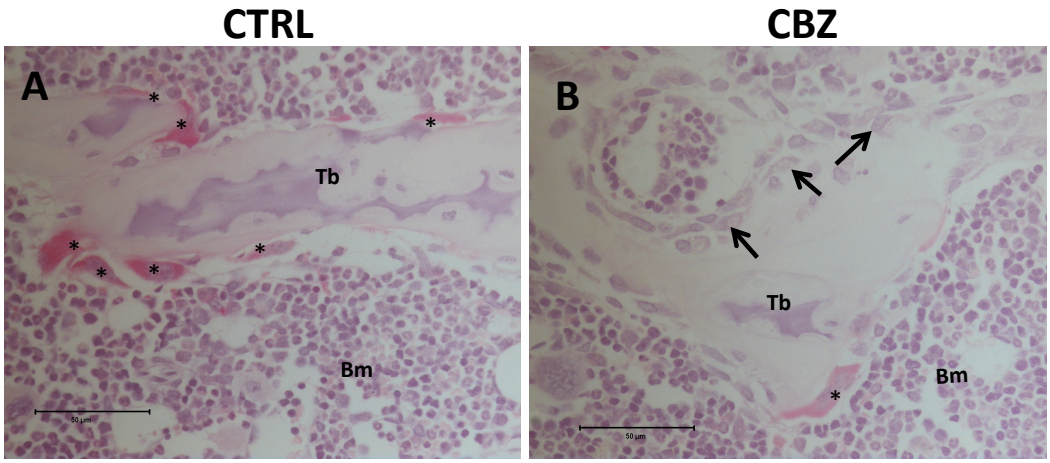


**Figure 42 Illustration of the effects of 5 doses of Cabozantinib on osteoclasts and osteoblasts *in vivo.***

(A) Representative TRAP-stained histological bone tissue sections from 8-9 week old mice illustrating the decrease in osteoclast numbers following 5 doses of 30mg/kg Cabozantinib (CBZ) or (B) control (CTRL). Osteoclasts are highlighted with black asterisk, osteoblasts with black arrowhead, 20x objective, scale bar is 50µm, Bm=Bone marrow, Tb=Trabecular bone.

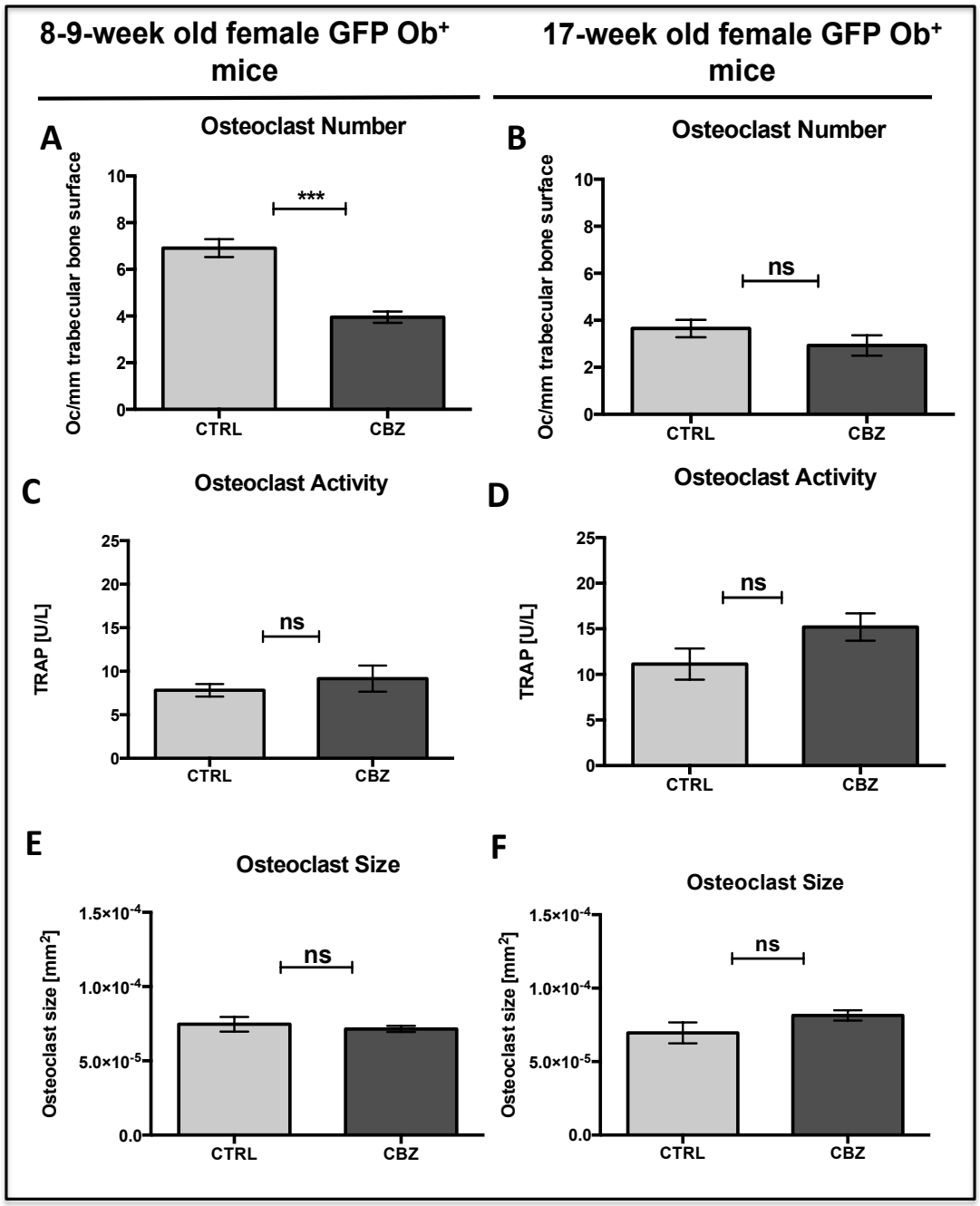


**Figure 43 Effects of 5-day treatment with Cabozantinib on osteoclasts.**
(A,C,E) 8-9 week old GFP $Ob^+$ and (B,D,F) 17-week old GFP $Ob^+$mice received 5 doses of 30mg/kg Cabozantinib (CBZ) or control (CTRL) daily (n=4/group). (A&B) osteoclast number/mm trabecular bone surface (C&D) osteoclast activity (serum TRAP levels) and (E&F) osteoclast size (in $mm^2$) were determined Student's t-test: ns is non significant, *** is $p \leq 0.001$. All data show Mean±SEM.

#### 4.6.1.3. Effects on bone volume and structure following 5 administrations of CBZ

To determine if the effects on osteoblasts and osteoclasts resulted in alterations of bone structure and volume, µCT analysis of proximal tibiae after administration of 30mg/kg CBZ or CTRL for 5-days was performed. There was significantly increased trabecular bone volume in 17-week old GFP $Ob^+$ mice ($p \leq 0.01$, Fig.44A, Table 18), whereas all other analysed bone parameters, including trabecular thickness and number remained unaffected. No CBZ-induced alterations in bone structure were determined in 8-9-week old animals (Fig. 44B, Table 18). Following CBZ treatment cortical bone volume was not altered in both animal models when compared to control receiving mice (Table 19).

Taken together, these data demonstrate that a 5-day course of CBZ treatment is sufficient to induce modifications of osteoblasts and osteoclasts, although longer-term administration of CBZ is likely to be required to cause significant alterations to bone structure.

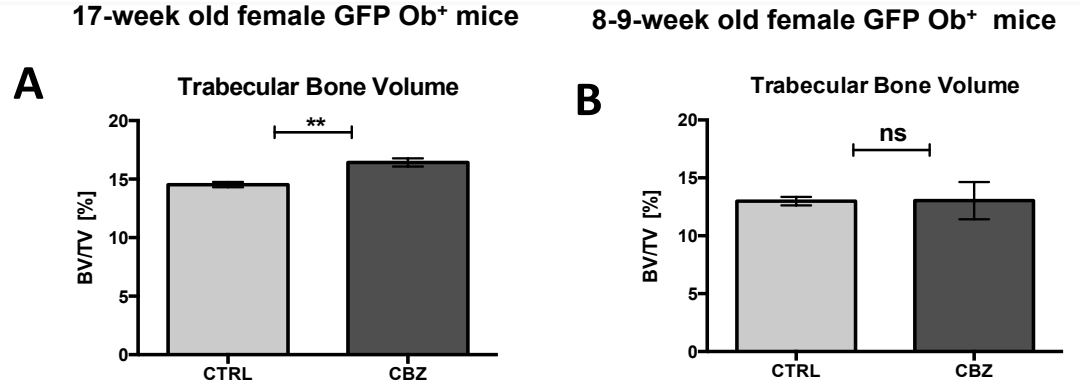


**Figure 44 Effects of 5-day treatment with Cabozantinib on trabecular bone volume.**
Trabecular bone volume (BV/TV in %) was analysed after 5 administrations of 30mg/kg Cabozantinib (CBZ) or control (CTRL) for (A) 17-week old GFP $Ob^+$ mice (n=4/group) and (B) 8-9-week old GFP $Ob^+$ mice (n=4/group). Student's t-test: ns is non significant, ** is $p \leq 0.01$. All data show Mean±SEM.

### 4.6.2. A 10-day course of Cabozantinib alters bone structure and modifies key bone cells

The 5-day administration of 30mg/kg CBZ (cumulative dose: 150mg/kg) rapidly modified osteoblast and osteoclast number with only modest effects on bone volume, therefore the dosing regimen was increased to a total of 8 administrations of CBZ over 10 days (cumulative dose: 240mg/kg, Fig. 37B).

#### 4.6.2.1. Effects on osteoblasts

8 doses of CBZ resulted in significantly increased osteoblast number/mm trabecular bone surface in 6-week old male BALB/c nude mice, compared to control (CTRL: 10.54 ± 1.23 vs. CBZ: 15.01 ± 1.12, $p \leq 0.05$, Fig.45A). However, there was no effect on osteoblast number in the other experimental animal models receiving this treatment regimen (6-week old female BALB/c nude: CTRL: 16.01 ± 1.48 vs. CBZ: 17.12 ± 0.97, Fig.45C; 9-week old GFP $Ob^+$: CTRL: 9.53 ± 0.66 vs. CBZ: 8.64 ± 1.33, Fig.45E). Similar to 5 doses of CBZ, administration of 8 doses did not alter serum PINP levels in 6-week old male BALB/c nude (CTRL: 332.0 ± 63.88ng/mL vs. CBZ: 431.6 ± 36.24ng/mL, Fig.45B), 6-week old female BALB/c nude (CTRL: 184.2 ± 31.33 ng/mL vs. CBZ: 151.2 ± 28.67ng/mL, Fig.45D) or 9-week old female GFP-$Ob^+$ (CTRL: 46.30 ± 1.81ng/mL vs. CBZ: 43.49 ± 7.18ng/mL, Fig.45F). In addition at day 5 and 12 after treatment termination no change in osteoblast number (Day 15: CTRL: 16.19 ± 1.86 vs. CBZ: 15.49 ± 1.08; Day 22: CTRL: 17.37 ± 2.34 vs. CBZ: 15.90 ± 0.88; 2-way ANOVA, Fig.49D) was observed. However, osteoblast activity was lower in CBZ treated mice when compared to control (Day 15: CTRL: 226.1 ± 27.75ng/mL vs. 131.3 ± 17.12 ng/mL, $p \leq 0.05$; Day 22: CTRL: 186.1 ± 32.59 ng/mL vs. CBZ: 94.11 ± 11.79ng/mL; 2-way ANOVA, Fig.49B). Representative TRAP-stained histological slides from 6-week old female BALB/c nude mice are shown in Fig.46A&B.

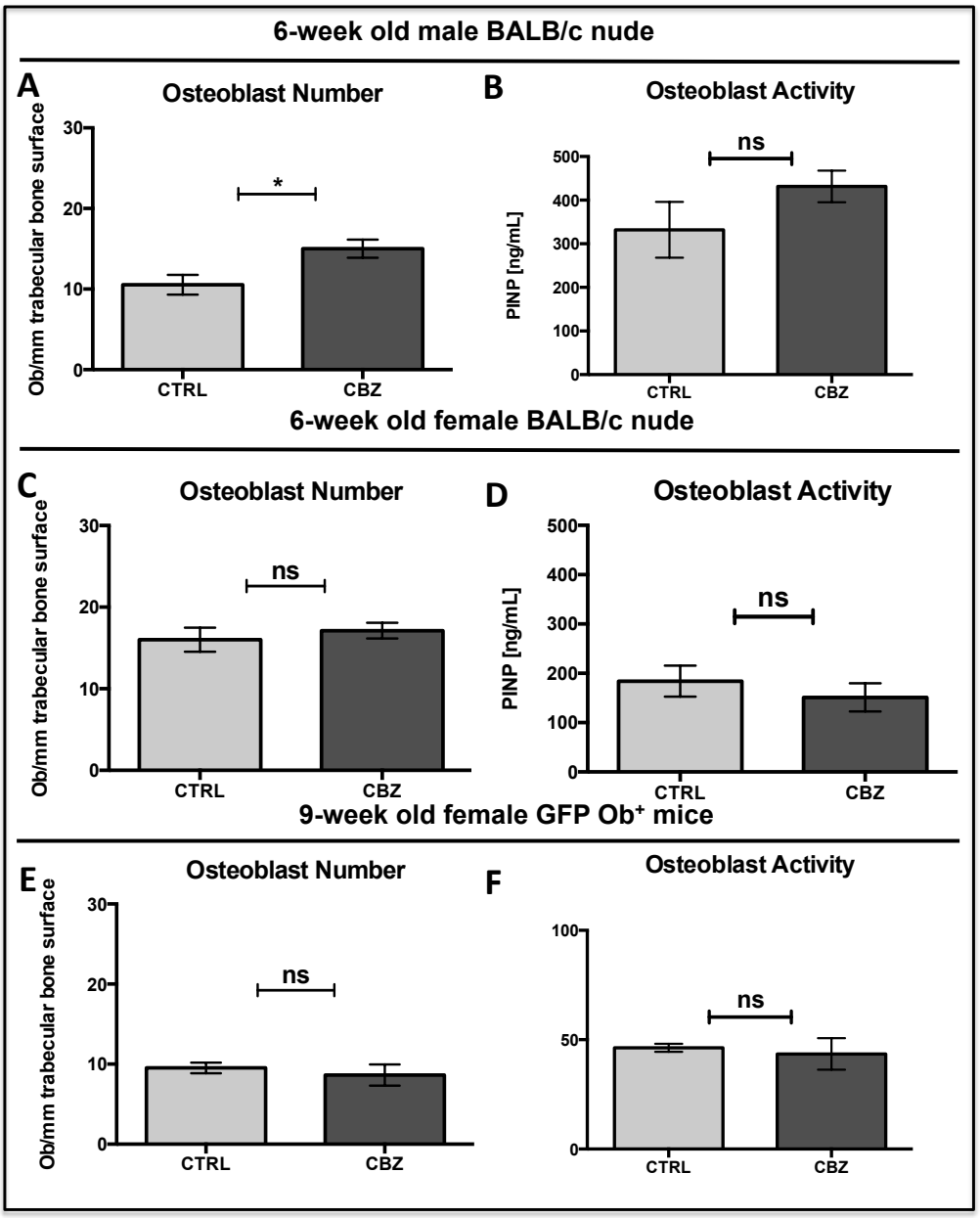


**Figure 45 Effects of 8 administrations of CBZ on osteoblasts *in vivo*.**
Osteoblast number/mm trabecular bone surface (A,C,E) and activity (measured by serum PINP levels) (B,D,F) were determined after 8 doses of 30mg/kg CBZ or sterile $H_2O$ control (CTRL) in 6-week old male BALB/c nude mice (n=4/group, A&B), 6-week old female BALB/c nude (n=5/group, C&D) and 9-week old female GFP $Ob^+$ mice (n=4/group, E&F). Student's t-test: ns is non-significant, * is $p \leq 0.05$. All data show Mean±SEM.

#### 4.6.2.2. Effects on osteoclasts

When compared to control, 8 doses of CBZ did not alter osteoclast number in 6-week old male BALB/c nude mice (CTRL: 5.63 ± 0.16 vs. CBZ: 6.56 ± 0.59, Fig.47A) but resulted in significantly increased osteoclast size (CTRL: $7.10x10^{-5} \pm 4.74x10^{-6}$ $mm^2$ vs. CBZ: $9.72x10^{-5} \pm 6.53x10^{-6}$ $mm^2$, $p \leq 0.05$, Fig.48A), which may indicate a loss of activity. In contrast, there was a significant decrease in osteoclast number both in 6-week old female BALB/c nude (CTRL: 8.29 ± 0.39 vs. CBZ: 6.78 ± 0.48, $p \leq 0.05$, Fig.46, Fig47C) and 9-week old GFP $Ob^+$ (CTRL: 5.99 ± 0.46 vs. CBZ: 4.15 ± 0.30, $p \leq 0.05$, Fig.47E) treated with CBZ. Osteoclast activity was not significantly altered in 6-week old female BALB/c nude mice (CTRL: 15.99 ± 0.75 U/L vs. CBZ: 13.81 ± 2.99 U/L, Fig.47D) and 9-week old GFP $Ob^+$ mice (CTRL: 11.64 ± 1.21 vs. CBZ: 12.97 ± 1.23 U/L, Fig.47F). However, increased osteoclast activity in 6-week old male BALB/c nude mice receiving CBZ was observed, although this did not reach statistical significance (CTRL: 13.98 ± 1.06 vs. CBZ: 18.52 ± 1.90,Fig.47B). CBZ-induced effects on osteoclast number were rapidly reversed after treatment termination (Day 10: CTRL: 8.29 ± 0.39 vs. CBZ: 6.78 ± 0.49; Day 15: 7.55 ± 0.45 vs. CBZ: 7.80 ± 0.23; Day 22: CTRL: 9.84 ± 0.35 vs. CBZ: 9.99 ± 0.60, Fig.49C), and osteoclast activity appeared to be elevated compared to control 12 days after administration of the last dose of CBZ, however no significant difference was determined (CTRL: 9.55 ± 0.85 U/L vs. CBZ: 13.23 ± 1.35 U/L, two-way ANOVA, Fig.49A).

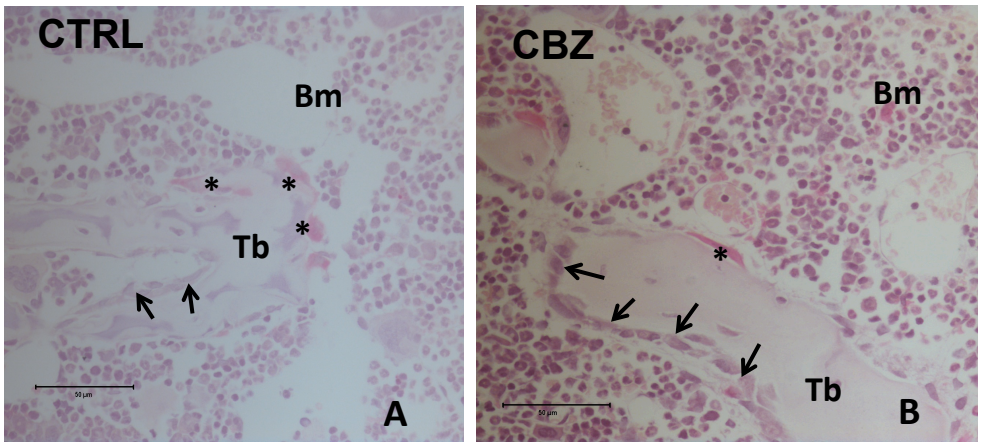


**Figure 46 Representative TRAP-stained histological sections of tibiae after 8 administrations of Cabozantinib**

Representative TRAP stained histological sections of 6-week old female BALB/c nude mice are shown in (A&B). Black asterisk highlights osteoclasts, black arrowheads indicate osteoblasts, 40x objective, scale bar is 50µm.

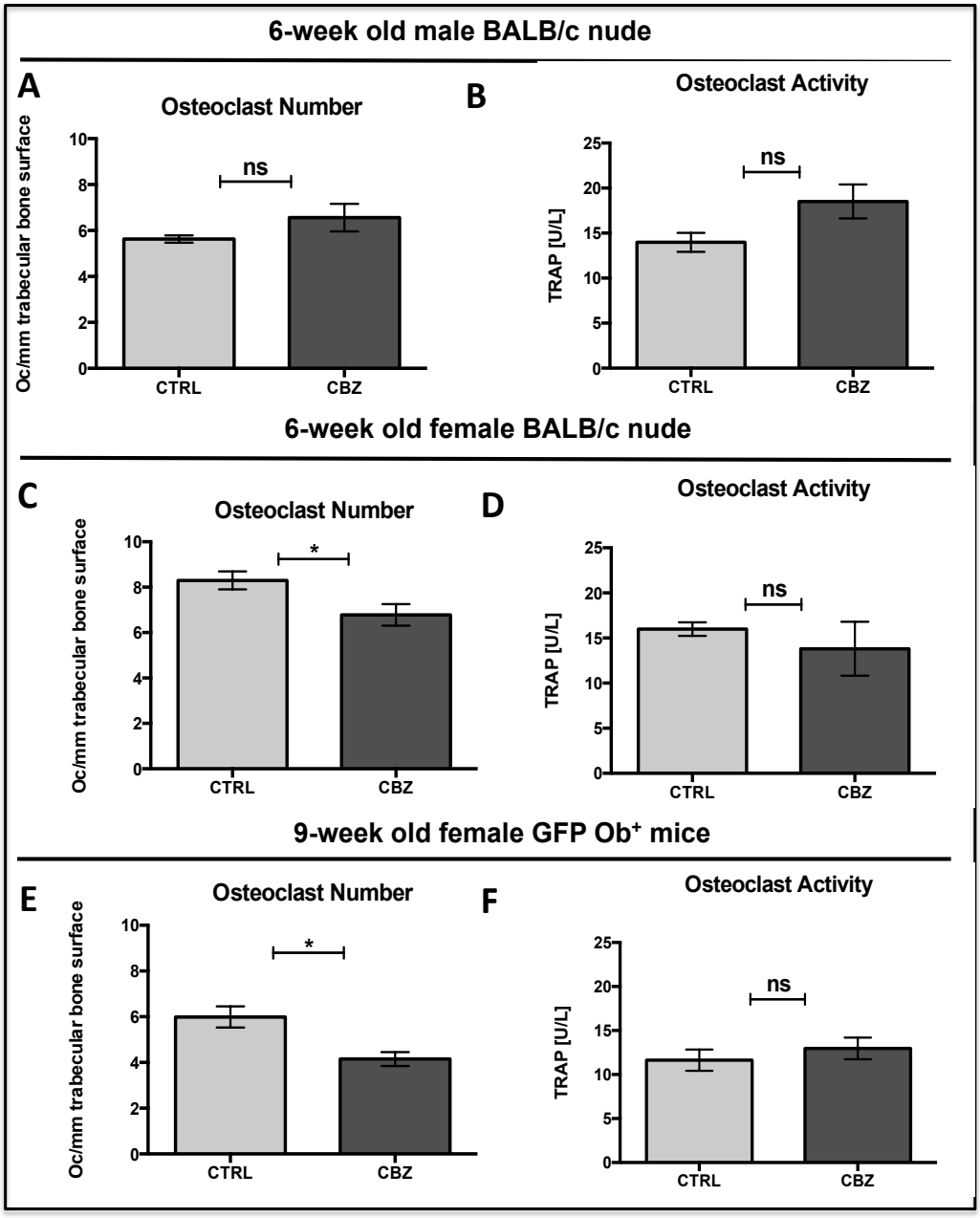


**Figure 47 Effects of 8 doses of CBZ on osteoclasts *in vivo*.**
(A,C,E) Osteoclast number/mm trabecular bone surface and (B,D,F) osteoclast activity (measured as serum TRAP levels) were determined after 8 doses of 30mg/kg Cabozantinib (CBZ) or sterile $H_2O$ control (CTRL) in 6-week old male BALB/c nude mice (n=4/group, A&B), 6-week old female BALB/c nude (n=5/group, C&D) and 9-week old female GFP $Ob^+$ mice (n=4/group, E&F) Student's t-test: ns is non-significant, * is $p \leq 0.05$. All data show Mean±SEM.

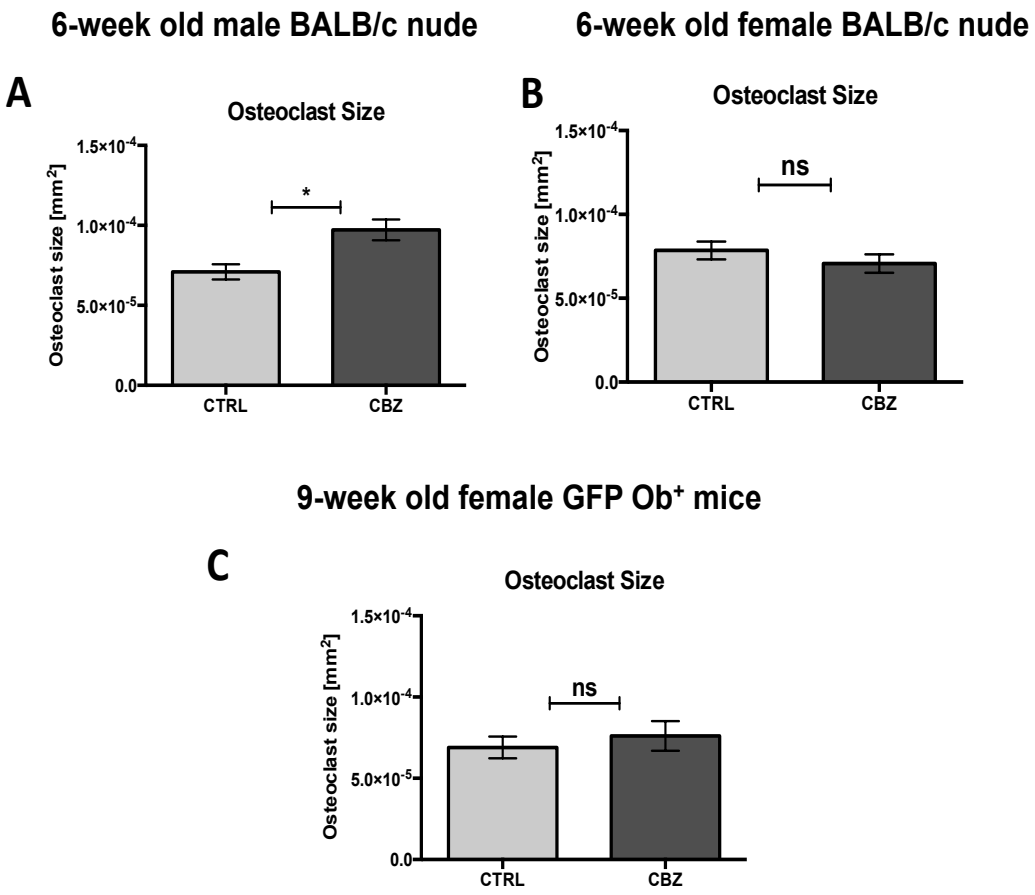


**Figure 48 Effects of 8 doses of CBZ on osteoclast size *in vivo*.**
Effects of CBZ on osteoclast size was determined after 8 doses of 30mg/kg Cabozantinib (CBZ) or sterile $H_2O$ control (CTRL) in (A) 6-week old male BALB/c nude mice (n=4/group), (B) 6-week old female BALB/c nude (n=5/group) and (C) 9-week old female GFP $Ob^+$ mice (n=4/group) Student's t-test: ns is non significant, * is $p \leq 0.05$. All data show Mean±SEM.

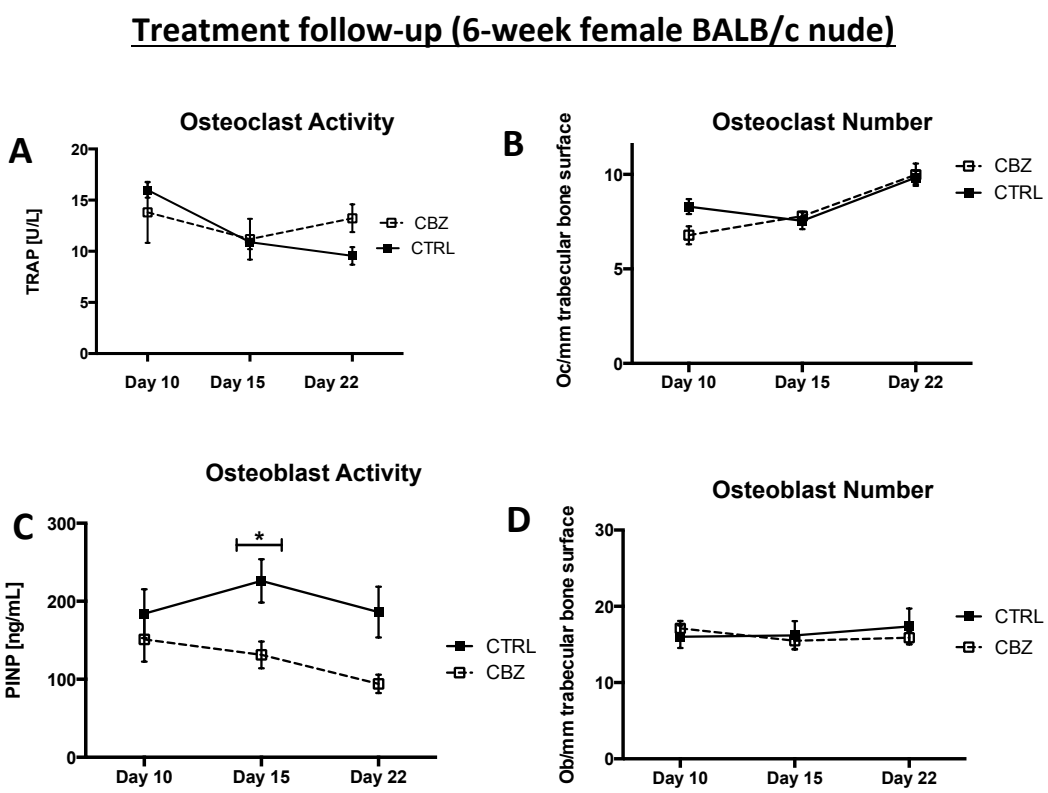


**Figure 49 Treatment follow-up of 8 doses of CBZ on osteoblasts and osteoclasts.**
6-week old female BALB/c nude mice received 8 doses of Cabozantinib (CBZ, 30mg/kg) or sterile $H_2O$ control (CTRL). (A) Osteoclast activiy (measured by serum TRAP levels), (C) osteoclast number, (B) osteoblast activity (serum PINP levels) and (D) osteoblast number was determined on day 10 (day of treatment termination) and effects on bone cells followed up 5 (Day 15) and 12 (Day 22) days post treatment termination. n=5/day and group. All data show Mean±SEM. two-way ANOVA, Bonferroni post-test, * is $p \leq 0.05$ no statistical significance at all other time points.

#### 4.6.2.3. Effects on bone volume and structure

I next assessed if 8 doses of CBZ (cumulative dose: 240mg/kg) caused alterations in trabecular bone volume, number and/or thickness of proximal tibiae. CBZ resulted in significantly increased trabecular thickness in all the animal models ($p \leq 0.01$, Table 18) when compared to control. 9-week old GFP $Ob^+$ mice treated with CBZ, also demonstrated increased trabecular number ($p \leq 0.05$, Table 18; 24% increase) and volume ($p \leq 0.01$, Table 18, ≈39% increase). These parameters were not significantly affected in BALB/c nude mice (Table 18) although there was a trend towards increased trabecular bone volume in 6-week old male BALB/c nude mice ($p=0.0694$, Table 18). The CBZ-induced increase in trabecular thickness was transient and normalised to control levels, 5 days after termination of treatment (Day 15, Table 18). Cortical bone volume remained unaffected by 8 administrations of CBZ in all animal models studied (Table 19).

**Table 18 Effects of CBZ on bone volume.**
Students t-test or [(1)] two-way ANOVA with Bonferroni post-test was used for statistical analysis. ns is non-significant, * is $p \leq 0.05$, ** is $p \leq 0.001$. All data show Mean±SEM.

| Analysis of treatment effects on bone volume and structure | | | | | | | | | |
|---|---|---|---|---|---|---|---|---|---|
| | BV/TV (%) | | | Tb.N. ($mm^{-1}$) | | | Tb.Th. (mm) | | |
| **5-day treatment schedule** | | | | | | | | | |
| | **CTRL** | **CBZ** | **p** | **CTRL** | **CBZ** | **p** | **CTRL** | **CBZ** | **p** |
| **GFP $Ob^+$ mice 8-9-week old** | 12.97 ± 0.36 | 13.04 ± 1.60 | ns | 2.86 ± 0.05 | 2.77 ± 0.36 | ns | 0.045 ± 0.001 | 0.047 ± 0.001 | ns |
| **GFP $Ob^+$ mice 17-week old** | 14.53 ± 0.22 | 16.42 ± 0.35 | ** | 2.57 ± 0.09 | 2.72 ± 0.05 | ns | 0.057 ± 0.002 | 0.060 ± 0.002 | ns |
| **10-day treatment schedule** | | | | | | | | | |
| **Male BALB/c nude 6-week old** | 12.16 ± 0.84 | 16.01 ± 1.53 | ns | 3.39 ± 0.24 | 3.84 ± 0.30 | ns | 0.036 ± 0.001 | 0.042 ± 0.001 | ** |
| **Female BALB/c nude 6-week old** | 11.61 ± 1.31 | 12.18 ± 1.47 | ns | 3.21 ± 0.31 | 2.82 ± 0.303 | ns | 0.036 ± 0.001 | 0.043 ± 0.001 | ** |
| **Female GFP $Ob^+$ mice 9-week old** | 13.48 ± 0.54 | 18.75 ± 1.09 | ** | 2.65 ± 0.13 | 3.29 ± 0.15 | * | 0.051 ± 0.001 | 0.057 ± 0.001 | ** |
| **Follow up treatment (6-week old female BALB/c nude)** | | | | | | | | | |
| **5 days post treatment termination** | 11.07 ± 1.29 | 9.86 ± 0.95 | ns [(1)] | 2.86 ± 0.33 | 2.41 ± 0.18 | ns [(1)] | 0.039 ± 0.001 | 0.041 ± 0.001 | ns [(1)] |
| **12 days post treatment termination** | 10.49 ± 0.85 | 11.64 ± 1.49 | ns [(1)] | 2.65 ± 0.19 | 2.83 ± 0,30 | ns [(1)] | 0.039 ± 0.001 | 0.041 ± 0.002 | ns [(1)] |

**Table 19 Effects of CBZ on cortical bone volume**
Students t-test or [(1)] two-way ANOVA with Bonferroni post-test was used for statistical analysis. ns is non-significant, * is p≤0.05, ** is p≤0.001. All data show Mean±SEM.

| Cortical bone volume [$mm^3$] | | | |
|---|---|---|---|
| | **CTRL** | **CBZ** | **p** |
| **5 doses of CBZ** | | | |
| 8-9-week old GFP $Ob^+$ mice | 0.75 ± 0.02 | 0.77 ± 0.03 | ns |
| 17-week old GFP $Ob^+$ mice | 0.90 ± 0.03 | 0.97 ± 0.04 | ns |
| **8 doses of CBZ** | | | |
| 6-week old male BALB/c nude | 0.60 ± 0.03 | 0.65 ± 0.05 | ns |
| 6 week old female BALB/c nude | 0.53 ± 0.03 | 0.56 ± 0.02 | ns |
| 9-week old female GFP $Ob^+$ | 0.83 ± 0.02 | 0.84 ± 0.03 | ns |
| **Treatment follow-up** | | | |
| 5 days post treatment termination | 0.62 ± 0.03 | 0.56 ± 0.03 | ns [(1)] |
| 12 days post treatment termination | 0.62 ± 0.03 | 0.64 ± 0.03 | ns [(1)] |

#### 4.6.2.4. Effects on bone formation

To monitor the rate of new bone formation, I analysed incorporation of calcein labels in vertebra (n=4/group) from 6-week old female BALB/c nude mice receiving 8 doses of 30mg/kg CBZ or CTRL respectively.

Cabozantinib treated animals had increased rate of bone formation (CTRL: 0.58 ± 0.09 $mm^2$ $x10^{-3}$/mm/day vs. CBZ: 0.96 ± 0.09 $mm^2x10^{-3}$/mm/day, p≤0.05, Fig.50C). No significant effect on mineral apposition (CTRL: 1.97 ± 0.26 µm/day vs. CBZ 2.51 ± 0.21 µm/day, Fig.50B) or double-labelled width (CTRL: 7.88 ± 1.03 µm vs. CBZ: 10.05 ± 0.85 µm, Fig.50D) were observed. However, a trend towards increased mineralising surface was observed following CBZ administration (CTRL: 30.06 ± 3.25 % vs. CBZ: 38.13 ± 1.52 %, p=0.0655, Fig.50A).

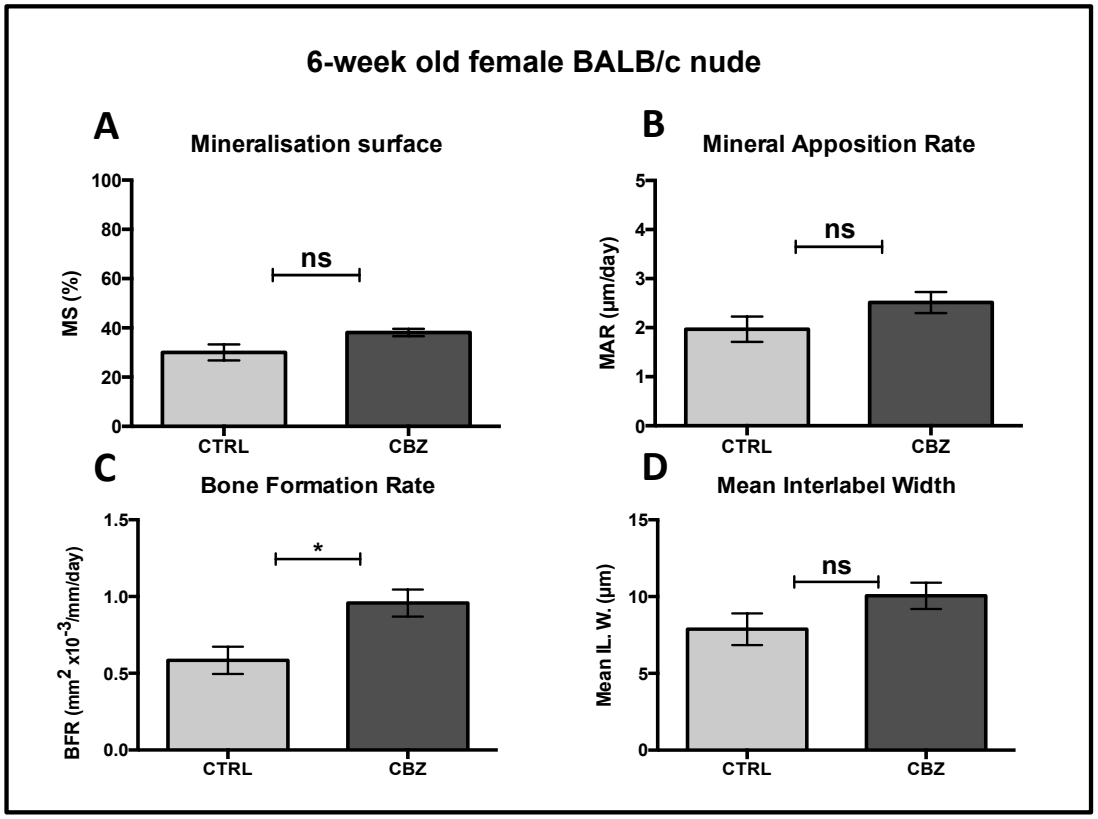


**Figure 50 Effects of CBZ on bone formation.**
The rate of new bone formation was assessed in lumbar vertebra 4 of 6-week old female BALB/c nude mice receiving 8 doses of 30mg/kg Cabozantinib (CBZ) or control (CTRL), n=4/group. It was interactively drawn around the calcein labels to determine differences in (A) mineralisation surface, (B) Mineral apposition rate, (C) Bone formation and (D) the Mean Interlabel Width between treatment groups. ns is non-significant * is $p<0.05$, Student's t-test. Only one level per sample was assessed. All data show Mean±SEM.

### 4.6.3. Effects of Cabozantinib on the epiphyseal growth plate

The epiphyseal growth plate is comprised of cartilage producing chondrocytes embedded in a proteoglycan-rich extracellular matrix. Significant modifications of the epiphysis in CBZ treated animals were observed and therefore I quantified the area of resting/proliferating and hypertrophic chondrocytes, respectively (in $mm^2$, Fig.38, Fig.51A) after a 5- and 8-dose regimen of CBZ or CTRL. Additionally I analysed tumour-free tibiae collected in previously published tumour models [231, 233], to assess effects of longer-term CBZ treatment.

Five daily administrations of CBZ resulted in a significant increase in the hypertrophic chondrocyte zone in both, 8-9- ($p\leq0.0001$, ≈76% increase, Fig.51B, Table 20) and 17-week old female GFP $Ob^+$ mice ($p\leq0.001$, Fig.51B, ≈135% increase, Table 20) Similarly, a 10-day course (8 administrations) of CBZ increased the hypertrophic chondrocyte area in all the animal models when compared to control ((6-week old male

BALB/c nude: p≤0.001, Fig.51C, ≈98% increase; 9-week old GFP $Ob^+$: p≤0.01, Fig.50D, ≈49% increase; 6-week old female BALB/c nude: p≤0.001, Fig.52A, ≈85% increase; Table 20). Next to the elongated hypertrophic zones, the chondrocyte stacks appeared disorganized in CBZ treated animals compared to control (Fig.51D&F). The CBZ-induced increase in growth plate thickness was reversed to control levels within 5 days of treatment termination (Fig.52A, Table 20). In addition to the increased hypertrophic chondrocyte area, the resting/proliferating chondrocyte area was significantly smaller in animals receiving 5 (8-9-week old GFP $Ob^+$: p≤0.05, ≈24% decrease; 17-week old female GFP $Ob^+$: p≤0.05, Fig.51B, ≈18% decrease, Table 20) and 10 doses of CBZ (9-week old GFP $Ob^+$: p≤0.001, ≈37% decrease, Fig.50D, Table 20; 6-week old female BALB/c nude: p≤0.01, Fig.52A, ≈30% decrease; Table 20). Treatment follow-up analysis in 6-week old female BALB/c nude mice revealed that the resting/proliferating chondrocyte area returned to control levels as within 5 days post CBZ treatment termination (Fig.52A, Table 20). These results suggest that CBZ induces reversible alterations to the epiphyseal growth plate by disrupting chondrocyte differentiation. Archived material from previously published studies allowed me to determine the effects on the growth plate on histological samples from contralateral, tumour free tibiae following longer-term treatment with CBZ (Table 20) [231, 233]. In agreement with the short-term studies, castrated male NOD/SCID mice that had received daily administration of 30mg/kg CBZ for 15 days had a significantly elongated hypertrophic chondrocyte area when compared to control mice (p≤0.001, Fig. 52B, ≈107% increase, Table 20). Similar results were observed after 6-week treatment with 60mg/kg CBZ (p≤0.01, ≈83% increase Fig 52C) of castrated male beige SCID mice and no alteration in the proliferative/resting chondrocyte zone was determined in either of these experiments (Fig.52B&C, Table 20).

**Table 20 Treatment effects of Cabozantinib (CBZ) on growth plate zones.**
The hypertrophic and resting/proliferating chondrocyte zone of the epiphyseal growth plate area (in $mm^2$) was analysed after 5 and 8 dose regimen of 30mg/kg CBZ or control (CTRL) on histological sections of tibiae using OsteoMeasure software and normalised to total growth plate area (in $mm^2$). Student's t-test was used for statistical analysis or (1) two-way ANOVA with Bonferroni post-test. ns is non-significant, * is p≤0.05, ** is p≤0.01, *** is p≤0.001, **** is p≤0.0001. All data show Mean±SEM.

| **Hypertrophic chondrocyte zone area ($mm^2$) /total growth plate area ($mm^2$)** | | | |
|---|---|---|---|
| | **CTRL** | **CBZ** | **p** |
| **5 doses of CBZ** | | | |
| 8-9-week old GFP $Ob^+$ mice | 0.305 ± 0.015 | 0.537 ± 0.017 | **** |
| 17-week old GFP $Ob^+$ mice | 0.171 ± 0.010 | 0.403 ± 0.025 | *** |
| **8 doses of CBZ** | | | |
| 6-week old male BALB/c nude | 0.276 ± 0.004 | 0.549 ± 0.041 | *** |
| 6 week old female BALB/c nude | 0.278 ± 0.016 | 0.514 ± 0.035 | *** |
| 8-9-week old female GFP $Ob^+$ | 0.275 ± 0.018 | 0.409 ± 0.028 | ** |
| **Treatment follow-up** | | | |
| 5 days post treatment termination | 0.292 ± 0.022 | 0.319 ± 0.005 | ns (1) |
| 12 days post treatment termination | 0.335 ± 0.020 | 0.282 ± 0.019 | ns (1) |
| **Longer term treatment** | | | |
| Castrated male NOD/SCID mice | 0.232 ± 0.024 | 0.481 ± 0.034 | *** |
| Castrated male beige SCID mice | 0.203 ± 0.023 | 0.372 ± 0.047 | ** |
| **Resting/Proliferating chondrocyte zone area ($mm^2$)/total growth plate area ($mm^2$)** | | | |
| | **CTRL** | **CBZ** | **p** |
| **5 doses of CBZ** | | | |
| 8-9-week old GFP $Ob^+$ | 0.297 ± 0.019 | 0.226 ± 0.012 | * |
| 17-week old GFP $Ob^+$ | 0.254 ± 0.016 | 0.207 ± 0.009 | * |
| **8 doses of CBZ** | | | |
| 6-week old male BALB/c nude | 0.269 ± 0.048 | 0.211 ± 0.018 | ns |
| 6 week old female BALB/c nude | 0.406 ± 0.021 | 0.285 ± 0.017 | ** |
| 8-9-week old female GFP $Ob^+$ | 0.337 ± 0.014 | 0.212 ± 0.006 | *** |
| **Treatment follow-up (6-week old female BALB/c nude)** | | | |
| 5 days post treatment termination | 0.387 ± 0.008 | 0.381 ± 0.016 | ns (1) |
| 12 days post treatment termination | 0.414 ± 0.011 | 0.392 ± 0.014 | ns (1) |
| **Longer term treatment** | | | |
| Castrated male NOD/SCID mice | 0.238 ± 0.021 | 0.205 ± 0.013 | ns |
| Castrated male beige SCID mice | 0.174 ± 0.013 | 0.200 ± 0.019 | ns |

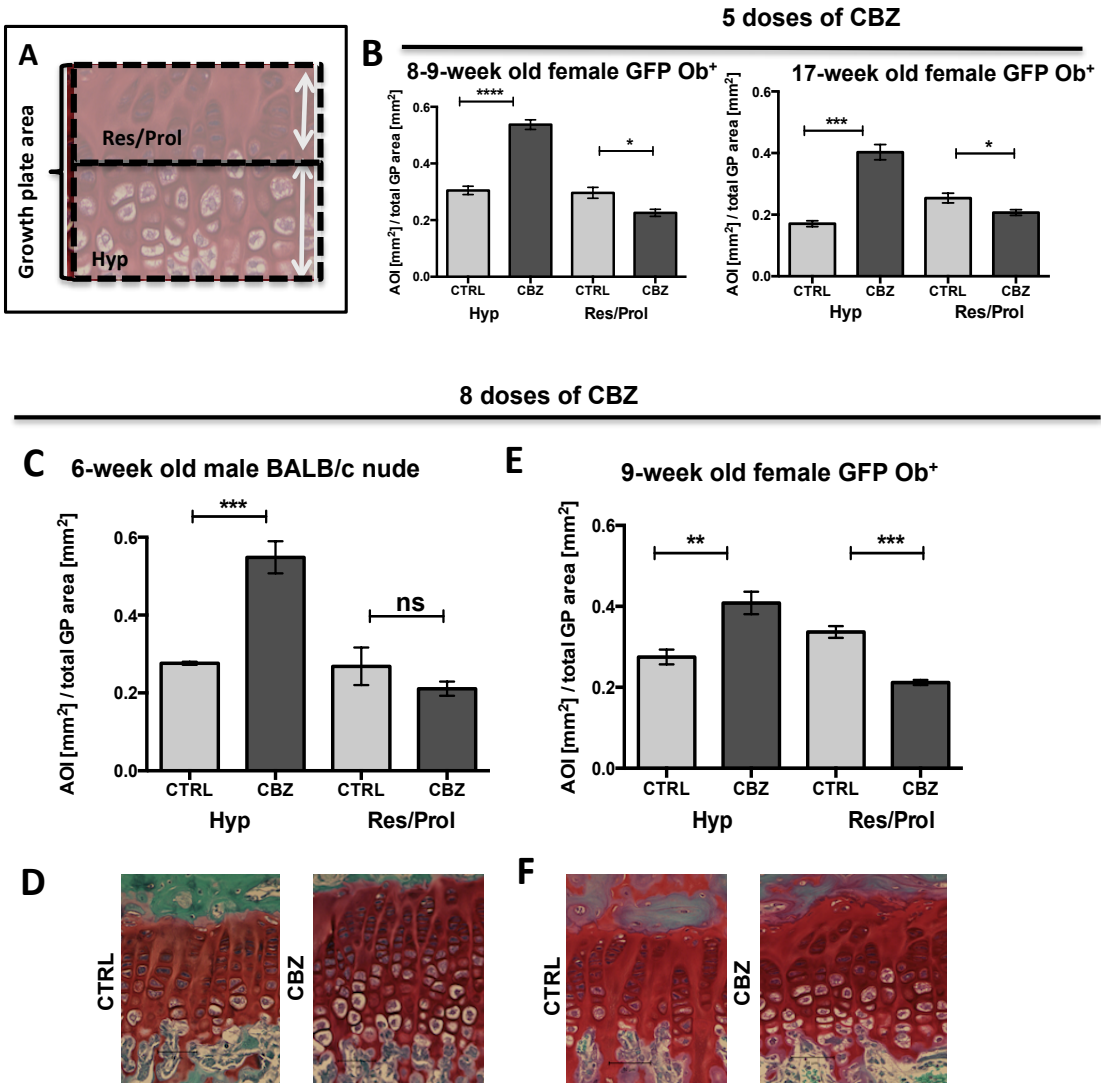


**Figure 51 Effects of CBZ on the epiphyseal growth plate.**
(A) Schematic illustration of growth plate areas quantified after administration of 30mg/kg Cabozantinib (CBZ) or sterile $H_2O$ control (CTRL). It was interactively drawn around the hypertrophic (Hyp) and resting/proliferating (Res/Prol) chondrocyte zone of the epiphysis using OsteoMeasure software. Effects of 5 doses (n=4/group) of CBZ or CTRL on the epiphyseal growth plate are shown in (B) for 8–9- and 17-week old female GFP $Ob^+$mice. Alterations in growth plate composition following 8 doses of CBZ or CTRL are presented in (C) 6-week old male BALB/c nude (n=4/group) and (E) 9-week old GFP Ob+ (n=4/group) mice. Representative Safranin-O stained sections of tibiae are shown in (D) for 6-week old male BALB/c nude and (F) 9-week old GFP $Ob^+$ mice. 20x objective, scale bar is 50 µm. Student's t-test * is $p \leq 0.05$, ** is $p \leq 0.01$, *** is $p \leq 0.001$, **** is $p \leq 0.0001$, ns is non-significant. AOI is area of interest. All data show mean ± SEM.

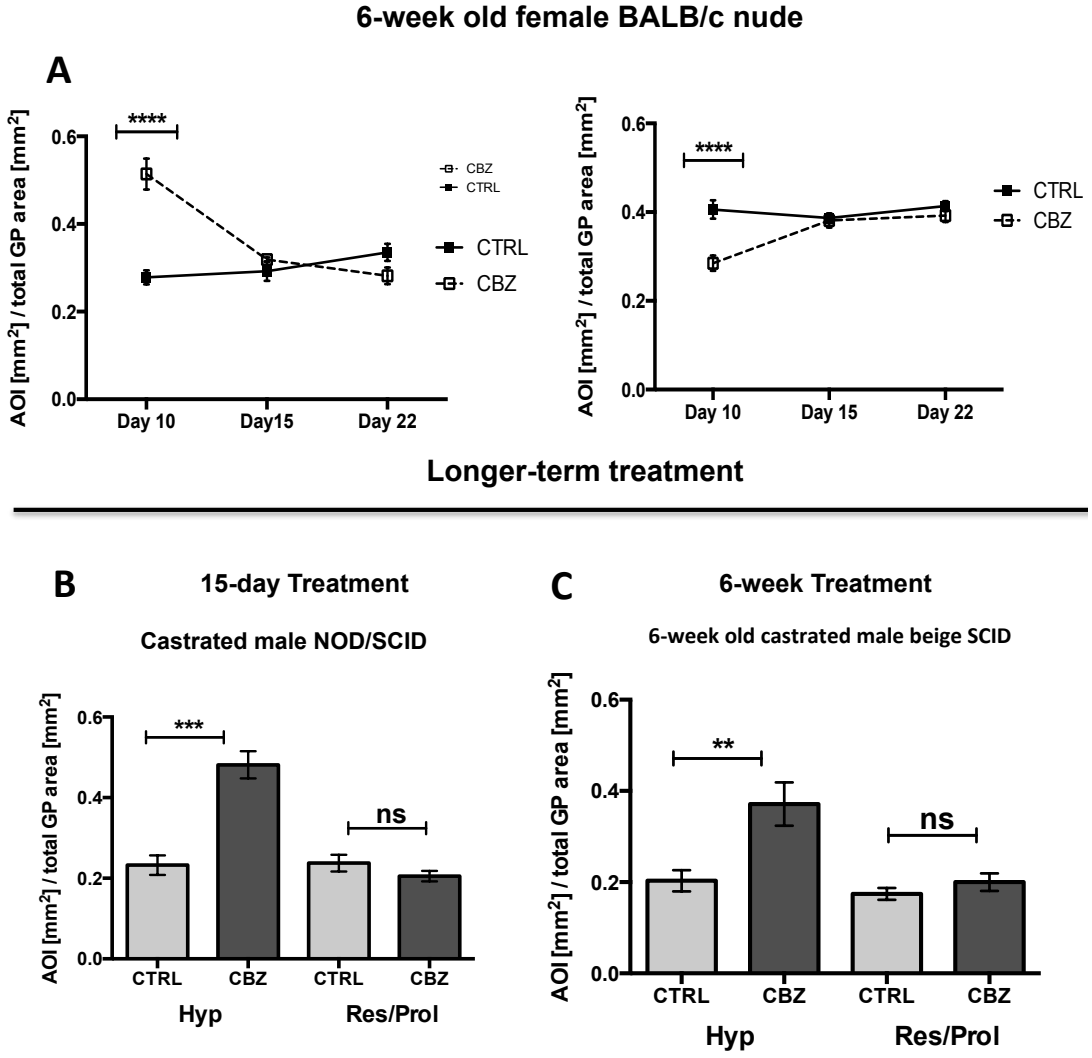


**Figure 52 Effects of Cabozantinib on the epiphyseal growth plate, follow-up and longer-term treatment.**

The hypertrophic (hyp) and resting/proliferating (res/prol) growth plate areas were quantified after administration of 30mg/kg Cabozantinib (CBZ) or sterile $H_2O$ control (CTRL) using OsteoMeasure software. Alterations in growth plate composition following 8 doses of CBZ or CTRL are presented in (A) for 6-week old female BALB/c nude mice (day 10: n=4 CBZ otherwise n=5/group/time point). Treatment was terminated at Day 10 and effects on growth plate areas assessed 5 and 12 days post treatment termination. Effects on the growth plate after 30mg/kg CBZ or CTRL daily for 15 days in castrated NOD/SCID mice (n=6 CTRL, n=7 CBZ), are presented in (D). (E) highlights effects after 60mg/kg CBZ or CTRL 5x weekly for 6 weeks in 6-week old of castrated male beige SCID mice (n=9 CTRL, n=10 CBZ). Student's t-test (B&C) or two-way ANOVA with Bonferroni post-test (A), ** is $p \leq 0.01$, *** is $p \leq 0.001$, **** is $p \leq 0.0001$, ns is non-significant. AOI is area of interest. All data show mean ± SEM.

### 4.6.4. Effects of Cabozantinib on bone marrow composition

#### 4.6.4.1. Effects on bone marrow megakaryocytes

During sample analyses I observed that CBZ caused alterations in bone marrow composition. In particular, CBZ-treated animals appeared to have increased numbers of red blood cells in the bone marrow associated with numerous megakaryocytes. I therefore determined the effects of CBZ on the number of megakaryocytes/$mm^2$ bone tissue by scoring H&E stained sections of tibiae as illustrated in Fig. 53A. In BALB/c nude mice, 8 administrations of CBZ resulted in increased numbers of megakaryocytes/$mm^2$ tissue area when compared to control (Male BALB/c nude: CTRL: 42.50 ± 3.09 vs. CBZ: 58.52 ± 0.88, $p \leq 0.01$, Fig. 53B; Female BALB/c nude: CTRL: 38.91 ± 2.37 vs. CBZ: 47.30 ± 1.77, $p \leq 0.05$, Fig.53B-D). Megakaryocyte numbers were reduced 5 days after the last administration of CBZ (CTRL: 37.76 ± 1.95 vs. CBZ: 27.43 ± 2.30, Fig.53C) and normalised to control levels by day 12 (CTRL: 39.25 ± 5.66 vs. CBZ: 37.44 ± 1.24, Fig. 53C).

#### 4.6.4.2. Effects on the bone marrow vasculature and haematopoietic cells

On the day of sacrifice dissected hind legs revealed significant alterations in bone marrow composition. Flushed bone marrow from mice receiving 8 doses of 30mg/kg CBZ appeared bright red when compared to bone marrow from CTRL treated mice (Fig.54A&B) indicating a potential increase in the number of erythrocytes and/or bleeding abnormalities. Excised spleens, a major site of blood formation, did not vary in size. However 3.5hrs after the last administration the spleen of the CBZ treated mouse appeared bright red when compared to the CTRL mouse – this would however require confirmation due to a lack of animals for this time point (Fig.54E). Similar effects were observed throughout all experiments performed, however less prominent in animals receiving 5 administrations of CBZ only. Figure 54 represents observations in 10-week old male C57BL/6J mice.

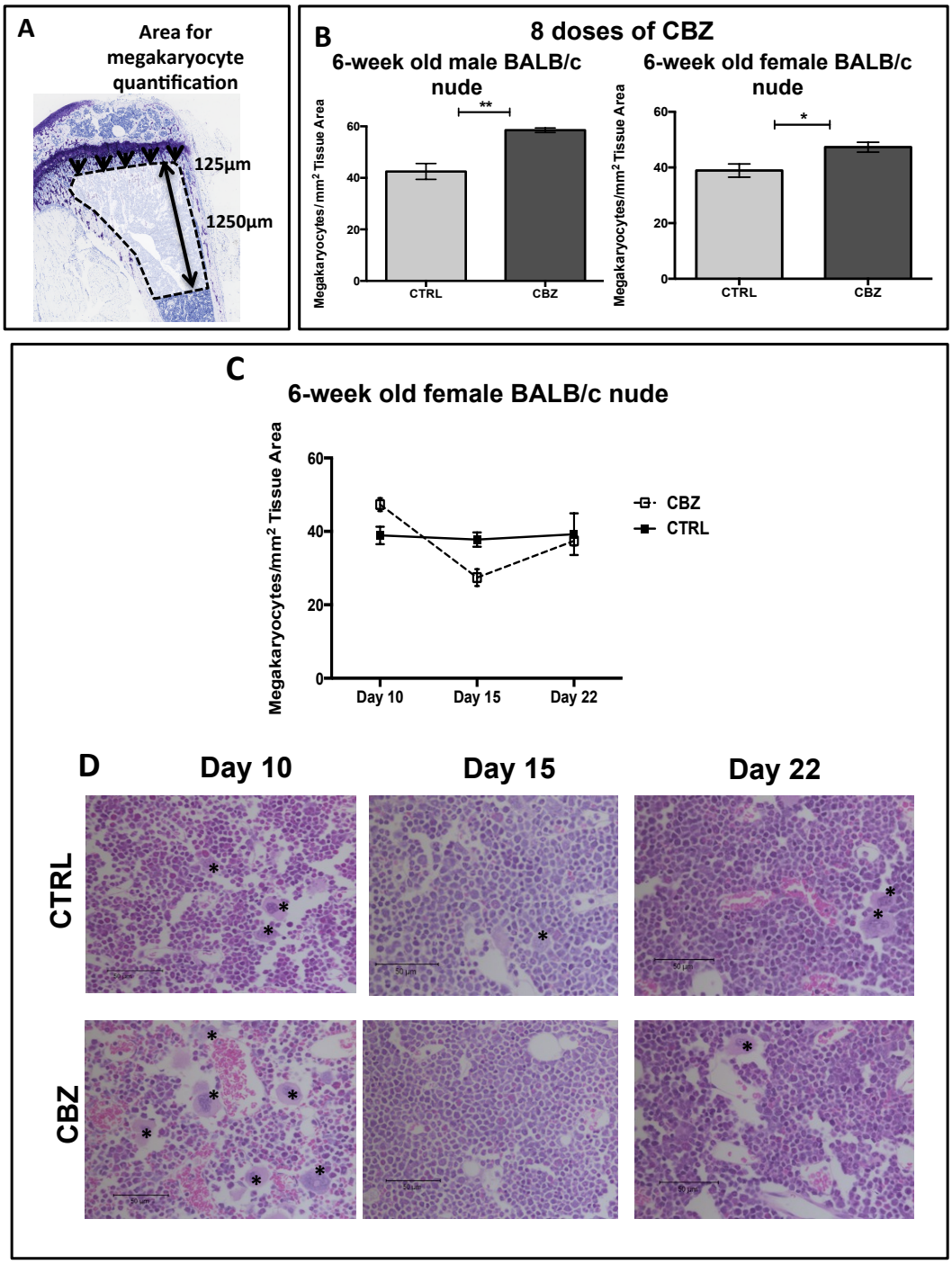


**Figure 53 Effects of Cabozantinib on bone marrow megakaryocytes.**
(A) Megakaryocytes/mm$^2$ tissue area were scored 125 µm away from the growth plate as illustrated. An area with a total length of 1250µm was scored. (B) Number of megakaryocytes was scored after 8 administrations of 30 mg/kg Cabozantinib (CBZ) or sterile $H_2O$ control (CTRL) for 10 days using 6-week old male (n=4/group) and female (n= 4-5/group) BALB/c nude mice. (C) Megakaryocyte number 5 (day 15) and 12 days (day 22) after the last CBZ administration in 6-week old female BALB/c nude mice. Representative H&E stained tissue sections illustrating effects on megakaryocytes and bone marrow cellularity are demonstrated in (D), 20x objective, scale bar is 50µm. Black asterisk points out megakaryocytes. (B) Student's t-test, * is $p \leq 0.05$, ** is $p \leq 0.01$. (C) Two-way ANOVA with Bonferroni post-test. All data show Mean ± SEM.

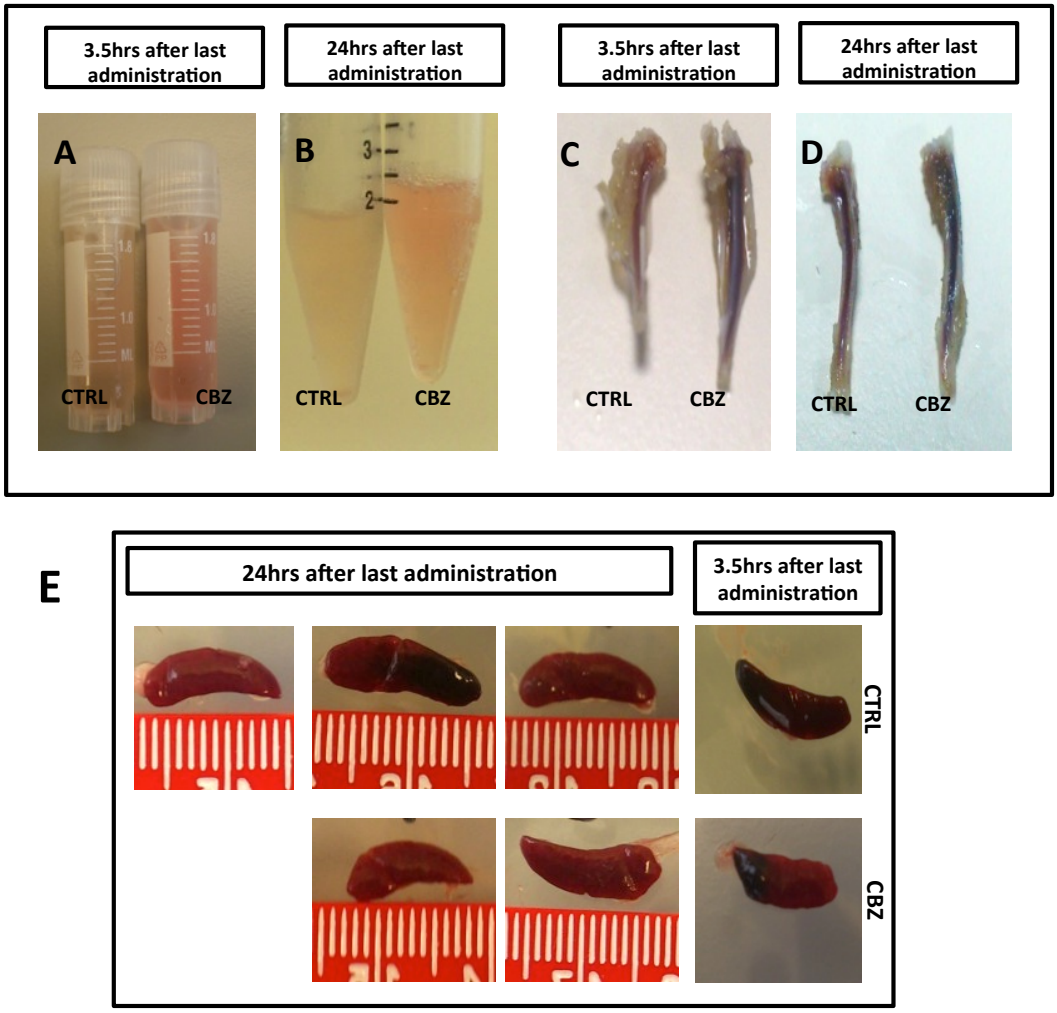


**Figure 54 visualisation of alterations in bone marrow cellulatrity following Cabozantinib treatment.**
(A) and (B) show bone marrow flushes from 10-week old male C57BL/6J mice that had received 8 administrations of 30mg/kg Cabozantinib (CBZ) or control (CTRL). Excised hind limbs are shown in (C) 3.5hrs and (D) 24hrs after the last treatment administrations. (E) presents excised spleens.

In addition to the changes to the BME described previously, histological analysis revealed that overall bone marrow cellularity was notably reduced in CBZ treated animals compared to control. Administration of 8 doses of CBZ resulted in vascular ectasia and spillage of mature (non-nucleated) red blood cells amongst the extra vascular bone marrow cells (Fig. 55D). Haemangioma-like bone marrow blood vessels, densely filled with erythrocytes, were observed, locally replacing the normal haematopoietic bone marrow. The dilated

vessels appeared thin walled compared to the ones observed in control bone marrow (Fig.55A-D). In addition there appeared to be a reduction in Endomucin+ve vascular endothelial cells in the area adjacent to the epiphyseal growth plate (Fig.56A-F). Assumptions about alterations in bone marrow vasculature are based on observations only and would require confirmation and further investigation. The effects were most prominent after 8 administrations of CBZ, with similar but less prominent alterations observed after 5 doses (Fig.56A-F). Alterations in bone marrow vasculature and spillage of erythrocytes were rapidly lost once CBZ treatment was terminated, with normal bone marrow restored by day 15 (Fig.53D).

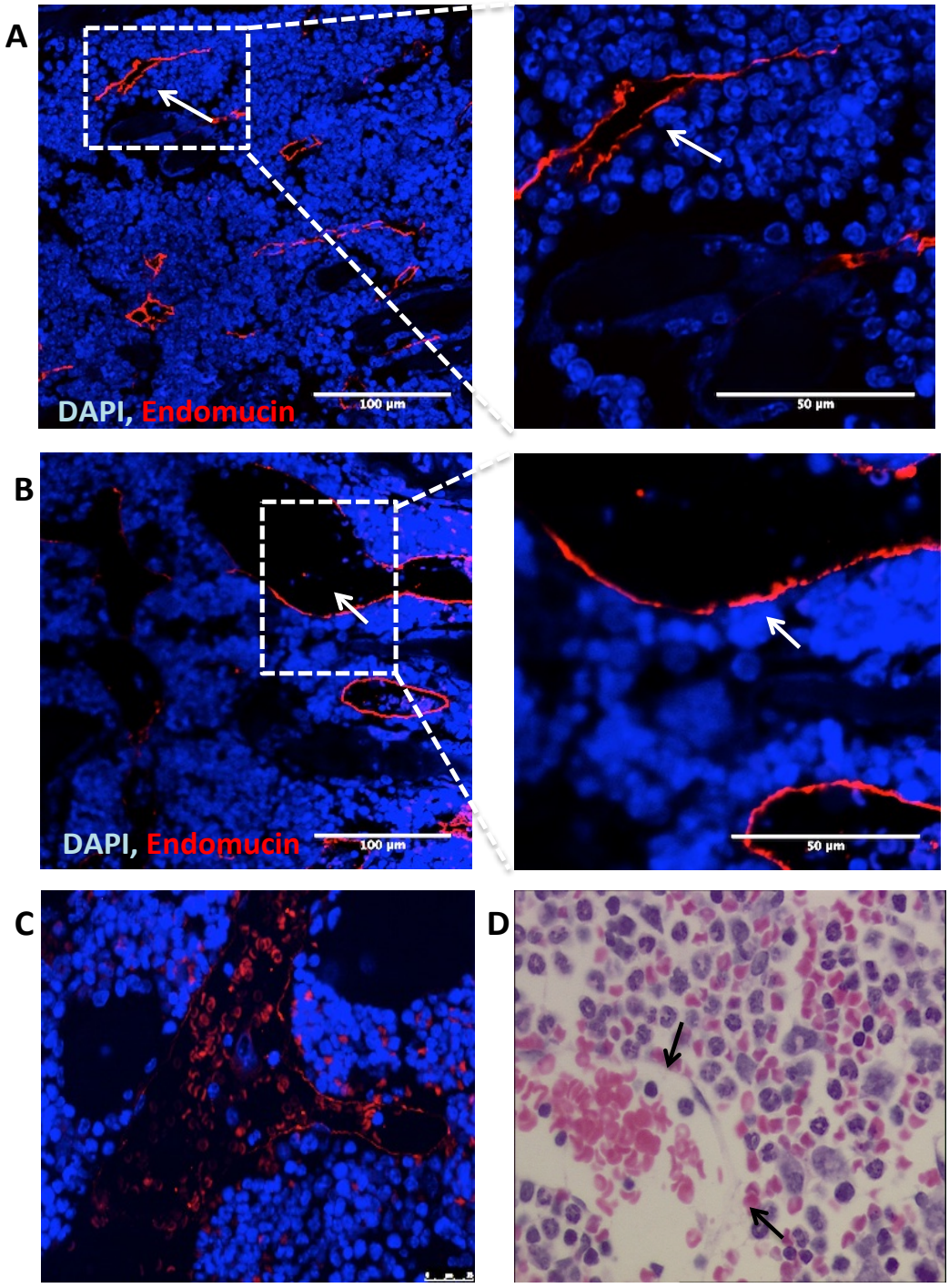


**Figure 55 Effects of 8 doses of Cabozantinib on the bone marrow vasculature *in vivo*.**
Immunofluorescence staining against the vascular endothelial marker Endomucin was performed on 3µm paraffin embedded sections of tibiae from 6-week old male BALB/c nude mice receiving (A) sterile $H_2O$ control (CTRL) or (B) 30mg/kg Cabozantinib (CBZ) 5x weekly for 10 days (8 doses in total). Bone marrow vessels appeared dilated and thin walled in CBZ receiving animals. Note the spillage of mature erythrocytes into the extravascular bone marrow in visualised in (C) by immunofluorescence and (D) by H&E staining. White arrowheads point out Endomucin positive vessels (in red). (A&C) 20x objective Nikon A1 Confocal microscope; (D) Leica DMRB upright microscope 20x objective.

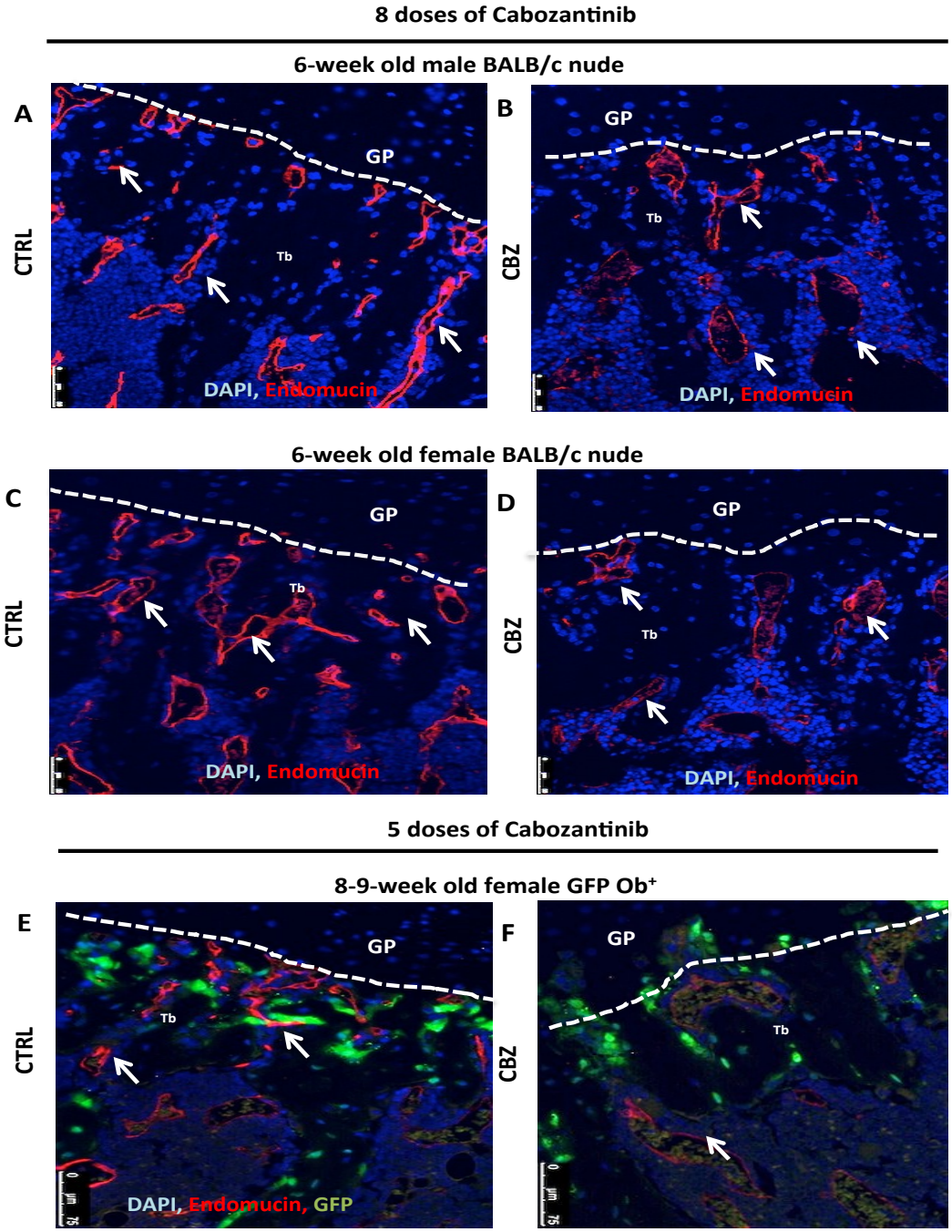


**Figure 56 Effects of Cabozantinib on the bone marrow vasculature in the metaphysis.**
Immunofluorescence staining against the vascular endothelial marker Endomucin was performed on 3µm paraffin embedded sections of tibiae from 6-week old (A&B) male and (C&D) female BALB/c nude mice receiving sterile $H_2O$ control (CTRL) or 30mg/kg Cabozantinib (CBZ) 5x weekly for 10 (8 doses in total) or 5 days (E&F, 8-9-week old female GFP $Ob^+$ mice). Representative Endomucin+ve vasculature pointed out by white arrow head, for GFP $Ob^+$ mice GFP+ve osteoblastic cells are shown in green (E&F), DAPI for nuclear cells in blue. White dotted line illustrates the last hypertrophic chondrocyte stacks of the growth plate (GP). Tb is trabecular bone. 20x objective, Leica DMI4000B. Scale bar is 50 or 75µm respectively.

To quantify the alterations in bone marrow cellularity observed after 8 doses of CBZ treatment flow cytometric analysis using antibodies against Ter119 (marker for erythrocytes), CD45 (cells of haematopoietic origin) and CD41 (platelets) were used in a

pilot experiment. Erythrocytes were identified as $Ter119^{+}/CD41^{-}/CD45^{-}$; platelets as $CD41^{+}$, $Ter119^{-}/CD45^{-}$. Analysis of CD45+ve cells revealed effects on haematopoietic cells.

As observed by histology 10-week old male C57BL/6J mice treated with 30mg/kg CBZ for 10 days showed increased percentage of erythrocytes in analysed bone marrow flushes at both time points (3.5hrs post treatment: CTRL: 47.8% vs. CBZ: 81.2%, n=1/group, Fig.57A; 24hrs after treatment: CTRL: 53.53 ± 4.28% vs. CBZ: 75.50 ± 8.60%, n=2-3/group, Fig.57B). In CBZ treated animals the percentage of nuclear haematopoietic cells in the bone marrow was reduced when compared to control receiving mice 3.5hrs (CTRL: 37.7% vs. CBZ: 15.6%, Fig.57B, n=1/group,) and 24hrs (CTRL: 36.57 ± 4.13% vs. CBZ: 20.10 ± 7.00%, FIg.57D, n=2-3/group) after the last treatment administration. The previously determined increase in megakaryocyte number may account for their inability to release platelets, their terminal differentiation state. Interestingly 3.5hrs after the last dose a lower percentage of CD41+ve cells was found in the bone marrow of the animals receiving CBZ (CTRL: 0.4% vs. CBZ: 0.1%, Fig.57E, n=1/group). No obvious alterations in CD41+ve cells was determined 24hrs after treatment termination (CTRL: 0.13 ± 0.03% vs. CBZ: 0.15 ± 0.05% n=2-3/group, Fig.57F). The flow cytometric analysis was performed in a small amount of animals only and would therefore require confirmation in a larger sample set.

Taken together, these data show that CBZ affects the BME through modification of multiple cell types, including bone cells and cells of the haematopoietic marrow.

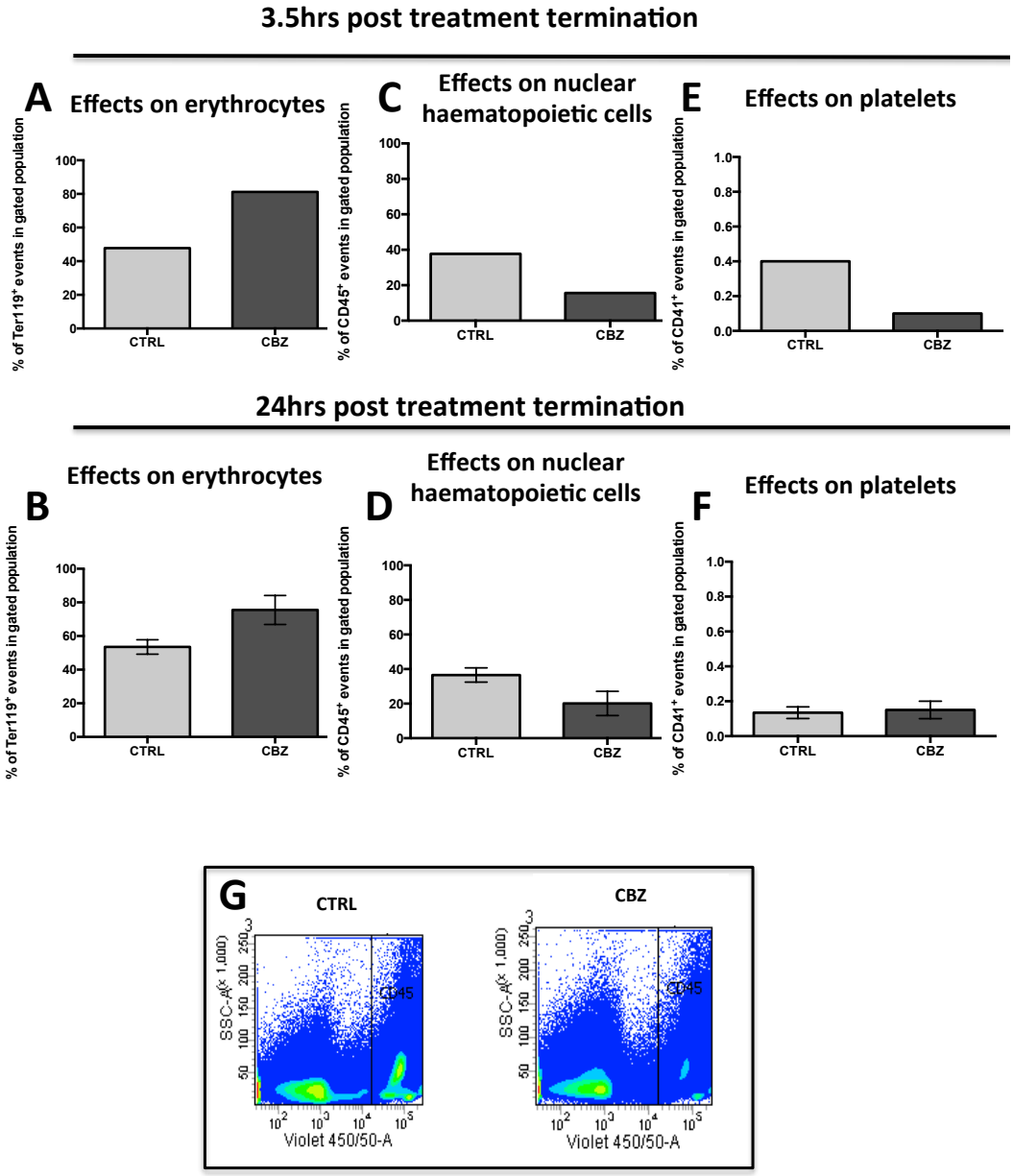


**Figure 57 Assessing effects of Cabozantinib treatment on bone marrow cellularity using flow cytometry.**

10-week old male C57BL/6J mice received 8 doses of 30mg/kg Cabozantinib (CBZ) or sterile $H_2O$ control (CTRL) and alterations in bone marrow cellularity were assessed using flow cytometric analysis 3.5 (A,C,E) and 24hrs (B,D,F) after the last CBZ administration. To quantify the alterations in bone marrow cellularity observed after 8 doses of CBZ treatment flow cytometric analysis using antibodies against Ter119 (marker for erythrocytes), CD45 (cells of hematopoietic origin) and CD41 (platelets) were used. Erythrocytes (A&B) were identified as $Ter119^+/CD41^-/CD45^-$; platelets (E&F) as $CD41^+/Ter119^-/CD45^-$. Analysis of CD45+ve cells revealed effects on hematopoietic cells (C&D). (G) shows representative flow cytometry readout for $CD45^+$ cells. 3.5hrs post treatment termination n=1/group, 24hrs post treatment termination n=3 for CTRL and n=2 for CBZ. All data show Mean ± SEM.

### 4.6.5. Effects of Cabozantinib on the expression of genes associated with bone remodelling

As I observed rapid alteration in bone cell number and bone structure following CBZ administration I assessed if treatment alters the expression of genes associated with bone remodelling, in particular RANK, RANKL and OPG, by qRT-PCR. In addition I determined gene expression levels of VEGFa and Sox9, a gene associated with chondrocyte proliferation. Samples used for gene expression analysis included tibiae and femurs of animals from treated or control groups respectively. 5 doses of CBZ did not alter the expression levels of any of assessed genes in 8-9-week old female GFP $Ob^+$ mice (Table 21). In 9-week old female GFP $Ob^+$ mice 8 doses of CBZ resulted in increased expression (=lower dCT value) of Sox9 (CTRL: 7.24 ± 0.14 vs. CBZ: 6.53 ± 0.06, $p \leq 0.01$, Table 22) and RANKL (CTRL: 9.10± 0.06 vs. CBZ: 8.73 ± 0.07, $p \leq 0.01$, Table 22) when compared to control mice potentially representing the alterations in the epiphyseal growth plate observed by histology.

**Table 21 Alteration in gene expression following 5 doses of Cabozantinib.**
Animals received 5 administrations of 30mg/kg Cabozantinib (CBZ) or sterile $H_2O$ control (CTRL) and gene expression of RANK, RANKL, OPG, Vegfa and Sox9 were assessed. Bone marrow was scraped out manually and tibia and femur pooled for each mouse. Biological replicates: n=4 for CTRL, n=3 for CBZ. All data show Mean ± SEM.

| 8-9-week old female GFP $Ob^+$ | | | | | | | |
|---|---|---|---|---|---|---|---|
| | Average Ct | | dCT | | Fold change | | |
| Gene | CTRL | CBZ | CTRL | CBZ | CTRL | CBZ | p |
| RANK | 27.08 ± 0.25 | 27.92 ± 0.28 | 8.756 ± 0.24 | 9.48 ± 0.32 | 1 | 0.61 | ns |
| RANKL | 27.02 ± 0.13 | 27.26 ± 0.12 | 8.69 ± 0.11 | 8.82 ± 0.10 | 1 | 0.92 | ns |
| OPG | 25.56 ± 0.21 | 26.36 ± 0.11 | 7.23 ± 0.25 | 7.92 ± 0.07 | 1 | 0.62 | ns |
| Vegfa | 24.71 ± 0.42 | 24.25 ± 0.48 | 8.69 ± 0.11 | 8.82 ± 0.10 | 1 | 1.53 | ns |
| Sox9 | 25.25 ± 0.55 | 25.79 ± 0.67 | 6.93 ± 0.34 | 7.30 ± 0.44 | 1 | 0.77 | ns |

**Table 22 Alteration in gene expression following 8 doses of Cabozantinib.**
Animals received 8 administrations of 30mg/kg Cabozantinib (CBZ) or sterile $H_2O$ control (CTRL) and gene expression of RANK, RANKL, OPG, Vegfa and Sox9 were assessed. Bone marrow was scraped out manually and the tibia and femur pooled for each mouse. n=4/group. All data show Mean ± SEM.

| 9-week old female GFP Ob$^+$ | | | | | | | |
|---|---|---|---|---|---|---|---|
| | Average Ct | | dCT | | Fold change | | |
| Gene | CTRL | CBZ | CTRL | CBZ | CTRL | CBZ | |
| RANK | 26.63 ± 0.19 | 26.84 ± 0.34 | 8.20 ± 0.13 | 8.66 ± 0.25 | 1 | 0.72 | ns |
| RANKL | 27.54 ± 0.09 | 26.91 ± 0.25 | 9.10 ± 0.06 | 8.73 ± 0.07 | 1 | 1.29 | ** |
| OPG | 25.83 ± 0.14 | 25.51 ± 0.31 | 7.39 ± 0.08 | 7.33 ± 0.13 | 1 | 1.05 | ns |
| Vegfa | 24.37 ± 0.39 | 23.89 ± 0.11 | 5.71 ± 0.18 | 5.16 ± 0.34 | 1 | 1.17 | ns |
| Sox9 | 25.68 ± 0.13 | 24.75 ± 0.29 | 7.24 ± 0.14 | 6.53 ± 0.06 | 1 | 1.59 | ** |

### 4.6.6. Assessment of the presence of MET and MET receptor phosphorylation

Yakes and colleagues assessed expression of MET and phosphorylation of MET (pMET) receptor in liver samples of naïve female nu/nu mice 2, 4, 8, 24, and 48hrs post administration of 100mg/kg CBZ or water vehicle [218]. In these experiments animals were administered 10mg HGF intravenously 10min pre harvest in order to stimulate receptor phosphorylation. I aimed to assess MET and pMET levels in my experiments using liver samples from 10-week old male C57BL/6J mice that had received 8 administrations of 30mg/kg CBZ 5x weekly. Yakes *et al.* observed inhibition of receptor phosphorylation 2-8hrs post CBZ treatment upon HGF stimulation. In contrast to I did not detect differences in MET and pMET levels in liver lysates between control and CBZ treated animals (Fig.58). However, in this study I did not use HGF stimulation as described in [218] which might account for the discrepancy in observed results.

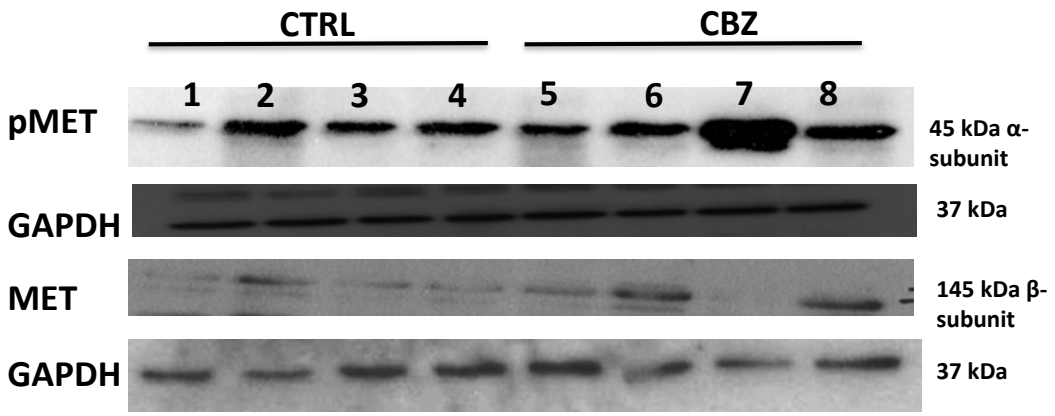


**Figure 58 Assessment or MET receptor phosphorylation (pMET) and MET expression by westernblot analysis.**

Met levels were assessed in liver lysates from 10-week old male C57BL/6J mice receiving 30mg/kg Cabozantinib (CBZ) or sterile $H_2O$ control (CTRL) 5x weekly for 10 days using Western blot. Total protein concentration loaded was 30ng/µL. GAPDH was used as a loading control. Loading: (1) CTRL, 3.5hrs post administration, (2-4) – CTRL, 24hrs post administration, (5) CBZ; 3.5hrs post administration, (6+8) CBZ; 24hrs post administration, (7) animal had to be sacrificed immediately after treatment, liver sample was collected 1hr post cull.

## 4.7. Discussion

The main objective of this study was to characterise the effects of the tyrosine kinase inhibitor (TKI) CBZ on the BME in the absence of tumour. Due to their expression on cells other than the tumour cells multiple TKIs such as Cabozantinib target signalling pathways (*e.g.* RET, VEGFR, MET) involved in tumourigenesis, angiogenesis and osteogenesis. Various TKI have been shown to affect bone metabolism raising the need to establish their impact on the BME. Imatinib, Dasatinib, Saracatinib and Sunitinib for example have demonstrated to reduce and or inhibit osteoclast resorption [208, 278, 279]. In 2006 Berman *et al.* reported a reduction in bone formation and resorption marker (osteocalcin and NTX) in patients receiving long-term therapy of Imatinib, a BCR-ABL, C-KIT and PDGFR targeted TKI [278]. This highlights that the effects of TKI including CBZ on bone cells combined with anti-tumour effects could reduce skeletal-related morbidity in patients with bone metastasis.

### 4.7.1. Effects on bone cells

Prior to the research presented in this chapter the *in vivo* effects of CBZ on osteoblasts and osteoclasts in the absence of tumour cells have not been investigated in detail. The majority of experiments investigating CBZ effects on tumour growth in bone have been performed in models of advanced prostate cancer [230, 231, 233], where substantial bone loss and large tumour burden has hampered analysis of CBZ responses on bone. This chapter therefore presents the first comprehensive analysis of the short-term effects of CBZ on osteoblast and osteoclast number in a range of BMEs including mice of different ages, sex and strain.

Osteoblasts and osteoclasts are key players in the vicious cycle driving progression of bone metastasis [121], and crucially both cell types express receptors (e.g. MET and VEGFR-2) targeted by CBZ [209, 210, 212]. In support of my hypothesis that CBZ mediates treatment response by inducing alterations to bone remodelling, I found that CBZ rapidly reduced the number of osteoclasts/mm trabecular bone surface, resulting in increased trabecular thickness after a cumulative dose of 240mg/kg (8 administrations) in naïve female mouse models. These findings are in agreement with data from studies performed in models of prostate cancer-induced bone disease [230, 233], where effects of CBZ on osteoclasts were assessed in tumour-free, contralateral tibiae [230, 232] and/or tumour free mice [233]. The authors reported reduced number of osteoclasts/mm trabecular bone surface along the edge of the growth plate (male NOD/SCID mice, daily 30mg/kg CBZ for 15 days)[233] and decreased osteoclast perimeter (male SCID mice, daily 60mg/kg CBZ for 3 weeks) [230]. In contrast others report no effect of CBZ on osteoclasts in mouse

models of prostate cancer [232]. In contrast to female mice, I did not determine alterations in osteoclast number in male BALB/c nude mice after 8 doses of CBZ. However, CBZ caused an increased osteoclast size in these male mice, indicating a potential loss of activity. Previous publications report an inhibition of differentiation and resorptive activity in RAW pre-osteoclasts [230, 276] but no effects of CBZ on the ability of mature osteoclasts to resorb bone *in vitro* [232]. TRAP5b levels were increased in male SCID mice but these findings could be masked by the presence of tumour in this model [230]. Based on their *in vitro* and *in vivo* observations the authors suggest that CBZ might not affect the resorptive activity of osteoclasts but rather inhibit osteoclast maturation and/or reduce their number [230]. The highly significant increase in the length of the hypertrophic chondrocyte zone after treatment termination however suggested that resorption may be impaired by CBZ. However, TRAP serum levels remained unaffected after 5 and 8 doses of CBZ in all animal models, suggesting that short-term treatment with CBZ may not affect bone resorption *in vivo* in the absence of tumour.

Osteoblast number/mm trabecular bone was significantly increased after 5 doses of CBZ (150mg/kg cumulative dose) however no effects on osteoblasts were observed after 8 administrations in female animals. In contrast male BALB/c nude mice showed a slight increase in osteoblast numbers. Others report reduced viability and osteocalcin levels (a marker for late osteoblast differentiation) in pre-osteoblastic MC3T3-E1 and mouse bone marrow stromal ST-2 cell cultures determined following CBZ treatment (0.01-5µmol/L) *in vitro* [230]. Data are contradictory with regards to effects on alkaline phosphatase activity (ALP, marker for early osteoblast differentiation) and mineralisation [230-232] suggesting that CBZ may act on bone through more than one mechanism. The biphasic effects on ALP could be caused by different concentrations of CBZ used in these experiments. Nude mice injected intratibially with the prostate cancer cell line $ARCaP_M$ receiving 10 or 30mg/kg CBZ daily for 7 weeks showed increased numbers of osteoblasts [232]. Similar results were determined in non-tumour bearing tibiae of male SCID mice with intratibial PC-$3^{luc}$ prostate tumours, following daily administration of 60mg/kg CBZ for 3 weeks [230]. Beside the alterations in bone cell number serum PINP levels remained unaffected after 5 and 8 doses of CBZ. This is in agreement with others who found that serum PINP and osteocalcin levels were unaffected by CBZ (60mg/kg/day) [230]. Calcein analysis of vertebrae from female mice receiving 8 doses of CBZ demonstrated that these animals had slightly increased bone formation rate (BFR) when compared to control; BFR takes into account how much bone surface is actively mineralising and is therefore depending on the number of active

osteoblasts). In contrast serum PINP levels were significantly lower in CBZ treated mice 5 days post treatment termination relative to control receiving mice.

Most likely the bone serum marker levels (TRAP and PINP) did not correspond with the observed alterations in bone cell number in my experiments, due to experimental design. Serum samples for bone marker measurements were only collected at the end of the experiment, reflecting one point in time and taking repeated blood samples is also not an option on our current project license. In contrast, histological analysis quantifies accumulated effects of CBZ over the entire experimental period. Additionally, serum TRAP/PINP levels represent levels released from the entire skeleton whereas I only quantified bone cell number in tibia/bone formation rate in vertebrae (representing accumulating effects), potentially contributing to the observed differences. In a recent Phase II randomized discontinuation trial (patients with castration resistant prostate cancer who received 100mg CBZ daily) serum ALP and CTX were reduced by 50% in 57% of evaluable patients [234]. Similar results - reduced levels of CTX and NTX - were obtained in a Phase II Nonrandomised Expansion Study conducted in patients with chemotherapy pre-treated metastatic castration-resistant prostate cancer [235], supporting the hypothesis that CBZ partially mediates treatment effects by targeting the BME.

In summary, it remains unclear why differential effects of CBZ on osteoblast and osteoclasts were observed in mice of different sex; and highlight the need to perform studies in different animal ages/sex in order to demonstrate consistency of therapeutic effects in model systems. My studies showed potential of CBZ to affect both cell types *in vivo* however the tight coupling between osteoblasts and osteoclasts makes it difficult to separate the direct/indirect effects of therapeutic agents on these cells, in particular when both cell types express the target receptor(s). It is possible that CBZ reduced RANKL expression by the osteoblasts in these studies, resulting in decreased osteoclast number. However it is not possible to accurately measure the levels of active RANKL in the BME and the role of soluble RANKL in regulating bone turnover is unclear. Given that short-term treatment with CBZ did not alter bone remodelling throughout the animal models used, further cell types of the BME were suggested as potential mediators of treatment effects. This is supported by the observations that CBZ-induced alterations of megakaryocyte number, bone marrow vasculature, trabecular thickness and elongated hypertrophic chondrocyte zone in the epiphyseal growth plate area were all consistently observed in both male and female mice.

### 4.7.2. Effects on bone volume and structure

Although 5 administrations of CBZ increased osteoblast and decreased osteoclast numbers, this short-term schedule did not result in any significant increase in trabecular bone volume, apart from in 17-week old female GFP $Ob^+$ mice. Increasing the schedule to 8 doses of CBZ over 10 days did result in increased trabecular thickness in all the models evaluated in addition to increased trabecular bone volume and number in 9-week old female GFP $Ob^+$ mice (Table 18). This increase was rapidly lost, returning to control levels 5 days after the last administration of CBZ (Table 18). Although the GFP $Ob^+$ mice represent a slightly different BME compared to BALB/c nude mice, the differential effects of CBZ on trabecular bone is potentially due to the difference in bone turnover between the mice aged 6 and 9 weeks. These findings highlight that long-term and continuous treatment might be required for bone volume to be altered, but following cessation of treatment the BME has the capacity to reverse the alterations. In contrast others found no increase in bone mineral content in tumour-free tibiae of mice receiving 60mg/kg CBZ for 3 weeks (PC3 tumours) and 5 weeks (Ace1 and C4-2B tumours), respectively suggesting that it may take longer to see treatment effects on bone than the 7-week treatment course [230]. However, 6-week treatment with 60mg/kg CBZ in castrated and intact mice injected with LnCaP 23.1 prostate cancer cells resulted in significantly increased trabecular bone volume and number in contralateral non-tumour bearing tibiae [231]. These differential effect of CBZ on bone volume and structure between studies may be due to the models and CBZ schedules used, and further studies are required to firmly establish the optimal CBZ dosing regimen required to increase bone volume.

### 4.7.3. Effects on growth plate composition

Importantly, my study is the first reporting effects of CBZ on chondrocytes *in vivo*. I observed substantial alterations in the epiphyseal growth plate of CBZ treated mice, including an expansion of the hypertrophic chondrocyte zone. This was prominent in the epiphysis of all animals irrespective of age, sex and treatment schedule. When analysing growth plates of tumour-free tibiae from animals receiving longer-term CBZ treatment [231, 233], similar effects were observed. During endochondral ossification, newly synthesised cartilage is replaced by woven bone in a highly organised process involving chondrocyte proliferation, maturation, hypertrophy and finally matrix calcification. There are conflicting views about the terminal fate of the chondrocyte, including their differentiation into osteoblastic cells [280] or apoptosis (reviewed in [281]). It has previously been reported that inhibition of VEGF signalling results in growth plate

thickening as a consequence of the expanded hypertrophic chondrocyte zone [212, 282] and this could also be the mechanism involved in the CBZ-induced effects. The growth plate normalised to control thickness 12 days after treatment termination, coinciding with an increase in osteoclast activity. During endochondral ossification, osteoclasts are recruited to the mineralising front of the growth plate, allowing resorption of cartilage and invasion of osteoblasts to mineralise the matrix, which is a potential explanation for the sudden increase in osteoclast activity once CBZ administration ceased. New blood vessel formation is apparent in the developing epiphysis and anti-VEGF treatment has been shown to modify the growth plate [283-285]. Similarly, CBZ treated mice appeared to have fewer Endomucin positive vessels in the epiphysis when compared to control mice (observations only). Children with open growth plates therefore require close monitoring when receiving anti-angiogenic therapy as they are in risk of developing growth plate abnormalities [286]. This approach might be appropriate also for CBZ, although preliminary safety data from a phase 1 trial of CBZ in paediatric cancer patients did not indicate clinical consequences of potential growth plate effects [287].

#### 4.7.4. Effects on bone marrow composition

During histological analysis I also noted alterations in the bone marrow composition in CBZ treated animals compared to control, including vascular ectasia and spillage of mature red blood cells in the extra vascular bone marrow. CBZ rapidly altered the structure of bone marrow vascular endothelial cells resulting in dilated blood vessels densely filled with erythrocytes in mice that had received 8 administrations of CBZ. Vessels appeared thin walled and the observed spillage of erythrocytes into the extravascular bone marrow suggests disintegration of the bone marrow vasculature. However, this would require further confirmation. Mice that received 15 days of treatment [233] appeared to have reduced haematopoietic cells in the marrow, increased numbers of adipocytes and reduced megakaryocyte cytoplasm, although I was unable to accurately quantify this due to the limited number of samples available from this study [233]. Analysis of histological sections from tibiae of mice receiving 60mg/kg CBZ 5x weekly for 6 weeks [231] showed similar changes in bone marrow composition in 3 out of 8 assessed mice, with additional animals displaying a more modest effect. These responses are likely a result of inhibition of VEGFR affecting the bone microvasculature. In support of this, a study using the soluble VEGF receptor chimeric protein Flt(1-3)-IgG reported an increase in thickness of secondary trabeculi *in vivo* in addition to disorganised and dilated blood vessels adjacent to the hypertrophic chondrocyte zone [212] with similar morphology as observed in my study.

Recently others report that human-tumour-derived VEGF induces bone marrow vessel dilation and observe similar effects in bone marrow vasculature in VEGF-tumour bearing mice as the here reported effects of CBZ on bone marrow vasculature. The authors suggest that bone marrow cell mobilisation and vessel dilation is VEGFR-2 dependent [288].

Moreover, alterations in endochondral ossification, in particular the transition from cartilage to bone, might affect the haematopoietic niche located within the bone marrow potentially accounting for the observed alterations in the haematopoietic composition after CBZ treatment. By generating transgenic mice expressing defective collagen X variants, Jacenko *et al.* demonstrated the close interdependence of endochondral ossification and haematopoiesis in the bone marrow [289]. In these experiments the authors observed a compression in the tibial growth plate and a reduction in the number of hypertrophic chondrocytes. Interestingly, histology and observations made on day of dissections from aging transgenic mice revealed marrow hypoplasia (fatty marrow), and a bone marrow with a predominance of erythrocytes – similar to observations made following CBZ treatment. In three-week old mice they observed a reduction in the overall number of nucleated cells within the bone marrow [289], similar to data obtained in my experiments. This highlights the importance of endochondral ossification in maintaining haematopoiesis and might partially explain observed effects on bone marrow composition following CBZ treatment.

Next to fatigue, hypertension and hand-foot syndrome were the most common experienced grade 3 adverse events caused by CBZ in patients with advanced prostate cancer [234]; lymphopenia, neutropenia and thrombocytopenia in addition to haemorrhage have been reported as common haematological adverse effects [229]. The bone marrow effects we observed may therefore reflect some of the known complications experienced by patients treated with CBZ. All animals appeared healthy after short-term treatment used in my study but at the biological level this does support the use of *in vivo* models to investigate effects on the BME.

One of the most intriguing findings in my studies was that CBZ treatment caused a significant increase in the number of megakaryocytes in the bone marrow, indicating that CBZ may have impaired terminal differentiation of megakaryocytes and release of platelets. The increase in red blood cells in the marrow could be in agreement with thrombocytopenia reported as a common laboratory abnormality in patients receiving CBZ [229]. However, as with all the CBZ-induced effects detected, megakaryocyte numbers and the associated bone marrow effects rapidly normalised to control levels once treatment

was terminated. Megakaryocytes also play a role in bone homeostasis, including in the maintenance of bone mass [290]. Mice deficient in the transcription factors required for megakaryocyte differentiation and maturation have high numbers of immature megakaryocytes in the bone marrow, accompanied by dramatically increased osteoblast numbers and bone volume [80]. *In vitro,* osteoblast proliferation is increased by the presence of megakaryocytes and direct cell-to cell contact between both cell types is suggested to occur via gap junctions [81] and/or integrins [82]. However, to what extent osteoblasts and megakaryocytes are in direct contact *in vivo* remains to be established. In the present study, megakaryocytes did not appear to be in close proximity to osteoblasts in 2D histological sections of tibiae. Megakaryocytes have also been demonstrated to inhibit formation of osteoclasts when added to pre-osteoclast cultures and to impair osteoclast function [291, 292]. It is therefore possible that CBZ may increase bone volume not only through direct effects on osteoblasts and osteoclasts, but also indirectly through increasing the number of megakaryocytes that in turn stimulate osteoblasts and inhibit osteoclast activity and maturation.

#### 4.7.5. Gene expression

To determine if expression of key genes involved in bone turnover were affected by CBZ treatment, I assessed expression levels of genes associated with bone remodelling (RANK, RANKL, OPG, Vegfa, and Sox9) in long bones of mice after 5 and 8 doses of CBZ treatment.

5 day treatment with CBZ did not affect expression of assessed genes whereas RANKL and Sox9 levels were increased following 8 doses of CBZ in 9-week old female GFP $Ob^{+}$ mice. Required for full osteoclastic differentiation, RANKL is expressed by a variety of cells in the bone marrow including osteoblasts, chondrocytes, osteocytes and endothelial cells [69]. CBZ treatment did not result in alterations in osteoblast number after 8 doses suggesting that osteoblastic cells might not be one of the sources of increased RANKL expression in these experiments. Another source of increased RANKL expression could be the hypertrophic chondrocyte. This would be in agreement with the observations of significantly enlarged hypertrophic chondrocyte zone in growth plates of CBZ receiving mice when compared to control. RANKL derived from hypertrophic chondrocytes is necessary for regulating osteoclast mediated bone resorption at the calcified bone:cartilage junction in bone. In agreement with this, various studies detected RANK expression in hypertrophic chondrocytes [293]. In addition, Collin-Osdoby *et al.* have shown that human microvascular endothelial cells express RANKL mRNA *in vitro* and might play an important role in bone remodelling as well as osteoclastogenesis [294]. One of the

major sources of RANKL in bone is the osteocyte [295, 296]. I did not investigate effects of CBZ on osteocytes, however, these cells could also be altered by drug administration and account for the observed effects on gene expression.

Sox9 is required for maintaining growth plate functionality by regulating chondrocyte proliferation and inducing hypertrophy – this was shown by Dy *et. al* who generated doxocycline inducible Cre transgene and Sox 9 null alleles in mice [297]. Sox 9 has first been suggested to inhibit chondrocyte proliferation but has also been demonstrated to be required for early chondrocyte differentiation [298]. Sox 9 was subsequently suggested to be a mediator of survival and hypertrophy and terminal maturation of chondrocytes [299]. The alteration in Sox 9 gene expression levels after CBZ treatment could therefore be a consequence of the observed increase in the hypertrophic chondrocyte zone in CBZ treated mice.

### 4.8. Summary and Conclusion

In summary, these data demonstrate that CBZ exerts effects on various cell types in the BME (Table 23). Data on osteoblasts and osteoclasts varied depending on animal model and treatment schedule used; suggesting that short-term treatment with CBZ does not affect bone remodelling in the absence of tumour. However further cell types including megakaryocytes, bone marrow vascular endothelial cells and chondrocytes were rapidly affected by CBZ suggesting that these cell types may contribute to the therapeutic effects of CBZ as well as off target effects. Response of key bone cells to CBZ administration is rapid and reversible once treatment is stopped, supporting the conclusion that continuous administration is required in order to maintain the effects of this agent (see Table 23 for a summary of treatment effects).

**Table 23 Summary of the effects of CBZ on the bone microenvironment.**
× = no effect, ↑ = increased, ↓ = decreased, Ob.N.= Osteoblast number, Ob.A.= Osteoblast activity, Oc.N.= Osteoclast number, Oc.A.= Osteoclast activity, GP = Growth plate area, MK = Number of megakaryocytes, n.a = not assessed.

| Summary of treatment effects | | | | | | |
|---|---|---|---|---|---|---|
| **Model system** | **Ob.N.** | **Ob.A.** | **Oc.N.** | **Oc.A** | **GP** | **MK** |
| **5 doses of CBZ** | | | | | | |
| **8-9-week old GFP Ob$^+$ mice** | ↑ | × | ↓ | × | ↑ | × |
| **17-week old GFP Ob$^+$ mice** | ↑ | × | × | × | ↑ | × |
| **8 doses of CBZ** | | | | | | |
| **6-week old male BALB/c nude** | ↑ | × | × | × | ↑ | ↑ |
| **6-week old female BALB/c nude** | × | × | ↓ | × | ↑ | ↑ |
| **9-week old femiale GFP Ob$^+$ mice** | × | × | ↓ | × | ↑ | × |
| **Treatment follow-up** | | | | | | |
| **6-week old female BALB/c nude** | | | | | | |
| **5 days post treatment termination** | × | × | × | × | ↓ | ↓ |
| **12 days post treatment termination** | | | | | | |
| **12 days post treatment termination** | × | × | × | ↑ | × | × |
| **Longer-term treatment** | | | | | | |
| **Castrated male NOD/SCID mice** | n.a | n.a | n.a | n.a | ↑ | n.a |
| **6-week old castrated male beige SCID mice** | n.a | n.a | n.a | n.a | ↑ | n.a |

# Chapter 5 - The role of the bone microenvironment in peripheral breast tumour re-growth following successful combination therapy

## 5.1. Summary

Cancer patients often receive a combination of therapies to increase their treatment response. Combined treatment with doxorubicin (DOX) followed by Zoledronic acid (ZOL) is shown to cause suppression of peripheral breast tumour growth *in vivo* in experimental models [241, 260]. Several clinical studies have suggested beneficial effects of ZOL when added to chemotherapy in the neoadjuvant setting [191, 192], and a recent meta analysis demonstrated a significant increase in complete pathological response in the breast when ZOL was added to chemotherapy in postmenopausal women [193]. The exact mechanism underlying the observed anti-tumour effects remain to be established. However, combining an anti-resorptive agent with chemotherapy supports a role for bone in the growth of primary breast tumours.

Signals from the bone microenvironment (BME) - including for example osteoclastic bone resorption – can cause bone marrow derived cells (BMDCs) including haematopoietic stem cells (HSCs) to leave their niche, proliferate and differentiate. BMDCs include cells that can produce tumour-growth-promoting factors and/or are recruited directly to the site of tumour growth.

The **hypothesis** to be tested in this chapter is that **ZOL-induced modification of the BME reduces peripheral breast cancer re-growth after cessation of combination therapy of the primary tumour.** This is the first study to determine whether reduced subcutaneous tumour growth following combination therapy is reversed by transplanting the tumours into new recipients with a modified BME. This will also give insight into whether effects of combination therapy are due to direct interactions between the drugs and tumour cells or through ZOL-induced alterations to the BME.

Weekly combination therapy successfully suppressed tumour growth whereas growth of re-transplanted tumour fragments resumed at equal rates whether transplanted into ZOL or PBS pre-treated hosts. Both ZOL and combination therapy caused modifications to numerous cell types in the BME. However, modification of the BME with ZOL was not sufficient to suppress peripheral breast cancer re-growth following cessation of combination therapy suggesting that modification of the BME only is not sufficient for sustained anti-tumour effects.

## 5.2. Introduction

### 5.2.1. Primary tumour growth and bone marrow-derived cells

Primary breast tumours are comprised of multiple components including both tumour cells as well as stromal cells. Stromal cells are increasingly recognised as key mediators of tumour development and disease progression [10]. Given that many of the stromal cells present within the TME are mobilised host cells from distant tissues including the bone marrow and spleen, growing attention is paid to bone marrow-derived cells (BMDCs) and their contribution to breast cancer growth. Upon cancer-cell-derived signals (cytokines and growth factors including G-CSF, VEGF, TGF-β, OPN, LOX and SDF-1 [27-29]) BMDCs including but not limited to cancer-associated fibroblasts, tumour-associated macrophages, infiltrating immune cells, myeloid-derived suppressor cells or corresponding precursors are actively recruited to the site of tumour growth, where they promote disease progression. Given that the bone marrow acts as a reservoir of BMDCs that can be recruited to the site of primary tumour growth, therapeutics that modulate the BME (including ZOL) may have consequences on primary breast cancer (re-) growth.

### 5.2.2. Combination therapy – clinical setting

In clinical practice, patients with advanced breast cancer often receive a combination of treatments that include bisphosphonates (BPs), chemotherapy and anti-hormone therapy. However, exact treatment intervals and sequence are not standardised and vary widely depending on disease progression. Bone-targeted agents, including BPs, and Denosumab are approved for treatment of patients with established bone metastases, but recent clinical trials also support their use in patients without evidence of skeletal involvement both in the adjuvant and neoadjuvant setting. Several studies have suggested beneficial effects of adding ZOL to chemotherapy in the neoadjuvant setting [191, 192]. A recently published meta-analysis assessed data from 750 patients with stage II/III breast cancer enrolled in 4 different randomised clinical trials comparing the use of ZOL in combination with neoadjuvant chemotherapy. Subgroup analysis showed that pathological response (pCR), the ultimate aim in neoadjuvant therapy, was nearly doubled in postmenopausal women; results similar as described with regards to the differential menopausal effect of ZOL in adjuvant therapy [132, 192]. Given these clinical trials the use of BPs in patients without evidence of skeletal involvement will increase. However, it remains speculative whether and how the BME mediates primary breast cancer (re-) growth and if this is influenced by bone-targeted agents.

### 5.2.3. Combination therapy – pre-clinical setting

Chemotherapeutic regimes used to treat breast cancer patients often include the anthracycline doxorubicin (Adriamycin®, herein referred to as DOX) or epirubicin (Ellence®). Neoadjuvant chemotherapies used in the AZURE trial included anthracyclines [192] and previous experiments in our laboratory have shown beneficial effects of clinically relevant doses of the anthracyclin DOX in combination with ZOL on peripheral as well as skeletal breast cancer growth [241, 247].

Briefly, DOX acts on cancer cells by inhibiting topoisomerase-II-mediated DNA repair, interfering with DNA unwinding [300] and generating free oxygen radicals that damage cell membranes [301]. Doxorubicin has been shown to decrease proliferation [302], to induce senescence [303] and cell death in breast cancer cells *in vitro* [139]. In clinical practice DOX is administered intravenously at a dose of 60-75mg/$m^2$ once every 21 days, or at 40-60mg/$m^2$ when used in combination with other chemotherapy drugs.

The nitrogen containing bisphosphonate ZOL, rapidly binds to bone mineral where it targets the bone resorbing osteoclast - its main target, by inhibiting key enzymes of the mevalonate pathway [138]. *In vitro* ZOL is also suggested to have direct anti-tumour effects as it induces apoptosis in a number of breast cancer cells including MCF7 and MDA-MB-231 [304, 305]. Numerous *in vitro* studies have also demonstrated direct potential of ZOL to affect tumour cell adhesion, invasion, proliferation and survival (briefly summarised in [140]). These studies however, did not use clinically relevant doses and time points. In my studies I therefore decided to use 100µg/kg ZOL, comparable to the 4mg dose administered to patients with cancer-induced bone disease. However, the weekly schedule used in this study is not comparable to the clinical practice of ZOL administration every 3-4 weeks.

*In vitro* combination of the bone targeted agent ZOL with chemotherapy (*e.g.* ZOL + paclitaxel *in vitro* [304], ZOL + DOX *in vitro and in vivo* [139, 241, 259, 260]) has been shown to be more effective than each agent on its own in inducing tumour cell apoptosis and reducing tumour growth [139, 241, 260, 304]. Initial *in vitro* studies by Neville-Webbe and colleagues revealed the importance of sequence and schedule of DOX and ZOL when given in combination [139]. In MCF-7 and MDA-MB-436 breast cancer cells, DOX (0.05µM) treatment for 24hrs followed by 1hr treatment with ZOL (25µM) induced apoptosis whereas neither treatment alone or the reverse order resulted in significant alterations in

tumour cell apoptosis [139]. Similar results were observed in the PC3 prostate cancer cell line [139]. Combination of DOX with clodronate (500μM) – a less potent non-nitrogen containing BP – did not synergistically induce apoptosis in MCF7 cells. However, sequential treatment of DOX followed by alendronate (AL), a nitrogen containing BP, increased apoptosis, although this was less prominent than combination therapy of DOX with ZOL [139]. Similar findings are reported using ZOL (10μM) in combination with (2nM) paclitaxel – with a 5- or 4- fold increase in apoptosis of MCF-7 cells upon combination therapy when compared to ZOL or paclitaxel given alone [304].

In clinical practice administration schedules vary widely and treatments might be administered at irregular intervals whereas these studies suggest that the order in which therapeutic agents are administered and the interval between them could be vital to treatment success. Previous work in our group has investigated the anti-tumour effects of DOX and ZOL *in vivo* [154, 241, 247, 259, 260] with effects on both breast cancer growth in bone, as well as extra-skeletal tumour growth. Administration of single agents initially reduced peripheral tumour growth but had no effect in the later stages, whereas peripheral tumour growth was nearly abolished in mice receiving sequential combination therapy [241, 260]. Importantly suppression of tumour growth was sustained for over 160 days post treatment termination, although the mechanisms regulating this effect remain to be established [260]. These intriguing data clearly suggest a role of the BME in peripheral tumour growth with potential to be mediated via the addition of bone-targeted agents.

*In vivo* the exposure of breast cancer cells to ZOL is most likely quite short due to the high affinity of the drug to bone and its short half-life in circulation. Administered as a 4mg dose infusion every 3-4 weeks in the treatment of cancer induced bone disease ZOL has a plasma half-life of 105min with a peak plasma concentration of 1-2μM [306]. Whereas in bone, a combination of direct and indirect effects of BPs contribute to inhibition of tumour growth and cancer-induced bone disease, though little is known about whether modification of the BME affects tumour growth distant to the bone, and the interaction of the BME and peripheral tumours remains speculative.

The majority of studies investigating the effects of BPs as single agents established their ability to inhibit bone metastases [143, 149, 257, 307] and only a limited number of studies have investigated the effects of bone-targeted agents on peripheral tumour growth (summarised in Table 24). A study by Coscia *et al.* has elegantly demonstrated ZOL's impact and benefit on tumour growth outside the bone in an experimental *in vivo* model [171].

However, the studies in Table 24 used multiple doses and continuous treatment, making it impossible to establish whether any observed treatment effects are mediated via direct effects of BPs on the tumour cells or via modification of the BME, or both.

### 5.2.4. Targeting the BME in peripheral breast cancer growth

The bone marrow hosts two distinct stem cell populations with each having different progenies – haematopoietic and mesenchymal stem cells (HSCs and MSCs). HSCs give rise to all lymphoid and myeloid lineage cells that finally produce blood circulating cells and immune cells [50]. MSCs, in contrast, differentiate to give rise to adipocytes, bone and connective tissue cells. In addition the bone marrow contains numerous blood vessels, endothelial cells arising from hemangioblasts similar to HSCs [30]. All of these mature cell populations (in the following chapter referred to as bone marrow derived cells (BMDCs)) as well as their precursors may be affected by BP treatment and thereby directly or indirectly contribute to primary tumour growth (Table 25, osteoblasts and osteoclasts are not included as previously discussed in depth in Chapter 3, Figure 59 below).

**Table 24 *In vivo* studies investigating the effects of BPs on extra skeletal (breast) cancer growth**

| Bisphosphonate | Mouse model | Cell line | Effect on peripheral tumour growth | Ref. |
|---|---|---|---|---|
| Risedronate - 150μg/kg daily for 25 days, once palpable | athymic BALB/c | B02-GFP/βGal cells ($5x10^6$), subcutaneous | No effect | [148] |
| NE-58051 - 150μg/kg daily for 25 days, once palpable | athymic BALB/c | B02-GFP/βGal cells ($5x10^6$), subcutaneous | No effect | [148] |
| ZOL - 0.1mg/kg ZOL or Pamidronate – 2mg/kg 5 days a week | BALB-neuT expressing rat oncogene c-erbB-2 (HER-2/neu) | Spontaneous mammary carcinoma formation | Delayed tumour onset, reduced tumour volume, reduced numbers of infiltrating CD11b/Gr-1/F4/80 positive cells within the tumour stroma | [37] |
| ZOL - 5μg/mouse 2x weekly, once tumours reached 200mg | 6-8-week-old male Fox Chase SCID mice | $2x10^6$ PC-3 cells or subcutaneously implanted LuCaP 23.1 tumour bits | No effect | [307] |
| ZOL - 100μg/kg once weekly for 4 weeks, cycle repeated after 3 weeks of rest | 7-week old BALB-neuT mice | Spontaneous mammary carcinoma formation | Extension in tumour-free survival, reduction in tumour multiplicity, growth delay, prolonged survival, reduced number of infiltrating CD11b+ macrophages | [171] |
| Risedronate analogue - AF647-RIS 0.9mg/kg or Pamidronate analogue - OsteoSense 680 0.7mg/kg; once palpable | 6-8-week old BALB/c nude | $5x10^5$ 4T1-luc2 breast cancer cells in the mammary fat pad | NBPs were internalised by TAMs | [39] |
| Risedronate at 150 μg/kg body weight every other day for 14 days; once $50mm^3$ tumour volume | 5-week-old female non obese diabetic/severe combined immunodeficient (NOD/SCID) | $5x\ 10^6$ B02 or T47D cells, subcutaneous | No inhibition of T47D and B02 tumour growth | [175] |
| 2mg/kg Doxorubicin follwed 24hrs by 100μg/kg ZOL; 27 days post tumour injection | 5-week-old female nonobese diabetic/severe combined immunodeficient (NOD/SCID) | B02 cells, subcutaneous | Slowed down tumour growth compared to placebo | [175] |

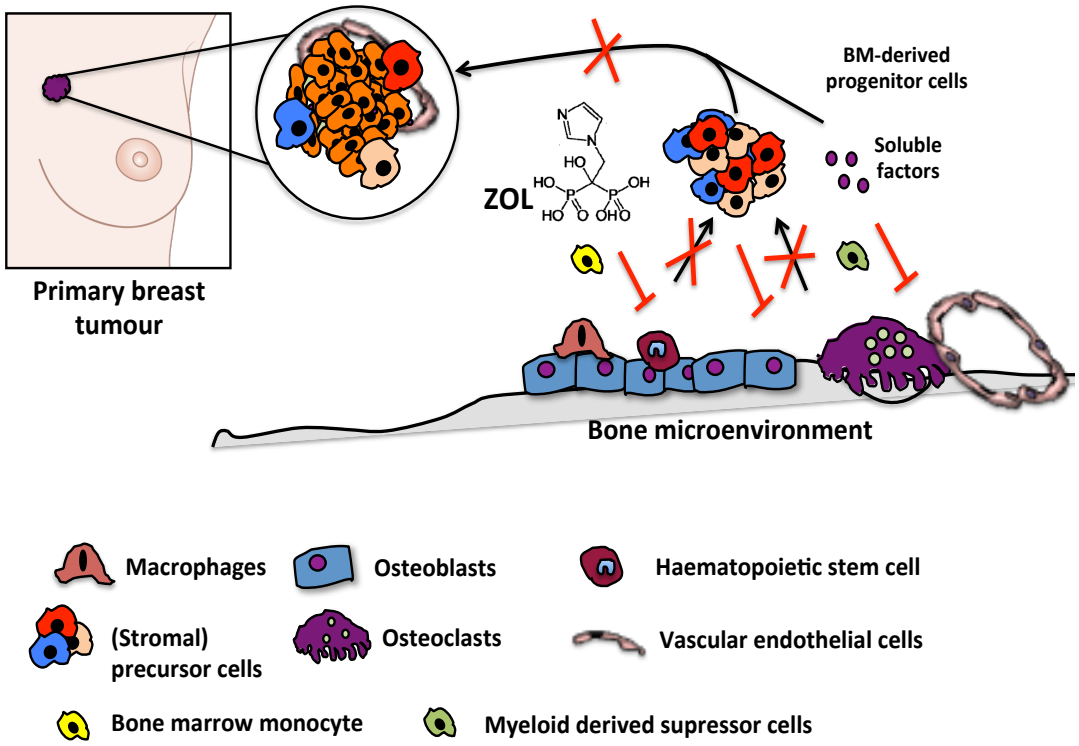


**Figure 59 Schematic illustration of the hypothesis that ZOL-induced modification of the BME affects primary breast cancer growth.**
The primary breast cancer is a heterogeneous microenvironment composed of various stromal cells. These stromal cells are recruited from haematopoietic organs including the bone marrow. Zoledronic acid (ZOL) is known to affect a variety of BMDCs and the availability of soluble factors that could all contribute to peripheral tumour growth.

**Table 25 Effects of bisphosphonate (BP) treatment on BMDCs.**
PAM=Pamidronate, AL=Alendronate, IB=Ibandronate

| Cellular components of the BME | | |
|---|---|---|
| **Cell type** | **BP** | **Effect** |
| **Endothelial cells**<br>- Human dermal microvascular endothelial cell (HuDMEC) [163]<br><br>- Human umbilical vein endothelial cells (HUVEC) [161, 162] | ***In vitro:***<br>- ZOL: 25-50µM [163], 0.3-30µM [161], 5 - 500µM [162]<br>- PAM/IB: 5 - 500 µmol [162]<br>***In vivo:***<br>- ZOL: 50-150 µg/kg daily in 8-week old male CD1 nude mice *[163]*<br>- ZOL: (1-100 µg/kg s.c) daily for 6 days in female Tiflbm:MAG mice [161]<br>- ZOL: 1mM Chicken Egg Chorioallantoic Membrane Assay [161]<br>- ZOL: 200µg/kg, 2x weekly; 4-week old male C57BL/6J mice) [159]<br>***Ex vivo:***<br>- ZOL: 50µM Aortic ring assay [161]<br>**Patients:**<br>- ZOL: 4mg or PAM 90mg every 3-4 weeks [164] | **Overall:** Anti-angiogenic<br>***In vitro:***<br>- Increased accumulation of Rap1a in HuDMEC and inhibited cell proliferation [163]<br>- Dose dependent inhibition of proliferation [161]<br>- Decreased cell viability [162]<br>***In vivo:***<br>-No effect on venular or arteriolar diameters [163]<br>- Inhibition of bFGF induced angiogenic response[161]<br>- Reduced vessel thickness and increased vessel numbers with overall vessel volume fraction not being affected [159]<br>**In clinic:**<br>- Decreased levels of circulating endothelial progenitor cells[164]<br>***Ex vivo:***<br>- Inhibition of capillary sprouting [161] |
| **Haematopoietic stem cells** | ***In vivo:***<br>-ZOL: 200µg/kg, 2x weekly; 4-week old male C57BL/6J mice) [159] | ***In vivo:***<br>- Expansion of HSC niche<br>- Increase in haematopoietic progenitor cells in bone marrow<br>- Trend towards increased numbers of long-term reconstitution haematopoietic stem cells in bone marrow |
| **γδ T cells** | ***In vitro:***<br>- PAM: 5 to 10 µM [176], 0.4-40µM [174]<br>***In patients:***<br>- PAM: 60 or 90mg [176] | ***In vitro:***<br>- Dose dependent expansion of γδ T cells [174]<br>- Induce proliferation [174]<br>- Activation and selective expansion of γδ T cells in cultures of peripheral-blood mononuclear cells from healthy subjects [176]<br>- Increased secretion of interferon-γ [176]<br>***In patients:***<br>- Acute-phase reaction → increased presence of $CD3^+$ γδ T cells in peripheral blood after first pamidronate treatment [176] |
| **Fibroblasts**<br>-human gingival fibroblasts | ***In vitro:***<br>- ZOL/PAM/IB: 5 - 500µM [162] | ***In vitro:***<br>- Inhibition of viability [162] |

| Cell type | BP | Effect |
|---|---|---|
| **Macrophages**<br>- J774 and RAW264 [156]<br><br>- J774 macrophages [38]<br><br>**-** Mouse macrophage-like J774.1 cells [308] | ***In vitro:***<br>- PAM, IB, AL: 100µM [156]<br>- ZOL: 5µM [38]<br>- AL, PAM, IB, ZOL: $10^{-6}$ to $10^{-4}$ M [308]<br>***In vivo:***<br>- ZOL: 100µg/kg [38]<br>- ZOL: 100µg/kg once weekly for 4 weeks, cycle repeated after 3 weeks of rest; 7-week old BALB-neuT mice [171]<br>- ZOL or PAM - 0.1mg/kg ZOL or PAM – 2mg/kg 5 days a week [37]<br>- ZOL: 100µg/kg, daily; K14-HPV16 transgenic mice [309] | ***In vitro:***<br>- Apoptosis of J774 cells [156]<br>- Apoptosis, increased levels of uRap1A [38]<br>- Apoptosis J774.1 [308]<br>***In vivo:***<br>- Increased accumulation of uRap1A [38]<br>- Reduced infiltration of CD11b+ve macrophages in s.c. tumours [37, 171]<br>- Reduced MMP-9 expression [37]<br>- Decreased infiltration of macrophages in tumour stroma [309]<br>- Reduced MMP-9 expression in tumour macrophages [309] |
| **Bone marrow monocytes (CD14+ve)** | ***In vivo:***<br>- RIS analogues: single injection with 0.9 mg/kg AF647-RIS (3 day old) New Zealand White rabbits [172] | ***In vivo:***<br>- Uptake of fluorescently labelled BPs and accumulation of uRap1a [172] |
| **Human placental mesenchymal stem cells (pMSCs)** | ***In vitro:***<br>- ZOL, AL: 0.25-200µM [165] | ***In vitro:***<br>- Negative effect on proliferation and migration<br>- Reduced tube formation<br>- Inhibited differentiation of pMSCs into endothelial cells |
| **$CD11b^+/Gr1^+$ Myeloid-derived suppressor cells**<br>- total bone marrow cells cultured with M-CSF OR 30% tumour supernatant [168] | ***In vitro:***<br>- ZOL: 0.03, 0.15 or 0.3 **µ**M for 6 days [168]<br>***In vivo:***<br>- ZOL: 100µg/kg, daily, 6-8-week old CBA-j mice [168]<br>- ZOL: 0.1mg/kg ZOL 5x weekly BALB-neuT mice[37] | ***In vitro:***<br>- Inhibiton of myeloid differentiation into macrophages [168]<br>***In vivo:***<br>- Increased MDSC in the spleen [168]<br>- Reduced presence of macrophages in spleen of ZOL treated mice suggesting impaired differentiation of MDSCs upon ZOL treatment [168]<br>- Reduced number of $CD11b^+/Gr\text{-}1^+/F4^+/80^+$ cells in tumour stroma and peripheral blood [37]<br>Reduction in clonogenic colony-forming progenitor cells present in bone marrow [37] |

In addition to various cell types also circulating cytokines that are known to promote tumour growth are affected by BP treatment (Table 26).

**Table 26 Effects of bisphosphonates (BP) on cytokines and growth factors**
PAM=Pamidronate, AL=Alendronate, IB=Ibandronate

| Factor | BP | Effect |
|---|---|---|
| **VEGF serum/plasma levels** | ***In patients:***<br>- PAM (90mg) [166]<br>- ZOL (4mg) [167]<br><br>***In vivo:***<br>- ZOL: 100µg/kg once weekly for 4 weeks, cycle repeated after 3 weeks of rest; 7-week old BALB-neuT mice [171]<br>- ZOL: 100µg/kg daily for 5 days a week; BALB-neuT mice [37] | ***In patients:***<br>- Reduced 1, 2 and 7 days post PAM infusion [166]<br>- Reduced 2, 7 and 21 days post ZOL infusion [167]<br><br>***In vivo:***<br>- Decreased serum VEGF levels [37, 171] |
| **γ-IFN and IL-6 serum/plasma levels** | ***In patients:***<br>- PAM (90mg) [166] | ***In patients:***<br>- Increased 1 day after infusion but rapidly decreased after 2 days [166] |
| **PDGF serum/plasma levels** | ***In patients:***<br>- ZOL (4mg) [167] | ***In patients:***<br>- Decreased 1 day after ZOL infusion [167] |
| **Interleukins**<br>- effusion fluid from the peritoneal cavity | ***In vivo:***<br>- ZOL: 100µg/kg, daily for 25 days, 6-8-week old CBA-j mice (mesothelioma bearing) | ***In vivo:***<br>- Increase in IL-6, IL-12 and IL-1b [168] |
| **Matrix metallo proteinases**<br>- MMP-9 | ***In vivo:***<br>- ZOL: 0.1mg/kg 5x weekly, BALB-neuT mice | ***In vivo:***<br>- Decreased pro-MMP9 serum levels [37] |

As illustrated and summarised above, BPs have the potential to affect a wide variety of BMDCs in addition to modifying the levels of growth factors and cytokines involved in tumour growth. This supports the hypothesis that treatment of the BME with ZOL may have consequences on extra-skeletal tumour growth.

### 5.3. Hypothesis

The hypothesis to be tested in this chapter is that **modification of the BME with the bone-targeted agent ZOL reduces re-growth of transplanted tumour fragments** after successful combination therapy by altering the availability of growth-supporitng BMDCs.

### 5.4. Aims and Objectives

- Establish an *in vivo* re-implantation model to study the role of the BME in primary breast cancer re-growth.
- Assess whether reduced tumour growth after DOX/ZOL combination therapy is reversed or maintained when tumours are transplanted into animals with a modified BME induced by ZOL pre-treatment.
- Determine if reduced tumour growth following combination therapy is mediated via modification of BMDCs.

## 5.5. Material and Methods

Here I investigated whether combination therapy (DOX + ZOL) affects subcutaneous tumour growth through modifying the BME, and determined whether tumour growth resumes following transplantation of treated tumour fragments (DOX+ZOL combination therapy) into hosts with a therapeutically altered BME. This aims to investigate whether modification of the bone microenvironment is sufficient to initiate anti-tumour effects or if both the tumour and BME need to be targeted. A summary of materials and methods can be seen in Table 27 below.

**Table 27 A summary of material and methods for Chapter 5.**

| Method | Parameters analysed | Equipment |
|---|---|---|
| Microcomputed tomography | Bone integrity of tibiae<br>-Trabecular bone volume (BV/TV in %)<br>-Trabecular number (TB.N. in $mm^{-1}$)<br>-Trabecular thickness (Tb.Th. in mm) | -SkyScan 1272 scanner (SkyScan)<br>-NRecon software<br>-CTAn software |
| **Histological assessment** | | |
| CD34 staining | CD34+ve tumour vasculature – microvascular density | -Leica DMI1000 microscope<br>-Chalkley grid |
| CD31 staining | CD31+ve tumour vasculature – microvascular density | -Leica DMI1000 microscope<br>-Chalkley grid |
| Haematoxylin and Eosin staining (H&E) | Nectotic core | -OsteoMeasure software (OsteoMetrics)<br>-DMRB upright microscope<br>-Olympus BX53 microscope |
| Ki-67 staining | Tumour cell proliferation | -OsteoMeasure software (OsteoMetrics)<br>-Olympus BX53 microscope |
| Immunofluorescence/confocal microscopy | Visualisation of Endomucin positive vascular endothelial cells in bone | -Nikon A1 confocal microscope with NIS Elements software (40x objective)<br>Nikon inverted Ti eclipse, NIS-Elements software Version 4.30, Plan Apo 20x (NA 0.75)<br>-Cryostat (MICROM HM560) |
| ***In vivo* work** | | |
| Monitoring tumour growth | Subcutaneous tumour growth | -Calipers |
| **Effects on Bone Marrow Derived Cells** | | |
| Flowcytometry | Presence of $CD11b^{+}/Gr1^{+}$ cells in bone marrow flushes | -LSRII |
| **Statistical analysis** | | |
| Statistical analysis | Experimental datasets | -Prism GraphPad |

### 5.5.1. Subcutaneous growth of MDA-G8 cells *in vivo*

The human triple negative breast cancer cell line MDA-MB-436 (hereafter referred to as MDA-G8) were transfected with GFP and kindly provided by Dr. Ottewell (University of Sheffield) [241]. Cells were cultured in RPMI supplemented with 10% FBS at 37°C, 5% $CO_2$. On the day of tumour cell injection, cells were harvested as described in Chapter 2, Section 2.2.3. 100µL cell suspension (5x$10^6$ cells/mL sterile PBS) was subcutaneously injected into the right flank of mice using 1mL syringes with 25G needles. Tumour size (depicted as tumour volume in $mm^3$) was measured 2-3 times weekly using callipers. Tumour volume was calculated assuming spherical dimensions by using the formula $V = \frac{4}{3} \times \pi \times r^3$ where r = $\frac{(\frac{\text{(Vertical + horizontal diameter)}}{2})}{2}$. Animals were culled according to regulated procedures once maximum tumour volume (1000$mm^3$) was reached, or earlier if severe skin blistering (ulceration) or signs of morbidity were observed.

### 5.5.2. Drug preparation and administration

#### 5.5.2.1. Zoledronic acid

Zoledronic acid (ZOL) was prepared as described in Chapter 2, Section 2.2.8.5. A 100µg/kg suspension was prepared fresh prior to injection, sterile filtered and 100µL injected intra peritoneal using 1mL syringes (25-gauge needle). The 100µg/kg dose used in these experiments is equivalent to the 4mg clinical dose used in the treatment of cancer-induced bone disease. However, the regime is different with ZOL administered weekly when compared to the clinical administration of every 3-4 weeks.

#### 5.5.2.2. Doxorubicin

Doxorubicin (2mg/kg, DOX) was prepared in PBS fresh on the day of use and sterile filtered prior to injection (Chapter 2, Section 2.2.8.4). Animals were placed in an incubator at 35°C for at least 15min to dilate the tail veins and facilitate intravenous drug administration. Mice were placed in a bench top restrainer fitted onto a heating pad. 100µL of the drug suspension were slowly injected into the tail vein using 1mL insulin syringes (27-gauge needle). Clinical grade doxorubicin at a stock concentration of 2mg/mL was kindly provided from Weston Park Cancer Hospital, Sheffield, UK.

### 5.5.3. Experimental design of *in vivo* studies

#### 5.5.3.1. Animal models

Experiments to investigate the role of the BME as a mediator of peripheral breast cancer growth were performed twice, one pilot experiment to establish the suitability of the model followed by an experiment with increased animal numbers. Mouse models included in both experiments are listed in Table 28 below.

**Table 28 Animal models used to establish the role of the BME as a mediator of peripheral breast cancer growth.**

| | Mouse strain | Age at study start | Treatment | Referred to |
|---|---|---|---|---|
| Pilot experiment | Female BALB/c-Nude[Foxn1-Crl] (n=15) | 6-8-week old | 1x weekly combination therapy for 5 weeks (DOX/ZOL: n=9, PBS: n=6) | Tumour fragment donor |
| | Female BALB/cOlaHsd-Foxn1nu (n=6) | 9-11-week old | 1x weekly ZOL (100µg/kg) for 2 weeks (n=3/group) | Tumour fragment recipient |
| Full study | Female BALB/c-Nude[Foxn1-Crl] (n=24) | 7-9-week old | 1x weekly combination therapy for 5 weeks (DOX/ZOL: n=14, PBS: n=10) | Tumour fragment donor |
| | Female BALB/c-Nude[Foxn1-Crl] (n=16) | 6-7-week old | 1x weekly ZOL (100µg/kg) for 2 weeks (n=8/group) | Tumour fragment recipient |

#### 5.5.3.2. Combination therapy schedule

Previous reports using *in vitro* experiments have shown the importance of sequence and schedule of DOX and ZOL when given as combination therapy [139]. DOX (0.05µM) treatment for 24hrs followed by 1hr treatment with ZOL (25µM) induced apoptosis in the human oestrogen-dependent breast cancer cell line MCF7, the oestrogen-independent cell line MDA-MB-436 and androgen-independent prostate cancer cells PC3. Based on the reported importance of administration sequence, I administered DOX (2mg/kg, 100µL, i.v.) 24hrs prior to ZOL (100µg/kg, 100µL, i.p.) once weekly to mice bearing MDA-G8 tumours, a dosing regime that has previously been demonstrated to abolish subcutaneous growth of this cell line in female MF1 nu/nu mice [241]. In the following sections this treatment regime is referred to as ''combination therapy''.

Mice were randomly assigned into two treatment groups receiving either **(1)** 2mg/kg Doxorubicin (100µL, i.v.) followed 24hrs later by 100µg/kg Zoledronic acid (100µL, i.p.) or **(2)** PBS (100µL, i.v.) followed 24hrs later by PBS (100µL, i.p.), once weekly for 5 weeks. Combination therapy was administered to 7-9-week old female BALB/c nude mice (Charles River, UK; BALB/c-Nude[Foxn1-Crl], n=14 DOX/ZOL, n=10 PBS) or 6-8-week old female BALB/c nude mice (BALB/c-Nude[Foxn1-Crl], Charles River, UK, n=9 DOX/ZOL and n=6 PBS) – see Table 28, Fig.60; with treatment being initiated 7-17 days post tumour cell

injection (Fig.60). These mice are in the following method section referred to as “tumour donors”.

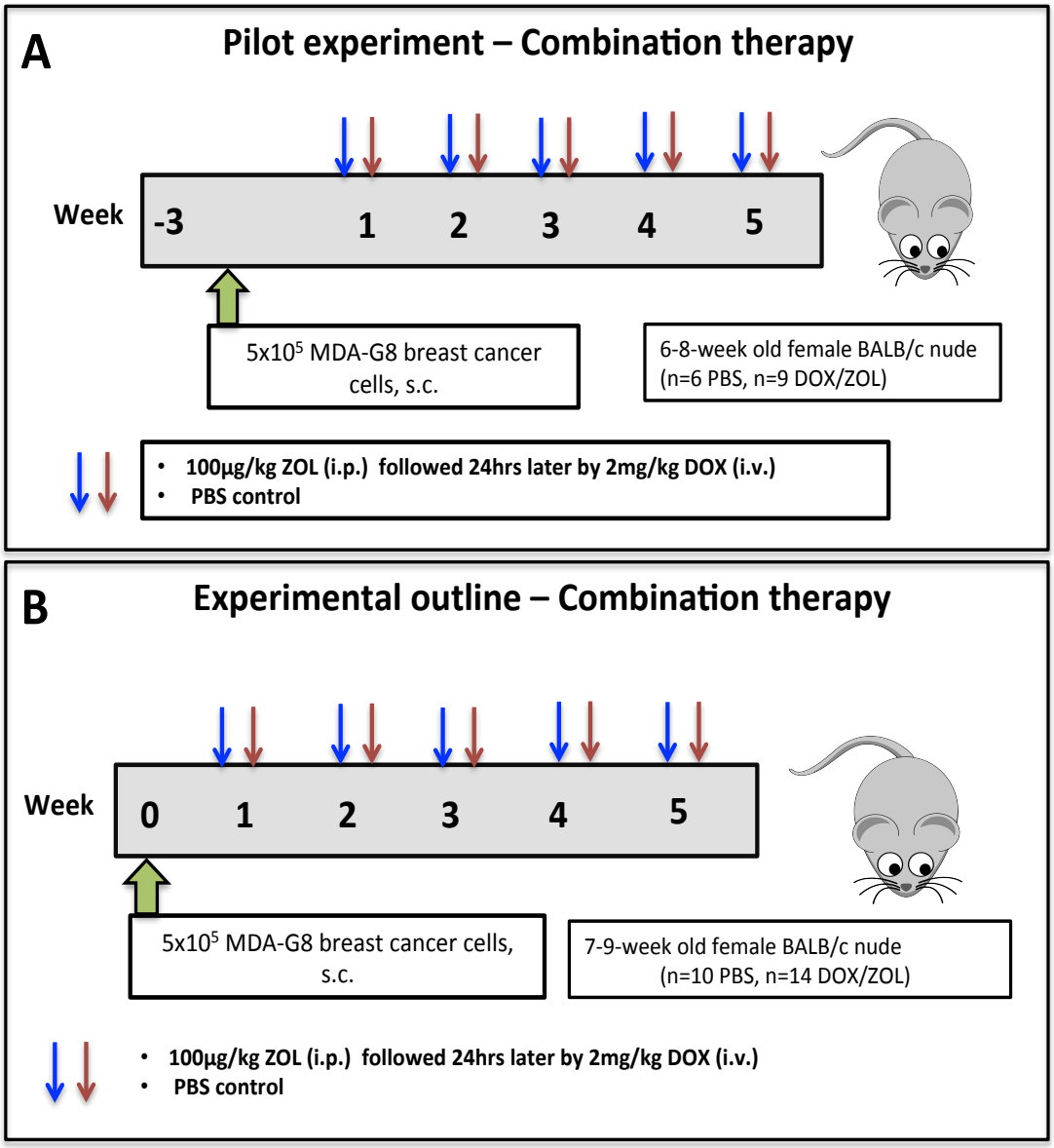


**Figure 60 Experimental outline for combination therapy administration.**
(A) 6-8-week and (B) 7-9-week old female BALB/c nude mice were subcutaneously injected with $5x10^5$ MDA-G8 breast cancer cells. Combination therapy (2mg/kg Doxorubicin (DOX) followed 24hrs later by 100µg/kg Zoledronic acid (ZOL), 1x weekly or PBS controls via respective administration routes was started (B) 7 and (A) 17 days post tumour cell injection.

#### 5.5.3.3. Zoledronic acid pre-treatment

In previous experiments I have determined that ZOL rapidly induces changes to the *in vivo* BME, including alterations in bone volume, bone cell number and extracellular matrix composition [158]. ZOL (2 doses) or PBS control was therefore used to induce therapeutic modification to the BME of 6-7-week old female BALB/c nude mice (BALB/c-Nude [Foxn1-Crl], n=8/group, Charles River, UK) or 9-11-week old female BALB/c nude mice (BALB/cOlaHsd-Foxn1nu, Harlan UK, n=3/group); the tumour fragment recipients - Table 28.

#### 5.5.3.4. Transplantation of tumour fragments

Transplantation of tumour fragments was performed 24hrs after both tumour donor and recipient mice had received the last dose of ZOL (Fig.62).

Tumour donor mice (DOX+ZOL treated mice) were culled by using an overdose of pentobarbitone and blood collected by cardiac puncture. Subcutaneous tumours were excised using sterile, autoclaved dissection tools and immediately transferred into sterile PBS. Tumours were then split into pieces of approximately equal size and remained in PBS until transplantation (within the next 10 minutes).

Fragments were transplanted into mice that had either received ZOL pre-treatment or PBS control. Recipient mice were anaesthetised using isoflurane, and a small incision made on the back. A pocket was formed underneath the skin using blunt scissors and the previously dissected tumour pieces positioned inside the pocket using sterile forceps. Wounds were closed using wound clippers (Harvard Apparatus). Wound clips were removed 1 week after surgery to ensure complete wound closure at the incision site (Fig.61). Surgery was kindly taught and assisted by Dr. Ottewell, University of Sheffield, UK.

A schematic summary of the experiments to establish the role of the BME in peripheral breast cancer growth can be seen in Figure 62 below.

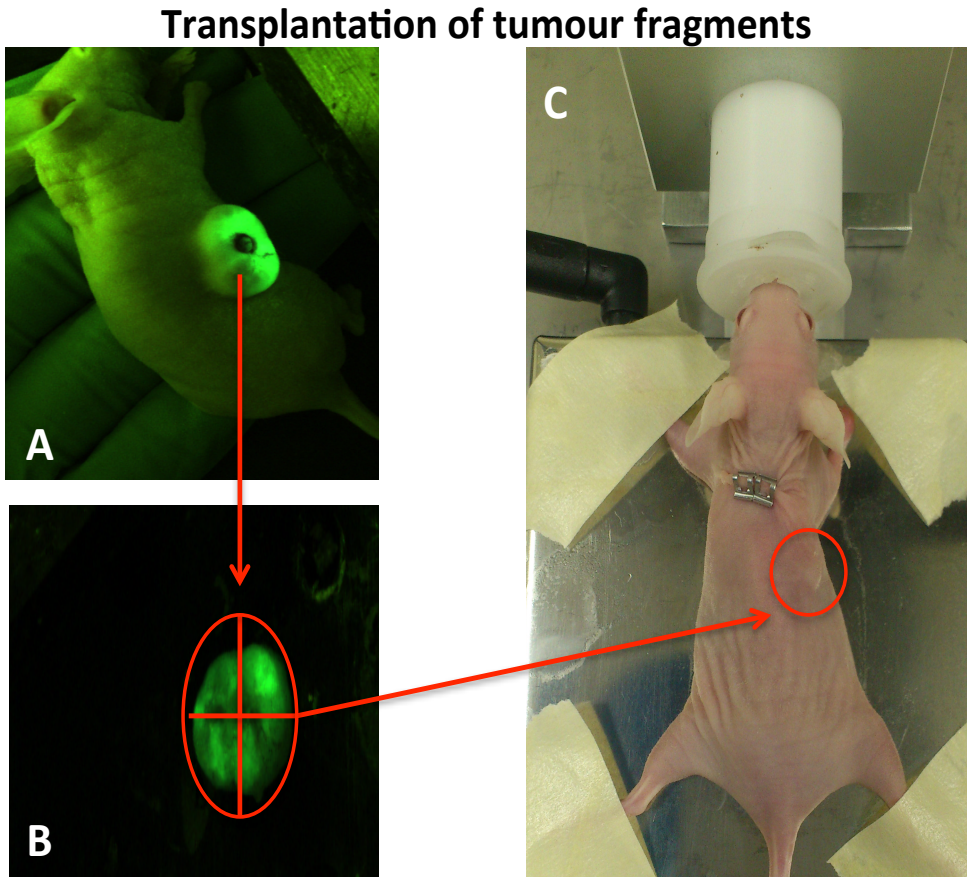


**Figure 61 Tumour fragment transplantation.**
24hrs after both tumour donor and recipient mice had received their last dose of Zoledronic acid, transplantation of tumour fragments was performed. Subcutaneous MDA-G8 tumours were isolated from "donor mice" (A), split into quarters (B) and subcutaneously transplanted into the right flank of "recipient mice" (C).

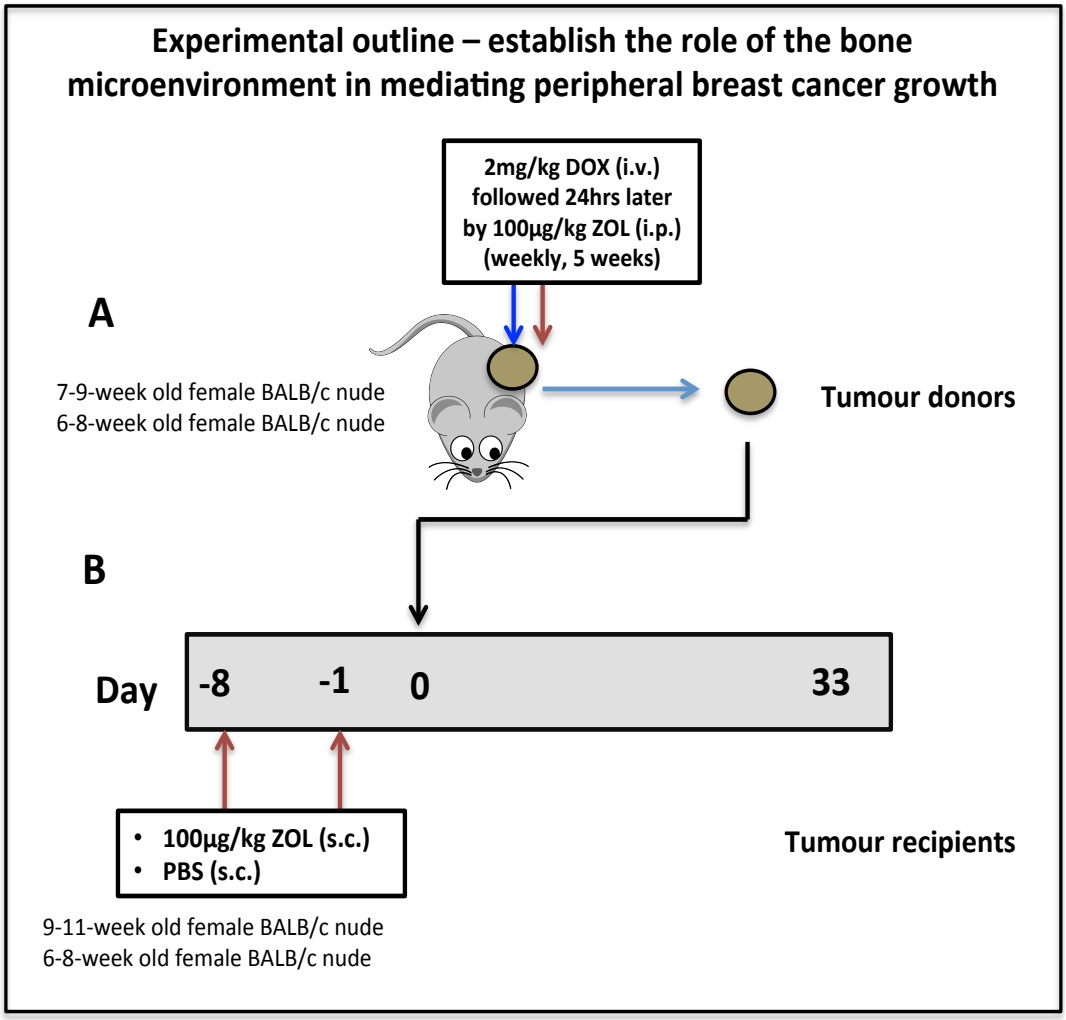


**Figure 62 Experimental outline to establish the role of the bone microenvironment in mediating peripheral breast cancer growth.**

Subcutaneous tumours (MDA-G8 cells) from mice receiving 5 weeks of combination therapy (2mg/kg Doxorubicin (DOX) followed 24hrs later by 100µg/kg Zoledronic acid (ZOL),1x weekly) were collected at experimental endpoint (A). Tumours were split into pieces and subcutaneously transplanted into female BALB/c nude mice (n=3-8/group). Recipient mice received either 2 doses of ZOL (100µg/kg, 100µL, 1x weekly) or PBS control (100µL) (B). Two separate experiments were performed using 6-8-week old (n=8/group, age indicated at pre-treatment start) or 9-11-week old female BALB/c nude (age indicated at pre-treatment start, n=3/group mice) as tumour recipients.

### 5.5.4. Assessing effects of combination therapy on myeloid-derived suppressor cells using flow cytometry

Myeloid-derived suppressor cells (MDSCs) are known to be overproduced in the bone marrow and spleen of cancer patients [170]. In addition they infiltrate into tumours and increase angiogenesis by expressing high levels of MMPs, thereby stimulating tumour growth [37, 41, 310], a process known the be reduced after ZOL treatment [170]. To determine if combination therapy induces alterations in the MDSC-pool in the bone marrow I quantified the percentage of this cell population using flow cytometry. In murine models MDSCs are classified as CD11b (a marker for myeloid cells of the macrophage lineage) and Gr-1 (a marker for granulocytes) positive [41, 170].

#### 5.5.4.1. Collection of bone marrow derived cells (BMDCs) for flow cytometry:

To collect BMDCs from mouse long bones I was kindly provided with a protocol from J-Ubellacker, Boston, USA. Briefly, on the day of cull excised femurs of mice were placed in ice-cold sterile PBS. Next the distal portion of the femur (attached to the hip) was cut off to expose the bone shaft. 25-G needles were used to punch a hole into the bottom of a PCR-tube, which was then placed into an eppendorf tube. Femurs were placed into the PCR-tubes and BMDCs obtained by centrifugation at 8000rpm (Heraeus FRESCO21; ≈6200xg) for 4min at 4°C. Red blood cells were lysed using RBC lysis buffer from eBioscience according to manufacturers instructions. Cells were resuspended in 3mL lysis buffer and incubated for 5min at ambient temperature followed by termination of the reaction by adding PBS. Next, samples were centrifuged at 1500rpm (MSE Mistral 2000; ≈403xg) for 5min and washed 2x in FACS buffer (2% FBS in PBS). Where possible one marrow from both femurs of each mouse were collected, pooled and frozen down in 2 aliquots in FBS containing 10% DMSO. Samples were stored at -80°C over night followed by transferral to liquid nitrogen until further analysis.

#### 5.5.4.2. Staining of bone marrow samples for flow cytometry

Bone marrow cells were rapidly thawed in a 37°C water bath and resuspended in 5mL FACS buffer (2%FBS in PBS). The cell suspension was passed through a 100µm nylon mesh, centrifuged at 1500rpm (5810R, Eppendorf; ≈ 370xg) for 5min and resuspended in 5mL FACS buffer. Cell number was determined using a haemocytometer and $1x10^6$ cells transferred into eppendorf tubes followed by centrifugation at 1500rpm Heraeus FRESCO21; ≈200xg) for 5min at 4°C. For analysis bone marrow samples from 2 mice/group were pooled (3 independent repeats to have n=3). Cell pellets were resuspended in corresponding antibody solutions (prepared in PBS, see Table 29 below, Anti-Mouse CD11b

Alexa Fluor® 488, eBioscience, Clone M1-70, Cat.No.:53-0112-80; Pe-Cy7 anti-mouse Ly-6G/Ly-6C (Gr-1), Clone RB6-8C5, Cat.No.:108415) and incubated for 30min at 4°C followed by 2 washes in FACS buffer. Samples were resuspended in 500µL FACS buffer and analysed using the LSRII flow cytometer. Using a low flow rate $1x10^4$ events per sample were recorded. Viability in each sample was assessed using TOPRO3. Samples were run by the Flow Cytometry Core Facility or by myself. The gating strategy used to obtain the percentage of viable $CD11b^+/Gr1^+$ cells in bone marrow samples is shown below (Fig.63). Analysis was performed with kind assistance from Dr. Russell Hughes, University of Sheffield.

**Table 29 Sample preparation for flow cytometry**

| Tube | Ab | Cells detected |
|---|---|---|
| 1 | Unstained | All cell populations |
| 2 | CD11b (0.005µg/µL*)<br><br>TOPRO3 was added later on to assess viability | Expressed on all cells of the myeloid linage, including leukocytes (mostly neutrophils), NK cells, mononuclear phagocytes (*e.g.* macrophages), granulocytes [311] |
| 3 | Gr-1 (0.0003125µg/µL*)<br><br>TOPRO3 was added later on to assess viability | Composed of Ly-6C and Ly-6G<br>Enriched on granulocytes; useful to determine relative amounts of granulocytes and monocytes or macrophages [311]<br>Ly-6C expressed on 50% of bone marrow cells [312] including CD8+ T-cells, on neutrophils and monocytes in bone marrow [313]<br>Ly-6G in bone marrow primarily on granulocytes [313] |
| 4 | CD11b (0.005µg/µL) + Gr-1 (0.0003125µg/µL)<br><br>TOPRO3 was added later on to assess viability | Myeloid Derived Supressor Cells (MDSCs) [41]<br>• immunosuppressive effects by inhibiting NK-, B- and T-cells<br>• infiltrate into tumours where they promote angiogenesis by expressing high levels of MMP9<br>• MDSCs are composed of immature myeloid cells at their early stages of differentiation |
| 5 | Unstained + TOPRO3 | Allows differentiation between viable and dead cells |
| * Antibodies were carefully titrated to determine the optimal working concentration. Serial dilutions were performed around the working concentration recommended by the manufacturer (CD11b: 0.00125 µg/µL -0.01 µg/µL; Gr-1: 0.000015625 µg/µL- 0.000250µg/µL). Cell number, temperature and instrument settings were kept constant. | | |

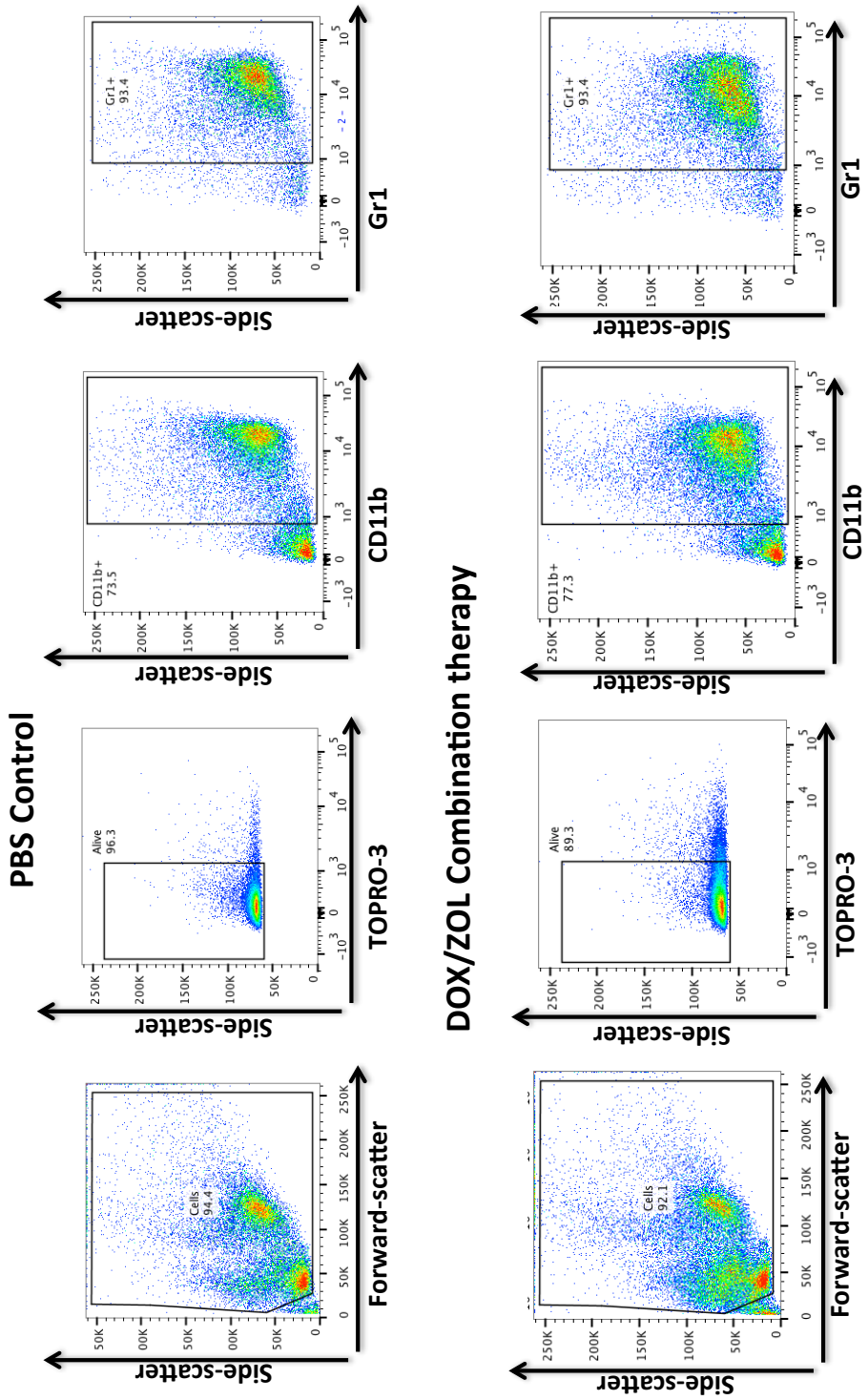


**Figure 63 Gating strategy to assess the presence of CD11b$^+$/Gr1$^+$ myeloid-derived suppressor cells in bone marrow samples.**

Presence of CD11b$^+$/Gr1$^+$ cells in bone marrow samples from mice receiving 5 rounds of combination therapy (DOX (2mg/kg) followed 24hrs later by ZOL (100µg/kg)) was compared to control mice. Forward-scatter side-scatter was used to gate on the total population of interest, followed by exclusion of dead cells based on positivity for TOPRO-3. Next a gate was drawn around CD11b+ve (Alexa Fluor488) and Gr1+ve (Pe-Cy7) cells.

### 5.5.5. Analysis of tumour samples by immunohistochemistry

For histological analysis subcutaneous tumour fragments were excised, fixed in ice cold 4%PFA (pH 7.4) for 48hrs followed by transferral into 70% ethanol and paraffin embedding. For immunohistochemistry 3µm thick sections were dewaxed in xylene, rehydrated through alcohols and stained as described below.

#### 5.5.5.1. Analysis of tumour samples by immunohistochemistry

Optimisation of the CD31 (1:200 – 1:400; DIA-310, Dianova) and CD34 (MCA1825GA, AbD Serotec; 1:200 to 1:400) antibody used in this chapter has kindly been performed by Maggie Glover (Histology Technician, University of Sheffield) and Jacob Skinner (placement student, Sheffield Hallam University). The Ki67 antibody (DAKO, Clone MIB-1) has been optimised and routinely applied to visualise proliferating tumour cells in our group at the concentration of 1:125 as published in [241].

#### 5.5.5.2. Immunohistochemistry to visualise CD31+ve vascular endothelial cells

To assess if anti-cancer therapy affects the presence of CD31+ve microvasculature of subcutaneous tumours, immunohistochemistry against the vascular endothelial cell marker CD31 was performed. CD31 (or platelet endothelial cell adhesion molecule-1, PECAM-1) is expressed on cell surfaces of platelets, neutrophils, embryonic and adult endothelial cells; and involved in cell-to-cell adhesion.

Following dewaxing (Xylene 2x 5min) and rehydration through alcohols (100% - 70%, 1min each) slides were incubated in 3% $H_2O_2$ in methanol for 30min at ambient temperature. Next slides were washed in running tap water for 5min and heat-induced antigen retrieval performed using the Dako Target Retrieval Solution (S1699) in a pressure cooker (2hrs). Non-specific staining was blocked using Avidin/Biotin blocking solution (Vector Laboratories) followed by incubation in 10% goat serum/1% casein for 30min at ambient temperature. The primary antibody (1:200, CD31, DIA-310, Dianova) was incubated in 2% goat serum over night at 4°C. After 3 washes in PBS+0.1% Tween the secondary antibody (1:200, 1hr RT, BA-9401, Vector) was applied for 1hr followed by washing in PBS+0.1% Tween with 30min incubation in ABC solution, DAB-reagent and mounting. Appropriate negative controls were included (omitting the primary antibody). Vascular staining was kindly assisted by Jacob Skinner (placement student, Sheffield Hallam University).

#### 5.5.5.3. Immunohistochemistry for CD34+ve vascular endothelial cells

CD34 is expressed on haematopoietic stem and progenitor cells and vascular endothelial progenitors. In addition CD34 has recently been associated with endothelial tip cells, that guide the sprouting capillary through the ECM to an angiogenic stimulus [314] and it is commonly used to indicate the presence of immature vessels.

Briefly, following dewaxing (Xylene 2x 5min) and rehydration through alcohols (100% - 70%, 1min each) slides were incubation in 3% $H_2O_2$ in methanol for 30min at ambient temperature followed by antigen retrieval in 0.01M citrate buffer (1.92g Citric Acid (GPR™ 27780) + 0.5mL Tween® 20 + 1000mL $dH_2O$, adjusted to pH 6 with 1M NaOH, microwaved on high for 4min) for 20min. Slides were washed in PBS+0.1% Tween, non-specific binding of the antigen was blocked using the Avidin/Biotin blocking kit (Vector Laboratories) followed by 30min incubation in 10% normal goat serum/1%casein. Primary antibody (CD34, MCA1825GA, AbD Serotec, 1:400 in PBS) was incubated at 4˚C over night. On the following day samples were washed in PBS-Tween, and the secondary antibody was applied for 1hr at ambient temperature (BA-9401 Biotinylated Goat-anti-Rat IgG, 1:200). This was followed by incubation using the ABC-kit, staining visualised using DAB, washing and mounting of the slides. Appropriate negative controls were included (omitting the primary antibody).

#### 5.5.5.4. Quantification of microvessel density of tumour samples

To determine if the anti-cancer treatment modifies microvessel density of subcutaneous MDA-G8 tumours, a Chalkley grid was used. Briefly, the Chalkley grid contains 25 dots within 4 quarters; each vessel that hits a dot is regarded as a Chalkley score. Where tumour size allowed, Chalkley scores of 5 randomly chosen fields of view (10x objective, Leica DMI1000) were recorded. Necrotic cores and apoptotic areas were avoided for analysis. 3 individual levels (20µm apart) for each tumour sample were assessed and the average score for all fields of view per sample determined. The average scores per sample were then divided by 0.79$cm^2$ (the area of the Chalkley graticule). The data are represented as Micro Vessel Density (MVD, being the average Chalkley score/$cm^2$).

#### 5.5.5.5. Immunohistochemistry for Ki-67+ve tumour cells

Immunohistochemistry for the cellular proliferation marker Ki-67 was used to visualise treatment effects on tumour cell proliferation. Following dewaxing (Xylene 2x 5min) and rehydration through alcohols (100% - 70%, 1min each) slides were incubated in 3% $H_2O_2$ in methanol for 10min at ambient temperature. Next slides were washed in PBS+0.1%

Tween, followed by antigen-retrieval in citrate buffer (microwave using 5min high and 5 min low power). After additional washing, samples were incubated in 1X Casein/PBS+0.1% Tween for 30min at ambient temperature followed by addition of human Ki-67 specific primary antibody (1:125, DAKO, Clone MIB-1, prepared in 1X Casein/PBS+0.1% Tween) over night at 4°C. On the following day the secondary antibody (anti-mouse biotin, Vector BA-2000, 1:200 diluted in 1X Casein/PBS+0.1% Tween) was applied for 30min at ambient temperature, followed by incubation in ABC-kit, visualisation of staining using DAB, washing and mounting of the slides. Appropriate negative controls were included (emitting the primary antibody).

#### 5.5.5.6. Quantification of Ki-67+ve tumour cells

To determine if the anti-cancer treatment modifies proliferation of subcutaneous MDA-G8 tumours the number of Ki-67+ve tumour cells/$mm^2$ tumour tissue was scored on 3 non-serial histological sections per sample. Where sample size allowed, Ki-67+ tumour cells in 5 randomly selected fields of view per section were counted using a 20x objective, OsteoMeasure software and a BX53 Olympus microscope.

### 5.5.6. Analysis of bone samples

Bone samples were embedded in paraffin or gelatine as described in Methods section (see Chapter 2, section 2.2.10.3).

#### 5.5.6.1. µCT analysis

To assess treatment-induced alterations in bone volume and structure left tibiae were collected in 4% PFA, scanned using the Skyscan 1272 as previously described in Chapter 2, section 2.2.10.4. Scans were reconstructed using Nrecon software and trabecular as well as total bone volume determined using CTan software, a lower threshold of 95 and an upper threshold of 255 were used.

#### 5.5.6.2. Visualisation of treatment induced alteration to bone marrow vasculature

Immunofluorescence staining for the vascular endothelial cell marker Endomucin was performed as described in Methods Chapter 2, Section 2.2.10.6.2.2. Slides were imaged using the Nikon A1 confocal microscope, NIS-Elements software, 403nm and 562nm lasers and a 20x oil objective. Pixel size was set to 1024x1024 and Z-stacks with a 20µm depth were scanned and reconstructed using Fiji (Image>Stacks>3D projections). 3D projections were then converted to RGB images. For a subset of samples tile scans (6x6) were imaged using the Nikon Dual cam system with Nikon Eclipse inverted microscope, 20x objective.

Appropriate negative controls were included (emitting the primary antibody). Qualitative analysis (structural changes in the vascular organisation) was confirmed by Prof. Nicola Brown, University of Sheffield, UK.

## 5.6. Results

### 5.6.1. Establishing optimal study conditions – a pilot experiment

To establish an *in vivo* model to study the effects of the BME on peripheral breast cancer (re-) growth, 6-8-week old female BALB/c nude mice were subcutaneously injected with $5x10^5$ MDA-G8 cells on day 0. Palpable tumours developed in 87% (13 out of 15) of mice 4 days post subcutaneous injection of MDA-G8 cells. For a subset of mice (n=3) administration of combination therapy was initiated 13 days post injection of MDA-G8 cells, when tumours had reached an average size of $92mm^3$. For the remaining mice, treatment was started 17 days after injection at an average tumour size of $44mm^3$ in the combination therapy group and $27mm^3$ in the control group.

#### 5.6.1.1. Response to combination therapy – pilot study data

Starting the administration of combination therapy at an average tumour size of $92mm^3$ did not reduce the growth rate of subcutaneous MDA-G8 cells, with either 3 or 4 rounds of combination therapy. The tumours were growing faster in these three mice and tumour volume was increased 32 days post injection when compared to control mice (Day 32: PBS: $119.9 \pm 35.59mm^3$, n=4 vs. ZOL: $385.9 \pm 94.04\ mm^3$, n=3, p=0.0571, Fig.64A-D).

In this pilot experiment the anticipated 5-week course of combination therapy could only be administered to 3 out of 9 mice whereas the others had to be culled prior to the experimental endpoint as a consequence of severe skin blistering, scabbing and/or ulceration in the tumour area – Table 30.

**Table 30 Rounds of combination therapy administered to mice included in this study.**

| Number of mice | Rounds of combination therapy (2mg/kg DOX followed 24hrs later by 100µg/kg ZOL) |
|---|---|
| 4 | 3 |
| 2 | 4 |
| 3 | 5 |

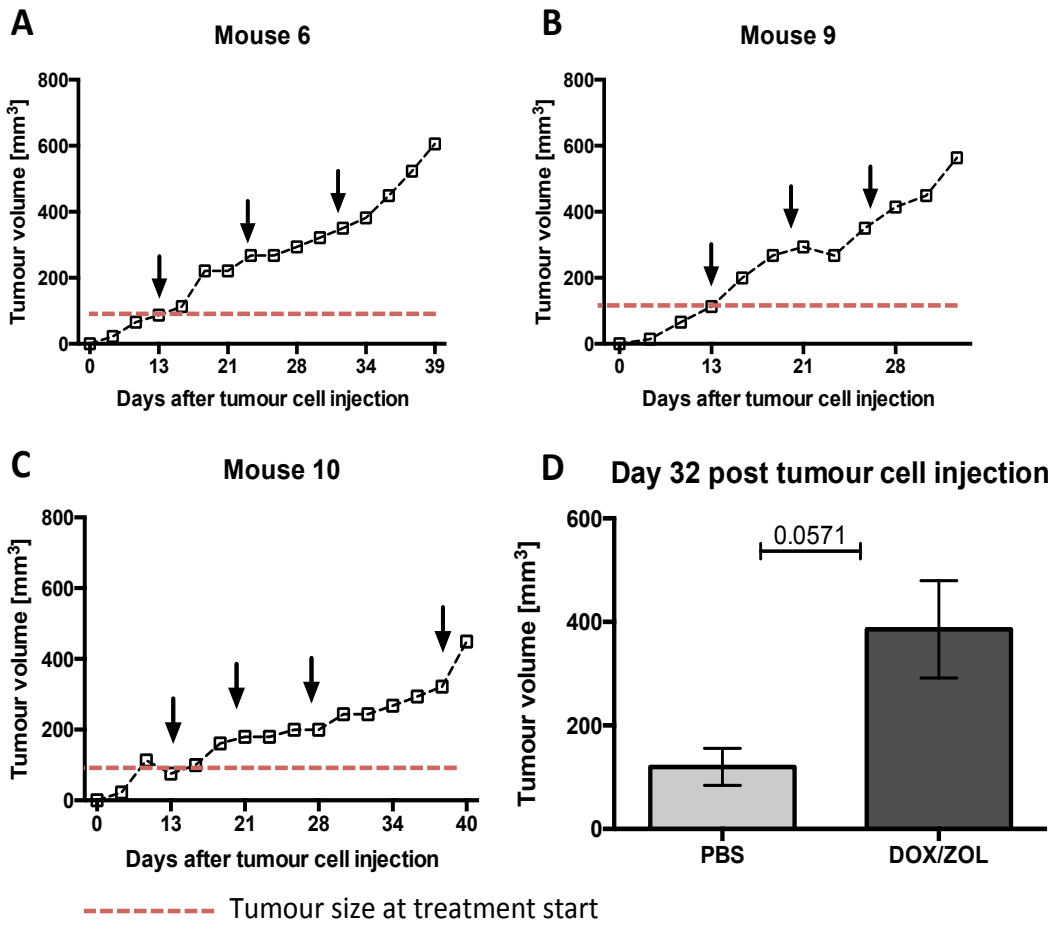


**Figure 64 Response to combination therapy when treatment was started at an average tumour volume of 92mm$^3$.**

5x10$^5$ MDA-G8 breast cancer cells were subcutaneously injected into the right flank of 6-8-week old female BALB/c nude mice. Administration of combination therapy (Doxorubicn (DOX) 2mg/kg followed 24hrs later by Zoledronic acid (ZOL) 100µg/kg) was started 13 days post tumour cell injection when tumours had reached an average size of 92mm$^3$. Combination therapy was administered once weekly. (A-C) Individual growth curves of subcutaneously implanted MDA-G8 cells. Black arrowheads indicate treatment administration. Dashed red line indicates tumour volume at treatment start. (D) Comparison of tumour volume at Day 32 (PBS: n=4, DOX/ZOL: n=3), Mann-Whitney test, Data show Mean±SEM.

The three remaining mice had an average tumour volume of 27mm$^3$ when combination therapy was initiated. In these mice combination therapy inhibited growth of MDA-G8 cells in 2 mice and reduced the growth rate in the third one (Fig.65). Five rounds of weekly combination therapy therefore significantly reduced subcutaneous growth of MDA-G8 cells when compared to control (Day 46: $p \leq 0.01$, 2way ANOVA, Fig.65A) resulting in decreased tumour volume at experimental endpoint (Day 46: PBS: 328.7 ± 88.28mm$^3$ vs. DOX/ZOL: 90.89 ± 66.15mm$^3$, n=3/group, Fig.65A).

These findings suggest that 5 rounds of combination therapy slow down the rate of subcutaneous breast cancer growth in this model. However, administration of combination therapy has to be started at the early stages of tumour formation to be effective, before the tumour volume reaches approximately 30mm$^3$. At this size there might have been sufficient recruitment of growth-promoting stromal cell precursors resulting in the tumours growing independent of the BME.

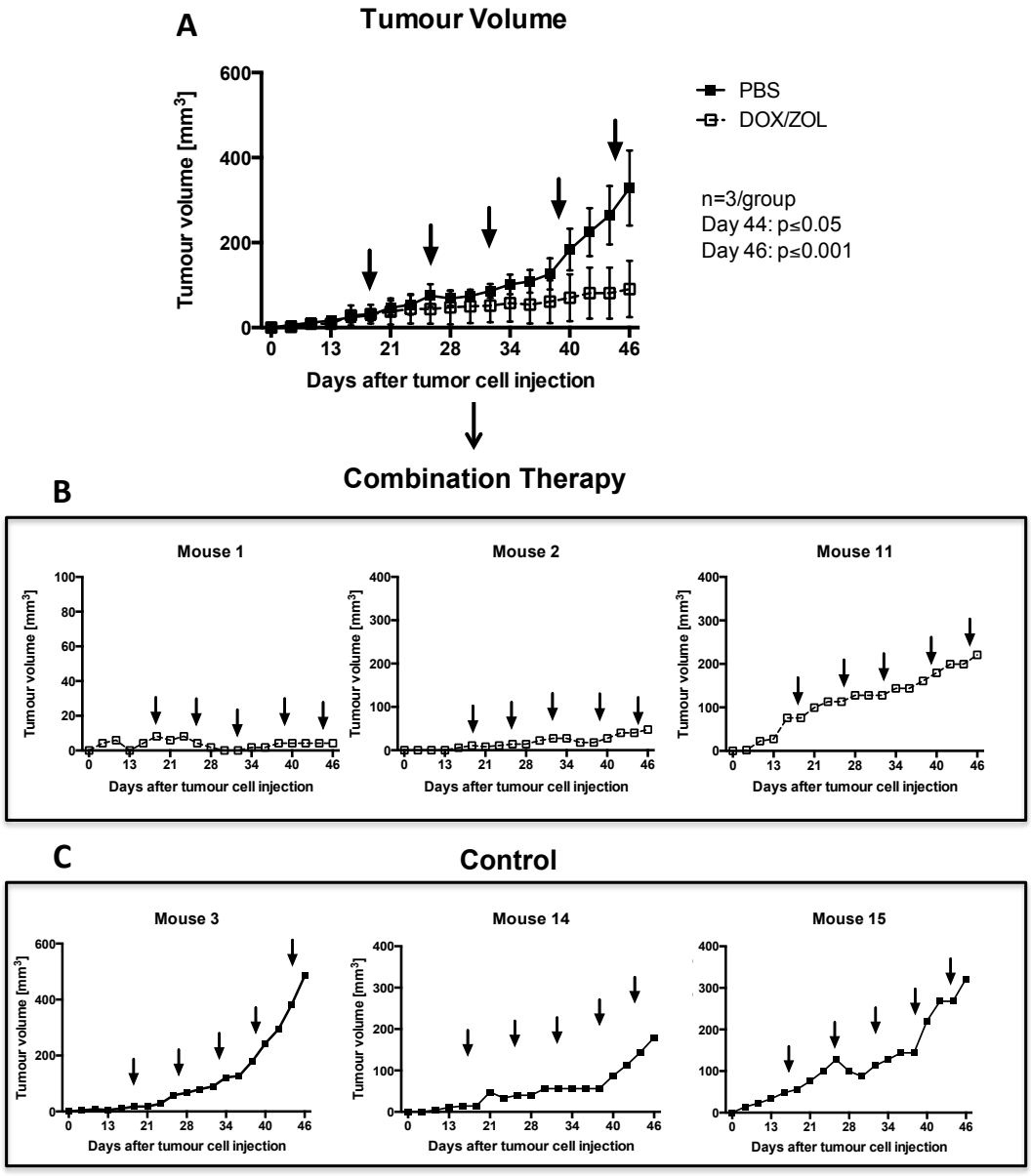


**Figure 65 Effects of combination therapy on subcutaneous growth of breast cancer – pilot data.** $5x10^5$ MDA-G8 breast cancer cells were subcutaneously injected into the right flank of 6-8-week old female BALB/c nude mice. Administration of combination therapy (Doxorubicn (DOX) 2mg/kg followed 24hrs later by Zoledronic acid (ZOL) 100µg/kg) was started 17 days post tumour cell injection. Combination therapy was administered once weekly. Control mice (n=3) received PBS control. (A) Comparison of tumour growth over time between the two treatment groups. Black arrowheads indicate treatment days. Two-way ANOVA with Bonferroni's post-test, Data show Mean±SEM. Individual growth curves of subcutaneously implanted MDA-G8 cells in mice receiving combination therapy (B) or PBS control (C).

#### 5.6.1.2. Transplantation of tumour fragments into hosts with a modified BME – pilot study

The role of the BME in mediating peripheral (primary) breast cancer remains poorly investigated. To assess if therapeutic modification of the BME affects peripheral tumour growth, isolated tumour fragments (average size of 22mm$^3$) from mice having received 5 rounds of combination therapy were subcutaneously transplanted into recipients that had either been pre-treated with ZOL (100µg/kg, 1x weekly for 2 weeks, n=3) or PBS control (n=3).

At experimental endpoint (Day 27) the mean tumour volume reached 232.3 ± 35.67mm$^3$ in the PBS pre-treated and 154.3 ± 71.68mm$^3$ in the ZOL pre-treatment group (Fig. 66A-C). Two of the tumour fragments that were subcutaneously transplanted into ZOL pre-treated recipients (Day 27: 113.04mm$^3$ and 56.09mm$^3$ respectively) demonstrated a slower growth rate whereas the third fragment demonstrated exponential growth from 22 days post transplantation onwards (Fig.66C). In contrast, after an initial lag-phase all three tumour fragments transplanted into control mice grew exponentially at comparable rates (Fig.66B). These findings supported the hypothesis that the BME may influence peripheral breast cancer growth.

These data demonstrate that fragments from tumours responding to combination therapy are able to re-grow when transplanted into recipient mice; providing evidence that the study should be repeated with sufficient power to detect any differences in influence of BME ZOL pre-treatment on peripheral tumour growth.

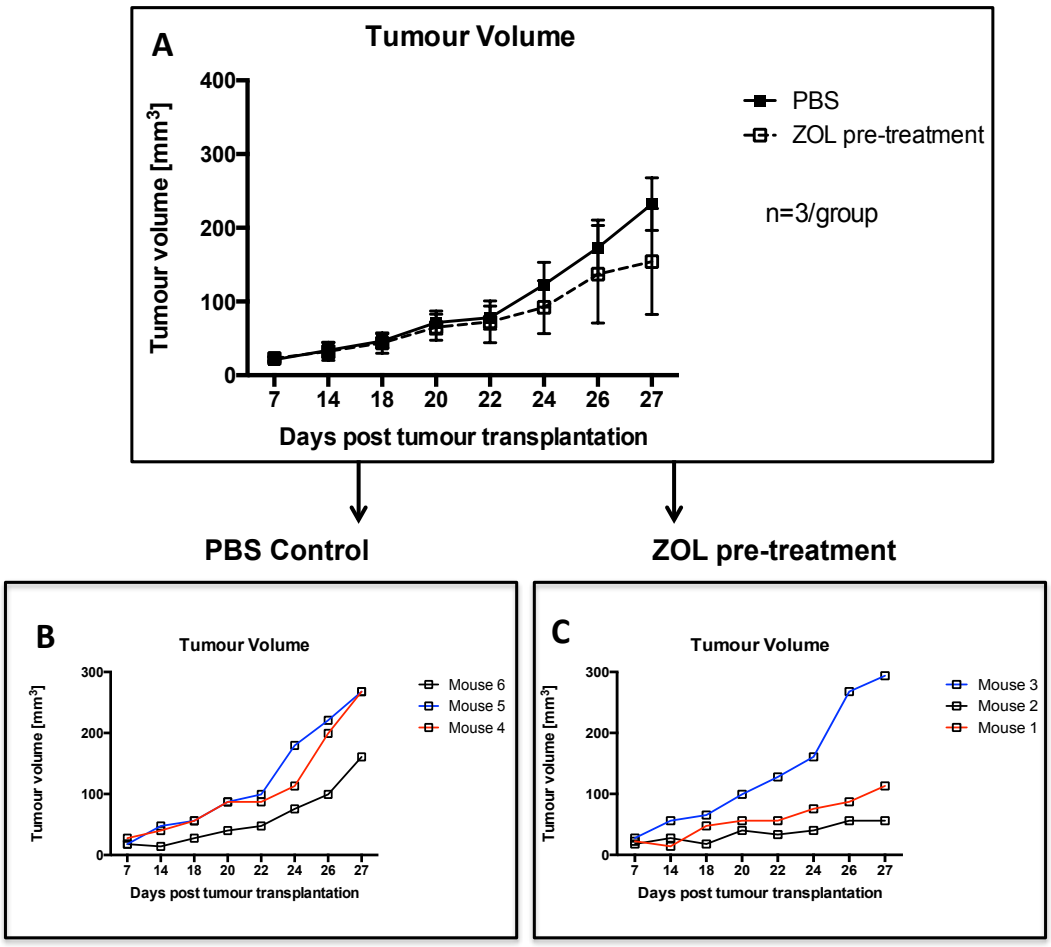


**Figure 66 Re-growth of subcutaneously transplanted tumour fragments after cessation of combination therapy.**

MDA-G8 breast tumour fragments (22mm$^3$) from mice receiving combination therapy (Doxorubicn (DOX) 2mg/kg followed 24hrs later by Zoledronic acid (ZOL) 100µg/kg) were subcutaneously transplanted into the right flank of 9-11-week old female BALB/c nude mice. Recipient mice had either received 2 pre-treatments with ZOL (100µg/kg, i.p., 1x weekly for 2 weeks) or PBS control. (A) shows tumour growth over time (n=3/group), individual growth curves are shown in (B) for PBS and (C) for ZOL pre-treated mice. Data show Mean±SEM.

### 5.6.2. Full study to assess the role of the BME in peripheral tumour growth

#### 5.6.2.1. Tumour volume and survival upon combination therapy

Briefly, 7-9-week old female BALB/c nude mice injected with $5x10^5$ MDA-G8 cells developed palpable tumours by day 4 (n=24, tumour take rate was 100%). 10 mice were randomly assigned to a PBS-receiving control group and the remaining 14 mice received combination therapy (2mg/kg DOX followed 24hrs later by 100µg/kg ZOL) once weekly for 5 weeks. As the previously performed pilot experiment showed that combination therapy needs to be administered at the early stages of tumour development, treatment was started 7 days after tumour cell injection once tumour growth was confirmed by a GFP signal (Light Tools). Average tumour volume at treatment start was ≤10$mm^3$.

To assess effects of weekly combination therapy on subcutaneous growth of MDA-G8 cells, tumour volume was monitored 2-3x weekly using calipers. Prior to the experimental endpoint (Day 35) 8 mice in the control group had to be culled due to the subcutaneous tumours reaching maximum size and/or ulceration. In contrast, only 3 mice receiving combination therapy were culled as a consequence of skin blistering/ulceration. Animals treated sequentially with DOX followed by ZOL therefore exhibited significant increases in survival due to reduced tumour size; only 8% of mice in the PBS group survived the entire experiment where as treatment with DOX+ZOL increased survival to 79% (Fig.67).

The last tumour measurements allowing statistical analysis were taken on Day 33 post tumour cell inoculation (PBS: n=5, DOX/ZOL: n=13). Weekly administration of combination therapy slowed down subcutaneous tumour growth (Day 33: $p<0.0001$, Fig.68A), with a significantly reduced tumour volume when compared to control (Day 33: PBS: 330.9 ± 125.3$mm^3$ vs. DOX/ZOL: 82.86 ± 13.93$mm^3$, $p\leq0.05$, Fig.68B).

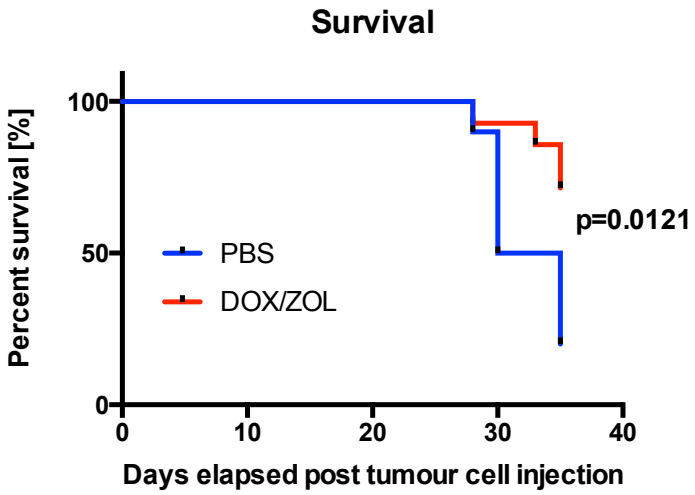


**Figure 67 Combination therapy increases survival.**
7-9-week old female BALB/c nude mice were subcutaneously injected with $5x10^5$ MDA-G8 breast cancer cells. Prior to the experimental endpoint (Day 35) 8 mice in the control group had to be culled due to the subcutaneous tumours reaching maximum size and/or ulceration. In contrast, only 3 mice receiving combination therapy were culled in the treatment group. Log-rank (Mantel-Cox) test.

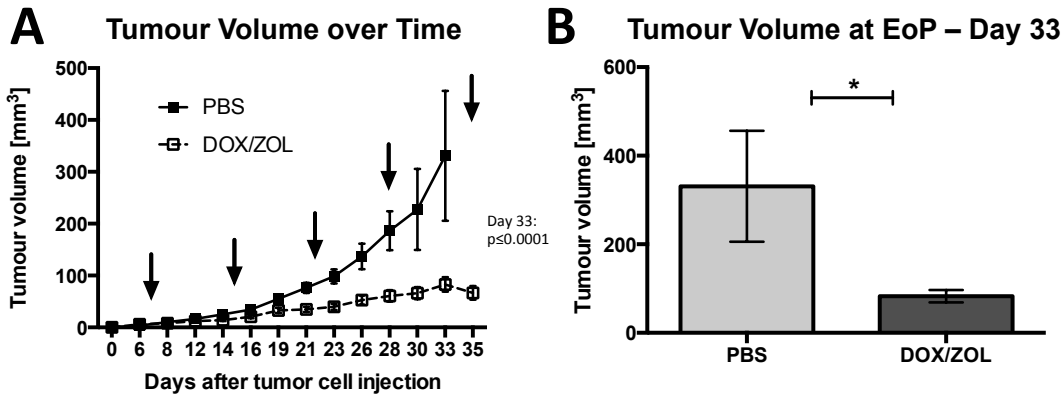


**Figure 68 Effects of combination therapy on subcutaneous growth of MDA-G8 tumours.**
$5x10^5$ MDA-G8 cells were subcutaneously injected into the right flank of 7-9-week old female BALB/c nude mice. Mice received combination therapy (Doxorubicn (DOX) 2mg/kg followed 24hrs later by Zoledronic acid (ZOL) 100µg/kg) or PBS control 1x weekly for 5 weeks (indicated with black arrow heads). Tumour growth was monitored 2-3x weekly using calipers. Data show Mean±SEM. (A) tumour growth over time, 2-way ANOVA with Bonferroni's post test (B) Mann-Whitney test, * is ≤0.05. Day 33: n=5 for PBS and n=13 for DOX/ZOL. EoP = end of protocol.

### 5.6.2.2. Effects of combination therapy on proliferation and vascularisation of subcutaneous tumours

To assess if combination therapy alters proliferation of subcutaneous tumours, staining against the cellular proliferation marker Ki-67 was performed on a subset of tumour samples. Ki-67 positive cells in 5 randomly selected fields of view were quantified on 3 non-serial levels per sample. This analysis showed a significant reduction in Ki-67+ve cells after 5 rounds of combination therapy when compared to control (PBS: 951.7±111.6/mm$^2$ vs. DOX/ZOL: 607.7±44.95, p≤0.05, Fig.69A), suggesting reduced tumour cell proliferation upon DOX/ZOL treatment – representative Ki-67 stained histological sections are shown below (Fig.69B).

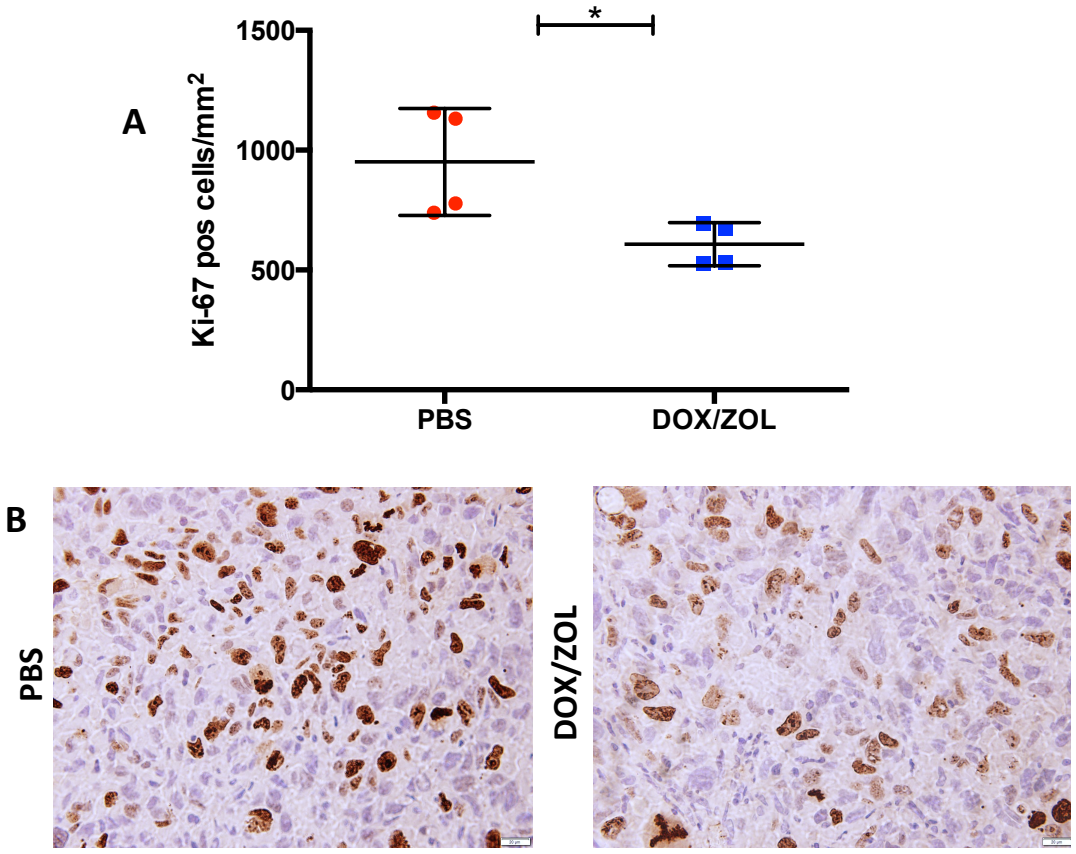


**Figure 69 Effects of combination therapy on proliferation of MDA-G8 tumour cells (Ki-67+ve).** Differences in proliferation of subcutaneous MDA-G8 tumours from mice receiving PBS control or 5 rounds of combination therapy (2mg/kg Doxorubicin (DOX, i.v.) followed 24hrs later by 100µg/kg Zoledronic acid (ZOL, i.p.)) was determined by scoring the presence of Ki-67+ve cells on three non-serial levels per sample. (A) shows data with 3 levels pre sample averaged, (B) representative sections, Ki-67+ve cells in brown. n=4/group. Data show Median±Range. Mann-Whitney test. 40x objective, scale bar is 20µm, * is p<0.05.

Effects of combination therapy on CD34 and CD31 positive vasculature within the subcutaneous tumours of DOX/ZOL treated mice was quantified by using a Chalkley grid method and compared to respective controls.

Microvascular density (here represented as Average Chalkley score/$cm^2$) of CD34+ve tumour vasculature was significantly reduced after combination therapy when compared to control (PBS: 2.58 ± 0.25$cm^2$ vs. ZOL: 1.43 ± 0.14$cm^2$, $p \leq 0.05$, Fig. 70A&B, representative histological slides shown in 70C&D). Similar effects were determined when analysing sections stained for CD31+ve tumour vasculature, however this trend ($p=0.0571$) did not reach statistical significance (PBS: 3.85 ± 0.35/$cm^2$ vs. DOX/ZOL: 2.64 ± 0.07/$cm^2$, Fig. 71A&B, representative histological slides shown in Fig.71C&D).

Collectively these data suggest that vascular density in tumours treated with DOX/ZOL combination therapy is reduced when compared to tumours of control mice.

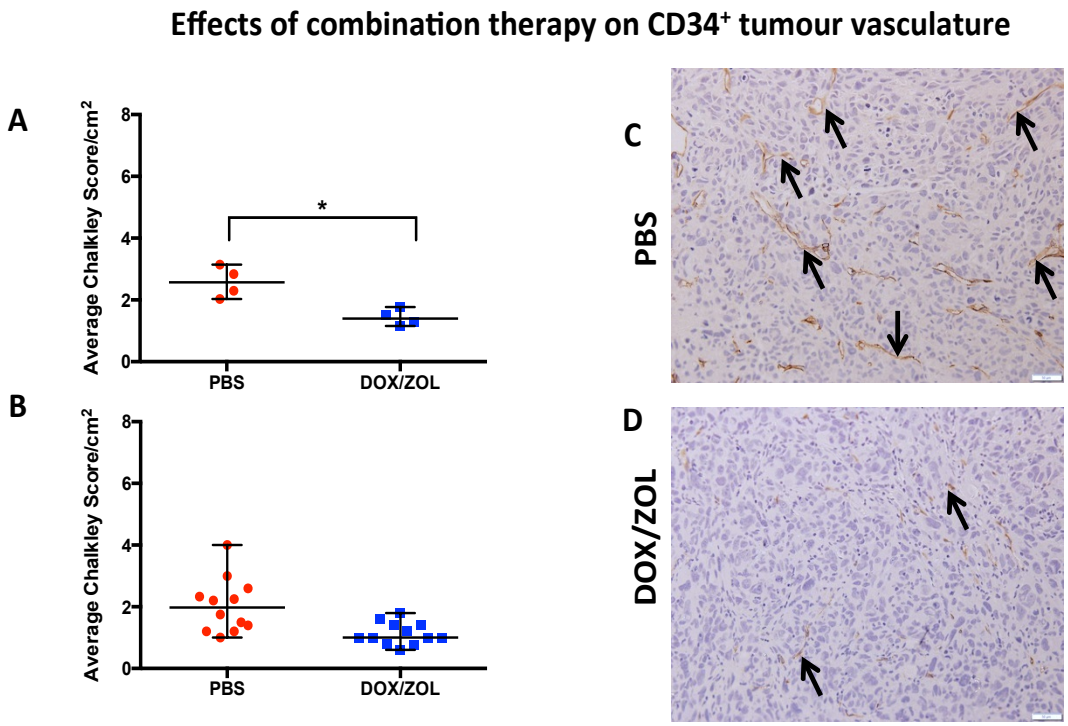


**Figure 70 Effects of combination therapy on CD34 positive vasculature of subcutaneous MDA-G8 breast tumours.**

Microvessel density (MVD, here represented as Average Chalkley Score/cm$^2$) of subcutaneous MDA-G8 tumours from mice receiving (C) PBS control or (D) 5 rounds of combination therapy (2mg/kg Doxorubicin (DOX, i.v.) followed 24hrs later by 100µg/kg Zoledronic acid (ZOL, i.p.) was determined using a Chalkley grid. Three non-serial levels were assessed per sample. (A) shows data with 3 levels averaged, (B) shows individual scoring data (no statistical analysis performed). n=4/group. Data show Median±Range. Mann-Whitney test, * is $p<0.05$. CD34+ve vasculature shown in brown, representative vasculature pointed out by black arrowheads, 20x objective, scale bar is 50µm. Olympus BX53, cellSense software.

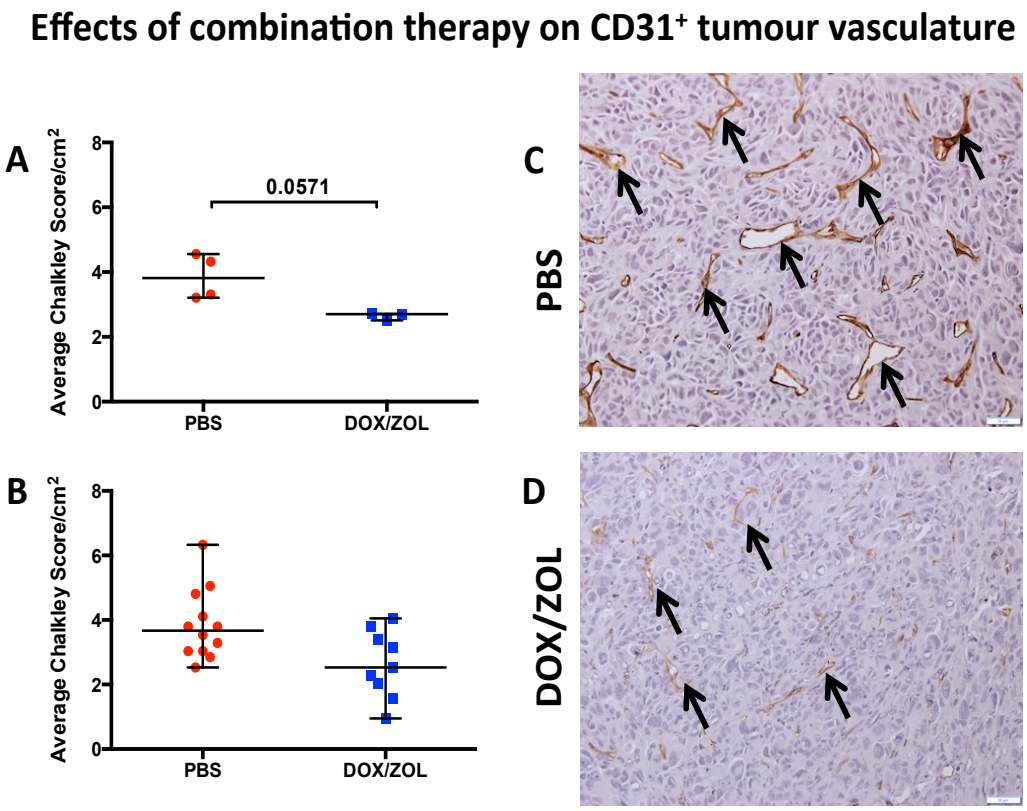


**Figure 71 Effects of combination therapy on CD31 positive vasculature of subcutaneous MDA-G8 tumours.**

Microvessel density (MVD, here represented as Average Chalkley Score/cm$^2$) of subcutaneous MDA-G8 breast tumours from mice receiving (C) PBS control or (D) 5 rounds of combination therapy (2mg/kg Doxorubicin (DOX, i.v.) followed 24hrs later by 100µg/kg Zoledronic acid (ZOL, i.p.) was determined using a Chalkley grid. Three non-serial levels were assessed per sample. (A) shows data of 3 non-serial levels averaged, (B) shows individual scoring data (no statistical analysis performed). n=4 for PBS and n=3 DOX/ZOL. Data show Median±Range. Mann-Whitney test. CD31+ve vasculature shown in brown, representative vasculature indicated with black arrowhead, 20x objective, scale bar is 50µm. Olympus BX53, cellSense software.

#### 5.6.2.3. Effects of combination therapy on bone and the BME

##### 5.6.2.3.1. Effects of combination therapy on bone volume and structure

Excised tibiae of 3 mice per group were randomly selected and effects of combination therapy on trabecular bone volume assessed using µCT analysis. The anti-resorptive capacity of ZOL is well established and the dose used in this experiment (100µg/kg) has shown to reduce osteoclast activity and number, as well as increased bone volume [154, 158, 241]. In agreement with this 5 administrations of combination therapy increased trabecular bone volume (PBS: 10.25 ± 0.36% vs. DOX/ZOL: 15.53 ± 0.91, p≤0.01, Fig.72A,D) and trabecular number (PBS: 2.40 ± 0.12$mm^{-1}$ vs. DOX/ZOL: 3.55 ± 0.12 $mm^{-1}$, p≤0.01 Fig.72B,D) when compared to control. Similarly, total bone volume (covering a height of interest of 3.0mm from the top bit of the tibia) was increased after 5 rounds of combination therapy (PBS: 3.22 ± 0.06$mm^3$ vs. DOX/ZOL: 4.27 ± 0.15$mm^3$, p≤0.01, Fig. 72E&F). There was no effect of DOX/ZOL on trabecular thickness (PBS: 0.04 ± 0.001mm vs. DOX/ZOL: 0.04 ± 0.001$mm^3$, Fig.72C).

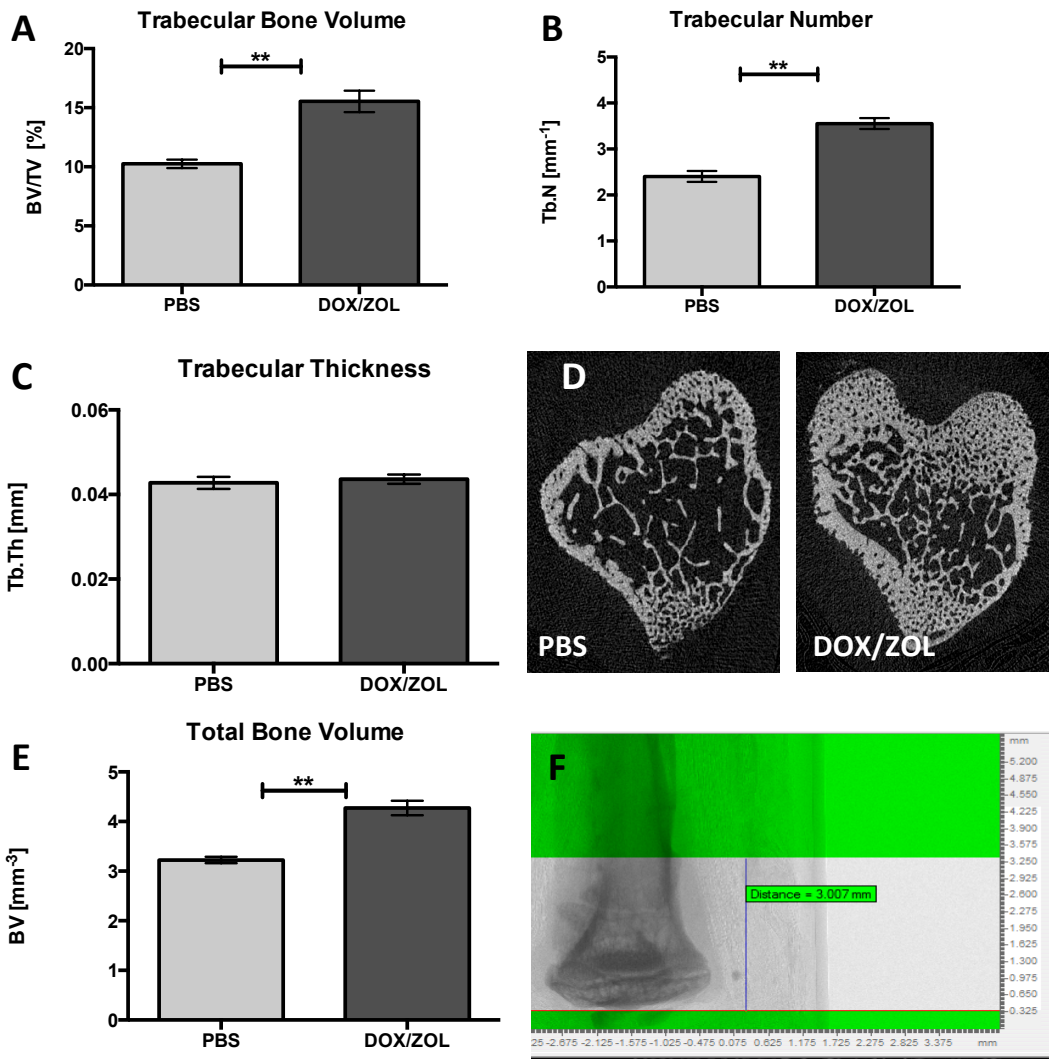


**Figure 72 Effects of combination therapy on bone volume of tibiae.**
7-9-week old female BALB/c nude mice received combination therapy (Doxorubicn (DOX) 2mg/kg followed 24hrs later by Zoledronic acid (ZOL) 100µg/kg) or PBS control 1x weekly for 5 weeks. Effects on (A) trabecular bone volume (in%), (B) trabecular number (in $mm^{-1}$) and (C) trabecular thickness (in mm) were assessed using µCT analysis. (D) Representative cross sections of tibiae. (E) Bone volume of the whole tibia (3mm in length) was determined (in $mm^3$), representative X-ray images shown in (F) (n=3/group), Data show Mean±SEM, Student's t-test, ** is $p<0.01$.

#### 5.6.2.3.2. Effects of combination therapy on the bone marrow vasculature

In addition to modifying subcutaneous breast cancer growth, sequential treatment with DOX and ZOL has also shown to reduce growth of MDA-MB-436 cells in bone [247], but

the precise mechanisms by which this occurs remain to be established. To assess if treatment induces alterations in the bone marrow vasculature in the metaphysis, an area preferentially colonised by breast cancer cells [90], immunofluorescence staining against the vascular endothelial cell marker Endomucin was performed on 30µm thick sections of tibiae. Scanning Z-stacks with a 20µm depth allowed visualisation of the three-dimensional bone marrow vasculature in the metaphysis, and tile scans (6x6) allowed qualitative assessment of the total bone marrow vasculature after combination therapy.

The microvasculature extending from the edge of the epiphysis appeared highly branched and interconnected in the PBS treated mice (Fig.73). In contrast, in DOX/ZOL treated mice the vasculature extending from the epiphysis into the metaphysis appeared tubular and column like with limited presence of connection loops or arches. Whether this is a result of the altered bone structure in this area (increased trabecular number) or direct therapeutic effects on endothelial cells remains to be established. Tile scans did not reveal any overt alterations in structural organisation or density of total bone marrow vasculature (qualitative data only, Fig.73A-H).

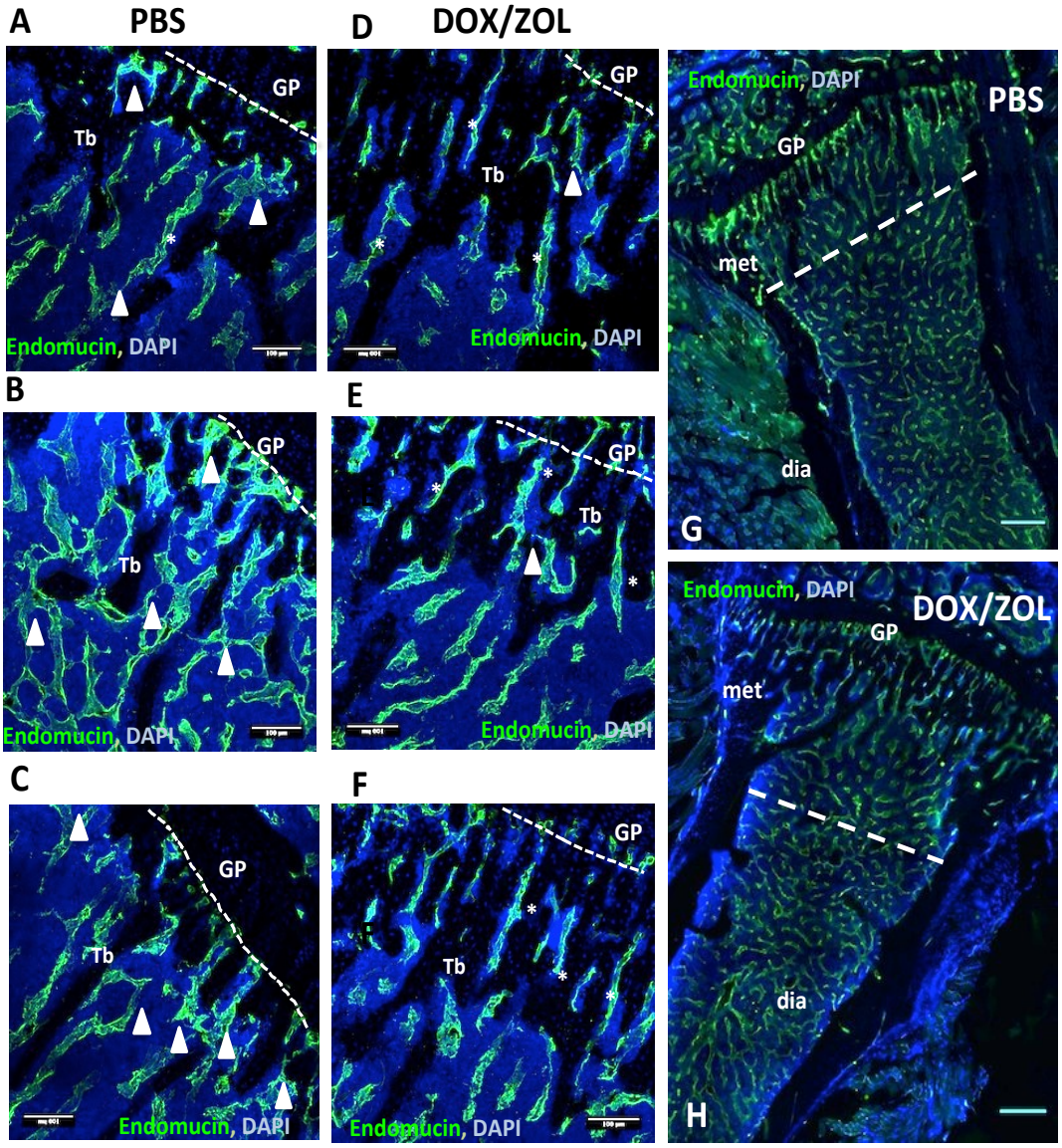


**Figure 73 Effects of combination therapy to the bone marrow vasculature.**

7-9-week old female BALB/c nude mice bearing subcutaneous MDA-G8 tumours received combination therapy (Doxorubicn (DOX) 2mg/kg followed 24hrs later by Zoledronic acid (ZOL) 100µg/kg) or PBS control 1x weekly for 5 weeks. Effects on bone marrow vasculature were visualised using immunofluorescence against the vascular endothelial cell marker Endomucin (Endomucin positive cells shown in green, nuclei shown in blue (DAPI)). (A-C) shows representative 3D projections of 30µm thick gelatine embedded sections of tibiae from PBS treated mice and (D-F) for combination therapy treated mice. Images were acquired using the Nikon A1 confocal microscope, 20x oil objective. Z stacks of 20µm depth were scanned and 3D projections merged into one RGB image. White triangles = branched vessels, white asterisk = columnar vasculature, dashed line = growth plate boarder, GP = growth plate. Scale bar is 100µm. Representative tile scans (6x6) showing vasculature within the whole bone after (G) PBS and (H) DOX/ZOL. Images acquired using the Nikon Eclipse Dual Cam system, 20x objective, Scale bar is 250µm. For (G&H): GP=growth plate, met = metaphysis, dia = diaphysis, transition form met to dia indicated by dashed line.

#### 5.6.2.3.3. Effects of combination therapy on MDSCs cells

$CD11b^+/Gr1^+$ MDSCs are known to be overproduced in both spleen and bone marrow of tumour bearing mice and patients [170], and are associated with tumour progression. To determine if DOX/ZOL combination therapy reduces subcutaneous tumour growth via reducing the levels of $CD11b^+/Gr1^+$ cells in bone marrow and/or impairing their recruitment to the site of tumour growth, the presence of $CD11b^+/Gr1^+$ cells in murine bone marrow flushes was quantified using flow cytometry.

There was a small but non-significant increase (apr. 6%) in the presence of viable CD11b+ve myeloid cells in the bone marrow of DOX/ZOL treated mice (PBS: 73.83±0.49%, vs, DOX/ZOL: 80.20 ± 2.950, Fig.74A). No difference in Gr-1+ve cells within the CD11b+ve population was determined (PBS: 94.13±0.50% vs. DOX/ZOL: 94.63±0.91%, Fig.74B). Similar to the percentage of CD11b+ve cells the percentage of viable $CD11b^+/Gr1^+$ dual positive cells showed a small but non-significant increase after DOX/ZOL treatment (69.53±0.83% vs. 75.97±3.52%, Fig.74C).

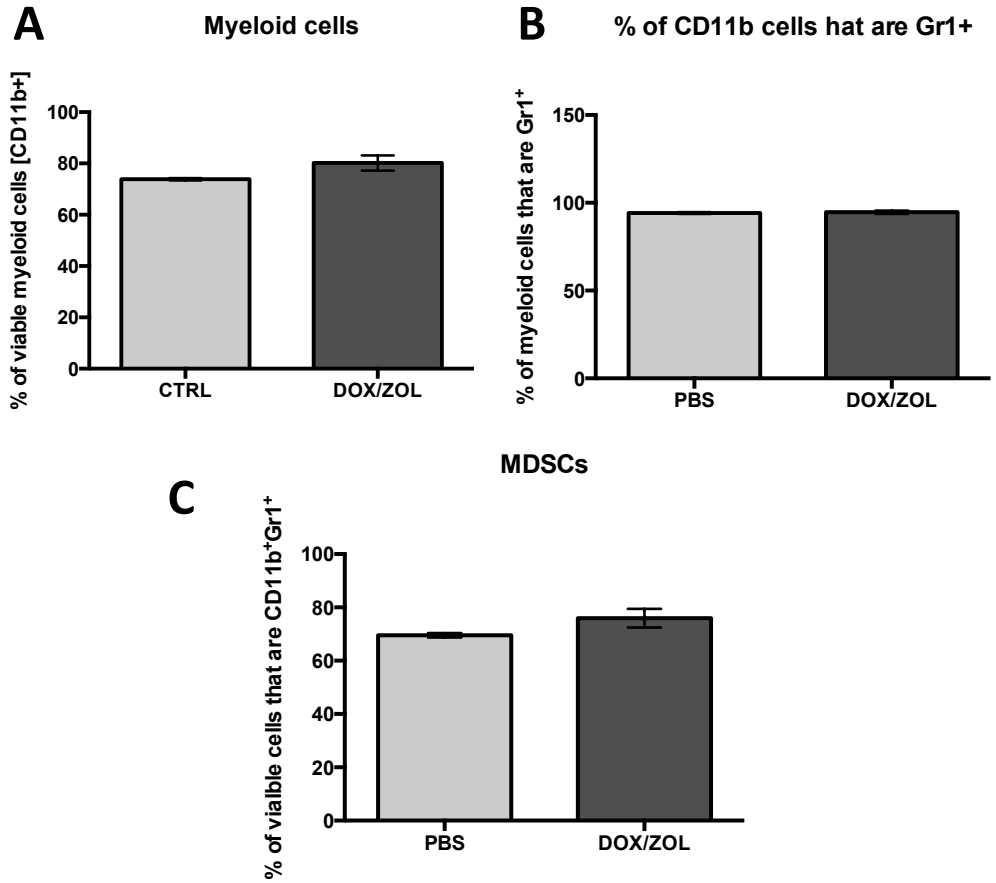


**Figure 74 Effects of combination therapy on MDSCs.**
7-9-week old female BALB/c nude mice bearing subcutaneous MDA-G8 tumours received combination therapy (Doxorubicn (DOX) 2mg/kg followed 24hrs later by Zoledronic acid (ZOL) 100µg/kg) or PBS control 1x weekly for 5 weeks. On day of sacrifice bone marrow was collected to analyse the presence of (A) CD11b+ve myeloid cells, (B) proportion of $CD11b^+$ myeloid cells that are positive for Gr1 and (C) MDSCs dual positive for CD11b/Gr1 by flow cytometry. Data show Mean±SEM, Student's t-test. n=3/group, 2 mice per sample pooled.

### 5.6.3. Does ZOL-induced modification of the BME affect growth of subcutaneously implanted tumour fragments from DOX/ZOL treated hosts?

#### 5.6.3.1. Confirmation of ZOL effects on bone

To confirm that ZOL administration actively induced alterations to the BME µCT analysis a subset of tibiae collected at the experimental endpoint was performed (PBS: n=6, ZOL: n=4). As expected, ZOL pre-treatment (100µg/kg, 1x weekly for 2 weeks) caused a significant increase in trabecular bone volume (ZOL: 37.04 ± 1.80% vs. PBS: 9.59 ± 0.40%, p≤0.0001, Fig.75A&C) and number (ZOL: 14.17 ± 0.93mm$^{-1}$ vs. PBS: 2.92 ± 0.14mm$^{-1}$, p≤0.0001, Fig.75B), thus providing a significantly altered BME.

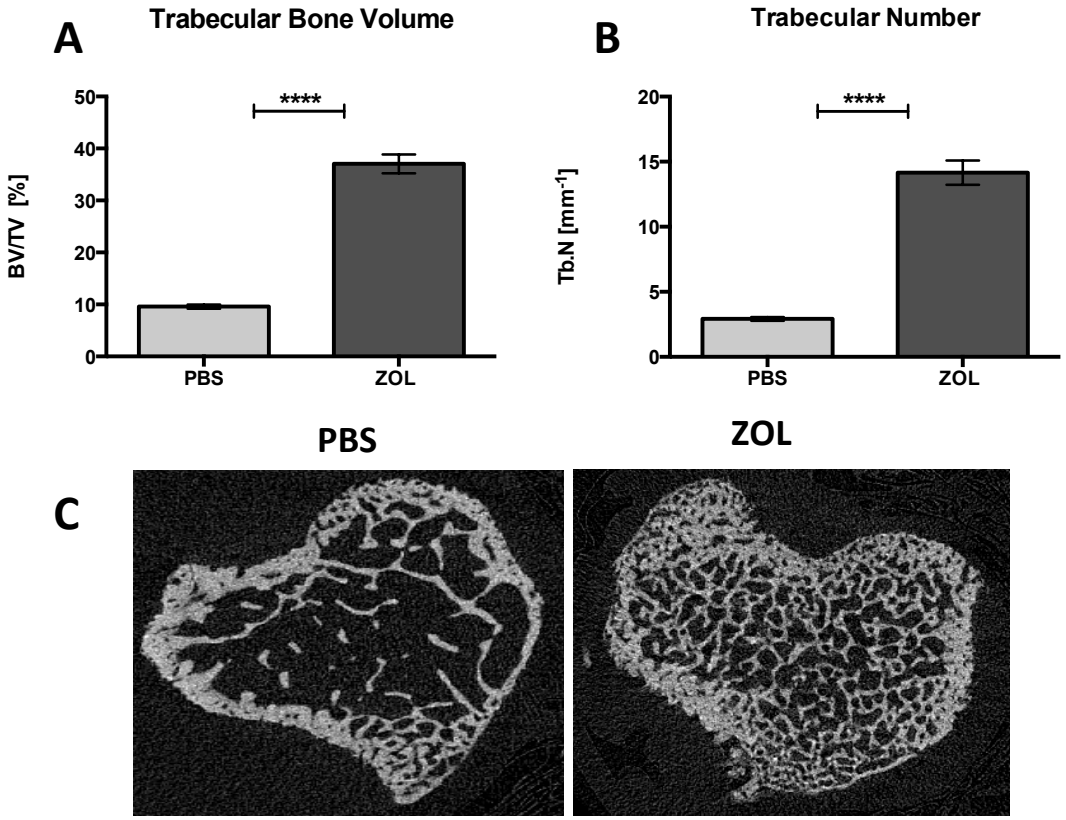


**Figure 75 Effects of ZOL pre-treatment on trabecular bone volume.**
6-8-week old female BALB/c nude mice received 1x weekly treatment with 100µg/kg Zoledronic acid (ZOL) or PBS control for 2 weeks, prior to tumour fragment transplantation. Bones were collected 33 days post tumour fragment transplantation. Effects on (A) trabecular bone volume (in%) and (B) trabecular number (in mm$^{-1}$) were assessed using µCT analysis. (C) Representative cross sections of tibiae. (n=6 for PBS, n=4 for ZOL), Student's t-test test, **** is p≤0.0001, Data show Mean±SEM.

#### 5.6.3.2. Re-growth of tumour transplants

As shown previously 5 weekly administrations of combination therapy significantly slowed down growth of subcutaneous MDA-G8 tumours when compared to control. Tumours from DOX/ZOL treated mice were isolated, subdivided into quarters (average of 14mm$^3$) and subcutaneously transplanted into recipient mice that were either pre-treated with 100µg/kg ZOL (1x weekly for 2 weeks) or PBS control (n=8/group). To assess if tumour growth resumes at equal rates, tumour size was monitored 2-3x weekly using calipers.

One mouse of the ZOL pre-treatment group was culled on Day 30, 3 days before the experimental endpoint due to skin blistering; 2 mice (n=1/group) were culled on day 32. No difference in tumour volume between the groups was determined at the experimental endpoint (PBS: 185.9 ± 51.05mm$^3$ vs. ZOL pre-treatment: 191.8 ± 36.99, PBS: n=6, ZOL: n=7 at day 33, Fig.76A&B). After the re-transplantation, tumour fragments started to re-grow in both recipients that were pre-treated with ZOL or PBS. Although re-growth of fragments transplanted into ZOL pre-treated hosts appeared to be slower in the initial stages, no difference in tumour size was determined at the experimental endpoint, potentially also due to the high variability within each experimental group (Fig.76C&D).

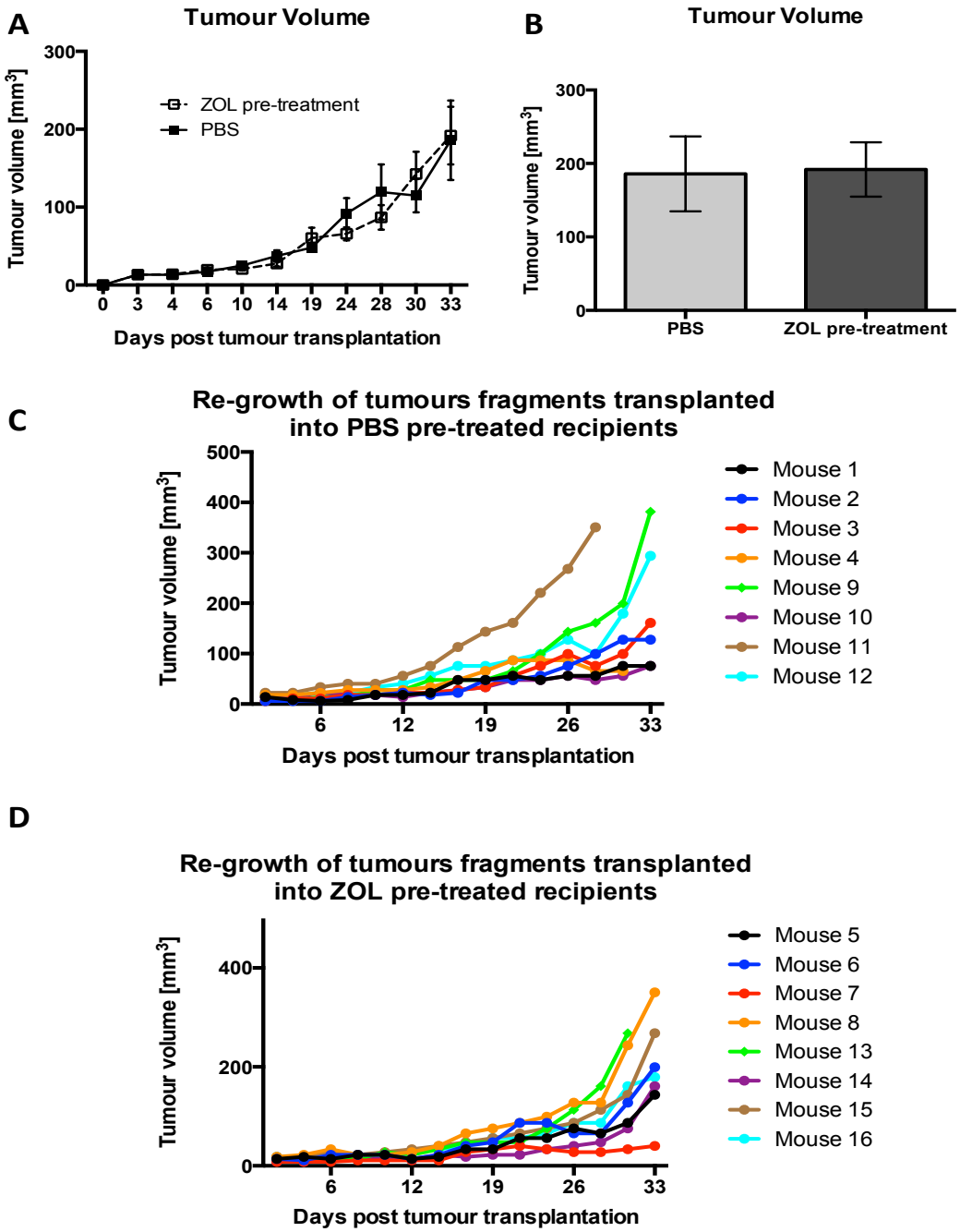


**Figure 76 Re-growth of subcutaneously transplanted MDA-G8 tumour fragments.**
Isolated MDA-G8 tumour fragments from female BALB/c nude mice treated with combination therapy (Doxorubicn (DOX) 2mg/kg followed 24hrs later by Zoledronic acid (ZOL) 100µg/kg) 1x weekly for 5 weeks were subcutaneously transplanted into 7-9-week old female BALB/c nude mice. Recipient mice had either received pre-treatment with 100µg/kg ZOL or PBS control. (A) tumour growth over time and (B) Tumour volume at experimental endpoint. Day 33: PBS: n=6, ZOL: n=7. Data show Mean±SEM. Individual growth rates for tumour fragments transplanted into PBS (C) and ZOL pre-treated (D) recipients.

### 5.6.3.3. Presence of CD34+ve and CD31+ve tumour vasculature

To determine whether pre-treating tumour recipients with ZOL affects vascularisation of transplanted tumour fragments, CD34+ve and CD31+ve tumour vasculature for a subset of mice was quantified using the Chalkley grid method. There was no significant difference in the number of CD31+ve (PBS: 4.50±0.18 vs. ZOL pre-treated: 3.88±0.24, Fig.77A&B) or $CD34^{+}$ (PBS: 2.66±0.36 vs. ZOL pre-treated: 2.23±0.26, Fig.77C&D) tumour blood vessels.

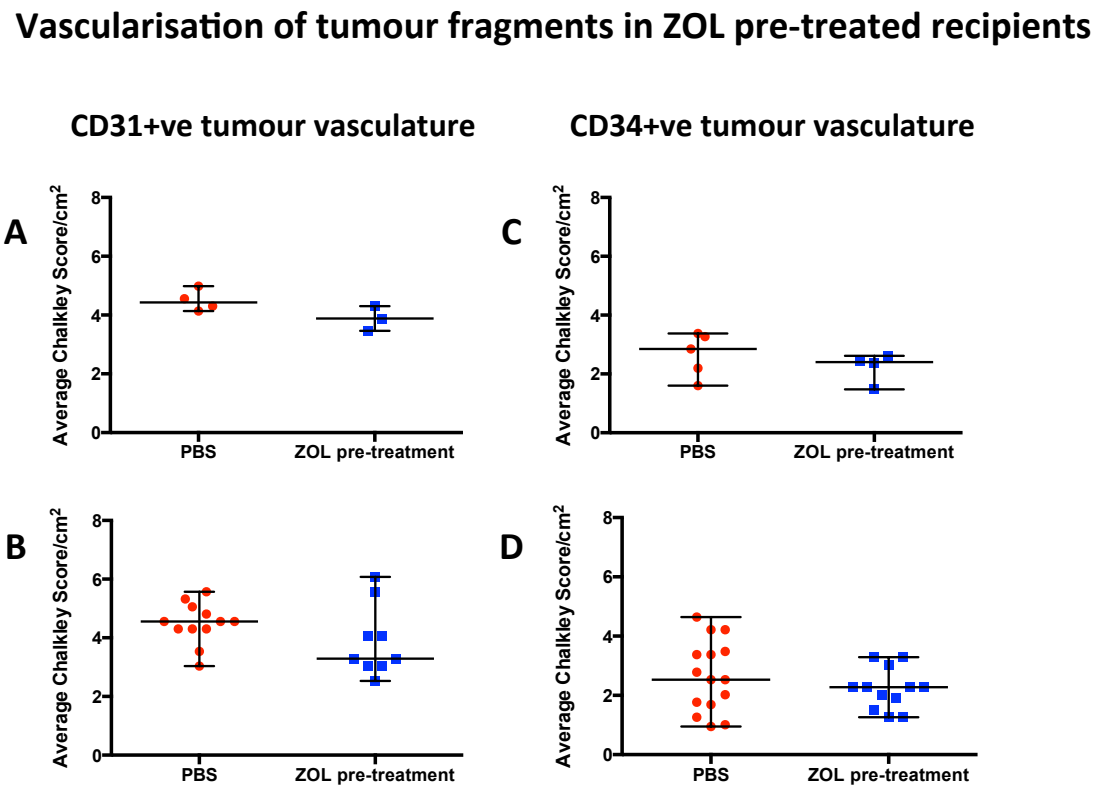


**Figure 77 Effects of ZOL pre-treatment on CD34+ve and CD31+ve vasculature of subcutaneously transplanted MDA-G8 tumour fragments from DOX/ZOL treated hosts.**
Microvessel density (MVD, presented as Average Chalkley score/$cm^2$) of subcutaneous MDA-G8 tumours from mice receiving PBS control or 100µg/kg Zoledronic acid pre-treatment (ZOL, i.p.) prior to transplantation of DOX/ZOL treated tumour fragments was determined using a Chalkley grid. Three non-serial levels were assessed per sample. (A&C) shows data with 3 levels averaged, (B&D) shows individual scoring data. n=3-5/group. Data show Median±Range. Mann-Whitney test. No statistical test applied for (B&D), shows individual scoring data only.

### 5.6.3.4. Effects on tumour cell necrosis

I also investigated whether there was a difference in tumour cell necrosis between the two groups of mice. The necrotic tumour area on 3 non-serial levels per sample was quantified using OsteoMeasure (performed by Maria ErazoBastidas, Research technician, University of Sheffield). No difference in necrotic area was determined between the treatment groups, suggesting that ZOL pre-treatment does not affect necrosis of subcutaneously transplanted tumour fragments (PBS: 29.52 ± 6.84% vs. ZOL pre-treatment: 31.66 ± 4.57%, Fig.78).

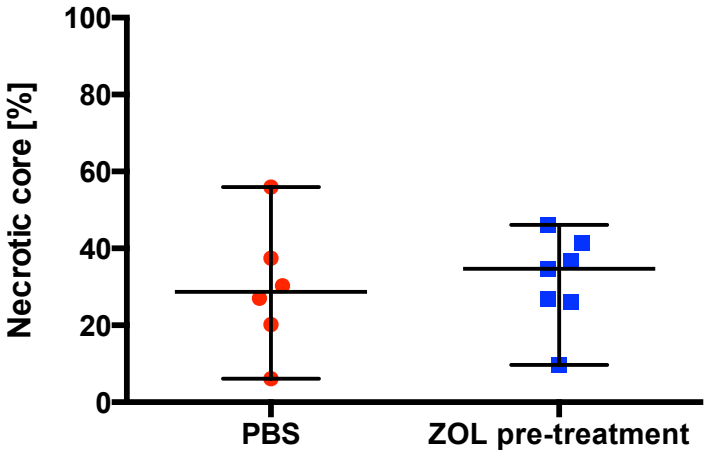


**Figure 78 Effects of ZOL pre-treatment on necrotic cores of subcutaneously transplanted MDA-G8 tumour fragments from DOX/ZOL treated hosts.**
The percentage of the necrotic area of subcutaneous MDA-G8 tumours from mice receiving PBS control or 100µg/kg Zoledronic acid pre-treatment (ZOL, i.p.) prior to transplantation of DOX/ZOL treated tumour fragments was determined using OsteoMeasure. Three non-serial levels were assessed per sample. PBS: n=6, ZOL: n=7). Data show Median±Range, Mann-Whitney test.

### 5.6.3.5. Effects on tumour cell proliferation

Ki-67 was used as a marker to identify proliferating tumour cells on histological sections of transplanted tumour fragments. Immunohistochemistry confirmed that both pre-treated and control tumours were actively proliferating, irrespective of tumour size at experimental endpoint (Fig.79).

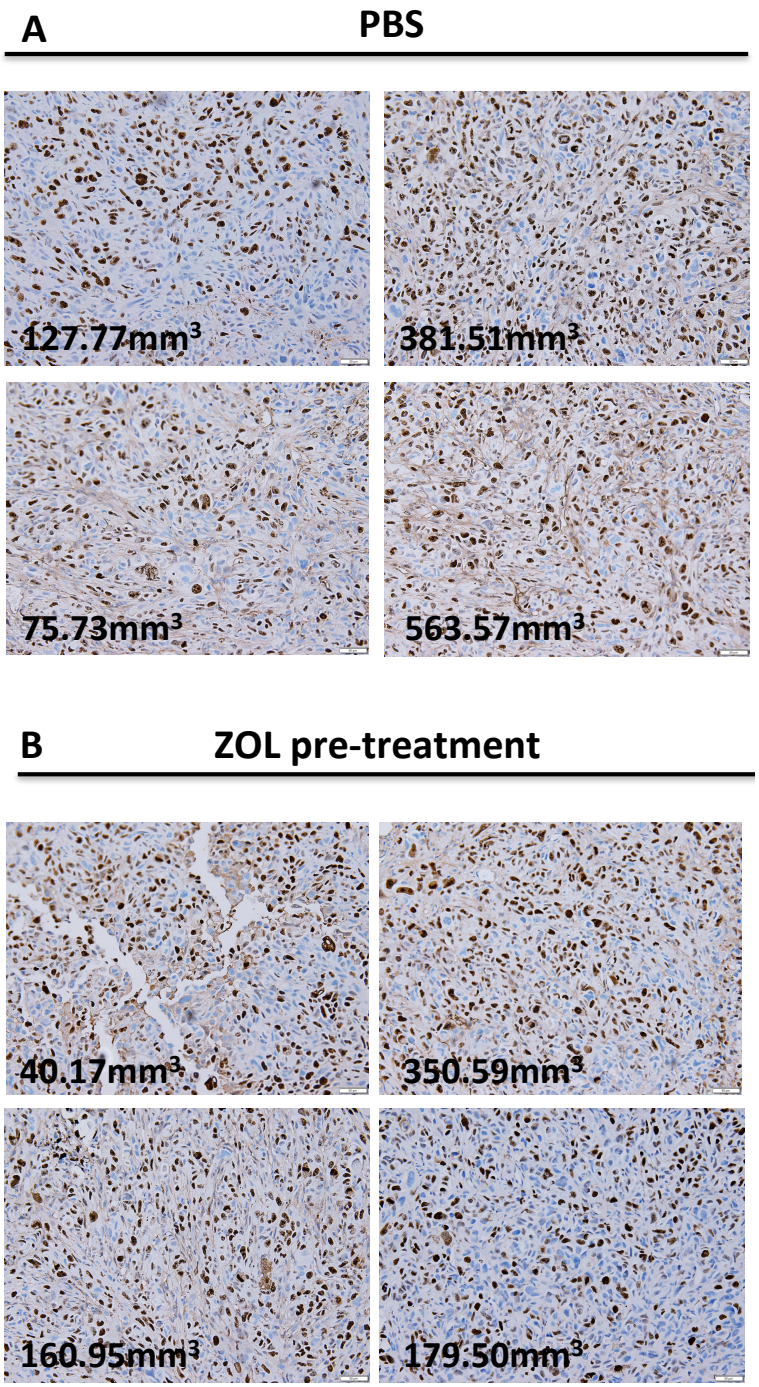


**Figure 79 Effects of ZOL pre-treatment on proliferation of subcutaneously transplanted MDA-G8 tumour fragments.**

Presence of proliferating (Ki-67+ve) MDA-G8 tumour cells (in brown) in tumour fragments from mice receiving PBS control or 100µg/kg Zoledronic acid pre-treatment (ZOL, i.p.). 20x objective, Olympus BX53, cellSense software, Scale bar is 50µm. Numbers indicate tumour volume at cull day.

## 5.7. Discussion

This study aimed to investigate the role of the bone microenvironment (BME) in mediating peripheral breast cancer (re)-growth. Experiments were designed to establish whether subcutaneous tumour growth resumes after successful combination therapy (DOX/ZOL), when tumour fragments are transplanted into recipients with a modified BME.

### 5.7.1. Effects of combination therapy on subcutaneous breast cancer growth

In clinical practice patients with advanced breast cancer often receive a combination of therapies, for example cytotoxic drugs accompanied with palliative bisphosphonate (BPs) treatment; and combination of therapies have shown synergistic anti-cancer response both *in vitro* and *in vivo* [154, 241, 247, 259, 260] (reviewed in [315]).

The majority of studies in breast cancer have investigated BPs in combination therapy in the metastatic setting, with only a limited number of studies investigating soft tissue and or peripheral tumours. Hiraga and colleagues observed an enhanced reduction in the area of established bone metastases in the 4T1/luc mouse model after combination therapy with tegafur-uracil (UFT, 20mg/kg/day, days 14-21) and ZOL (250µg/kg on day 7), when compared to UFT or ZOL alone. However, no effects were demonstrated using the single agent or the combination on orthotopic mammary fat tumours [316]. Combination of ZOL (0.2µg/mouse every other day, started 3 days prior to tumour cell injection) with doxycyline releasing pellets (10mg pellets with timed-release over 21 days, resulting in 15mg/kg/day, initiated at the same time as ZOL treatment) decreased MDA-MB-231 breast cancer burden in bone and the surrounding bone associated soft tissues in female BALB/c nu/nu mice [317]. Studies by Ottewell and colleagues, demonstrated reduced intraosseous MDA-MB-231/BO2 tumour burden, reduced presence of BrdU positive tumour cells accompanied by a reduction in caspase-3 positive tumour cells in nude mice using combination therapy of DOX followed 24hrs later by ZOL, which was not observed with single agents [259]. BPs in combination therapy have also been investigated in other cancer types including prostate, lung and colon (reviewed in greater detail in [147]). For example, ZOL (0.1mg/kg, twice weekly) in combination with Docetaxel (20mg/kg, every 2 weeks) for 7 weeks significantly reduced prostate specific antigen (PSA) serum levels, a measure of reduced tumour growth, in male SCID mice bearing intratibial LnCap prostate cancer cells when compared to single agents. However, ZOL as single agent decreased tumour volume, but as this was further enhanced with combination therapy the authors suggested that ZOL sensitizes LuCap cells to docetaxel treatment, resulting in an additive rather than synergistic anti-tumour effect of the two drugs [318].

Given that most studies explored treatment effects in bone metastases, the models used do not allow us to determine whether the anti-tumour effects are induced directly, indirectly via the BME, or a combination of the two. Recently ZOL in combination with the anti-EGFR monoclonal antibodies cetuximab has been shown to reduce growth of subcutaneous LS147T and SW48 colon tumours in male BALB/c nu/nu mice compared to control or treatment with single agents. This suggests synergy between the two therapeutic agents [319] and supports the hypothesis that addition of bone-targeted therapy modifies peripheral tumour growth.

Here I show that 5 rounds of combination therapy (DOX+ZOL) are effective in reducing subcutaneous MDA-G8 breast cancer growth, as in agreement with previously published studies by Ottewell *et al.* [241, 260]. However, the current study did not demonstrate complete suppression of tumour growth as described in these studies [241, 260]. This might be due to experimental variables including the use of different animal models (*e.g.* 6-week old female MF1 nude or CD1 nu/nu mice [241, 260] vs. 6-9-week old female BALB/c nude mice); or differential tumour volume at treatment start, a factor that I determined to be crucial for effective response to combination therapy. A human specific antibody was used to determine differences in tumour cell proliferation upon combination therapy showing a significant reduction in the number of Ki-67+ve cells/$mm^2$ tumour tissue area after combination therapy when compared to control, supporting the tumour volume measurements. In addition I observed reduced microvascular density (CD34+ve and CD31+ve vasculature) of subcutaneous tumours after 5 rounds of combination therapy. Single treatments with ZOL and DOX have previously been described not to affect microvascular density of subcutaneous MDA-G8 tumours when administered for 6 weeks; reduced presence of CD34+ve vasculature was only observed when both agents were combined [259].

### 5.7.2. Effects of combination therapy on the BME

Besides alterations in tumour microvasculature, the bone microvasculature appeared altered following combination therapy. In particular, the structural organisation of Endomucin positive vascular endothelial cells in the metaphysis changed from a distinct branched, tubular and interconnected network in the control mice to column like vasculature extending from the epiphysis in the treatment group. These observations require confirmation and quantification in independent experiments. In addition, it is well established that a single dose as well as repeated administration of combination therapy increases trabecular bone volume [154, 241] and this was also observed in my

experiments. However, whether alterations observed in the organisation of the metaphyseal bone marrow microvasculature after combination therapy are due to direct effects on vascular endothelial cells and/or due to the increase in trabecular bone in this particular area, reducing physical space, remains subject to further analysis. Whereas the role of the bone marrow vasculature in both aging and tumour cell colonisation and dormancy has been identified/explored [51, 52, 160, 320], the consequences of treatment-induced alteration to the bone marrow microvasculature and any resulted effects on peripheral breast cancer growth is unknown.

Given that tumour-growth-promoting cells (CAFs, TAM, etc.) are recruited from haematopoietic organs including the bone marrow to support disease progression, this suggests that an intact bone marrow vascular network is crucial for the trafficking of BMDCs and tumour-growth promoting soluble factors (*e.g.* VEGF, MMPs, etc.) that are released during bone remodelling. I therefore proposed that following combination therapy BMDCs including $CD11b^{+}/Gr1^{+}$ myeloid derived suppressor cells (MDSCs) are retained in the BM, reducing their presence in the circulation and their recruitment to the peripheral tumour, which could partially contribute to the reduced subcutaneous tumour growth.

Overall, I observed a small but non-significant increase in the percentage of CD11b+ve myeloid cells in the bone marrow of DOX/ZOL treated mice when compared to control. CD11b is expressed on a variety of BMDCs including leukocytes, monocytes, neutrophils, natural killer cells, granulocytes and macrophages. Therefore, to determine if specific CD11b+ve cell populations increase in the bone marrow after combination therapy, multiple markers would be needed (*e.g.* mature monocytes are-CD11b, CD11c, CD13, CD14, CD33, and CD64 positive [321]). Well defined in murine models, the phenotype of immature myeloid cells, or MDSCs, consists of dual expression of Gr-1 and CD11b; human phenotypes remain poorly defined. MDSCs have been described as a heterogeneous population of immature myeloid cells, generally overproduced in peripheral blood and bone marrow of cancer patients, associated with poor prognosis, clinical cancer stage and metastatic tumour burden [322]. Gabitass and colleagues for example observed increased presence of MDSCs ($HLADR^{-}Lin1^{low/-}$ $CD33^{+}CD11b^{+}$) in peripheral blood of pancreatic, oesophageal and gastric cancer patients when compared to healthy volunteers [323]. This is in agreement with data from Porembka *et al.* ($CD15^{+}CD11b^{+}$) [170], who also demonstrated, in humans, that these cells are actively recruited to pancreatic tumours thereby accelerating tumour growth [170]. In the same

publication they report that ZOL treatment (30μg/kg 3x weekly) reduced intra-tumoural accumulation of MDSCs, delayed tumour growth as well as increased survival in a murine model of pancreatic cancer ($0.1x10^6$ Pan02 pancreatic adenocarcinoma cells). Given that the cell line used in these experiments is non-metastatic and the observed shift of the tumour microenvironment towards an immunostimulatory phenotype with increased levels of IFN-γ accompanied by decreased IL-10 levels [170], supports the hypothesis that ZOL-induced alterations to the BME affect non-skeletal tumour growth. Soki *et al.* did not observe effects on Gr1+ve cells in bone marrow of ZOL treated 4-week old C57BLJ/6 mice when compared to control (ZOL: 200μg/kg 2x weekly for 4 weeks) [159]. Repeated and continuous ZOL treatment is also suggested to inhibit differentiation of myeloid cells *in vitro*, and data from *in vivo* studies report reduced infiltration of CD11b+ve macrophages into mammary carcinomas, decreased presence of macrophages in the spleen of ZOL treated mice (mesothelioma model) suggesting impaired differentiation of MDSCs upon ZOL treatment [168], with others showing reduced number of $CD11b^+/Gr\text{-}1^+/F4^+/80^+$ cells in tumour stroma and peripheral blood [37]. A significant increase (about 37%) in MDSCs in bone marrow of myeloma bearing mice when compared to control, paralleling myeloma burden in bone, has also been reported. By isolating MDSCs from spleens of tumour bearing mice, studies have shown differentiation into bone resorbing osteoclasts *in vitro,* whereas MDSCs isolated from naïve mice did not. *In vitro* ZOL inhibited osteoclast formation in tumour-induced MDSC cultures and *in vivo* ZOL (0.1mg/kg, 2x weekly for 4 weeks) reduced the increase in MDSCs by 30% upon development of myeloma burden in bone when compared to control [324].

A study by Diaz-Montero *et al.* investigated levels of MDSC in newly diagnosed cancer patients (solid malignancies) undergoing doxorubicin–cyclophosphamide chemotherapy. There was a significant correlation between both percentage and absolute number of circulating MDSC and clinical cancer stage, with highest levels of MDSCs found in patients with metastatic cancer. Standard doxorubicin–cyclophosphamide chemotherapy on an every 14-day schedule was associated with a significant increase in MDSC in peripheral blood of breast cancer patients [322]. In the 4T1 breast cancer model administration of 2.5mg and 5mg/kg DOX significantly reduced the proportion and absolute number of 4T1 tumour-induced MDSC in the spleen and blood when compared to control, potentially mediated by DOX-induced apoptosis of MDSCs [325]. A key characteristic of MDSCs is their ability to suppress the activation and proliferation of T cells, however the immunosuppressive function of the residual MDSCs was significantly

impaired [325]. In my experiments T-cell depleted BALB/c nude mice were used, so the immunosuppressive effect of MDSCs on T cells was not present and could not be evaluated.

The experiments discussed above did not assess effects of chemotherapy on bone marrow derived MDSCs. I could not detect any overt effects on the percentage of CD11b/Gr1$^{+}$ cells in the bone marrow after 5 rounds of weekly DOX/ZOL combination therapy when compared to control. These results suggest that this schedule of combination therapy does not modify CD11b$^{+}$/Gr1$^{+}$ BMDCs, however, a more detailed analysis with increased sample size and multiple markers will allow a more comprehensive investigation of the potential consequences of the treatment regime on BMDCs.

In summary, these data show that 5 rounds of DOX/ZOL combination therapy are effective in reducing subcutaneous tumour growth, highlighting that treatment has to be initiated early for successful therapy. However the precise molecular and cellular mechanisms regulating the synergistic effects of DOX/ZOL in xenograft models of subcutaneous breast cancer growth remain to be determined.

### 5.7.3. Role of the BME in mediating peripheral breast cancer re-growth following cessation of combination therapy

Studies by Ottewell *et al.* also showed that suppression of peripheral tumour growth was maintained once combination therapy was withdrawn [260]. I therefore specifically designed my experiments to elucidate the role of the BME in subcutaneous tumour re-growth, and whether this was affected by bone-targeted therapy. Isolated fragments from successfully treated DOX/ZOL tumours were therefore transplanted into hosts with a ZOL-modified BME or control mice.

Only a limited number of studies have investigated the effects of bone-targeted agents on peripheral breast tumour growth, with the majority reporting minimal to no effect [37, 39, 148, 307]. In addition, when reduced tumour growth and/or increased survival was observed, all animals eventually died from progressive disease; similar to effects observed when using ZOL-monotherapy in animal models of bone metastases [146, 147, 273]. A recently published study reports beneficial effects of ZOL in prostate cancer models bearing subcutaneous tumours. Here the authors show that ZOL (100μg/kg once weekly for 6 weeks) prevents cancer associated fibroblast (CAF)-induced enhancement of subcutaneous prostate cancer cell growth ($1x10^{6}$ PC3 cells plus $0.5x10^{6}$ CAFs were injected), potentially mediated via ZOL's ability to impair stromal CAFs and fibroblast

reactivity [169]. Nevertheless, the dose and administration schedule in these studies were not clinically relevant, thus preventing conclusions to be drawn as to whether the effects of ZOL on peripheral tumours were direct or via the BME. In addition I am not aware of studies assessing the role of a ZOL-modified BME in primary breast cancer re-growth. Whereas BPs have been well studied in the adjuvant setting [135, 180], their role in neoadjuvant therapy, given before the main treatment to reduce tumour size, remains poorly defined. A recent meta-analysis of clinical trials investigated the effects of adding ZOL to neoadjuvant chemotherapy in patients with stage II and III breast cancer concluded that there was no benefit of adding ZOL to neoadjuvant chemotherapy in the overall study population [193]. However, addition of ZOL resulted in significant increase in pathological complete response in the breast in postmenopausal women [193]. The models used in my experiments did however not represent a post-menopausal setting, given the use of young animals (6-8-weeks at treatment start without ovariectomy).

Myself and others have previously established that ZOL induces rapid and significant alterations to the BME highlighting that although the main target of BPs is the osteoclast, also other BMDCs including HSCs [159], osteoblasts [158] or tumour associated macrophages [171] could contribute to the observed anti-tumour effects of BPs in skeletal and extra-skeletal settings. Unpublished data from our group showed that following transplantation of tumour fragments from untreated hosts into recipients that were pre-treated with DOX/ZOL or PBS control for 6 weeks, tumour growth resumed in both treated or control mice. However there was a difference in doubling time (Untreated: 10 days vs. Treated: 5 days). To assess if growth of regressed subcutaneous tumours resumes when transplanted into hosts with a therapeutically altered microenvironment, Wind and colleagues then transplanted fragments from successfully treated DOX/ZOL treated tumours into mice that were either pre-treated with PBS control or 6 cycles of weekly DOX/ZOL combination therapy. These experiments showed that regressed tumours were able to continue their growth irrespective of pre-treatment. Similar results were obtained in my experiments where I transplanted tumour fragments after cessation of combination therapy into recipients with a ZOL pre-treated microenvironment. After an initial lag-phase tumours started to grow exponentially in a subset of mice in both groups. These data suggest that re-growth of previously treated tumour fragments is irrespective of the BME. Although tumour fragments appeared to grow slower in the initial phase after transplantation no difference in doubling time or volume at experimental endpoint was determined. Active tumour cell proliferation was confirmed by Ki-67 staining. Observations

of differences in tumour growth rate might be hampered by the high variance of tumour volumes in these studies (PBS: 75.73mm$^3$ to 563.57mm$^3$ and ZOL pre-treatment: 40.17 mm$^3$ to 448.69mm$^3$). In addition no difference in CD34+ve, CD31+ve vascular cells within the tumour or tumour cell necrosis was observed. However, analysis was complicated, as some samples were split into pieces prior to processing.

Intratumoural heterogeneity, the existence of multiple sub-clones with different molecular profiles within one tumour, as well as the complex tumour stroma provides a major clinical challenge [326]. Using the tumour re-transplantation model rather than inoculating breast cancer cells into mice with a ZOL pre-treated BME allowed me to recapitulate this heterogenous tumour microenvironment. Injecting tumour cells rather than transplanting tumour fragments would be more relevant to study the role of the BME on peripheral breast cancer development. My studies therefore aimed to represent the heterogeneity in a clinical setting, where small residual tumours regrow after initial therapy. Although care was taken to transplant equally sized fragments into recipient mice, the above mentioned intratumoural heterogeneity does also complicate the analysis of the here-performed experiments. Given the nature of these studies transplanted tumour fragments were comprised of varying cellular composition (tumour heterogeneity, necrotic areas, stromal cells). Additionally the fate of these fragments during the initial days after transplantation are speculative given the initial lack of blood vessels to supply oxygen and nutrients as well as hypoxia and tumour cell apoptosis. Indeed shrinkage of the tumour transplants was observed during the first days, with growth resuming at later time points. In addition, transplanted tumour fragments may already contain sufficient infiltrated stromal cells that aid engraftment and re-growth following transplantation in the new host, irrespective of any newly recruited stroma. Any alterations in stroma-recruitment following ZOL treatment may therefore not be sufficient to affect re-growth of transplanted tumour fragments. Thus, the nature of using the complex system of tumour re-transplantation is a possible explanation for the high variation of tumour re-growth observed in the recipient mice (both ZOL and control pre-treated). In separate, ongoing studies we have demonstrated that effects of ZOL in expanding cells of the haematopoietic niche is rapid but also transient (Haider & Ubellacker, unpublished). Experimentally, tumour fragments were transplanted 24hrs after recipient mice had received the final dose of ZOL and whether this was the ideal time point to establish the full consequences of the BME on peripheral growth remains to be established. Nevertheless choosing the 24hr time point guaranteed that circulating levels of ZOL were minimal, due to the short plasma half-

life of the drug. Besides no difference in tumour size I could also not determine differences in tumour cell necrosis or vascularisation between fragments that were transplanted into ZOL or control pre-treated recipients.

### 5.8. Summary and Conclusion

In summary these data show that modification of the BME with ZOL is not sufficient to supress peripheral breast cancer re-growth following cessation of combination therapy, suggesting that both the tumour and microenvironment need to be targeted for successful anti-cancer therapy.

# Chapter 6 – Discussion, Future Work and Conclusion

## 6.1. Discussion and future work

Breast cancer preferentially metastasises to bone, hence calling for therapeutic intervention that targets not only the tumour but also the bone microenvironment (BME). Decision-making for the use of anti-cancer therapy is primarily based on tumour characteristics. However, our increased understanding of the interactions between cancer cells and their surrounding microenvironment (TME) highlights the importance of considering the response of the TME when selecting and designing treatment approaches. In metastatic breast cancer the presence of proliferating tumour cells in bone disturbs the physiological balance of bone remodelling due to increased osteoclast activity, which results in osteolytic lesions [121, 130, 327, 328]. To date bone-targeted therapeutics include the standard of care anti-resorptive agents (*e.g.* Zoledronic acid, ZOL), and novel agents with promising results in clinical trials are emerging (*e.g.* the tyrosine kinase inhibitor Cabozantinib, CBZ). Stromal cells including osteoblasts and osteoclasts as well as soluble factors in the TME are therefore increasingly investigated and enhanced anti-cancer effects are reported when combining therapies that target both the cancer cells and their microenvironment [241, 247, 259, 260].

Work presented in this thesis has utilised a range of *in vivo* model systems and methodologies to investigate the response of the *in vivo* BME to anti-cancer therapy, its role in tumour cell homing to bone and peripheral breast cancer re-growth.

### 6.1.1. Modification of the BME with ZOL and consequences on tumour cell homing to bone

Although the BP ZOL has shown to reduce human breast cancer recurrence in bone and its routine use to reduce skeletal-related events in human cancer-induced bone disease, there was minimal data available on the effects of ZOL on cells other than the osteoclast prior to data presented in Chapter 3. This seems somewhat surprising given that BPs were identified by chemists in the middle of the 19$^{th}$ century and used in skeletal disorders that are characterised by excessive bone resorption [329]. Effects of BPs on osteoblasts and endothelial cells for example have been mainly investigated *in vitro*, and the pharmacological property of the drug questions the relevance of these data [159, 161, 162, 165, 249, 262, 267, 269]. The lack of studies exploring the effects of BPs on osteoblasts *in vivo* is potentially due to the difficulty of identifying these cells on histological sections. Whereas osteoclasts are easily identified based on their bright, pink appearance following TRAP-staining, the lack of specific markers to detect osteoblasts using immunohistochemistry for example makes quantification a challenge. Osteoblasts are

generally identified according to their distinct morphology using H&E stained sections [90, 330-332]. To establish osteoblast quantification I received training by key experts at the University of Sheffield and my histophatological results were reviewed and confirmed by pathologists Dr. Hunter and Dr. Heymann (both University of Sheffield). Others have previously quantified osteoblasts lining trabecular bone surfaces using pre-defined areas of $0.75mm^2$ with an offset of 0.25mm from the growth plate [332, 333]. In Chapter 3 I present data that breast cancer cells preferentially localise to trabecular bone areas, and similar results have been reported by others [90]; however, a wide variation in the location of tumour cells within the metaphysis has previously been observed [90]. Experimentally I therefore decided to quantify the number of osteoblasts and osteoclasts on all trabecular bone surfaces 125µm away from the growth plate. In addition, specialised mouse models expressing GFP +ve cells of the osteoblastic lineage were used in a proportion of experiments, that facilitate the visualisation of treatment effects on these cells.

It is well established that long-term treatment with BPs increases bone volume due to reduced osteoclast activity [157, 241, 262, 266]. A study by Pozzi and colleagues demonstrated activity of the BP ZOL on osteoblasts *in vivo,* with a trend towards reduced osteoblast numbers per bone perimeter after repeated treatment with 0.5-1mg/kg ZOL weekly for 3 weeks, in addition to significantly reduced serum osteocalcin levels in C57BL6 mice. However, the dose and treatment schedules in these experiments are not comparable to the clinical setting [262]. Here I present the first evidence that a single, clinical relevant dose of ZOL (100µg/kg in mice) causes substantial alterations to the BME *in vivo* including an increase in trabecular bone volume and a reduction in number and activity of both osteoblasts and osteoclasts as early as 3 days post treatment when compared to control. In addition, ZOL appears to induce changes to the structural organisation of the bone marrow vasculature and increases the presence of proteoglycan-rich ECM in the metaphysis, with potential consequences for the physical location and cellular/molecular interactions of the metastasis niche.

Dissemination of tumour cells occurs early in the disease and in about 30% of patients with early-stage breast cancer, presence of micro-metastases in the bone marrow at the time of diagnosis has been reported [97]. Although our knowledge covering how tumour cells influence the BME and vice versa continues to increase, our understanding of the crucial, early events occurring in bone metastasis remains speculative; this is largely due to the lack of methodologies to accurately study these early events. Others have used the bioluminescence signal to study the homing of B02 breast cancer cells to bone 14 days

post tumour cell inoculation in the presence and absence of ZOL treatment [146]. However, this method does not allow the detection of individual tumour cells or their precise location in bone. Two- or multi-photon microscopy is therefore the current standard technique to visualise single cancer cells in bone [85, 115]. Despite this technique allowing high resolution imaging, it remains challenging to investigate the surrounding cells of the BME. In my thesis I combined the use of two-photon and fluorescence microscopy with standard histology, to explore whether osteoblasts are key cells of the complex network of bone marrow-derived cells (BMDCs) that create the metastasis niche and determined whether tumour cell homing, one of the critical key step in the development of osteolytic bone disease, is affected by bone targeted therapy (ZOL).

Previous studies have injected breast cancer cells 24hrs post ZOL pre-treatment [146], a time point where bone volume as well as osteoblasts and osteoclasts are not affected by ZOL [158]. However my previous analysis on the early effects of ZOL on the naïve BME allowed me to determine when tumour cells arrive in bone so this coincides with the time point when ZOL-induced BME modifications have reached their peak (Day 5 post ZOL). In postmenopausal women ZOL has been shown to reduce breast cancer recurrence in bone, and increased risk of bone metastasis has been associated with high PINP serum levels (marker of osteoblast activity) [132]. This suggests a key role of osteoblasts in the development of bone metastasis and breast cancer recurrence in bone. However, *in vivo* the tight coupling between osteoblasts and osteoclasts makes it difficult to separate the direct and indirect effects of therapeutic agents on these cells; a single quantification of the bone serum marker levels (TRAP and PINP), is not helpful, so repeated measurements are required.

Previous work has highlighted the prevalence of osteoblasts in the BME comprising microscopic bone lesions [94], and suggests that osteoclasts are not critical in the earliest stages of bone metastasis but rather at later stages of disease progression [93]. This is supported by my data showing that inhibition of osteoclasts with ZOL does not inhibit tumour cell homing to bone [158]. However, in agreement with findings from Wang and colleagues my data suggest that BCs preferentially home to osteoblast-rich trabecular areas. This is further strengthened by the observation that in breast cancer patients, actively proliferating macrometastases have been found in close proximity to endosteal surfaces [112], and that heterotypic adherens junctions between E-cadherins expressed on breast cancer cells and N-cadherins expressed on $ALP^+$ osteogenic cells are formed during the early stages of bone metastasis [94].

However, BCs might not only localise close to endosteal surfaces due to the presence of osteoblasts, since these areas were also comprised of proteoglycan-rich extracellular matrix (ECM). Although tumour cell adhesion to the ECM is the first step in the metastatic cascade, the mechanism by which ZOL affects interaction of breast cancer cells with ECM components such as for example proteoglycans and hyaluronan implicated for breast cancer cell adhesion, invasion, proliferation and migration are less well reported. In addition, integrins, cell surface glycoproteins mediating cell-cell and cell-ECM adhesion may be affected by ZOL treatment with potential consequences on the metastatic process. Indeed, ZOL has been shown to have anti-adhesive properties in breast cancer cells *in vitro* [334]. When compared to control, ZOL (5-90μM for 48 and 96hrs) caused a down-regulation of the integrin heterodimers αvβ3 (−34%), αvβ5 (−98%) as well as α5β1 (−40%) in MDA-MB-231 breast cancer cells, which was accompanied by reduced adhesion to various ECM matrices *in vitro* [334]. In breast cancer cells ZOL also reduced the expression of MMP-9 and -2, MMPs that play a crucial role in invasion and metastasis [334]. Others also reported that ZOL treatment significantly impaired the adhesion of MDA-MB-231 breast cancer cells to vitronectin and gelatine matrices (both αvβ3 ligands) when compared to control, which correlated with reduced αv and αvβ3 cell surface expression. In contrast no difference in adhesion onto fibronectin (α5β1-ligand) and collagen type 1 (α2β1-ligand) was observed [335]. These findings may provide a further explanation for why the location of tumour cells in bone is altered in a ZOL-modified BME.

The metaphysis is a highly vascularised structure. Given the role of osteoblasts in bone development, regeneration, and remodelling [336], studies have suggested coupled invasion of osteoblasts with growing PECAM-1+ve blood vessels to the site of bone turnover in response to environmental cues in experimental fracture models [53]. Studies by Kusumbe and colleagues revealed that osteoblasts are selectively positioned around endosteal Endomucin$^{high}$CD31$^{high}$ vessels in the metaphysis [51, 160], the area preferentially colonised by breast cancer cells [90, 158]. These observations suggest a potential overlap of the endosteal and vascular niche in bone, and whether both contribute to tumour cell homing remains to be elucidated. However, given the tight coupling between osteogenesis and angiogenesis [51], alterations in tumour cell location in bone following modification of both, osteoblasts and endothelial cells in my experiments, strengthens the notion of a joint role for both niches in tumour cell homing to bone. Additionally I observed single tumour cells in close proximity to both vascular endothelial cells and bone surfaces using immunofluorescence; however quantification methods to

determine the temporal-spatial relationship between bone marrow vasculature and tumour cells need to be developed.

For my studies I largely focused on the two key bone cells, osteoblasts and osteoclasts; although also other cells of the BME, including HSCs, may contribute to tumour cell homing. In collaboration with Dr. Sandra McAllisters group in Boston I investigated the effects of ZOL on HSCs, another potential component of the metastatic niche [31, 95, 96]. Using prostate cancer models Shiozawa and colleagues have shown that tumour cells compete with HSCs for the occupancy of the hematopoietic niche [95]. HSCs are thought to reside in close proximity to the endosteal and vascular niches [101-103, 337, 338]. It is well established that elevated numbers of osteoblasts increase HSCs in the bone marrow [102-104], concomitantly osteoblast depletion decreases the numbers of HSCs [339]. In addition osteoclast-induced bone resorption results in the release of soluble growth factors such as G-CSF, TGF-$\beta$, as well as bone minerals and proteins that affect HSC maintenance and mobilisation [32]. Homing of HSCs to the marrow niche is partially regulated by CXCR4/CXCL12 chemotactic signalling [110], and there is evidence that tumour cell homing to bone is also mediated through this pathway [95].

Following up to work presented in my thesis, a detailed, real-time characterisation of the temporal-spatial relationship between various niche components including osteoblasts, vascular endothelial cells, HSCs and tumour cells would be required. By using lipophilic dyes as well as expression of fluorescent reporters, intra-vital microscopy would offer a significant advantage over longitudinal imaging by bioluminescence, which lacks the resolution to detect single cells. This approach remains challenging given the need for high-resolution imaging and deep-tissue-penetration. Intra-vital imaging of cellular trafficking within the bone marrow space has been successfully applied to study the HSC niche [338, 340] and bone marrow colonisation by multiple myeloma cells [115]. These studies were predominantly performed by imaging the calvarial bone marrow, whereas intra-vital imaging of the long bones, the location where xenograft models commonly develop breast cancer bone metastases, remains challenging. To my knowledge there is only one study by McDonald and colleagues who have developed a method for dynamic longitudinal imaging of dormant myeloma cells within intact long bones of mice [115]. In these experiments colonising myeloma cells migrating from the bone marrow space towards endocortical bone surfaces, where they appeared to arrest, were visualised. Performing similar experiments in breast and/or prostate cancer models would significantly contribute to our understanding of how the BME regulates the development of bone metastases. However,

longitudinal intra-vital imaging of the development of bone metastasis has various limitations including the stress of the procedure to animals, given the repeated and prolonged anaesthesia and surgery. In addition, the critical step of tumour cell homing to bone may only be captured within the first hours post tumour cell injection.

### 6.1.2. Characterise the effects of CBZ on the BME *in vivo*

Novel, small molecule tyrosine kinase inhibitors such as CBZ, have been shown to affect bone [208, 231, 341], but most studies investigated the effects of such agents in the presence of tumour, which masks the specific contribution of bone cells to observed anti-cancer response. Currently CBZ is approved for metastatic medullary thyroid cancer and advanced renal cell carcinoma [229, 239]; clinical trials in prostate cancer bone metastasis [234, 235] support the notion that treatment effects are mediated via key bone cells. I carried out the first detailed characterisation of the response of the naïve *in vivo* BME to CBZ across a range of animal models (studies were kindly supported by Exelixis). This allowed me to assess the response of the BME to CBZ in different microenvironments with regards to age, sex and strain. With aging the composition of the BME changes, including the presence of myeloid and lymphoid lineages in the bone marrow in addition to alterations in intrinsic HSC properties such as proliferation and differentiation [342]. In addition, mesenchymal stem cells change their proliferation and differentiation capacity during aging, which is potentially associated with the increased bone loss in adulthood. Also BME-derived growth factors exhibit age-related changes [242]. I therefore included young (6-week old) and older mice with a more mature skeleton (17-weeks) in my experiments and observed differential effects of CBZ in these models. Similar differential effects were also seen in male vs. female mice, potentially due to presence of different sex hormones and receptors. This emphasises the need to establish the response of anti-cancer therapeutics in a variety of animal models to provide detailed mechanistic information. The models used in my studies also lacked the presence of an active immune system, which eliminates the ability to establish the role of the adaptive immune system in mediating the response to CBZ. Investigating the effects of CBZ in immunocompetent models would allow evaluation of the role of the immune system in the response to drug treatment.

Briefly, administration of CBZ caused substantial alterations to the different cell types in bone irrespective of the absence of tumour, suggesting a key role of bone cells in mediating the response to CBZ therapy. To date limited studies in xenograft models of breast cancer have been conducted [218], and studies using CBZ in models of advanced

breast cancer should be performed. Experiments using CBZ in combination with additional anti-cancer drugs may also provide increased efficacy when compared to the mono-therapy. Indeed, CBZ has demonstrated promising effects in patients with advanced castration resistant prostate cancer who had received at least one previous docetaxel chemotherapy regimen [235]. CBZ is currently also being investigated in combination with fulvestran (hormonal therapy) and trastuzumab (monoclonal antibody that interferes with the HER2/neu receptor) in patients with advanced breast cancer (Clinical trials.gov identifier NCT01441947 and NCT02260531). Due to funding limitations I was not able to assess how the CBZ-mediated alterations of the BME may affect establishment and progression of breast cancer bone metastasis. It still remains unclear whether changes in bone scans following CBZ treatment are due to bone modulation alone or due to a specific anti-cancer effect on metastasis. Therefore serum bone markers such as alkaline-phosphatase are still used as non-specific surrogate markers for response to CBZ in patients with advanced prostate cancer alongside PSA-levels and pain assessment [235].

Based on the findings presented in Chapter 4, the importance of considering the BME in designing new anti-cancer treatment regimes has been established and will allow the design of treatment regimes with enhanced efficacy.

### 6.1.3. The role of the BME in mediating peripheral breast cancer growth

Patients with advanced breast cancer often receive a combination of drugs that target both the BME and the tumour cells (*e.g.* the bone-targeted agent ZOL). In addition to the use in advanced breast cancer, ZOL is increasingly investigated in the adjuvant (therapy given in addition to the main therapy to maximise treatment effectiveness) or neoadjuvant setting (given before the main treatment); and in both the patients menopausal status has emerged as the critical factor for treatment success [133, 135, 180, 182, 193] – see Table 2&3, Chapter 1. However, the role of the BME in mediating peripheral breast cancer growth remains poorly understood. Based on the intriguing findings in clinical trials [133, 135, 180, 182, 193], two interesting questions remain to be addressed [343], which are as follows: (1) "**What is the mechanism of action?"** and (2) "**Why are benefits observed in postmenopausal women only?"**. One potential mechanism of action in postmenopausal women was recently suggested by the ANZAC trial (AdditioN of Zoledronic Acid to Chemotherapy), which showed that addition of ZOL to neoadjuvant chemotherapy resulted in decreased serum levels of follistatin, an activin inhibitor and member of the TGF-β family. Interestingly this was not observed in premenopausal women. Therefore postmenopausal women receiving ZOL may therefore have a higher biological availability

of activin compared to premenopausal women, thus promoting the tumour suppressor action of this TGF-β family member after ZOL treatment [196]. In addition, given the reported effects of ZOL on cells other than the osteoclast [154, 155, 159, 168, 171, 173, 270, 308], it is highly likely that treatment effects are mediated via ZOL's impact on the BME.

Here I present the first experimental evidence that modification of the BME with ZOL is not sufficient to supress peripheral MDA-G8 breast cancer re-growth following cessation of combination therapy; suggesting that ZOL-induced modification of the BME is not sufficient to reduce peripheral breast cancer re-growth. Briefly, tumour fragments from mice receiving combination therapy (Doxorubicin followed by ZOL) were subcutaneously transplanted into naïve BALB/c nude mice with either a physiological or therapeutically altered BME (ZOL-pre-treatment). Despite ZOL-induced alterations to the BME, growth of subcutaneously re-transplanted tumour fragments resumed at equal rates whether transplanted into ZOL or PBS pre-treated hosts. Adjuvant and neoadjuvant ZOL only demonstrated benefits in clinical studies in postmenopausal women [133, 135, 180, 182, 193], and my experiments were not performed in a postmenopausal model system. It would therefore be relevant to repeat these studies in ovariectomised mice. In addition, adjuvant Denosumab, another bone-targeted agent, has been demonstrated to prevent fractures in aromatase inhibitor-treated postmenopausal women [203]. These findings highlight the potential to investigate whether the anti-RANKL-targeted Denosumab also improves the neoadjuvant response to chemotherapy.

Furthermore, transplanted tumour fragments are likely to be very heterogeneous given that different cell types and various stromal cells comprise different regions of the tumour. Importantly, breast cancer subtypes show significant molecular as well as genetic heterogeneity [344, 345], and within each breast cancer different mutations could drive disease progression. Intratumoural heterogeneity, the existence of multiple sub-clones with different molecular profiles within one tumour, provides a major clinical challenge [326]. Therefore the model of tumour-transplant in my experiments does represent the heterogeneity in a clinical setting, where small residual tumours regrow after initial therapy. However, the transplanted tumour heterogeneity is a possible explanation for the high variation of tumour re-growth observed in the recipient mice (both ZOL and control pre-treated). The tumours may have recruited sufficient BMDCs whilst still in the host, contributing to re-growth upon transplantation irrespective of the BME and precursor cell recruitment in the recipients. There may have already been a switch from

microenvironment-dependent to microenvironment-independent tumour growth, prior to the time of tumour transplantation.

It is currently not clear whether bone marrow-derived cells (BMDCs) are only required for the early stages of disease development or also for maintaining and promoting the growth established tumours. Studies from Lyden *et al.* showed that bone marrow-derived precursor cells are required for the early stages of tumour angiogenesis, whereas residual BMDCs may account for later growth of intradermally implanted B6RV2 lymphoma cells. These studies also showed that impaired recruitment of endothelial and haematopoietic progenitor cells from the bone marrow inhibits tumour angiogenesis and thus tumour growth [33].

The contribution of BMDCs to tumour growth is complex, involving their mobilisation, recruitment and incorporation into the tumour stroma, with each step offering an individual therapeutic window. Combining treatment approaches that target the recruitment and mobilisation of BMDCs in addition to other components of the TME may provide a significant improvement in the efficacy of anti-cancer therapy.

Studies suggest that disease progression might not only be mediated via direct BMDC recruitment but also through systemic factors [11, 27]. The role of systemic factors, derived from both the BME and the TME, in mediating breast cancer growth remains relatively unexplored. Soluble factors associated with BMDC mobilisation include VEGF, angiopoietin, SDF-1 and GM-CSF [28, 32, 42, 255, 346]. Targeting these factors and/or their receptors is a potential therapeutic approach although this will not only affect BMDCs. Granulocyte-macrophagecolony-stimulating-factor (GM-CSF) for example is known to have biphasic effects on osteoclastogenesis and may therefore affect peripheral tumour growth by altering the levels of tumour-growth promoting factors that are released form the BME during active bone resorption. Dai and colleagues assessed whether blocking GM-CSF-induced osteoclastogenesis by ZOL pre-treatment prevents GM-CSF-induced breast cancer growth in bone in a mouse model of chemotherapy-induced leukopenia. In these studies administration of murine GM-CSF increased the growth of MDA-231-lux breast cancer cells in bone, which was associated with increased osteoclast activity when compared to control. *In vitro* GM-CSF had no effect on breast cancer cell proliferation supporting an indirect mechanism *in vivo* [347]. Elucidating if alteration of the BME with GM-CSF and other stromal factors including SDF-1, known to regulate HSCs and progenitor trafficking [14, 255], or CXCL5, responsible for recruitment of myeloid derived suppressor cells

(MDSCs) into the breast carcinoma TME [41] affects primary tumour growth would be interesting to explore. With regards to MDSCs, I aimed to explore the effects of DOX/ZOL combination therapy on $CD11b^{+}/Gr1^{+}$ MDSCs. Here I observed a small, but non-significant increase in the presence of these cells in the BM of treated mice when compared to control. Using more complex flow-cytometric experiments with multiple markers for different BMDC populations and their progenitors would establish if reduced peripheral breast cancer growth after combination therapy is mediated via BMDCs (part of ongoing collaborative experiments with the McAllister group, Boston, USA). Although I have demonstrated that ZOL (alone or in combination therapy) rapidly affects the cellular and extra cellular composition of the BME, I was not able to measure the effects on these bone marrow-derived cytokines and growth factors that may contribute to BMDCs recruitment and mobilisation. Repeated blood sampling from animals was not permitted under the project license. This may also not be practical as only limited amounts of blood can be taken each time, providing insufficient quantity of serum/plasma for down-stream analysis.

In summary, further work is required to elucidate the extent of BMDCs and precursors contribution to the growth of peripheral tumours. In addition identifying the role of specific molecules that may play a key role in cancer progression is needed, to increase our understanding of the complex tumour-stroma interactions.

### 6.2. Summary of future work

A summary of proposed future work to follow-up on work presented in this thesis is listed below:

- Establish methodologies to quantify the effects of anti-cancer therapy on the *in vivo* bone marrow vasculature.
- Visualise the temporal-spatial relation ship of disseminated tumour cells, osteoblasts and vascular endothelial cells in bone using immunofluorescence (+/- therapeutic modification).
- Obtain histological samples from patients with breast cancer bone metastasis to validate whether breast cancer micrometastases are indeed found in close proximity to both endosteal and vascular niches. Ideally these samples would include biopsies from BP-treated patients.

- Establish effects of bone-targeted agents on tumour growth promoting BMDCs and precursor populations using a variety of model systems (*e.g.* immunocompromised vs. immunocompetent, pre- vs. post menopausal, male vs. female).
- Establish whether tumour cell homing to bone and metastatic outgrowth differs between subclones of breast cancer cells with differential molecular profile (*e.g.* a GM-CSF$^{high}$ vs GM-CSF$^{low}$ breast cancer cell) and whether this is affected by a ZOL pre-treated BME (this is part of an on-going collaboration with Dr. McAllister's laboratory in Boston, USA).
- Assess effects of bone-targeted agents on circulating cytokines, chemokines and growth factors (*e.g.* LOX, OPN, VEGF, GM-CSF etc.) associated with tumour growth and BMDCs mobilisation using a variety of model systems (*e.g.* immunocompromised vs. immunocompetent, pre- vs. post menopausal, male vs. female).
- Obtain clinical samples including blood, plasma, bone marrow or histopathological slides) from clinical trials (*e.g.* the AZURE trial) to determine effect of ZOL on bone marrow cell populations in the adjuvant setting.
- Establish the effects of CBZ alone or in combination in immunocompetent mouse models and assess how the CBZ-mediated alterations of the BME may affect establishment and progression of breast cancer bone metastasis.
- Determine response of the *in vivo* BME to CBZ in combination with other therapeutic agents (*e.g.* bisphosphonates, chemotherapy, denosumab etc.) and potential consequences in xenograft models of breast cancer bone metastasis.
- Establish effects of combination therapy (DOX/ZOL) on BMDC recruitment to periphral tumours in greater detail.
- Establish the role of primary-tumour derived systemic factors (*e.g.* OPN) on tumour cell dormancy and metastatic outgrowth in bone.

## 6.3. Conclusion

This thesis provides the first detailed characterisation of the acute and short-term effects of the bisphosphonate Zoledronic acid (ZOL) and the tyrosine kinase inhibitor Cabozantinib (CBZ) on the naïve *in vivo* bone microenvironment (BME) and highlights the importance of the BME in mediating response to anti-cancer therapy. In addition I demonstrate that breast cancer cells appear to preferentially localise to trabecular bone surfaces that are rich in osteoblasts, which could be modulated when tumour cells arrive in a therapeutically altered microenvironment. An increased understanding of the role of osteoblasts in the early stages of bone metastasis will therefore aid in providing new therapeutic approaches for inhibiting the disease progression towards osteolytic bone disease, which still remains incurable. I also performed the first studies demonstrating that modification of the BME is not sufficient to supress peripheral breast cancer re-growth following cessation of combination therapy, suggesting that both the tumour and microenvironment need to be targeted for successful anti-cancer therapy.

Further work is required to elucidate the contribution of the BME to peripheral breast cancer growth. Increasing our understanding of the complex tumour-microenvironment crosstalk will ultimately help to advance current treatment options as well as the design of novel therapeutic approaches for both primary and advanced breast cancer.

## 7. References


[1] J. Ferlay, E. Steliarova-Foucher, J. Lortet-Tieulent, S. Rosso, J.W. Coebergh, H. Comber, D. Forman, F. Bray, Cancer incidence and mortality patterns in Europe: estimates for 40 countries in 2012, Eur J Cancer 49(6) (2013) 1374-403.

[2] CancerResearchUK, http://www.cancerresearchuk.org/health-professional/cancer-statistics/statistics-by-cancer-type/breast-cancer/survival - heading-Two. (Accessed 17.02.2016.

[3] R.E. Coleman, Metastatic bone disease: clinical features, pathophysiology and treatment strategies, Cancer Treat Rev 27(3) (2001) 165-76.

[4] CancerResearchUK, http://www.cancerresearchuk.org/health-professional/cancer-statistics/statistics-by-cancer-type/breast-cancer/survival - heading-Three. (Accessed 17.02.2016.

[5] M.J. Bissell, D. Radisky, Putting tumours in context, Nat Rev Cancer 1(1) (2001) 46-54.

[6] J. Folkman, The role of angiogenesis in tumor growth, Semin Cancer Biol 3(2) (1992) 65-71.

[7] J. Folkman, Proceedings: Tumor angiogenesis factor, Cancer Res 34(8) (1974) 2109-13.

[8] D. Hanahan, R.A. Weinberg, Hallmarks of cancer: the next generation, Cell 144(5) (2011) 646-74.

[9] D. Hanahan, R.A. Weinberg, The hallmarks of cancer, Cell 100(1) (2000) 57-70.

[10] D. Hanahan, L.M. Coussens, Accessories to the crime: functions of cells recruited to the tumor microenvironment, Cancer Cell 21(3) (2012) 309-22.

[11] S.S. McAllister, R.A. Weinberg, The tumour-induced systemic environment as a critical regulator of cancer progression and metastasis, Nat Cell Biol 16(8) (2014) 717-27.

[12] F.R. Balkwill, M. Capasso, T. Hagemann, The tumor microenvironment at a glance, J Cell Sci 125(Pt 23) (2012) 5591-6.

[13] R. Kalluri, M. Zeisberg, Fibroblasts in cancer, Nat Rev Cancer 6(5) (2006) 392-401.

[14] Y. Kojima, A. Acar, E.N. Eaton, K.T. Mellody, C. Scheel, I. Ben-Porath, T.T. Onder, Z.C. Wang, A.L. Richardson, R.A. Weinberg, A. Orimo, Autocrine TGF-β and stromal cell-derived factor-1 (SDF-1) signaling drives the evolution of tumor-promoting mammary stromal myofibroblasts, Proceedings of the National Academy of Sciences of the United States of America 107(46) (2010) 20009-20014.

[15] E.L. Spaeth, J.L. Dembinski, A.K. Sasser, K. Watson, A. Klopp, B. Hall, M. Andreeff, F. Marini, Mesenchymal Stem Cell Transition to Tumor-Associated Fibroblasts Contributes to Fibrovascular Network Expansion and Tumor Progression, PLoS ONE 4(4) (2009) e4992.

[16] R. Montesano, K. Matsumoto, T. Nakamura, L. Orci, Identification of a fibroblast-derived epithelial morphogen as hepatocyte growth factor, Cell 67(5) (1991) 901-8.

[17] K.S. Siveen, G. Kuttan, Role of macrophages in tumour progression, Immunology Letters 123(2) (2009) 97-102.

[18] E.Y. Lin, J.-F. Li, L. Gnatovskiy, Y. Deng, L. Zhu, D.A. Grzesik, H. Qian, X.-n. Xue, J.W. Pollard, Macrophages Regulate the Angiogenic Switch in a Mouse Model of Breast Cancer, Cancer Research 66(23) (2006) 11238-11246.

[19] E.Y. Lin, J.W. Pollard, Tumor-Associated Macrophages Press the Angiogenic Switch in Breast Cancer, Cancer Research 67(11) (2007) 5064-5066.

[20] B. Qian, Y. Deng, J.H. Im, R.J. Muschel, Y. Zou, J. Li, R.A. Lang, J.W. Pollard, A Distinct Macrophage Population Mediates Metastatic Breast Cancer Cell Extravasation, Establishment and Growth, PLoS ONE 4(8) (2009) e6562.

[21] C.B. Williams, E.S. Yeh, A.C. Soloff, Tumor-associated macrophages: unwitting accomplices in breast cancer malignancy, Npj Breast Cancer 2 (2016) 15025.

[22] M. McCourt, J.H. Wang, S. Sookhai, H.P. Redmond, Activated human neutrophils release hepatocyte growth factor/scatter factor, European Journal of Surgical Oncology 27(4) 396-403.

[23] G. Bergers, R. Brekken, G. McMahon, T.H. Vu, T. Itoh, K. Tamaki, K. Tanzawa, P. Thorpe, S. Itohara, Z. Werb, D. Hanahan, Matrix metalloproteinase-9 triggers the angiogenic switch during carcinogenesis, Nat Cell Biol 2 (2000).

[24] G. Bergers, L.E. Benjamin, Tumorigenesis and the angiogenic switch, Nat Rev Cancer 3(6) (2003) 401-410.

[25] J. Folkman, Angiogenesis: an organizing principle for drug discovery?, Nature reviews. Drug discovery 6(4) (2007) 273-86.

[26] B.S. Wiseman, Z. Werb, Stromal effects on mammary gland development and breast cancer, Science 296(5570) (2002) 1046-9.

[27] S.S. McAllister, A.M. Gifford, A.L. Greiner, S.P. Kelleher, M.P. Saelzler, T.A. Ince, F. Reinhardt, L.N. Harris, B.L. Hylander, E.A. Repasky, R.A. Weinberg, Systemic endocrine instigation of indolent tumor growth requires osteopontin, Cell 133(6) (2008) 994-1005.

[28] R.N. Kaplan, R.D. Riba, S. Zacharoulis, A.H. Bramley, L. Vincent, C. Costa, D.D. MacDonald, D.K. Jin, K. Shido, S.A. Kerns, Z. Zhu, D. Hicklin, Y. Wu, J.L. Port, N. Altorki, E.R. Port, D. Ruggero, S.V. Shmelkov, K.K. Jensen, S. Rafii, D. Lyden, VEGFR1-positive haematopoietic bone marrow progenitors initiate the pre-metastatic niche, Nature 438(7069) (2005) 820-7.

[29] T.R. Cox, R.M. Rumney, E.M. Schoof, L. Perryman, A.M. Høye, A. Agrawal, D. Bird, N.A. Latif, H. Forrest, H.R. Evans, I.D. Huggins, G. Lang, R. Linding, A. Gartland, J.T. Erler, The hypoxic cancer secretome induces pre-metastatic bone lesions through lysyl oxidase, Nature 522(7554) (2015) 106-10.

[30] G.C. Schatteman, M. Dunnwald, C. Jiao, Biology of bone marrow-derived endothelial cell precursors, Am J Physiol Heart Circ Physiol 292(1) (2007) H1-18.

[31] Y. Shiozawa, A.M. Havens, K.J. Pienta, R.S. Taichman, The bone marrow niche: habitat to hematopoietic and mesenchymal stem cells, and unwitting host to molecular parasites, Leukemia 22(5) (2008) 941-50.

[32] I. Petit, M. Szyper-Kravitz, A. Nagler, M. Lahav, A. Peled, L. Habler, T. Ponomaryov, R.S. Taichman, F. Arenzana-Seisdedos, N. Fujii, J. Sandbank, D. Zipori, T. Lapidot, G-CSF induces stem cell mobilization by decreasing bone marrow SDF-1 and up-regulating CXCR4, Nat Immunol 3(7) (2002) 687-694.

[33] D. Lyden, K. Hattori, S. Dias, C. Costa, P. Blaikie, L. Butros, A. Chadburn, B. Heissig, W. Marks, L. Witte, Y. Wu, D. Hicklin, Z. Zhu, N.R. Hackett, R.G. Crystal, M.A.S. Moore, K.A. Hajjar, K. Manova, R. Benezra, S. Rafii, Impaired recruitment of bone-marrow-derived endothelial and hematopoietic precursor cells blocks tumor angiogenesis and growth, Nat Med 7(11) (2001) 1194-1201.

[34] K. Hattori, B. Heissig, Y. Wu, S. Dias, R. Tejada, B. Ferris, D.J. Hicklin, Z. Zhu, P. Bohlen, L. Witte, J. Hendrikx, N.R. Hackett, R.G. Crystal, M.A.S. Moore, Z. Werb, D. Lyden, S. Rafii, Placental growth factor reconstitutes hematopoiesis by recruiting VEGFR1+ stem cells from bone-marrow microenvironment, Nat Med 8(8) (2002) 841-849.

[35] T. Zhang, Y.W. Lee, Y.F. Rui, T.Y. Cheng, X.H. Jiang, G. Li, Bone marrow-derived mesenchymal stem cells promote growth and angiogenesis of breast and prostate tumors, Stem Cell Research & Therapy 4(3) (2013) 70-70.

[36] A. Mantovani, P. Allavena, S. Sozzani, A. Vecchi, M. Locati, A. Sica, Chemokines in the recruitment and shaping of the leukocyte infiltrate of tumors, Seminars in Cancer Biology 14(3) (2004) 155-160.

[37] C. Melani, S. Sangaletti, F.M. Barazzetta, Z. Werb, M.P. Colombo, Amino-biphosphonate-mediated MMP-9 inhibition breaks the tumor-bone marrow axis responsible for myeloid-derived suppressor cell expansion and macrophage infiltration in tumor stroma, Cancer Res 67(23) (2007) 11438-46.

[38] T.L. Rogers, N. Wind, R. Hughes, F. Nutter, H.K. Brown, I. Vasiliadou, P.D. Ottewell, I. Holen, Macrophages as potential targets for zoledronic acid outside the skeleton-evidence from in vitro and in vivo models, Cell Oncol (Dordr) 36(6) (2013) 505-14.

[39] S. Junankar, G. Shay, J. Jurczyluk, N. Ali, J. Down, N. Pocock, A. Parker, A. Nguyen, S. Sun, B. Kashemirov, C.E. McKenna, P.I. Croucher, A. Swarbrick, K. Weilbaecher, T.G. Phan, M.J. Rogers, Real-time intravital imaging establishes tumor-associated macrophages as the extraskeletal target of bisphosphonate action in cancer, Cancer Discov 5(1) (2015) 35-42.

[40] J.W. Pollard, Tumour-educated macrophages promote tumour progression and metastasis, Nat Rev Cancer 4(1) (2004) 71-78.

[41] L. Yang, C.M. Edwards, G.R. Mundy, Gr-1+CD11b+ myeloid-derived suppressor cells: formidable partners in tumor metastasis, J Bone Miner Res 25(8) (2010) 1701-6.

[42] R.N. Kaplan, B. Psaila, D. Lyden, Bone marrow cells in the 'pre-metastatic niche': within bone and beyond, Cancer Metastasis Rev 25(4) (2006) 521-9.

[43] C.S. Simmonds, C.S. Kovacs, Role of parathyroid hormone (PTH) and PTH-related protein (PTHrP) in regulating mineral homeostasis during fetal development, Crit Rev Eukaryot Gene Expr 20(3) (2010) 235-73.

[44] C.S. Kovacs, Vitamin D in pregnancy and lactation: maternal, fetal, and neonatal outcomes from human and animal studies, Am J Clin Nutr 88(2) (2008) 520S-528S.

[45] C.S. Kovacs, C.L. Ho-Pao, J.L. Hunzelman, B. Lanske, J. Fox, J.G. Seidman, C.E. Seidman, H.M. Kronenberg, Regulation of murine fetal-placental calcium metabolism by the calcium-sensing receptor, J Clin Invest 101(12) (1998) 2812-20.

[46] L. Ardeshirpour, P. Dann, D.J. Adams, T. Nelson, J. VanHouten, M.C. Horowitz, J.J. Wysolmerski, Weaning triggers a decrease in receptor activator of nuclear factor-kappaB ligand expression, widespread osteoclast apoptosis, and rapid recovery of bone mass after lactation in mice, Endocrinology 148(8) (2007) 3875-86.

[47] R.M. Locklin, S. Khosla, R.T. Turner, B.L. Riggs, Mediators of the biphasic responses of bone to intermittent and continuously administered parathyroid hormone, Journal of Cellular Biochemistry 89(1) (2003) 180-190.

[48] A.L. Boskey, Bone composition: relationship to bone fragility and antiosteoporotic drug effects, Bonekey Rep 2 (2013) 447.

[49] G.A. Rodan, Introduction to bone biology, Bone 13 Suppl 1 (1992) S3-6.

[50] C.T. Jordan, I.R. Lemischka, Clonal and systemic analysis of long-term hematopoiesis in the mouse, Genes Dev 4(2) (1990) 220-32.

[51] A.P. Kusumbe, S.K. Ramasamy, R.H. Adams, Coupling of angiogenesis and osteogenesis by a specific vessel subtype in bone, Nature 507(7492) (2014) 323-8.

[52] T. Itkin, S. Gur-Cohen, J.A. Spencer, A. Schajnovitz, S.K. Ramasamy, A.P. Kusumbe, G. Ledergor, Y. Jung, I. Milo, M.G. Poulos, A. Kalinkovich, A. Ludin, O. Kollet, G. Shakhar, J.M. Butler, S. Rafii, R.H. Adams, D.T. Scadden, C.P. Lin, T. Lapidot, Distinct bone marrow blood vessels differentially regulate haematopoiesis, Nature (2016).

[53] C. Maes, T. Kobayashi, M.K. Selig, S. Torrekens, S.I. Roth, S. Mackem, G. Carmeliet, H.M. Kronenberg, Osteoblast precursors, but not mature osteoblasts, move into developing and fractured bones along with invading blood vessels, Dev Cell 19(2) (2010) 329-44.

[54] T. Mizoguchi, S. Pinho, J. Ahmed, Y. Kunisaki, M. Hanoun, A. Mendelson, N. Ono, H.M. Kronenberg, P.S. Frenette, Osterix marks distinct waves of primitive and definitive stromal progenitors during bone marrow development, Dev Cell 29(3) (2014) 340-9.

[55] H.R. Dudley, D. Spiro, THE FINE STRUCTURE OF BONE CELLS, The Journal of Biophysical and Biochemical Cytology 11(3) (1961) 627-649.

[56] H. Nakamura, Morphology, Function, and Differentiation of Bone Cells, Journal of Hard Tissue Biology 16(1) (2007) 15-22.

[57] E. Bonucci, G. Gherardi, Osteocyte ultrastructure in renal osteodystrophy, Virchows Archiv A 373(3) 213-231.

[58] R. Baron, L. Neff, D. Louvard, P.J. Courtoy, Cell-mediated extracellular acidification and bone resorption: evidence for a low pH in resorbing lacunae and localization of a 100-kD lysosomal membrane protein at the osteoclast ruffled border, J Cell Biol 101(6) (1985) 2210-22.

[59] J.W. Penn, A.O. Grobbelaar, K.J. Rolfe, The role of the TGF-β family in wound healing, burns and scarring: a review, International Journal of Burns and Trauma 2(1) (2012) 18-28.

[60] V.S. Rajkumar, X. Shiwen, M. Bostrom, P. Leoni, J. Muddle, M. Ivarsson, B. Gerdin, C.P. Denton, G. Bou-Gharios, C.M. Black, D.J. Abraham, Platelet-Derived Growth Factor-β Receptor Activation Is Essential for Fibroblast and Pericyte Recruitment during Cutaneous Wound Healing, The American Journal of Pathology 169(6) (2006) 2254-2265.

[61] L.M. Cheng, Y. Yan, Q.R. Wang, Expression of hematopoietic inhibitory factors in mouse fibroblasts, macrophages and endothelial cells, Cell Biology International 27(9) (2003) 739-745.

[62] D. Brouty‐Boyé, C. Doucet, D. Clay, M.C.L. Bousse‐Kerdiles, T.J. Lampidis, B. Azzarone, Phenotypic diversity in human fibroblasts from myelometaplasic and non‐myelometaplasic hematopoietic tissues, International Journal of Cancer 76(5) (1998) 767-773.

[63] F. Rougier, F. Dupuis, Y. Denizot, Human bone marrow fibroblasts - an overview of their characterization, proliferation and inflammatory mediator production, Hematology and Cell Therapy 38(3) (1996) 241-246.

[64] R.S. Watnick, The Role of the Tumor Microenvironment in Regulating Angiogenesis, Cold Spring Harbor Perspectives in Medicine 2(12) (2012).

[65] H.M. Frost, Bone dynamics in metabolic bone disease, J Bone Joint Surg Am 48(6) (1966) 1192-203.

[66] G.A. Rodan, T.J. Martin, Role of osteoblasts in hormonal control of bone resorption—A hypothesis, Calcified Tissue International 33(1) (1981) 349-351.

[67] H. Yasuda, N. Shima, N. Nakagawa, K. Yamaguchi, M. Kinosaki, S. Mochizuki, A. Tomoyasu, K. Yano, M. Goto, A. Murakami, E. Tsuda, T. Morinaga, K. Higashio, N. Udagawa, N. Takahashi, T. Suda, Osteoclast differentiation factor is a ligand for osteoprotegerin/osteoclastogenesis-inhibitory factor and is identical to TRANCE/RANKL, Proc Natl Acad Sci U S A 95(7) (1998) 3597-602.

[68] H. Takayanagi, S. Kim, T. Koga, H. Nishina, M. Isshiki, H. Yoshida, A. Saiura, M. Isobe, T. Yokochi, J. Inoue, E.F. Wagner, T.W. Mak, T. Kodama, T. Taniguchi, Induction and activation of the transcription factor NFATc1 (NFAT2) integrate RANKL signaling in terminal differentiation of osteoclasts, Dev Cell 3(6) (2002) 889-901.

[69] D.L. Lacey, E. Timms, H.L. Tan, M.J. Kelley, C.R. Dunstan, T. Burgess, R. Elliott, A. Colombero, G. Elliott, S. Scully, H. Hsu, J. Sullivan, N. Hawkins, E. Davy, C. Capparelli, A. Eli, Y.X. Qian, S. Kaufman, I. Sarosi, V. Shalhoub, G. Senaldi, J. Guo, J. Delaney, W.J. Boyle, Osteoprotegerin ligand is a cytokine that regulates osteoclast differentiation and activation, Cell 93(2) (1998) 165-76.

[70] H. Hsu, D.L. Lacey, C.R. Dunstan, I. Solovyev, A. Colombero, E. Timms, H.L. Tan, G. Elliott, M.J. Kelley, I. Sarosi, L. Wang, X.Z. Xia, R. Elliott, L. Chiu, T. Black, S. Scully, C. Capparelli, S. Morony, G. Shimamoto, M.B. Bass, W.J. Boyle, Tumor necrosis factor receptor family member RANK mediates osteoclast differentiation and activation induced by osteoprotegerin ligand, Proc Natl Acad Sci U S A 96(7) (1999) 3540-5.

[71] M.C. Horowitz, Y. Xi, K. Wilson, M.A. Kacena, Control of osteoclastogenesis and bone resorption by members of the TNF family of receptors and ligands, Cytokine Growth Factor Rev 12(1) (2001) 9-18.

[72] K. Fuller, B. Wong, S. Fox, Y. Choi, T.J. Chambers, TRANCE is necessary and sufficient for osteoblast-mediated activation of bone resorption in osteoclasts, J Exp Med 188(5) (1998) 997-1001.

[73] A.R. Guntur, C.J. Rosen, IGF-1 regulation of key signaling pathways in bone, Bonekey Rep 2 (2013) 437.

[74] L.J. Raggatt, N.C. Partridge, Cellular and molecular mechanisms of bone remodeling, J Biol Chem 285(33) (2010) 25103-8.

[75] H. Yoshida, S. Hayashi, T. Kunisada, M. Ogawa, S. Nishikawa, H. Okamura, T. Sudo, L.D. Shultz, The murine mutation osteopetrosis is in the coding region of the macrophage colony stimulating factor gene, Nature 345(6274) (1990) 442-4.

[76] J. Gohda, T. Akiyama, T. Koga, H. Takayanagi, S. Tanaka, J. Inoue, RANK-mediated amplification of TRAF6 signaling leads to NFATc1 induction during osteoclastogenesis, EMBO J 24(4) (2005) 790-9.

[77] A.M. Parfitt, The coupling of bone formation to bone resorption: a critical analysis of the concept and of its relevance to the pathogenesis of osteoporosis, Metab Bone Dis Relat Res 4(1) (1982) 1-6.

[78] C. Zhao, N. Irie, Y. Takada, K. Shimoda, T. Miyamoto, T. Nishiwaki, T. Suda, K. Matsuo, Bidirectional ephrinB2-EphB4 signaling controls bone homeostasis, Cell Metabolism 4(2) (2006) 111-121.

[79] J. Ryu, H.J. Kim, E.-J. Chang, H. Huang, Y. Banno, H.-H. Kim, Sphingosine 1-phosphate as a regulator of osteoclast differentiation and osteoclast–osteoblast coupling, The EMBO Journal 25(24) (2006) 5840-5851.

[80] M.A. Kacena, R.A. Shivdasani, K. Wilson, Y. Xi, N. Troiano, A. Nazarian, C.M. Gundberg, M.L. Bouxsein, J.A. Lorenzo, M.C. Horowitz, Megakaryocyte-osteoblast interaction revealed in mice deficient in transcription factors GATA-1 and NF-E2, J Bone Miner Res 19(4) (2004) 652-60.

[81] W.A. Ciovacco, C.G. Goldberg, A.F. Taylor, J.M. Lemieux, M.C. Horowitz, H.J. Donahue, M.A. Kacena, The role of gap junctions in megakaryocyte-mediated osteoblast proliferation and differentiation, Bone 44(1) (2009) 80-6.

[82] J.M. Lemieux, M.C. Horowitz, M.A. Kacena, Involvement of integrins alpha(3)beta(1) and alpha(5)beta(1) and glycoprotein IIb in megakaryocyte-induced osteoblast proliferation, J Cell Biochem 109(5) (2010) 927-32.

[83] P.I. Croucher, M.M. McDonald, T.J. Martin, Bone metastasis: the importance of the neighbourhood, Nat Rev Cancer 16(6) (2016) 373-386.

[84] K.J. Luzzi, I.C. MacDonald, E.E. Schmidt, N. Kerkvliet, V.L. Morris, A.F. Chambers, A.C. Groom, Multistep Nature of Metastatic Inefficiency : Dormancy of Solitary Cells after Successful Extravasation and Limited Survival of Early Micrometastases, The American Journal of Pathology 153(3) (1998) 865-873.

[85] N. Wang, F. Docherty, H.K. Brown, K. Reeves, A. Fowles, M. Lawson, P.D. Ottewell, I. Holen, P.I. Croucher, C.L. Eaton, Mitotic quiescence, but not unique “stemness,” marks the phenotype of bone metastasis-initiating cells in prostate cancer, The FASEB Journal 29(8) (2015) 3141-3150.

[86] S. Paget, The distribution of secondary growths in cancer of the breast., The Lancet (1889) 571--573.

[87] E. Grimaud, L. Soubigou, S. Couillaud, P. Coipeau, A. Moreau, N. Passuti, F. Gouin, F. Redini, D. Heymann, Receptor Activator of Nuclear Factor κB Ligand (RANKL)/Osteoprotegerin (OPG) Ratio Is Increased in Severe Osteolysis, The American Journal of Pathology 163(5) (2003) 2021-2031.

[88] Z. Saidak, C. Boudot, R. Abdoune, L. Petit, M. Brazier, R. Mentaverri, S. Kamel, Extracellular calcium promotes the migration of breast cancer cells through the activation of the calcium sensing receptor, Exp Cell Res 315(12) (2009) 2072-80.

[89] C.M. van Golen, T.S. Schwab, B. Kim, M.E. Soules, S. Su Oh, K. Fung, K.L. van Golen, E.L. Feldman, Insulin-Like Growth Factor-I Receptor Expression Regulates Neuroblastoma Metastasis to Bone, Cancer Research 66(13) (2006) 6570-6578.

[90] H.K. Brown, P.D. Ottewell, C.A. Evans, I. Holen, Location matters: osteoblast and osteoclast distribution is modified by the presence and proximity to breast cancer cells in vivo, Clin Exp Metastasis 29(8) (2012) 927-38.

[91] S. Malladi, Danilo G. Macalinao, X. Jin, L. He, H. Basnet, Y. Zou, E. de Stanchina, J. Massagué, Metastatic Latency and Immune Evasion through Autocrine Inhibition of WNT, Cell 165(1) (2016) 45-60.

[92] Z.S. Templeton, W.-R. Lie, W. Wang, Y. Rosenberg-Hasson, R.V. Alluri, J.S. Tamaresis, M.H. Bachmann, K. Lee, W.J. Maloney, C.H. Contag, B.L. King, Breast Cancer Cell Colonization of the Human Bone Marrow Adipose Tissue Niche(), Neoplasia (New York, N.Y.) 17(12) (2015) 849-861.

[93] J.L. Zalucha, Y. Jung, J. Joseph, J. Wang, J.E. Berry, Y. Shiozawa, R.S. Taichman, The Role of Osteoclasts in Early Dissemination of Prostate Cancer Tumor Cells, J Cancer Stem Cell Res 3 (2015).

[94] H. Wang, C. Yu, X. Gao, T. Welte, A.M. Muscarella, L. Tian, H. Zhao, Z. Zhao, S. Du, J. Tao, B. Lee, T.F. Westbrook, S.T. Wong, X. Jin, J.M. Rosen, C.K. Osborne, X.H. Zhang, The osteogenic niche promotes early-stage bone colonization of disseminated breast cancer cells, Cancer Cell 27(2) (2015) 193-210.

[95] Y. Shiozawa, E.A. Pedersen, A.M. Havens, Y. Jung, A. Mishra, J. Joseph, J.K. Kim, L.R. Patel, C. Ying, A.M. Ziegler, M.J. Pienta, J. Song, J. Wang, R.D. Loberg, P.H. Krebsbach, K.J. Pienta, R.S. Taichman, Human prostate cancer metastases target the hematopoietic stem cell niche to establish footholds in mouse bone marrow, J Clin Invest 121(4) (2011) 1298-312.

[96] Y. Shiozawa, E.A. Pedersen, L.R. Patel, A.M. Ziegler, A.M. Havens, Y. Jung, J. Wang, S. Zalucha, R.D. Loberg, K.J. Pienta, R.S. Taichman, GAS6/AXL axis regulates prostate cancer invasion, proliferation, and survival in the bone marrow niche, Neoplasia 12(2) (2010) 116-27.

[97] S. Braun, F.D. Vogl, B. Naume, W. Janni, M.P. Osborne, R.C. Coombes, G. Schlimok, I.J. Diel, B. Gerber, G. Gebauer, J.Y. Pierga, C. Marth, D. Oruzio, G. Wiedswang, E.F. Solomayer, G. Kundt, B. Strobl, T. Fehm, G.Y. Wong, J. Bliss, A. Vincent-Salomon, K. Pantel, A pooled analysis of bone marrow micrometastasis in breast cancer, N Engl J Med 353(8) (2005) 793-802.

[98] B. Costa-Silva, N.M. Aiello, A.J. Ocean, S. Singh, H. Zhang, B.K. Thakur, A. Becker, A. Hoshino, M.T. Mark, H. Molina, J. Xiang, T. Zhang, T.-M. Theilen, G. Garcia-Santos, C. Williams, Y. Ararso, Y. Huang, G. Rodrigues, T.-L. Shen, K.J. Labori, I.M.B. Lothe, E.H. Kure, J. Hernandez, A. Doussot, S.H. Ebbesen, P.M. Grandgenett, M.A. Hollingsworth, M. Jain, K. Mallya, S.K. Batra, W.R. Jarnagin, R.E. Schwartz, I. Matei, H. Peinado, B.Z. Stanger, J. Bromberg, D. Lyden, Pancreatic cancer exosomes initiate pre-metastatic niche formation in the liver, Nat Cell Biol 17(6) (2015) 816-826.

[99] H.S. Kuznetsov, T. Marsh, B.A. Markens, Z. Castaño, A. Greene-Colozzi, S.A. Hay, V.E. Brown, A.L. Richardson, S. Signoretti, E.M. Battinelli, S.S. McAllister, Identification of Luminal Breast Cancers that Establish a Tumor Supportive Macroenvironment Defined by Pro-Angiogenic Platelets and Bone Marrow Derived Cells, Cancer Discovery (2012).

[100] J.M. Ubellacker, S.S. McAllister, The unresolved role of systemic factors in bone metastasis, Journal of Bone Oncology.

[101] C.M. Ghajar, H. Peinado, H. Mori, I.R. Matei, K.J. Evason, H. Brazier, D. Almeida, A. Koller, K.A. Hajjar, D.Y. Stainier, E.I. Chen, D. Lyden, M.J. Bissell, The perivascular niche regulates breast tumour dormancy, Nat Cell Biol 15(7) (2013) 807-17.

[102] L.M. Calvi, Osteoblastic activation in the hematopoietic stem cell niche, Ann N Y Acad Sci 1068 (2006) 477-88.

[103] L.M. Calvi, G.B. Adams, K.W. Weibrecht, J.M. Weber, D.P. Olson, M.C. Knight, R.P. Martin, E. Schipani, P. Divieti, F.R. Bringhurst, L.A. Milner, H.M. Kronenberg, D.T. Scadden, Osteoblastic cells regulate the haematopoietic stem cell niche, Nature 425(6960) (2003) 841-6.

[104] J. Zhang, C. Niu, L. Ye, H. Huang, X. He, W.-G. Tong, J. Ross, J. Haug, T. Johnson, J.Q. Feng, S. Harris, L.M. Wiedemann, Y. Mishina, L. Li, Identification of the haematopoietic stem cell niche and control of the niche size, Nature 425(6960) (2003) 836-841.

[105] R.S. Taichman, Blood and bone: two tissues whose fates are intertwined to create the hematopoietic stem-cell niche, Blood 105(7) (2005) 2631-9.

[106] B. Psaila, D. Lyden, I. Roberts, Megakaryocytes, malignancy and bone marrow vascular niches, J Thromb Haemost 10(2) (2012) 177-88.

[107] G.B. Adams, K.T. Chabner, I.R. Alley, D.P. Olson, Z.M. Szczepiorkowski, M.C. Poznansky, C.H. Kos, M.R. Pollak, E.M. Brown, D.T. Scadden, Stem cell engraftment at the endosteal niche is specified by the calcium-sensing receptor, Nature 439(7076) (2006) 599-603.

[108] T. Ponomaryov, A. Peled, I. Petit, R.S. Taichman, L. Habler, J. Sandbank, F. Arenzana-Seisdedos, A. Magerus, A. Caruz, N. Fujii, A. Nagler, M. Lahav, M. Szyper-Kravitz, D. Zipori, T. Lapidot, Induction of the chemokine stromal-derived factor-1 following DNA damage improves human stem cell function, Journal of Clinical Investigation 106(11) (2000) 1331-1339.

[109] A. Muller, B. Homey, H. Soto, N. Ge, D. Catron, M.E. Buchanan, T. McClanahan, E. Murphy, W. Yuan, S.N. Wagner, J.L. Barrera, A. Mohar, E. Verastegui, A. Zlotnik, Involvement of chemokine receptors in breast cancer metastasis, Nature 410(6824) (2001) 50-56.

[110] H.E. Broxmeyer, C.M. Orschell, D.W. Clapp, G. Hangoc, S. Cooper, P.A. Plett, W.C. Liles, X. Li, B. Graham-Evans, T.B. Campbell, G. Calandra, G. Bridger, D.C. Dale, E.F. Srour, Rapid mobilization of murine and human hematopoietic stem and progenitor cells with AMD3100, a CXCR4 antagonist, The Journal of Experimental Medicine 201(8) (2005) 1307-1318.

[111] Y. Kang, P.M. Siegel, W. Shu, M. Drobnjak, S.M. Kakonen, C. Cordón-Cardo, T.A. Guise, J. Massagué, A multigenic program mediating breast cancer metastasis to bone, Cancer Cell 3(6) 537-549.

[112] T.T. Price, M.L. Burness, A. Sivan, M.J. Warner, R. Cheng, C.H. Lee, L. Olivere, K. Comatas, J. Magnani, H. Kim Lyerly, Q. Cheng, C.M. McCall, D.A. Sipkins, Dormant breast cancer micrometastases reside in specific bone marrow niches that regulate their transit to and from bone, Science Translational Medicine 8(340) (2016) 340ra73-340ra73.

[113] P.D. Ottewell, The role of osteoblasts in bone metastasis, Journal of Bone Oncology.

[114] J.M. Butler, H. Kobayashi, S. Rafii, Instructive role of the vascular niche in promoting tumour growth and tissue repair by angiocrine factors, Nat Rev Cancer 10(2) (2010) 138-146.

[115] M.A. Lawson, M.M. McDonald, N. Kovacic, W. Hua Khoo, R.L. Terry, J. Down, W. Kaplan, J. Paton-Hough, C. Fellows, J.A. Pettitt, T. Neil Dear, E. Van Valckenborgh, P.A. Baldock, M.J. Rogers, C.L. Eaton, K. Vanderkerken, A.R. Pettit, J.M.W. Quinn, A.C.W. Zannettino, T.G. Phan, P.I. Croucher, Osteoclasts control reactivation of dormant myeloma cells by remodelling the endosteal niche, Nat Commun 6 (2015).

[116] J.A. Aguirre-Ghiso, Models, mechanisms and clinical evidence for cancer dormancy, Nature reviews. Cancer 7(11) (2007) 834-846.

[117] Q. Lewis, D.O.a.I.H. Penelope, Bone Metastasis: Molecular Mechanisms Implicated in Tumour Cell Dormancy in Breast and Prostate Cancer, Current Cancer Drug Targets 15(6) (2015) 469-480.

[118] X. Lu, E. Mu, Y. Wei, S. Riethdorf, Q. Yang, M. Yuan, J. Yan, Y. Hua, B.J. Tiede, X. Lu, B.G. Haffty, K. Pantel, J. Massagué, Y. Kang, VCAM-1 promotes osteolytic expansion of indolent bone micrometastasis of breast cancer by engaging α4β1-positive osteoclast progenitors, Cancer cell 20(6) (2011) 701-714.

[119] O. Straume, T. Shimamura, M.J.G. Lampa, J. Carretero, A.M. Øyan, D. Jia, C.L. Borgman, M. Soucheray, S.R. Downing, S.M. Short, S.-Y. Kang, S. Wang, L. Chen, K. Collett, I. Bachmann, K.-K. Wong, G.I. Shapiro, K.H. Kalland, J. Folkman, R.S. Watnick, L.A. Akslen, G.N. Naumov, Suppression of heat shock protein 27 induces long-term dormancy in human breast cancer, Proceedings of the National Academy of Sciences of the United States of America 109(22) (2012) 8699-8704.

[120] A. Zaslavsky, K.-H. Baek, R.C. Lynch, S. Short, J. Grillo, J. Folkman, J.E. Italiano, S. Ryeom, Platelet-derived thrombospondin-1 is a critical negative regulator and potential biomarker of angiogenesis, Blood 115(22) (2010) 4605-4613.

[121] S.M. Käkönen, G.R. Mundy, Mechanisms of osteolytic bone metastases in breast carcinoma, Cancer 97(3 Suppl) (2003) 834-9.

[122] R.J. Thomas, T.A. Guise, J.J. Yin, J. Elliott, N.J. Horwood, T.J. Martin, M.T. Gillespie, Breast Cancer Cells Interact with Osteoblasts to Support Osteoclast Formation, Endocrinology 140(10) (1999) 4451-4458.

[123] M. Bendre, D.C. Montague, T. Peery, N.S. Akel, D. Gaddy, L.J. Suva, Interleukin-8 stimulation of osteoclastogenesis and bone resorption is a mechanism for the increased osteolysis of metastatic bone disease, Bone 33 (2003).

[124] S.E. Aldridge, T.W. Lennard, J.R. Williams, M.A. Birch, Vascular endothelial growth factor acts as an osteolytic factor in breast cancer metastases to bone, Br J Cancer 92 (2005).

[125] Y.-C. Chen, D.M. Sosnoski, A.M. Mastro, Breast cancer metastasis to the bone: mechanisms of bone loss, Breast Cancer Research 12(6) (2010) 1-11.

[126] P.D. Ottewell, N. Wang, H.K. Brown, C.A. Fowles, P.I. Croucher, C.L. Eaton, I. Holen, OPG-Fc inhibits ovariectomy-induced growth of disseminated breast cancer cells in bone, International Journal of Cancer 137(4) (2015) 968-977.

[127] E. Tian, F. Zhan, R. Walker, E. Rasmussen, Y. Ma, B. Barlogie, J.D. Shaughnessy, The role of the Wnt-signaling antagonist DKK1 in the development of osteolytic lesions in multiple myeloma, N Engl J Med 349 (2003).

[128] M.A. Forget, S. Turcotte, D. Beauseigle, J. Godin-Ethier, S. Pelletier, J. Martin, S. Tanguay, R. Lapointe, The Wnt pathway regulator DKK1 is preferentially expressed in hormone-resistant breast tumours and in some common cancer types, British Journal of Cancer 96(4) (2007) 646-653.

[129] G.R. Mundy, Mechanisms of bone metastasis, Cancer 80 (1997).

[130] T.A. Guise, K.S. Mohammad, G. Clines, E.G. Stebbins, D.H. Wong, L.S. Higgins, R. Vessella, E. Corey, S. Padalecki, L. Suva, J.M. Chirgwin, Basic Mechanisms Responsible for Osteolytic and Osteoblastic Bone Metastases, Clinical Cancer Research 12(20) (2006) 6213s-6216s.

[131] M.C. Winter, H.C. Thorpe, R. Burkinshaw, S.J. Beevers, R.E. Coleman, The addition of zoledronic acid to neoadjuvant chemotherapy may influence pathological response – exploratory evidence for direct anti-tumor activity in breast cancer, Cancer Research 69(2 Supplement) (2009) 5101.

[132] R. Coleman, D. Cameron, D. Dodwell, R. Bell, C. Wilson, E. Rathbone, M. Keane, M. Gil, R. Burkinshaw, R. Grieve, P. Barrett-Lee, D. Ritchie, V. Liversedge, S. Hinsley, H. Marshall, A. investigators, Adjuvant zoledronic acid in patients with early breast cancer: final efficacy analysis of the AZURE (BIG 01/04) randomised open-label phase 3 trial, Lancet Oncol 15(9) (2014) 997-1006.

[133] R.E. Coleman, H. Marshall, D. Cameron, D. Dodwell, R. Burkinshaw, M. Keane, M. Gil, S.J. Houston, R.J. Grieve, P.J. Barrett-Lee, D. Ritchie, J. Pugh, C. Gaunt, U. Rea, J. Peterson, C. Davies, V. Hiley, W. Gregory, R. Bell, Breast-Cancer Adjuvant Therapy with Zoledronic Acid, New England Journal of Medicine 365(15) (2011) 1396-1405.

[134] R. Coleman, M. Gnant, G. Morgan, P. Clezardin, Effects of bone-targeted agents on cancer progression and mortality, J Natl Cancer Inst 104(14) (2012) 1059-67.

[135] R. Coleman, R. de Boer, H. Eidtmann, A. Llombart, N. Davidson, P. Neven, G. von Minckwitz, H.P. Sleeboom, J. Forbes, C. Barrios, A. Frassoldati, I. Campbell, O. Paija, N. Martin, A. Modi, N. Bundred, Zoledronic acid (zoledronate) for postmenopausal women with early breast cancer receiving adjuvant letrozole (ZO-FAST study): final 60-month results, Annals of Oncology 24(2) (2013) 398-405.

[136] P.P. Lehenkari, M. Kellinsalmi, J.P. Näpänkangas, K.V. Ylitalo, J. Mönkkönen, M.J. Rogers, A. Azhayev, H.K. Väänänen, I.E. Hassinen, Further Insight into Mechanism of Action of Clodronate:

Inhibition of Mitochondrial ADP/ATP Translocase by a Nonhydrolyzable, Adenine-Containing Metabolite, Molecular Pharmacology 61(5) (2002) 1255-1262.

[137] J.R. Michael, New Insights Into the Molecular Mechanisms of Action of Bisphosphonates, Current Pharmaceutical Design 9(32) (2003) 2643-2658.

[138] H. Mönkkönen, S. Auriola, P. Lehenkari, M. Kellinsalmi, I.E. Hassinen, J. Vepsäläinen, J. Mönkkönen, A new endogenous ATP analog (ApppI) inhibits the mitochondrial adenine nucleotide translocase (ANT) and is responsible for the apoptosis induced by nitrogen-containing bisphosphonates, Br J Pharmacol 147(4) (2006) 437-45.

[139] H.L. Neville-Webbe, A. Rostami-Hodjegan, C.A. Evans, R.E. Coleman, I. Holen, Sequence- and schedule-dependent enhancement of zoledronic acid induced apoptosis by doxorubicin in breast and prostate cancer cells, Int J Cancer 113(3) (2005) 364-71.

[140] P. Clézardin, F.H. Ebetino, P.G. Fournier, Bisphosphonates and cancer-induced bone disease: beyond their antiresorptive activity, Cancer Res 65(12) (2005) 4971-4.

[141] P. Clézardin, J. Gligorov, P. Delmas, Mechanisms of action of bisphosphonates on tumor cells and prospects for use in the treatment of malignant osteolysis, Joint Bone Spine 67(1) (2000) 22-9.

[142] S. Boissier, M. Ferreras, O. Peyruchaud, S. Magnetto, F.H. Ebetino, M. Colombel, P. Delmas, J.M. Delaissé, P. Clézardin, Bisphosphonates inhibit breast and prostate carcinoma cell invasion, an early event in the formation of bone metastases, Cancer Res 60(11) (2000) 2949-54.

[143] A.C. Hirbe, A.J. Roelofs, D.H. Floyd, H. Deng, S.N. Becker, L.G. Lanigan, A.J. Apicelli, Z. Xu, J.L. Prior, M.C. Eagleton, D. Piwnica-Worms, M.J. Rogers, K. Weilbaecher, The bisphosphonate zoledronic acid decreases tumor growth in bone in mice with defective osteoclasts, Bone 44(5) (2009) 908-16.

[144] M. Neudert, C. Fischer, B. Krempien, F. Bauss, M.J. Seibel, Site-specific human breast cancer (MDA-MB-231) metastases in nude rats: model characterisation and in vivo effects of ibandronate on tumour growth, Int J Cancer 107(3) (2003) 468-77.

[145] P.G.J. Fournier, F. Daubiné, M.W. Lundy, M.J. Rogers, F.H. Ebetino, P. Clézardin, Lowering Bone Mineral Affinity of Bisphosphonates as a Therapeutic Strategy to Optimize Skeletal Tumor Growth Inhibition In vivo, Cancer Research 68(21) (2008) 8945-8953.

[146] F. Daubiné, C. Le Gall, J. Gasser, J. Green, P. Clézardin, Antitumor effects of clinical dosing regimens of bisphosphonates in experimental breast cancer bone metastasis, J Natl Cancer Inst 99(4) (2007) 322-30.

[147] H.K. Brown, I. Holen, Anti-tumour effects of bisphosphonates--what have we learned from in vivo models?, Curr Cancer Drug Targets 9(7) (2009) 807-23.

[148] P.G. Fournier, V. Stresing, F.H. Ebetino, P. Clézardin, How do bisphosphonates inhibit bone metastasis in vivo?, Neoplasia 12(7) (2010) 571-8.

[149] A. Sasaki, B.F. Boyce, B. Story, K.R. Wright, M. Chapman, R. Boyce, G.R. Mundy, T. Yoneda, Bisphosphonate risedronate reduces metastatic human breast cancer burden in bone in nude mice, Cancer Res 55(16) (1995) 3551-7.

[150] L. Gao, H. Deng, H. Zhao, A. Hirbe, J. Harding, L. Ratner, K. Weilbaecher, HTLV-1 Tax transgenic mice develop spontaneous osteolytic bone metastases prevented by osteoclast inhibition, Blood 106(13) (2005) 4294-4302.

[151] T. Chen, J. Berenson, R. Vescio, R. Swift, A. Gilchick, S. Goodin, P. LoRusso, P. Ma, C. Ravera, F. Deckert, H. Schran, J. Seaman, A. Skerjanec, Pharmacokinetics and Pharmacodynamics of Zoledronic Acid in Cancer Patients with Bone Metastases, The Journal of Clinical Pharmacology 42(11) (2002) 1228-1236.

[152] J.E. Brown, S.P. Ellis, J.E. Lester, S. Gutcher, T. Khanna, O.-P. Purohit, E. McCloskey, R.E. Coleman, Prolonged Efficacy of a Single Dose of the Bisphosphonate Zoledronic Acid, Clinical Cancer Research 13(18) (2007) 5406-5410.

[153] M. Sato, W. Grasser, N. Endo, R. Akins, H. Simmons, D.D. Thompson, E. Golub, G.A. Rodan, Bisphosphonate action. Alendronate localization in rat bone and effects on osteoclast ultrastructure, J Clin Invest 88(6) (1991) 2095-105.

[154] H.K. Brown, P.D. Ottewell, C.A. Evans, R.E. Coleman, I. Holen, A single administration of combination therapy inhibits breast tumour progression in bone and modifies both osteoblasts and osteoclasts, Journal of Bone Oncology 1(2) (2012) 47-56.

[155] T.L. Rogers, I. Holen, Tumour macrophages as potential targets of bisphosphonates, J Transl Med 9 (2011) 177.

[156] M.J. Rogers, K.M. Chilton, F.P. Coxon, J. Lawry, M.O. Smith, S. Suri, R.G. Russell, Bisphosphonates induce apoptosis in mouse macrophage-like cells in vitro by a nitric oxide-independent mechanism, J Bone Miner Res 11(10) (1996) 1482-91.

[157] N. Jain, R.S. Weinstein, Giant osteoclasts after long-term bisphosphonate therapy: diagnostic challenges, Nat Rev Rheumatol 5(6) (2009) 341-6.

[158] M.-T. Haider, I. Holen, T.N. Dear, K. Hunter, H.K. Brown, Modifying the osteoblastic niche with zoledronic acid in vivo—Potential implications for breast cancer bone metastasis, Bone 66(100) (2014) 240-250.

[159] F.N. Soki, X. Li, J. Berry, A. Koh, B.P. Sinder, X. Qian, K.M. Kozloff, R.S. Taichman, L.K. McCauley, The effects of zoledronic acid in the bone and vasculature support of hematopoietic stem cell niches, J Cell Biochem 114(1) (2013) 67-78.

[160] S.K. Ramasamy, A.P. Kusumbe, L. Wang, R.H. Adams, Endothelial Notch activity promotes angiogenesis and osteogenesis in bone, Nature 507(7492) (2014) 376-80.

[161] J. Wood, K. Bonjean, S. Ruetz, A. Bellahcène, L. Devy, J.M. Foidart, V. Castronovo, J.R. Green, Novel antiangiogenic effects of the bisphosphonate compound zoledronic acid, J Pharmacol Exp Ther 302(3) (2002) 1055-61.

[162] C. Walter, M.O. Klein, A. Pabst, B. Al-Nawas, H. Duschner, T. Ziebart, Influence of bisphosphonates on endothelial cells, fibroblasts, and osteogenic cells, Clin Oral Investig 14(1) (2010) 35-41.

[163] M. Michailidou, H.K. Brown, D.V. Lefley, A. Evans, S.S. Cross, R.E. Coleman, N.J. Brown, I. Holen, Microvascular endothelial cell responses in vitro and in vivo: modulation by zoledronic acid and paclitaxel?, J Vasc Res 47(6) (2010) 481-93.

[164] A. Allegra, G. Oteri, E. Nastro, A. Alonci, G. Bellomo, V. Del Fabro, E. Quartarone, C. Alati, F.S. De Ponte, D. Cicciù, C. Musolino, Patients with bisphosphonates-associated osteonecrosis of the jaw have reduced circulating endothelial cells, Hematol Oncol 25(4) (2007) 164-9.

[165] D. Sharma, S.M. Hamlet, E.B. Petcu, S. Ivanovski, The effect of bisphosphonates on the endothelial differentiation of mesenchymal stem cells, Sci Rep 6 (2016) 20580.

[166] D. Santini, B. Vincenzi, G. Avvisati, G. Dicuonzo, F. Battistoni, M. Gavasci, A. Salerno, V. Denaro, G. Tonini, Pamidronate induces modifications of circulating angiogenetic factors in cancer patients, Clin Cancer Res 8(5) (2002) 1080-4.

[167] D. Santini, B. Vincenzi, G. Dicuonzo, G. Avvisati, C. Massacesi, F. Battistoni, M. Gavasci, L. Rocci, M.C. Tirindelli, V. Altomare, M. Tocchini, M. Bonsignori, G. Tonini, Zoledronic acid induces significant and long-lasting modifications of circulating angiogenic factors in cancer patients, Clin Cancer Res 9(8) (2003) 2893-7.

[168] J.D. Veltman, M.E. Lambers, M. van Nimwegen, R.W. Hendriks, H.C. Hoogsteden, J.P. Hegmans, J.G. Aerts, Zoledronic acid impairs myeloid differentiation to tumour-associated macrophages in mesothelioma, Br J Cancer 103(5) (2010) 629-41.

[169] G. Comito, C. Pons Segura, M. Letizia Taddei, M. Lanciotti, S. Serni, A. Morandi, P. Chiarugi, E. Giannoni, Zoledronic acid impairs stromal reactivity by inhibiting M2-macrophages polarization and prostate cancer-associated fibroblasts, Oncotarget; Advance Online Publications: Page 5 (2016).

[170] M.R. Porembka, J.B. Mitchem, B.A. Belt, C.S. Hsieh, H.M. Lee, J. Herndon, W.E. Gillanders, D.C. Linehan, P. Goedegebuure, Pancreatic adenocarcinoma induces bone marrow mobilization of myeloid-derived suppressor cells which promote primary tumor growth, Cancer Immunol Immunother 61(9) (2012) 1373-85.

[171] M. Coscia, E. Quaglino, M. Iezzi, C. Curcio, F. Pantaleoni, C. Riganti, I. Holen, H. Mönkkönen, M. Boccadoro, G. Forni, P. Musiani, A. Bosia, F. Cavallo, M. Massaia, Zoledronic acid repolarizes tumour-associated macrophages and inhibits mammary carcinogenesis by targeting the mevalonate pathway, J Cell Mol Med 14(12) (2010) 2803-15.

[172] A.J. Roelofs, F.P. Coxon, F.H. Ebetino, M.W. Lundy, Z.J. Henneman, G.H. Nancollas, S. Sun, K.M. Blazewska, J.L. Bala, B.A. Kashemirov, A.B. Khalid, C.E. McKenna, M.J. Rogers, Fluorescent risedronate analogues reveal bisphosphonate uptake by bone marrow monocytes and localization around osteocytes in vivo, J Bone Miner Res 25(3) (2010) 606-16.

[173] A.M. Wolf, H. Rumpold, H. Tilg, G. Gastl, E. Gunsilius, D. Wolf, The effect of zoledronic acid on the function and differentiation of myeloid cells, Haematologica 91(9) (2006) 1165-71.

[174] V. Kunzmann, E. Bauer, J. Feurle, F. Weissinger, H.P. Tony, M. Wilhelm, Stimulation of gammadelta T cells by aminobisphosphonates and induction of antiplasma cell activity in multiple myeloma, Blood 96(2) (2000) 384-92.

[175] I. Benzaïd, H. Mönkkönen, E. Bonnelye, J. Mönkkönen, P. Clézardin, In vivo phosphoantigen levels in bisphosphonate-treated human breast tumors trigger Vγ9Vδ2 T-cell antitumor cytotoxicity through ICAM-1 engagement, Clin Cancer Res 18(22) (2012) 6249-59.

[176] V. Kunzmann, E. Bauer, M. Wilhelm, Gamma/delta T-cell stimulation by pamidronate, N Engl J Med 340(9) (1999) 737-8.

[177] E. Terpos, C.B. Confavreux, P. Clezardin, Bone antiresorptive agents in the treatment of bone metastases associated with solid tumours or multiple myeloma, BoneKEy Rep 4 (2015).

[178] I.J. Diel, A. Jaschke, E.F. Solomayer, C. Gollan, G. Bastert, C. Sohn, F. Schuetz, Adjuvant oral clodronate improves the overall survival of primary breast cancer patients with micrometastases to the bone marrow—a long-term follow-up, Annals of Oncology 19(12) (2008) 2007-2011.

[179] T. Powles, A. Paterson, E. McCloskey, P. Schein, B. Scheffler, A. Tidy, S. Ashley, I. Smith, L. Ottestad, J. Kanis, Reduction in bone relapse and improved survival with oral clodronate for adjuvant treatment of operable breast cancer [ISRCTN83688026], Breast Cancer Res 8(2) (2006) R13.

[180] M. Gnant, B. Mlineritsch, H. Stoeger, G. Luschin-Ebengreuth, D. Heck, C. Menzel, R. Jakesz, M. Seifert, M. Hubalek, G. Pristauz, T. Bauernhofer, H. Eidtmann, W. Eiermann, G. Steger, W. Kwasny, P. Dubsky, G. Hochreiner, E.P. Forsthuber, C. Fesl, R. Greil, V. Austrian Breast and Colorectal Cancer Study Group, A.stria, Adjuvant endocrine therapy plus zoledronic acid in premenopausal women with early-stage breast cancer: 62-month follow-up from the ABCSG-12 randomised trial, Lancet Oncol 12(7) (2011) 631-41.

[181] R. de Boer, N. Bundred, H. Eidtmann, P. Neven, G. von Minckwitz, N. Martin, A. Modi, R. Coleman, S1-3: Long-Term Survival Outcomes among Postmenopausal Women with Hormone Receptor-Positive Early Breast Cancer Receiving Adjuvant Letrozole and Zoledronic Acid: 5-Year Follow-Up of ZO-FAST, Cancer Research 71(24 Supplement) (2011) S1-3-S1-3.

[182] R. Coleman, T. Powles, A. Paterson, M. Gnant, S. Anderson, I. Diel, J. Gralow, G. von Minckwitz, V. Moebus, J. Bergh, K.I. Pritchard, J. Bliss, D. Cameron, V. Evans, H. Pan, R. Peto, R. Bradley, R. Gray, E.B.C.T.C.G. (EBCTCG), Adjuvant bisphosphonate treatment in early breast cancer: meta-analyses of individual patient data from randomised trials, Lancet 386(10001) (2015) 1353-61.

[183] P.D. Ottewell, N. Wang, H.K. Brown, K.J. Reeves, C.A. Fowles, P.I. Croucher, C.L. Eaton, I. Holen, Zoledronic acid has differential anti-tumour activity in the pre-and post-menopausal bone microenvironment in vivo, Clinical cancer research : an official journal of the American Association for Cancer Research 20(11) (2014) 2922-2932.

[184] M. Gnant, B. Mlineritsch, H. Stoeger, G. Luschin-Ebengreuth, M. Knauer, M. Moik, R. Jakesz, M. Seifert, S. Taucher, V. Bjelic-Radisic, M. Balic, H. Eidtmann, W. Eiermann, G. Steger, W. Kwasny, P. Dubsky, U. Selim, F. Fitzal, G. Hochreiner, V. Wette, P. Sevelda, F. Ploner, R. Bartsch, C. Fesl, R. Greil, V.A. on behalf of the Austrian Breast and Colorectal Cancer Study Group, Zoledronic acid combined with adjuvant endocrine therapy of tamoxifen versus anastrozol plus ovarian function suppression in premenopausal early breast cancer: final analysis of the Austrian Breast and Colorectal Cancer Study Group Trial 12, Annals of Oncology 26(2) (2015) 313-320.

[185] J.W. Denham, D. Joseph, D.S. Lamb, N.A. Spry, G. Duchesne, J. Matthews, C. Atkinson, K.-H. Tai, D. Christie, L. Kenny, S. Turner, N.K. Gogna, T. Diamond, B. Delahunt, C. Oldmeadow, J. Attia, A. Steigler, Short-term androgen suppression and radiotherapy versus intermediate-term androgen suppression and radiotherapy, with or without zoledronic acid, in men with locally advanced prostate cancer (TROG 03.04 RADAR): an open-label, randomised, phase 3 factorial trial, The Lancet Oncology 15(10) (2014) 1076-1089.

[186] M. Wirth, T. Tammela, V. Cicalese, F. Gomez Veiga, K. Delaere, K. Miller, A. Tubaro, M. Schulze, F. Debruyne, H. Huland, A. Patel, F. Lecouvet, C. Caris, W. Witjes, Prevention of Bone Metastases in Patients with High-risk Nonmetastatic Prostate Cancer Treated with Zoledronic Acid: Efficacy and Safety Results of the Zometa European Study (ZEUS), European Urology 67(3) (2015) 482-491.

[187] C.L. Vale, S. Burdett, L.H.M. Rydzewska, L. Albiges, N.W. Clarke, D. Fisher, K. Fizazi, G. Gravis, N.D. James, M.D. Mason, M.K.B. Parmar, C.J. Sweeney, M.R. Sydes, B. Tombal, J.F. Tierney, Addition of docetaxel or bisphosphonates to standard of care in men with localised or metastatic, hormone-sensitive prostate cancer: a systematic review and meta-analyses of aggregate data, The Lancet Oncology 17(2) (2016) 243-256.

[188] E.V. McCloskey, J.A. Dunn, J.A. Kanis, I.C.M. MacLennan, M.T. Drayson, A. the Medical Research Council Working Party on Leukaemia in, Long-term follow-up of a prospective, double-blind, placebo-controlled randomized trial of clodronate in multiple myeloma, British Journal of Haematology 113(4) (2001) 1035-1043.

[189] G.J. Morgan, J.A. Child, W.M. Gregory, A.J. Szubert, K. Cocks, S.E. Bell, N. Navarro-Coy, M.T. Drayson, R.G. Owen, S. Feyler, A.J. Ashcroft, F.M. Ross, J. Byrne, H. Roddie, C. Rudin, G. Cook, G.H. Jackson, P. Wu, F.E. Davies, G. on behalf of the National Cancer Research Institute Haematological Oncology Clinical Studies, Effects of zoledronic acid versus clodronic acid on skeletal morbidity in patients with newly diagnosed multiple myeloma (MRC Myeloma IX): secondary outcomes from a randomised controlled trial, The Lancet Oncology 12(8) (2011) 743-752.

[190] G.J. Morgan, F.E. Davies, W.M. Gregory, S.E. Bell, A.J. Szubert, G. Cook, M.T. Drayson, R.G. Owen, F.M. Ross, G.H. Jackson, J.A. Child, Long-term Follow-up of MRC Myeloma IX Trial: Survival Outcomes with Bisphosphonate and Thalidomide Treatment, American Association for Cancer Research 19(21) (2013) 6030-6038.

[191] R. Aft, M. Naughton, K. Trinkaus, M. Watson, L. Ylagan, M. Chavez-MacGregor, J. Zhai, S. Kuo, W. Shannon, K. Diemer, V. Herrmann, J. Dietz, A. Ali, M. Ellis, P. Weiss, T. Eberlein, C. Ma, P.M. Fracasso, I. Zoberi, M. Taylor, W. Gillanders, T. Pluard, J. Mortimer, K. Weilbaecher, Effect of zoledronic acid on disseminated tumour cells in women with locally advanced breast cancer: an open label, randomised, phase 2 trial, Lancet Oncol 11(5) (2010) 421-8.

[192] R.E. Coleman, M.C. Winter, D. Cameron, R. Bell, D. Dodwell, M.M. Keane, M. Gil, D. Ritchie, J.L. Passos-Coelho, D. Wheatley, R. Burkinshaw, S.J. Marshall, H. Thorpe, A.B. Investigators, The effects of adding zoledronic acid to neoadjuvant chemotherapy on tumour response: exploratory evidence for direct anti-tumour activity in breast cancer, Br J Cancer 102(7) (2010) 1099-105.

[193] J.R. Kroep, A. Charehbili, R.E. Coleman, R.L. Aft, Y. Hasegawa, M.C. Winter, K. Weilbaecher, K. Akazawa, S. Hinsley, H. Putter, G.J. Liefers, J.W. Nortier, N. Kohno, Effects of neoadjuvant chemotherapy with or without zoledronic acid on pathological response: A meta-analysis of randomised trials, Eur J Cancer 54 (2016) 57-63.

[194] CancerResearchUK, http://www.cancerresearchuk.org/health-professional/cancer-statistics/statistics-by-cancer-type/breast-cancer/incidence-in-situ - heading-One. (Accessed 26.06.2016.

[195] A. Charehbili, S. van de Ven, V.T.H.B.M. Smit, E. Meershoek-Klein Kranenbarg, N.A.T. Hamdy, H. Putter, J.B. Heijns, L.J.C. van Warmerdam, L. Kessels, M. Dercksen, M.J. Pepels, E. Maartense, H.W.M. van Laarhoven, B. Vriens, M.N. Wasser, A.E. van Leeuwen-Stok, G.J. Liefers, C.J.H. van de Velde, J.W.R. Nortier, J.R. Kroep, G. on behalf of the Dutch Breast Cancer Research, Addition of zoledronic acid to neoadjuvant chemotherapy does not enhance tumor response in patients with HER2-negative stage II/III breast cancer: the NEOZOTAC trial (BOOG 2010-01), Annals of Oncology 25(5) (2014) 998-1004.

[196] M.C. Winter, C. Wilson, S.P. Syddall, S.S. Cross, A. Evans, C.E. Ingram, I.J. Jolley, M.Q. Hatton, J.V. Freeman, S. Mori, I. Holen, R.E. Coleman, Neoadjuvant Chemotherapy with or without Zoledronic Acid in Early Breast Cancer—A Randomized Biomarker Pilot Study, American Association for Cancer Research 19(10) (2013) 2755-2765.

[197] D.A. Hanley, J.D. Adachi, A. Bell, V. Brown, Denosumab: mechanism of action and clinical outcomes, International Journal of Clinical Practice 66(12) (2012) 1139-1146.

[198] S. Morony, C. Capparelli, I. Sarosi, D.L. Lacey, C.R. Dunstan, P.J. Kostenuik, Osteoprotegerin Inhibits Osteolysis and Decreases Skeletal Tumor Burden in Syngeneic and Nude Mouse Models of Experimental Bone Metastasis, Cancer Research 61(11) (2001) 4432-4436.

[199] S. Morony, K. Warmington, S. Adamu, F. Asuncion, Z. Geng, M. Grisanti, H.L. Tan, C. Capparelli, C. Starnes, B. Weimann, C.R. Dunstan, P.J. Kostenuik, The Inhibition of RANKL Causes Greater Suppression of Bone Resorption and Hypercalcemia Compared with Bisphosphonates in Two Models of Humoral Hypercalcemia of Malignancy, Endocrinology 146(8) (2005) 3235-3243.

[200] D.R. Clohisy, M.L. Ramnaraine, S. Scully, M. Qi, G. Van, H.L. Tan, D.L. Lacey, Osteoprotegerin inhibits tumor-induced osteoclastogenesis and bone tumor growth in osteopetrotic mice, Journal of Orthopaedic Research 18(6) (2000) 967-976.

[201] A.T. Stopeck, A. Lipton, J.-J. Body, G.G. Steger, K. Tonkin, R.H. de Boer, M. Lichinitser, Y. Fujiwara, D.A. Yardley, M. Viniegra, M. Fan, Q. Jiang, R. Dansey, S. Jun, A. Braun, Denosumab Compared With Zoledronic Acid for the Treatment of Bone Metastases in Patients With Advanced Breast Cancer: A Randomized, Double-Blind Study, Journal of Clinical Oncology 28(35) (2010) 5132-5139.

[202] K. Fizazi, M. Carducci, M. Smith, R. Damião, J. Brown, L. Karsh, P. Milecki, N. Shore, M. Rader, H. Wang, Q. Jiang, S. Tadros, R. Dansey, C. Goessl, Denosumab versus zoledronic acid for treatment of bone metastases in men with castration-resistant prostate cancer: a randomised, double-blind study, Lancet 377(9768) (2011) 813-822.

[203] M. Gnant, G. Pfeiler, P.C. Dubsky, M. Hubalek, R. Greil, R. Jakesz, V. Wette, M. Balic, F. Haslbauer, E. Melbinger, V. Bjelic-Radisic, S. Artner-Matuschek, F. Fitzal, C. Marth, P. Sevelda, B. Mlineritsch, G.G. Steger, D. Manfreda, R. Exner, D. Egle, J. Bergh, F. Kainberger, S. Talbot, D. Warner, C. Fesl, C.F. Singer, A.B.a.C.C.S. Group, Adjuvant denosumab in breast cancer (ABCSG-18): a multicentre, randomised, double-blind, placebo-controlled trial, Lancet 386(9992) (2015) 433-43.

[204] H.-P. Gerber, N. Ferrara, Pharmacology and Pharmacodynamics of Bevacizumab as Monotherapy or in Combination with Cytotoxic Therapy in Preclinical Studies, Cancer Research 65(3) (2005) 671-680.

[205] K.D. Miller, L.I. Chap, F.A. Holmes, M.A. Cobleigh, P.K. Marcom, L. Fehrenbacher, M. Dickler, B.A. Overmoyer, J.D. Reimann, A.P. Sing, V. Langmuir, H.S. Rugo, Randomized Phase III Trial of Capecitabine Compared With Bevacizumab Plus Capecitabine in Patients With Previously Treated Metastatic Breast Cancer, Journal of Clinical Oncology 23(4) (2005) 792-799.

[206] L.a. Mina, M. Yu, C. Johnson, C. Burkhardt, K.D. Miller, R. Zon, A phase II study of combined VEGF inhibitor (bevacizumab+sorafenib) in patients with metastatic breast cancer: Hoosier Oncology Group Study BRE06-109, Investigational new drugs 31(5) (2013) 1307-10.

[207] D. Li, K. Xie, G. Ding, J. Li, K. Chen, H. Li, J. Qian, C. Jiang, J. Fang, Tumor resistance to anti-VEGF therapy through up-regulation of VEGF-C expression, Cancer Letters 346(1) (2014) 45-52.

[208] J.O. Alemán, A. Farooki, M. Girotra, Effects of tyrosine kinase inhibition on bone metabolism: untargeted consequences of targeted therapies, Endocr Relat Cancer 21(3) (2014) R247-59.

[209] M. Grano, F. Galimi, G. Zambonin, S. Colucci, E. Cottone, a.Z. Zallone, P.M. Comoglio, Hepatocyte growth factor is a coupling factor for osteoclasts and osteoblasts in vitro, Proceedings of the National Academy of Sciences of the United States of America 93(15) (1996) 7644-8.

[210] M.M. Deckers, M. Karperien, C. van der Bent, T. Yamashita, S.E. Papapoulos, C.W. Löwik, Expression of vascular endothelial growth factors and their receptors during osteoblast differentiation, Endocrinology 141(5) (2000) 1667-74.

[211] J. Tombran-Tink, C.J. Barnstable, Osteoblasts and osteoclasts express PEDF, VEGF-A isoforms, and VEGF receptors: possible mediators of angiogenesis and matrix remodeling in the bone, Biochem Biophys Res Commun 316(2) (2004) 573-9.

[212] H.P. Gerber, T.H. Vu, A.M. Ryan, J. Kowalski, Z. Werb, N. Ferrara, VEGF couples hypertrophic cartilage remodeling, ossification and angiogenesis during endochondral bone formation, Nat Med 5(6) (1999) 623-8.

[213] H. Otomo, A. Sakai, S. Uchida, S. Tanaka, M. Watanuki, S. Moriwaki, S. Niida, T. Nakamura, Flt-1 tyrosine kinase-deficient homozygous mice result in decreased trabecular bone volume with reduced osteogenic potential, Bone 40(6) (2007) 1494-501.

[214] V. Gattei, D. Aldinucci, J.M. Quinn, M. Degan, M. Cozzi, V. Perin, A.D. Iuliis, S. Juzbasic, S. Improta, N.A. Athanasou, L.K. Ashman, A. Pinto, Human osteoclasts and preosteoclast cells (FLG 29.1) express functional c-kit receptors and interact with osteoblast and stromal cells via membrane-bound stem cell factor, Cell Growth Differ 7(6) (1996) 753-63.

[215] V. Gattei, A. Celetti, A. Cerrato, M. Degan, A. De Iuliis, F.M. Rossi, G. Chiappetta, C. Consales, S. Improta, V. Zagonel, D. Aldinucci, V. Agosti, M. Santoro, G. Vecchio, A. Pinto, M. Grieco, Expression of the RET receptor tyrosine kinase and GDNFR-alpha in normal and leukemic human hematopoietic cells and stromal cells of the bone marrow microenvironment, Blood 89(8) (1997) 2925-37.

[216] K.J. Gotink, H.M. Verheul, Anti-angiogenic tyrosine kinase inhibitors: what is their mechanism of action?, Angiogenesis 13(1) (2010) 1-14.

[217] J. Zhang, P.L. Yang, N.S. Gray, Targeting cancer with small molecule kinase inhibitors, Nat Rev Cancer 9(1) (2009) 28-39.

[218] F.M. Yakes, J. Chen, J. Tan, K. Yamaguchi, Y. Shi, P. Yu, F. Qian, F. Chu, F. Bentzien, B. Cancilla, J. Orf, A. You, a.D. Laird, S. Engst, L. Lee, J. Lesch, Y.-C. Chou, A.H. Joly, Cabozantinib (XL184), a novel MET and VEGFR2 inhibitor, simultaneously suppresses metastasis, angiogenesis, and tumor growth, Molecular cancer therapeutics 10(12) (2011) 2298-308.

[219] S.L. Organ, M.-S. Tsao, An overview of the c-MET signaling pathway, Therapeutic advances in medical oncology 3(1 Suppl) (2011) S7-S19.

[220] A.-K. Olsson, A. Dimberg, J. Kreuger, L. Claesson-Welsh, VEGF receptor signalling ? in control of vascular function, Nat Rev Mol Cell Biol 7(5) (2006) 359-371.

[221] S. Pennacchietti, P. Michieli, M. Galluzzo, M. Mazzone, S. Giordano, P.M. Comoglio, Hypoxia promotes invasive growth by transcriptional activation of the met protooncogene, Cancer Cell 3(4) (2003) 347-361.

[222] K.M. Weidner, J. Behrens, J. Vandekerckhove, W. Birchmeier, Scatter factor: molecular characteristics and effect on the invasiveness of epithelial cells, J Cell Biol 111(5 Pt 1) (1990) 2097-108.

[223] V. Brinkmann, H. Foroutan, M. Sachs, K.M. Weidner, W. Birchmeier, Hepatocyte growth factor/scatter factor induces a variety of tissue-specific morphogenic programs in epithelial cells, J Cell Biol 131(6 Pt 1) (1995) 1573-86.

[224] F. Bussolino, M.F. Di Renzo, M. Ziche, E. Bocchietto, M. Olivero, L. Naldini, G. Gaudino, L. Tamagnone, a. Coffer, P.M. Comoglio, Hepatocyte growth factor is a potent angiogenic factor which stimulates endothelial cell motility and growth, The Journal of cell biology 119(3) (1992) 629-41.

[225] C. Birchmeier, W. Birchmeier, E. Gherardi, G.F. Vande Woude, Met, metastasis, motility and more, Nature reviews. Molecular cell biology 4(12) (2003) 915-25.

[226] K.P. Raghav, W. Wang, S. Liu, M. Chavez-MacGregor, X. Meng, G.N. Hortobagyi, G.B. Mills, F. Meric-Bernstam, G.R. Blumenschein, A.M. Gonzalez-Angulo, cMET and phospho-cMET protein levels in breast cancers and survival outcomes, Clin Cancer Res 18(8) (2012) 2269-77.

[227] A. Fasolo, C. Sessa, L. Gianni, M. Broggini, Seminars in clinical pharmacology: an introduction to MET inhibitors for the medical oncologist, Annals of Oncology 24(1) (2013) 14-20.

[228] DrugBank, http://www.drugbank.ca/drugs/DB08875. (Accessed 03.07.16.

[229] R. Elisei, M.J. Schlumberger, S.P. Müller, P. Schöffski, M.S. Brose, M.H. Shah, L. Licitra, B. Jarzab, V. Medvedev, M.C. Kreissl, B. Niederle, E.E. Cohen, L.J. Wirth, H. Ali, C. Hessel, Y. Yaron, D. Ball, B. Nelkin, S.I. Sherman, Cabozantinib in progressive medullary thyroid cancer, J Clin Oncol 31(29) (2013) 3639-46.

[230] J. Dai, H. Zhang, A. Karatsinides, J.M. Keller, K.M. Kozloff, D.T. Aftab, F. Schimmoller, E.T. Keller, Cabozantinib inhibits prostate cancer growth and prevents tumor-induced bone lesions, Clin Cancer Res 20(3) (2014) 617-30.

[231] H.M. Nguyen, N. Ruppender, X. Zhang, L.G. Brown, T.S. Gross, C. Morrissey, R. Gulati, R.L. Vessella, F. Schimmoller, D.T. Aftab, E. Corey, Cabozantinib inhibits growth of androgen-sensitive and castration-resistant prostate cancer and affects bone remodeling, PLoS One 8(10) (2013) e78881.

[232] F. Schimmoller, M. Zayzafoon, L.W.K. Chung, H.E. Zhau, K.M. Fagerlund, D.T. Aftab, Abstract A233: Cabozantinib (XL184), a dual MET-VEGFR2 inhibitor, blocks osteoblastic and osteolytic progression of human prostate cancer xenografts in mouse bone, Molecular Cancer Therapeutics 10(11 Supplement) (2011) A233-A233.

[233] T.J. Graham, G. Box, N. Tunariu, M. Crespo, T.J. Spinks, S. Miranda, G. Attard, J. de Bono, S.A. Eccles, F.E. Davies, S.P. Robinson, Preclinical Evaluation of Imaging Biomarkers for Prostate Cancer Bone Metastasis and Response to Cabozantinib, Journal of the National Cancer Institute 106(4) (2014).

[234] D.C. Smith, M.R. Smith, C. Sweeney, A.A. Elfiky, C. Logothetis, P.G. Corn, N.J. Vogelzang, E.J. Small, A.L. Harzstark, M.S. Gordon, U.N. Vaishampayan, N.B. Haas, A.I. Spira, P.N. Lara, C.-C. Lin, S. Srinivas, A. Sella, P. Schöffski, C. Scheffold, A.L. Weitzman, M. Hussain, Cabozantinib in Patients With Advanced Prostate Cancer: Results of a Phase II Randomized Discontinuation Trial, Journal of Clinical Oncology 31(4) (2013) 412-419.

[235] M.R. Smith, C.J. Sweeney, P.G. Corn, D.E. Rathkopf, D.C. Smith, M. Hussain, D.J. George, C.S. Higano, A.L. Harzstark, A.O. Sartor, N.J. Vogelzang, M.S. Gordon, J.S. de Bono, N.B. Haas, C.J. Logothetis, A. Elfiky, C. Scheffold, A.D. Laird, F. Schimmoller, E.M. Basch, H.I. Scher, Cabozantinib in chemotherapy-pretreated metastatic castration-resistant prostate cancer: results of a phase II nonrandomized expansion study, J Clin Oncol 32(30) (2014) 3391-9.

[236] M.G. Doran, D.E. Spratt, J. Wongvipat, D. Ulmert, B.S. Carver, C.L. Sawyers, M.J. Evans, Cabozantinib Resolves Bone Scans in Tumor-Naïve Mice Harboring Skeletal Injuries, Molecular imaging 13 (2014) 10.2310/7290.2014.00026.

[237] E. Basch, K.A. Autio, M.R. Smith, A.V. Bennett, A.L. Weitzman, C. Scheffold, C. Sweeney, D.E. Rathkopf, D.C. Smith, D.J. George, C.S. Higano, A.L. Harzstark, A.O. Sartor, M.S. Gordon, N.J. Vogelzang, J.S. de Bono, N.B. Haas, P.G. Corn, F. Schimmoller, H.I. Scher, Effects of Cabozantinib on Pain and Narcotic Use in Patients with Castration-resistant Prostate Cancer: Results from a Phase 2 Nonrandomized Expansion Cohort, Eur Urol 67(2) (2015) 310-8.

[238] S.M. Tolaney, D.R. Ziehr, H. Guo, W.T. Barry, M.J. Higgins, S.J. Isakoff, J.E. Brock, E. Ivanova, C. Paweletz, M. Demeo, N.H. Ramaiya, B. Overmoyer, R.K. Jain, D.G. Duda, E.P. Winer, A Phase II study

of cabozantinib for metastatic triple-negative breast cancer (TNBC). J Clin Oncol, 2015 ASCO Annual Meeting, 2015.

[239] T.K. Choueiri, B. Escudier, T. Powles, P.N. Mainwaring, B.I. Rini, F. Donskov, H. Hammers, T.E. Hutson, J.-L. Lee, K. Peltola, B.J. Roth, G.A. Bjarnason, L. Géczi, B. Keam, P. Maroto, D.Y.C. Heng, M. Schmidinger, P.W. Kantoff, A. Borgman-Hagey, C. Hessel, C. Scheffold, G.M. Schwab, N.M. Tannir, R.J. Motzer, Cabozantinib versus Everolimus in Advanced Renal-Cell Carcinoma, New England Journal of Medicine 373(19) (2015) 1814-1823.

[240] FDA, Highlights of prescribing information CABOMETYX™ (cabozantinib) tablets, for oral use.

[241] P.D. Ottewell, H. Mönkkönen, M. Jones, D.V. Lefley, R.E. Coleman, I. Holen, Antitumor effects of doxorubicin followed by zoledronic acid in a mouse model of breast cancer, J Natl Cancer Inst 100(16) (2008) 1167-78.

[242] I. Bellantuono, A. Aldahmash, M. Kassem, Aging of marrow stromal (skeletal) stem cells and their contribution to age-related bone loss, Biochimica et Biophysica Acta (BBA) - Molecular Basis of Disease 1792(4) (2009) 364-370.

[243] NanoDrop, http://www.bio.davidson.edu/GCAt/protocols/NanoDrop_tip.pdf.

[244] S.A. Bustin, Absolute quantification of mRNA using real-time reverse transcription polymerase chain reaction assays, Journal of Molecular Endocrinology 25(2) (2000) 169-193.

[245] http://www3.appliedbiosystems.com/cms/groups/portal/documents/generaldocuments/cms_075428.pdf.

[246] http://www.thermofisher.com/uk/en/home/life-science/pcr/real-time-pcr/qpcr-education/real-time-pcr-troubleshooting-tool/gene-expression-quantitation-troubleshooting/poor-pcr-efficiency.html.

[247] P.D. Ottewell, J.K. Woodward, D.V. Lefley, C.A. Evans, R.E. Coleman, I. Holen, Anticancer mechanisms of doxorubicin and zoledronic acid in breast cancer tumor growth in bone, Mol Cancer Ther 8(10) (2009) 2821-32.

[248] L.S. Loftus, S. Edwards-Bennett, G.H. Sokol, Systemic therapy for bone metastases, Cancer Control 19(2) (2012) 145-53.

[249] G.I. Im, S.A. Qureshi, J. Kenney, H.E. Rubash, A.S. Shanbhag, Osteoblast proliferation and maturation by bisphosphonates, Biomaterials 25(18) (2004) 4105-15.

[250] S.P. Luckman, D.E. Hughes, F.P. Coxon, R. Graham, G. Russell, M.J. Rogers, Nitrogen-containing bisphosphonates inhibit the mevalonate pathway and prevent post-translational prenylation of GTP-binding proteins, including Ras, J Bone Miner Res 13(4) (1998) 581-9.

[251] J. Massagué, A.C. Obenauf, Metastatic colonization by circulating tumour cells, Nature 529(7586) (2016) 298-306.

[252] G. Riethmüller, C.A. Klein, Early cancer cell dissemination and late metastatic relapse: clinical reflections and biological approaches to the dormancy problem in patients, Semin Cancer Biol 11(4) (2001) 307-11.

[253] Y. Hüsemann, J.B. Geigl, F. Schubert, P. Musiani, M. Meyer, E. Burghart, G. Forni, R. Eils, T. Fehm, G. Riethmüller, C.A. Klein, Systemic spread is an early step in breast cancer, Cancer Cell 13(1) (2008) 58-68.

[254] T. Ponomaryov, A. Peled, I. Petit, R.S. Taichman, L. Habler, J. Sandbank, F. Arenzana-Seisdedos, A. Magerus, A. Caruz, N. Fujii, A. Nagler, M. Lahav, M. Szyper-Kravitz, D. Zipori, T. Lapidot, Induction of the chemokine stromal-derived factor-1 following DNA damage improves human stem cell function, J Clin Invest 106(11) (2000) 1331-9.

[255] R.S. Taichman, C. Cooper, E.T. Keller, K.J. Pienta, N.S. Taichman, L.K. McCauley, Use of the stromal cell-derived factor-1/CXCR4 pathway in prostate cancer metastasis to bone, Cancer Res 62(6) (2002) 1832-7.

[256] F. Balkwill, The significance of cancer cell expression of the chemokine receptor CXCR4, Seminars in Cancer Biology 14(3) (2004) 171-179.

[257] G. van der Pluijm, I. Que, B. Sijmons, J.T. Buijs, C.W. Löwik, A. Wetterwald, G.N. Thalmann, S.E. Papapoulos, M.G. Cecchini, Interference with the microenvironmental support impairs the de novo formation of bone metastases in vivo, Cancer Res 65(17) (2005) 7682-90.

[258] F. Nutter, I. Holen, H.K. Brown, S.S. Cross, C.A. Evans, M. Walker, R.E. Coleman, J.A. Westbrook, P.J. Selby, J.E. Brown, P.D. Ottewell, Different molecular profiles are associated with breast cancer cell homing compared with colonisation of bone: evidence using a novel bone-seeking cell line, Endocr Relat Cancer 21(2) (2014) 327-41.

[259] P.D. Ottewell, B. Deux, H. Mönkkönen, S. Cross, R.E. Coleman, P. Clezardin, I. Holen, Differential effect of doxorubicin and zoledronic acid on intraosseous versus extraosseous breast tumor growth in vivo, Clin Cancer Res 14(14) (2008) 4658-66.

[260] P.D. Ottewell, D.V. Lefley, S.S. Cross, C.A. Evans, R.E. Coleman, I. Holen, Sustained inhibition of tumor growth and prolonged survival following sequential administration of doxorubicin and zoledronic acid in a breast cancer model, Int J Cancer 126(2) (2010) 522-32.

[261] G.A. Rodan, H.A. Fleisch, Bisphosphonates: mechanisms of action, J Clin Invest 97(12) (1996) 2692-6.

[262] S. Pozzi, S. Vallet, S. Mukherjee, D. Cirstea, N. Vaghela, L. Santo, E. Rosen, H. Ikeda, Y. Okawa, T. Kiziltepe, J. Schoonmaker, W. Xie, T. Hideshima, E. Weller, M.L. Bouxsein, N.C. Munshi, K.C. Anderson, N. Raje, High-dose zoledronic acid impacts bone remodeling with effects on osteoblastic lineage and bone mechanical properties, Clin Cancer Res 15(18) (2009) 5829-39.

[263] L.I. Plotkin, R.S. Weinstein, A.M. Parfitt, P.K. Roberson, S.C. Manolagas, T. Bellido, Prevention of osteocyte and osteoblast apoptosis by bisphosphonates and calcitonin, J Clin Invest 104(10) (1999) 1363-74.

[264] P.A. Phadke, R.R. Mercer, J.F. Harms, Y. Jia, A.R. Frost, J.L. Jewell, K.M. Bussard, S. Nelson, C. Moore, J.C. Kappes, C.V. Gay, A.M. Mastro, D.R. Welch, Kinetics of metastatic breast cancer cell trafficking in bone, Clin Cancer Res 12(5) (2006) 1431-40.

[265] J.E. Fisher, E. Rosenberg, A.C. Santora, A.A. Reszka, In vitro and in vivo responses to high and low doses of nitrogen-containing bisphosphonates suggest engagement of different mechanisms for inhibition of osteoclastic bone resorption, Calcif Tissue Int 92(6) (2013) 531-8.

[266] R.S. Weinstein, P.K. Roberson, S.C. Manolagas, Giant osteoclast formation and long-term oral bisphosphonate therapy, N Engl J Med 360(1) (2009) 53-62.

[267] F. von Knoch, C. Jaquiery, M. Kowalsky, S. Schaeren, C. Alabre, I. Martin, H.E. Rubash, A.S. Shanbhag, Effects of bisphosphonates on proliferation and osteoblast differentiation of human bone marrow stromal cells, Biomaterials 26(34) (2005) 6941-9.

[268] N. Maruotti, A. Corrado, A. Neve, F.P. Cantatore, Bisphosphonates: effects on osteoblast, Eur J Clin Pharmacol 68(7) (2012) 1013-8.

[269] O. Fromigué, J.J. Body, Bisphosphonates influence the proliferation and the maturation of normal human osteoblasts, J Endocrinol Invest 25(6) (2002) 539-46.

[270] V. Viereck, G. Emons, V. Lauck, K.H. Frosch, S. Blaschke, C. Gründker, L.C. Hofbauer, Bisphosphonates pamidronate and zoledronic acid stimulate osteoprotegerin production by primary human osteoblasts, Biochem Biophys Res Commun 291(3) (2002) 680-6.

[271] E.J. Mackie, L. Tatarczuch, M. Mirams, The skeleton: a multi-functional complex organ: the growth plate chondrocyte and endochondral ossification, J Endocrinol 211(2) (2011) 109-21.

[272] M.M. Deckers, E.R. Van Beek, G. Van Der Pluijm, A. Wetterwald, L. Van Der Wee-Pals, M.G. Cecchini, S.E. Papapoulos, C.W. Löwik, Dissociation of angiogenesis and osteoclastogenesis during endochondral bone formation in neonatal mice, J Bone Miner Res 17(6) (2002) 998-1007.

[273] I. Holen, R.E. Coleman, Anti-tumour activity of bisphosphonates in preclinical models of breast cancer, Breast Cancer Res 12(6) (2010) 214.

[274] S. Mohan, D.J. Baylink, Bone growth factors, Clin Orthop Relat Res (263) (1991) 30-48.

[275] Y. Zhao, R. Bachelier, I. Treilleux, P. Pujuguet, O. Peyruchaud, R. Baron, P. Clément-Lacroix, P. Clézardin, Tumor alphavbeta3 integrin is a therapeutic target for breast cancer bone metastases, Cancer Res 67(12) (2007) 5821-30.

[276] P.H. Stern, K. Alvares, Antitumor agent cabozantinib decreases RANKL expression in osteoblastic cells and inhibits osteoclastogenesis and PTHrP-stimulated bone resorption, J Cell Biochem 115(11) (2014) 2033-8.

[277] D. Novack, Bone Histomorphometry 101, http://www.musculoskeletalcore.wustl.edu/mm/files/Bone Histomorphometry 101.pdf. (Accessed 23.07.2016 2016).

[278] E. Berman, M. Nicolaides, R.G. Maki, M. Fleisher, S. Chanel, K. Scheu, B.A. Wilson, G. Heller, N.P. Sauter, Altered bone and mineral metabolism in patients receiving imatinib mesylate, N Engl J Med 354(19) (2006) 2006-13.

[279] R.A. Hannon, G. Clack, M. Rimmer, A. Swaisland, J.A. Lockton, R.D. Finkelman, R. Eastell, Effects of the Src kinase inhibitor saracatinib (AZD0530) on bone turnover in healthy men: a randomized, double-blind, placebo-controlled, multiple-ascending-dose phase I trial, J Bone Miner Res 25(3) (2010) 463-71.

[280] X. Zhou, K. von der Mark, S. Henry, W. Norton, H. Adams, B. de Crombrugghe, Chondrocytes transdifferentiate into osteoblasts in endochondral bone during development, postnatal growth and fracture healing in mice, PLoS Genet 10(12) (2014) e1004820.

[281] C.S. Adams, I.M. Shapiro, The fate of the terminally differentiated chondrocyte: evidence for microenvironmental regulation of chondrocyte apoptosis, Crit Rev Oral Biol Med 13(6) (2002) 465-73.

[282] S.R. Wedge, D.J. Ogilvie, M. Dukes, J. Kendrew, J.O. Curwen, L.F. Hennequin, A.P. Thomas, E.S. Stokes, B. Curry, G.H. Richmond, P.F. Wadsworth, ZD4190: an orally active inhibitor of vascular endothelial growth factor signaling with broad-spectrum antitumor efficacy, Cancer Res 60(4) (2000) 970-5.

[283] C. Maes, P. Carmeliet, K. Moermans, I. Stockmans, N. Smets, D. Collen, R. Bouillon, G. Carmeliet, Impaired angiogenesis and endochondral bone formation in mice lacking the vascular endothelial growth factor isoforms VEGF164 and VEGF188, Mech Dev 111(1-2) (2002) 61-73.

[284] C. Maes, S. Goossens, S. Bartunkova, B. Drogat, L. Coenegrachts, I. Stockmans, K. Moermans, O. Nyabi, K. Haigh, M. Naessens, L. Haenebalcke, J.P. Tuckermann, M. Tjwa, P. Carmeliet, V. Mandic, J.P. David, A. Behrens, A. Nagy, G. Carmeliet, J.J. Haigh, Increased skeletal VEGF enhances beta-catenin activity and results in excessively ossified bones, EMBO J 29(2) (2010) 424-41.

[285] A.P. Hall, F.R. Westwood, P.F. Wadsworth, Review of the effects of anti-angiogenic compounds on the epiphyseal growth plate, Toxicol Pathol 34(2) (2006) 131-47.

[286] S.D. Voss, J. Glade-Bender, S.L. Spunt, S.G. DuBois, B.C. Widemann, J.R. Park, S.E. Leary, M.D. Nelson, P.C. Adamson, S.M. Blaney, B. Weigel, Growth plate abnormalities in pediatric cancer patients undergoing phase 1 anti-angiogenic therapy: a report from the Children's Oncology Group Phase I Consortium, Pediatr Blood Cancer 62(1) (2015) 45-51.

[287] M.K. Chuk, B.C. Widemann, A.C. H., J.M. Reid, A. Kim, J.J. Wright, M. Lodish, E. Fox, B. Weigel, S. Blane, A phase I study of cabozantinib (XL184) in children and adolescents with recurrent or refractory solid tumors, including CNS tumors: A Children's Oncology Group phase I consortium trial., J Clin Oncol, 2014 ASCO Annual Meeting, 2014, p. 5s.

[288] S. Lim, Y. Zhang, D. Zhang, F. Chen, K. Hosaka, N. Feng, T. Seki, P. Andersson, J. Li, J. Zang, B. Sun, Y. Cao, VEGFR2-mediated vascular dilation as a mechanism of VEGF-induced anemia and bone marrow cell mobilization, Cell Rep 9(2) (2014) 569-80.

[289] O. Jacenko, D.W. Roberts, M.R. Campbell, P.M. McManus, C.J. Gress, Z. Tao, Linking hematopoiesis to endochondral skeletogenesis through analysis of mice transgenic for collagen X, Am J Pathol 160(6) (2002) 2019-34.

[290] M.A. Kacena, W.A. Ciovacco, Megakaryocyte-bone cell interactions, Adv Exp Med Biol 658 (2010) 31-41.

[291] C.A. Beeton, S. Bord, D. Ireland, J.E. Compston, Osteoclast formation and bone resorption are inhibited by megakaryocytes, Bone 39(5) (2006) 985-90.

[292] M.A. Kacena, T. Nelson, M.E. Clough, S.K. Lee, J.A. Lorenzo, C.M. Gundberg, M.C. Horowitz, Megakaryocyte-mediated inhibition of osteoclast development, Bone 39(5) (2006) 991-9.

[293] V. Kartsogiannis, H. Zhou, N.J. Horwood, R.J. Thomas, D.K. Hards, J.M. Quinn, P. Niforas, K.W. Ng, T.J. Martin, M.T. Gillespie, Localization of RANKL (receptor activator of NF kappa B ligand) mRNA and protein in skeletal and extraskeletal tissues, Bone 25(5) (1999) 525-34.

[294] P. Collin-Osdoby, L. Rothe, F. Anderson, M. Nelson, W. Maloney, P. Osdoby, Receptor activator of NF-kappa B and osteoprotegerin expression by human microvascular endothelial cells, regulation by inflammatory cytokines, and role in human osteoclastogenesis, J Biol Chem 276(23) (2001) 20659-72.

[295] T. Nakashima, M. Hayashi, T. Fukunaga, K. Kurata, M. Oh-Hora, J.Q. Feng, L.F. Bonewald, T. Kodama, A. Wutz, E.F. Wagner, J.M. Penninger, H. Takayanagi, Evidence for osteocyte regulation of bone homeostasis through RANKL expression, Nat Med 17(10) (2011) 1231-4.

[296] J. Xiong, M. Onal, R.L. Jilka, R.S. Weinstein, S.C. Manolagas, C.A. O'Brien, Matrix-embedded cells control osteoclast formation, Nat Med 17(10) (2011) 1235-41.

[297] P. Dy, W. Wang, P. Bhattaram, Q. Wang, L. Wang, R.T. Ballock, V. Lefebvre, Sox9 directs hypertrophic maturation and blocks osteoblast differentiation of growth plate chondrocytes, Dev Cell 22(3) (2012) 597-609.

[298] H. Akiyama, M.C. Chaboissier, J.F. Martin, A. Schedl, B. de Crombrugghe, The transcription factor Sox9 has essential roles in successive steps of the chondrocyte differentiation pathway and is required for expression of Sox5 and Sox6, Genes Dev 16(21) (2002) 2813-28.

[299] D. Ikegami, H. Akiyama, A. Suzuki, T. Nakamura, T. Nakano, H. Yoshikawa, N. Tsumaki, Sox9 sustains chondrocyte survival and hypertrophy in part through Pik3ca-Akt pathways, Development 138(8) (2011) 1507-19.

[300] F.A. Fornari, J.K. Randolph, J.C. Yalowich, M.K. Ritke, D.A. Gewirtz, Interference by doxorubicin with DNA unwinding in MCF-7 breast tumor cells, Mol Pharmacol 45(4) (1994) 649-56.

[301] V. Berlin, W.A. Haseltine, Reduction of adriamycin to a semiquinone-free radical by NADPH cytochrome P-450 reductase produces DNA cleavage in a reaction mediated by molecular oxygen, J Biol Chem 256(10) (1981) 4747-56.

[302] E. Tarasewicz, R. Hamdan, J. Straehla, A. Hardy, O. Nunez, S. Zelivianski, D. Dokic, J.S. Jeruss, CDK4 inhibition and doxorubicin mediate breast cancer cell apoptosis through Smad3 and survivin, Cancer Biol Ther 15(10) (2014) 1301-11.

[303] L.W. Elmore, C.W. Rehder, X. Di, P.A. McChesney, C.K. Jackson-Cook, D.A. Gewirtz, S.E. Holt, Adriamycin-induced senescence in breast tumor cells involves functional p53 and telomere dysfunction, J Biol Chem 277(38) (2002) 35509-15.

[304] S.P. Jagdev, R.E. Coleman, C.M. Shipman, A. Rostami-H, P.I. Croucher, The bisphosphonate, zoledronic acid, induces apoptosis of breast cancer cells: evidence for synergy with paclitaxel, Br J Cancer 84(8) (2001) 1126-34.

[305] S.G. Senaratne, G. Pirianov, J.L. Mansi, T.R. Arnett, K.W. Colston, Bisphosphonates induce apoptosis in human breast cancer cell lines, Br J Cancer 82(8) (2000) 1459-68.

[306] D.B. Kimmel, Mechanism of action, pharmacokinetic and pharmacodynamic profile, and clinical applications of nitrogen-containing bisphosphonates, J Dent Res 86(11) (2007) 1022-33.

[307] E. Corey, L.G. Brown, J.E. Quinn, M. Poot, M.P. Roudier, C.S. Higano, R.L. Vessella, Zoledronic acid exhibits inhibitory effects on osteoblastic and osteolytic metastases of prostate cancer, Clin Cancer Res 9(1) (2003) 295-306.

[308] M.F. Moreau, C. Guillet, P. Massin, S. Chevalier, H. Gascan, M.F. Baslé, D. Chappard, Comparative effects of five bisphosphonates on apoptosis of macrophage cells in vitro, Biochem Pharmacol 73(5) (2007) 718-23.

[309] E. Giraudo, M. Inoue, D. Hanahan, An amino-bisphosphonate targets MMP-9-expressing macrophages and angiogenesis to impair cervical carcinogenesis, J Clin Invest 114(5) (2004) 623-33.

[310] C. Melani, C. Chiodoni, G. Forni, M.P. Colombo, Myeloid cell expansion elicited by the progression of spontaneous mammary carcinomas in c-erbB-2 transgenic BALB/c mice suppresses immune reactivity, Blood 102(6) (2003) 2138-45.

[311] P.J. Murray, T.A. Wynn, Protective and pathogenic functions of macrophage subsets, Nat Rev Immunol 11(11) (2011) 723-737.

[312] B.A. Houlden, P.M. Hogarth, I.F.C. McKenzie, Interrelationships of the "Ly-6 complex" antigens, Immunogenetics 23(4) (1986) 226-232.

[313] T.J. Fleming, M.L. Fleming, T.R. Malek, Selective expression of Ly-6G on myeloid lineage cells in mouse bone marrow. RB6-8C5 mAb to granulocyte-differentiation antigen (Gr-1) detects members of the Ly-6 family, The Journal of Immunology 151(5) (1993) 2399-2408.

[314] M.J. Siemerink, I. Klaassen, C.J.F. Van Noorden, R.O. Schlingemann, Endothelial Tip Cells in Ocular Angiogenesis: Potential Target for Anti-Angiogenesis Therapy, Journal of Histochemistry and Cytochemistry 61(2) (2013) 101-115.

[315] D. Miles, G. von Minckwitz, A.D. Seidman, Combination Versus Sequential Single-Agent Therapy in Metastatic Breast Cancer, The Oncologist 7(suppl 6) (2002) 13-19.

[316] T. Hiraga, A. Ueda, D. Tamura, K. Hata, F. Ikeda, P.J. Williams, T. Yoneda, Effects of oral UFT combined with or without zoledronic acid on bone metastasis in the 4T1/luc mouse breast cancer, International Journal of Cancer 106(6) (2003) 973-979.

[317] W.C.M. Duivenvoorden, S. Vukmirović-Popović, M. Kalina, E. Seidlitz, G. Singh, Effect of zoledronic acid on the doxycycline-induced decrease in tumour burden in a bone metastasis model of human breast cancer, British Journal of Cancer 96(10) (2007) 1526-1531.

[318] K.D. Brubaker, L.G. Brown, R.L. Vessella, E. Corey, Administration of zoledronic acid enhances the effects of docetaxel on growth of prostate cancer in the bone environment, BMC Cancer 6 (2006) 15-15.

[319] J. Kato, M. Futamura, M. Kanematsu, S. Gaowa, R. Mori, T. Tanahashi, N. Matsuhashi, K. Yoshida, Combination therapy with zoledronic acid and cetuximab effectively suppresses growth of colorectal cancer cells regardless of KRAS status, International Journal of Cancer 138(6) (2016) 1516-1527.

[320] A.P. Kusumbe, S.K. Ramasamy, T. Itkin, M.A. Mäe, U.H. Langen, C. Betsholtz, T. Lapidot, R.H. Adams, Age-dependent modulation of vascular niches for haematopoietic stem cells, Nature 532(7599) (2016) 380-384.

[321] W. Gorczyca, Z.-Y. Sun, W. Cronin, X. Li, S. Mau, S. Tugulea, Chapter 10 - Immunophenotypic Pattern of Myeloid Populations by Flow Cytometry Analysis, in: E.H.A.O.W.T.a.D.W. Zbigniew Darzynkiewicz (Ed.), Methods in Cell Biology, Academic Press2011, pp. 221-266.

[322] C.M. Diaz-Montero, M.L. Salem, M.I. Nishimura, E. Garrett-Mayer, D.J. Cole, A.J. Montero, Increased circulating myeloid-derived suppressor cells correlate with clinical cancer stage, metastatic tumor burden, and doxorubicin-cyclophosphamide chemotherapy, Cancer Immunol Immunother 58(1) (2009) 49-59.

[323] R.F. Gabitass, N.E. Annels, D.D. Stocken, H.A. Pandha, G.W. Middleton, Elevated myeloid-derived suppressor cells in pancreatic, esophageal and gastric cancer are an independent prognostic

factor and are associated with significant elevation of the Th2 cytokine interleukin-13, Cancer Immunol Immunother 60(10) (2011) 1419-30.

[324] J. Zhuang, J. Zhang, S.T. Lwin, J.R. Edwards, C.M. Edwards, G.R. Mundy, X. Yang, Osteoclasts in Multiple Myeloma Are Derived from Gr-1+CD11b+Myeloid-Derived Suppressor Cells, PLoS ONE 7(11) (2012) e48871.

[325] D. Alizadeh, M. Trad, N.T. Hanke, C.B. Larmonier, N. Janikashvili, B. Bonnotte, E. Katsanis, N. Larmonier, Doxorubicin Eliminates Myeloid-Derived Suppressor Cells and Enhances the Efficacy of Adoptive T-Cell Transfer in Breast Cancer, Cancer Research 74(1) (2014) 104-118.

[326] V.R. Zellmer, S. Zhang, Evolving concepts of tumor heterogeneity, Cell & Bioscience 4(1) (2014) 1-8.

[327] G.R. Mundy, Bone Remodeling and its Disorders, Martin Dunitz Ltd, London, 1999.

[328] A. Lipton, Pathophysiology of bone metastases: how this knowledge may lead to therapeutic intervention, J Support Oncol 2(3) (2004) 205-13; discussion 213-4, 216-7, 219-20.

[329] H. Fleisch, The role of bisphosphonates in breast cancer: Development of bisphosphonates, Breast Cancer Research 4(1) (2002) 30-34.

[330] D.J. Heath, A.D. Chantry, C.H. Buckle, L. Coulton, J.D. Shaughnessy, H.R. Evans, J.A. Snowden, D.R. Stover, K. Vanderkerken, P.I. Croucher, Inhibiting Dickkopf-1 (Dkk1) Removes Suppression of Bone Formation and Prevents the Development of Osteolytic Bone Disease in Multiple Myeloma, Journal of Bone and Mineral Research 24(3) (2009) 425-436.

[331] S.T. Mohanty, L. Kottam, A. Gambardella, M.J. Nicklin, L. Coulton, D. Hughes, A.G. Wilson, P.I. Croucher, I. Bellantuono, Alterations in the self-renewal and differentiation ability of bone marrow mesenchymal stem cells in a mouse model of rheumatoid arthritis, Arthritis Research & Therapy 12(4) (2010) R149-R149.

[332] S. Deleu, M. Lemaire, J. Arts, E. Menu, E. Van Valckenborgh, I. Vande Broek, H. De Raeve, L. Coulton, B. Van Camp, P. Croucher, K. Vanderkerken, Bortezomib Alone or in Combination with the Histone Deacetylase Inhibitor JNJ-26481585: Effect on Myeloma Bone Disease in the 5T2MM Murine Model of Myeloma, Cancer Research 69(13) (2009) 5307-5311.

[333] A.D. Chantry, D. Heath, A.W. Mulivor, S. Pearsall, M. Baud'huin, L. Coulton, H. Evans, N. Abdul, E.D. Werner, M.L. Bouxsein, M.L. Key, J. Seehra, T.R. Arnett, K. Vanderkerken, P. Croucher, Inhibiting activin-A signaling stimulates bone formation and prevents cancer-induced bone destruction in vivo, Journal of Bone and Mineral Research 25(12) (2010) 2633-2646.

[334] P.G. Dedes, C. Gialeli, A.I. Tsonis, I. Kanakis, A.D. Theocharis, D. Kletsas, G.N. Tzanakakis, N.K. Karamanos, Expression of matrix macromolecules and functional properties of breast cancer cells are modulated by the bisphosphonate zoledronic acid, Biochim Biophys Acta 1820(12) (2012) 1926-39.

[335] M. Wilke, A. Göbel, M. Rauner, P. Benad-Mehner, N. Schütze, S. Füssel, P. Hadji, L.C. Hofbauer, T.D. Rachner, Zoledronic acid and atorvastatin inhibit αvβ3-mediated adhesion of breast cancer cells, Journal of Bone Oncology 3(1) (2014) 10-17.

[336] N. Dirckx, M. Van Hul, C. Maes, Osteoblast recruitment to sites of bone formation in skeletal development, homeostasis, and regeneration, Birth Defects Research Part C: Embryo Today: Reviews 99(3) (2013) 170-191.

[337] P. Bianco, Bone and the hematopoietic niche: a tale of two stem cells, Blood 117(20) (2011) 5281-5288.

[338] N.M. Rashidi, M.K. Scott, N. Scherf, A. Krinner, J.S. Kalchschmidt, K. Gounaris, M.E. Selkirk, I. Roeder, C. Lo Celso, In vivo time-lapse imaging shows diverse niche engagement by quiescent and naturally activated hematopoietic stem cells, Blood 124(1) (2014) 79-83.

[339] D. Visnjic, Z. Kalajzic, D.W. Rowe, V. Katavic, J. Lorenzo, H.L. Aguila, Hematopoiesis is severely altered in mice with an induced osteoblast deficiency, Blood 103(9) (2004) 3258-3264.

[340] G.B. Adams, I.R. Alley, U.-i. Chung, K.T. Chabner, N.T. Jeanson, C. Lo Celso, E.S. Marsters, M. Chen, L.S. Weinstein, C.P. Lin, H.M. Kronenberg, D.T. Scadden, Hematopoietic stem cells depend upon G(s)α-mediated signalling to engraft bone marrow, Nature 459(7243) (2009) 103-107.

[341] M.T. Haider, K.D. Hunter, S.P. Robinson, T.J. Graham, E. Corey, T.N. Dear, R. Hughes, N.J. Brown, I. Holen, Rapid modification of the bone microenvironment following short-term treatment with Cabozantinib in vivo, Bone 81 (2015) 581-592.

[342] Y.-M. Yang, P. Li, D.-C. Cui, R.-J. Dang, L. Zhang, N. Wen, X.-X. Jiang, Effect of aged bone marrow microenvironment on mesenchymal stem cell migration, Age 37(2) (2015) 16.

[343] M. Gnant, Editorial comment on 'Effects of neoadjuvant chemotherapy with or without zoledronic acid on pathological response: A meta-analysis of randomised trials', European Journal of Cancer 59 (2016) 125-127.

[344] A. Prat, J.S. Parker, O. Karginova, C. Fan, C. Livasy, J.I. Herschkowitz, X. He, C.M. Perou, Phenotypic and molecular characterization of the claudin-low intrinsic subtype of breast cancer, Breast Cancer Res 12(5) (2010) R68.

[345] A. Prat, C.M. Perou, Deconstructing the molecular portraits of breast cancer, Mol Oncol 5(1) (2011) 5-23.

[346] B. Heissig, K. Hattori, S. Dias, M. Friedrich, B. Ferris, N.R. Hackett, R.G. Crystal, P. Besmer, D. Lyden, M.A. Moore, Z. Werb, S. Rafii, Recruitment of stem and progenitor cells from the bone marrow niche requires MMP-9 mediated release of kit-ligand, Cell 109(5) (2002) 625-37.

[347] J. Dai, Y. Lu, C. Yu, J.M. Keller, A. Mizokami, J. Zhang, E.T. Keller, Reversal of chemotherapy-induced leukopenia using granulocyte macrophage colony-stimulating factor promotes bone metastasis that can be blocked with osteoclast inhibitors, Cancer Res 70(12) (2010) 5014-23.